UNIVERSITY OF SOUTHAMPTON

MODELLING MECHANICAL RESPONSES TO HUMAN WHOLE-BODY VIBRATION

SATOSHI KITAZAKI, B.Eng., M.Eng.

DOCTOR OF PHILOSOPHY

FACULTY OF ENGINEERING AND APPLIED SCIENCE
INSTITUTE OF SOUND AND VIBRATION RESEARCH

OCTOBER, 1994

UNIVERSITY OF SOUTHAMPTON

ABSTRACT

FACULTY OF ENGINEERING AND APPLIED SCIENCE
INSTITUTE OF SOUND AND VIBRATION RESEARCH

Doctor of Philosophy

MODELLING MECHANICAL RESPONSES TO HUMAN WHOLE-BODY VIBRATION

by Satoshi Kitazaki

Understanding of mechanical responses of the human body is important to minimise adverse effects of vibration on health, activities and comfort. Although a considerable number of investigations has been made in this area, the mechanical responses are not yet understood due to the complexity and uncertainty of the body structure. In this research, a series of models for mechanical responses to the human whole-body vibration has been developed, using the finite element method. Beam, spring and mass elements were used to model the spinal column, visceral column, head, torso segments, pelvis and buttocks tissue in the mid-sagittal plane. The material properties were based on data from cadavers reported in the literature. Firstly, the models were validated and modified, comparing their responses with available experimental data for the driving point response. Subsequently, experimental work was conducted to develop the models further. Experimental modal analysis was applied to whole-body vibration. Acceleration transfer functions from vertical seat motion to motion of the head, spine, pelvis and the viscera in the mid-sagittal plane were measured, using a data correction method developed to eliminate the effects of local tissue-accelerometer vibration from accelerations measured on the body surface. The natural frequencies and the vibration mode shapes of the body in three different postures were extracted by the analysis. The final model was developed, comparing the natural frequencies and the vibration mode shapes of the model with the measurements.

The final model demonstrated that the principal resonance of the human body at about 5 Hz consisted of an entire body mode with vertical and fore-and-aft pelvic motion due to deformation of tissue beneath the pelvis in phase with a vertical visceral mode. The second principal resonance at about 8 Hz was found to correspond to a rotational mode of the pelvis. The model produced ten modes below 20 Hz (seven modes below 10 Hz), including the principal and the second principal modes, and the rest of the modes were mostly bending modes of the spine. The model showed that the shifts of the principal and the second principal resonances of the body due to postural change were caused by shifts of the natural frequencies for the entire body mode and the rotational mode of the pelvis. It was suggested that an increase in contact areas between the buttocks and the thighs and the seat surface, when changing posture from erect to slouched, decreased the axial stiffness beneath the pelvis with the non-linear force-deflection relationship of tissue, resulting in decreases in the natural frequencies. It was also found that a change in posture from erect to slouched increased the contribution of the shear deformation of tissue beneath the pelvis to the entire body mode, and the natural frequency was decreased with the much lower shear stiffness of tissue than the axial stiffness.

CONTENTS

ABSTRACT i

ACKNOWLEDGEMENTS vii

CHAPTER 1 GENERAL INTRODUCTION 1

CHAPTER 2 LITERATURE REVIEW

2.1 INTRODUCTION 3

2.2 ANATOMICAL BASIS

2.2.1 Vibration axes and planes of the body 3

2.2.2 Structure of whole skeletal system 4

2.2.3 Structure of vertebral column 5

2.2.4 Structure of each vertebra 6

2.2.5 Vertebral joints 8

2.2.6 Body cavities 12

2.3 MEASUREMENT OF MECHANICAL RESPONSES TO WHOLE-BODY VIBRATION

2.3.1 Introduction 13

2.3.2 Description and calculation of transfer functions 14

2.3.3 Driving point mechanical impedance and apparent mass ... 16

2.3.3.1 Effect of posture 17

2.3.3.2 Effect of muscle tension 18

2.3.3.3 Effect of constraint 19

2.3.3.4 Inter-subject variability 19

2.3.3.5 Non-linearity 20

2.3.4 Transmissibility to the head 23

2.3.4.1 Effect of posture 24

2.3.4.2 Effect of muscle tension 28

2.3.4.3 Inter-subject variability 28

2.3.4.4 Non-linearity 29

2.3.5 Transmissibility to the spine 30

2.3.5.1 General responses of the spine 32

2.3.5.2 Effect of posture 34
2.3.5.3 Effect of muscle tension 35
2.3.5.4 Non-linearity 36
2.3.6 Other responses of the body 37
2.3.6.1 Response of the viscera 38
2.3.6.2 Response of the pelvis 40
2.3.6.3 Response of the upper torso 42
2.3.7 Discussion
2.3.7.1 General responses of the human body 43
2.3.7.2 Effect of posture 45
2.3.7.3 Effect of muscle tension 46
2.3.7.4 Inter-subject variability 47
2.3.7.5 Non-linearity 49
2.4 MODELLING MECHANICAL RESPONSES TO WHOLE-BODY VIBRATION
2.4.1 Introduction 50
2.4.2 Lumped parameter models 52
2.4.3 Continuum models 59
2.4.4 Discrete models 64
2.4.5 Discussion 70
2.5 CONCLUSIONS FROM LITERATURE REVIEW 73

CHAPTER 3 MODELLING MECHANICAL RESPONSES TO WHOLE-BODY VIBRATION: PART 1

3.1 INTRODUCTION 75
3.2 THEORY
3.2.1 The finite element method and Ansys 75
3.2.2 Modal analysis 76
3.2.3 Harmonic response analysis
3.2.3.1 Mode-superposition method 77
3.2.3.2 Driving point impedance and apparent mass 78
3.2.3.3 Acceleration transfer function 79
3.2.4 Master degrees of freedom 79
3.2.5 Additional considerations for the human body structure
3.2.5.1 Modal analysis 79

3.2.5.2 Harmonic response analysis 82

3.3 MODEL 1: SIMPLIFIED MODEL BASED ON BELYTSCHKO'S MODEL

3.3.1 Model description 85

3.3.2 Geometry and material properties 87

3.3.3 Calculation conditions 92

3.3.4 Results and discussion 93

3.4 MODEL 2: MODIFIED SIMPLIFIED MODEL

3.4.1 Model description 97

3.4.2 Geometry and material properties 98

3.4.3 Results and discussion 99

3.5 MODEL 3: EXPANDED MODEL

3.5.1 Model description 106

3.5.2 Geometry and material properties 107

3.5.3 Results and discussion 114

3.6 CONCLUSIONS FROM MODELLING: PART 1 120

CHAPTER 4 EXPERIMENTAL DETERMINATION OF MODE SHAPES OF WHOLE-BODY VIBRATION

4.1 INTRODUCTION 122

4.2 A DATA CORRECTION METHOD FOR SURFACE MEASUREMENT OF VIBRATION ON THE HUMAN BODY

4.2.1 Introduction 122

4.2.2 Theory

4.2.2.1 Definition of the correction frequency function 124

4.2.2.2 Description of the correction frequency function 126

4.2.2.3 Estimation of the natural frequency and damping ratio of the local system 127

4.2.3 Experimental methods 130

4.2.4 Results 132

4.2.5 Discussion 138

4.2.6 Conclusions 147

4.3 EXPERIMENTAL MODAL ANALYSIS OF WHOLE-BODY VIBRATION

4.3.1 Introduction 147

4.3.2 Theory

4.3.2.1 Fundamentals of the experimental modal analysis 147

4.3.2.2 Additional considerations for the application of experimental modal analysis to whole-body vibration 150
4.3.2.3 Modal assurance criteria 153
4.3.3 Methods
4.3.3.1 Experimental methods 154
4.3.3.2 Calculation of pelvic motion 157
4.3.3.3 Estimation of spinal curves 158
4.3.4 Results 159
4.3.5 Discussion 175
4.3.6 Conclusions 181
4.4 MEASUREMENT OF THE APPARENT MASS WITH CONSTRAINTS
4.4.1 Introduction 182
4.4.2 Experimental methods 182
4.4.3 Results 183
4.4.4 Discussion 185
4.4.5 Conclusions 190
4.5 CONCLUSIONS FROM EXPERIMENTAL WORK 191

CHAPTER 5 MODELLING MECHANICAL RESPONSES TO WHOLE-BODY VIBRATION: PART 2

5.1 INTRODUCTION 192
5.2 MODEL 4: MODIFIED EXPANDED MODEL
5.2.1 Model description 192
5.2.2 Geometry and material properties
5.2.2.1 Geometry 193
5.2.2.2 Inertial properties 202
5.2.2.3 Stiffness data 204
5.2.2.4 Effective damping ratios 209
5.2.3 Calculation conditions 210
5.2.4 Results and discussion 210
5.3 CONCLUSIONS FROM MODELLING: PART 2 232

CHAPTER 6 GENERAL CONCLUSIONS AND RECOMMENDATIONS 234

APPENDICES

APPENDIX 1	Responses of a single degree-of-freedom system	239
APPENDIX 2	Fundamentals of the finite element method	242
APPENDIX 3	A straight-line technique for extracting modal properties from frequency response data	252
APPENDIX 4	Modal matrices	257
APPENDIX 5	Cubic spline interpolation	263
APPENDIX 6	Ansys command list for the modal analysis of the modified expanded model	265

REFERENCES 281

ACKNOWLEDGEMENTS

This research was sponsored by Nissan Motor Co., Ltd, 1 Natsushima-cho, Yokosuka, 237, Japan. I would like to show my deepest gratitude to Professor Michael J. Griffin for his extremely kind support with a lot of advice and suggestions for this research. This research would not have been completed without understanding and kind cooperation of my superiors in Nissan, Mr.E.Yaguchi, Mr.T.Yanagishima and Mr.T.Jindo., colleagues in the personnel section who gave me one year extension to stay in England, and other colleagues who compensated my absence in Nissan. I also would like to thank all the members of the Human Factors Research Unit, I.S.V.R., University of Southampton, especially Dr.C.H.Lewis, Dr.G.S.Paddan, and Mrs.A.J.Messenger for their kind technical advice, and Mr.C.A.C.J.Littler, Mr.G.C.Parker, and Mr.A.C.Stone for their help in my experiments as technicians. I cannot forget kind participation of all my subjects in the experiments who had to endure the torture for three hours with accelerometers attached on the body. I would like to express special thanks to Mrs.J.M.Spetch and Miss D.L.Janney who kindly helped me with completing this research as a librarian and a secretary of the unit. I will never forget all my friends in England who helped me with enjoying the life and encouraged me to work.

Finally, I thank my parents, Mr.T.Kitazaki and Mrs.K.Kitazaki. I would not have been able to live in a foreign country on my own for three years and complete this research without their mental support.

CHAPTER 1

GENERAL INTRODUCTION

We are almost consistently exposed to vibration in our daily life. Especially when travelling in vehicles such as cars and trains, the whole body in a sitting position is excited in response to vibration given to the buttocks from the seat. As transportation is developed in the modern society, such situations have largely increased. In engineering, considerable effort has been made to reduce vibration levels of machines and it has been quite successful. However, in contrast, the effects of vibration on humans have not yet been entirely understood due to the complexity and uncertainty of the body structure.

British standard 6841 (1987) classifies the effects of whole body vibration as those on health, activities, comfort and motion sickness which is helpful to conduct the efficient research in this area. When professional drivers such as bus drivers, truck drivers and drivers of earth-moving machines are considered, vibration affects their health, causing back pain and spinal injuries, due to long exposure times and high levels of vibration. Passengers in buses and trains and non-professional drivers of cars are usually exposed to vibration for shorter durations and vibration is not as hazardous as for the professional drivers. However, they feel vibration as discomfort which may cause physical and mental fatigue. Vibration also interferes with activities. It may degrade manual control or visual performance of drivers, and activities of passengers such as holding a cup of coffee and reading a book. Motion sickness is caused by vibration with frequencies lower than 0.5 Hz (British standard 6841). However, the frequencies are different from those causing the other three effects and it is excluded from the scope of this research.

Humans have a multiple response to vibration with different technical aspects such as mechanical, physiological, and psychological responses (Griffin, 1990), and researchers with the different backgrounds have been involved in this area. The effects on health and activities contain mechanical and physiological aspects, and the effect on comfort includes psychological, physiological and mechanical aspects. Spinal injury may be a breakdown or degeneration of the vertebrae which may be caused by internal stress within the spine. It has been suggested that vibration or shock induces axial, bending or torsional deformation of the spine, resulting in excessive stress concentration on some vertebrae, and long-term exposure may induce their fatigue-induced breakdown and consequent

degenerative change with the involvement of other physiological factors. Some effects of vibration on manual control may be explained by the mechanical responses of the body. The human body has resonances of substructures such as the spine and the arms, and vibration given to the buttocks from the seat travels through the body to the hands, inducing a shaking of the hands that may interfere with control. There can also be a compensatory effort from subjects not to spill coffee in a cup, for example, which involves physiological processes, acquiring information from the eyes and trying to control movement of the hands using the muscles. Visual performance can be degraded by the presence of vibration. It is known that there are physiological compensatory movements of eyes at low frequencies such as the pursuit reflex (below 1 or 2 Hz for display vibration and observer-and-display vibration), and the vestibulo-ocular reflex (below 8 or 10 Hz for observer vibration). However, above these frequencies, such compensation is not effective enough and the visual performance is degraded largely due to mechanical responses such as the translational and rotational motion of the head and the eyes in response to the vibration input. Comfort in vibration may be a dominantly psychological response. However, mechanical responses such as motion of the viscera and the head possibly induce the psychological response of discomfort, as well as physiological responses such as changes in perspiration and respiration.

Understanding mechanical responses of the human body to vibration should contribute to avoid spinal injuries and reduce activity interference. It will also help understanding comfort. Many workers have investigated the mechanical responses of the body, considering an analogy with mechanical structures. However, the complexity of the human body has impeded a large progress in this area. This research was conducted so as to model the mechanical responses of the human body to vibration and widen the understandings of the responses.

This thesis is divided into six chapters. Following this chapter, chapter 2 is literature review in which literature on measurement and modelling of mechanical responses to whole-body vibration is reviewed so as to summarise current information. Chapter 3 describes models which are developed, comparing their responses with experimental data reported in the literature. Chapter 4 contains experimental work which is conducted so as to determine the mode shapes of whole-body vibration and also includes some other supplementary experiments. In chapter 5, a final model is developed, comparing the natural frequencies and the vibration mode shapes of the model with the measurements. Chapter 6 describes the general conclusions and recommendations.

CHAPTER 2

LITERATURE REVIEW

2.1 INTRODUCTION

Various mechanical responses to whole-body vibration have been measured by many workers so as to investigate the effects of vibration on health, activities, and comfort. A number of precious findings have been obtained through experimental investigations. However, because the human body is a uncertain structure with large variability between subjects as well as within a subject, the experimental findings are not always consistent. Biodynamic models have been developed so as to interpret the measured responses with a physical and theoretical understanding, and also to predict responses which are not easy to measure such as spinal stress. However, because of the complexity of the human body, many different models have been proposed, depending on the type and degree of idealisation of the body structure as well as the purpose of use.

The literature review begins with the anatomical basis to help understanding of the following sections, then it is divided into three main sections, which are measurement of mechanical responses to whole-body vibration, modelling mechanical responses to whole-body vibration, and conclusions.

2.2 ANATOMICAL BASIS (extracted from Tortora and Anagnostakos, 1990, and Oliver and Middleditch, 1991)

2.2.1 Vibration axes and planes of the body

International Standard 2631 (1985) defines an orthogonal coordinate system for directions of whole-body vibration as x-axis for the fore-and-aft, y-axis for the lateral and z-axis for the vertical direction as shown in Figure 2.1. The origin of the coordinate system is defined at the heart by the standard. This research adopts the orthogonal coordinate system whose directions are the same as those in International Standard. However, the location of the origin is defined in each case for convenience of measurement and modelling.

The anatomical directional terms are also sometimes used to avoid confusion. The terms,

superior, inferior, anterior, posterior and medial are defined as the directions towards the head, the feet, the front of the body, the back of the body and the midline of the body respectively in the anatomical position in which a subject is standing erect, facing the observer (Figure 2.1). The structural planes of the human body are also defined anatomically. A sagittal plane is a vertical plane which divides the body into right and left sides. A mid-sagittal plane is a sagittal plane which passes through the midline of the body and divides the body into equal right and left sides. A frontal plane is a vertical plane orthogonal to the sagittal plane which divides the body into anterior and posterior portions. A horizontal plane is a plane in parallel to the ground which divides the body into superior and inferior portions.

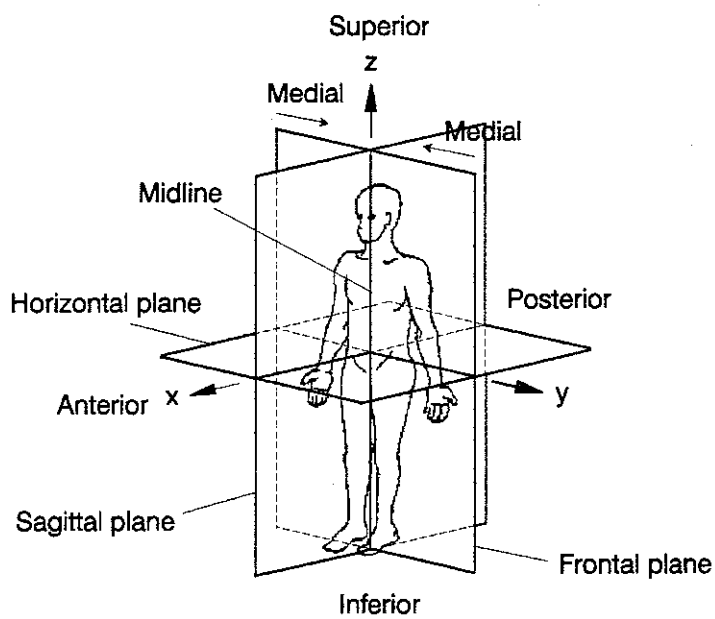

Figure 2.1 Coordinate system for whole-body vibration and anatomical terms for directions and planes.

2.2.2 Structure of whole skeletal system

The adult human skeleton usually consists of 206 named bones (Figure 2.2) grouped into two principal divisions: the axial skeleton and the appendicular skeleton. The axial division of the skeleton contains the bones which lie around the longitudinal axis of the body such as the skull, vertebral column and the ribs. The appendicular division contains the bones of the upper and lower extremities (limbs) and the shoulder and pelvic girdles which connect the extremities to the axial skeleton.

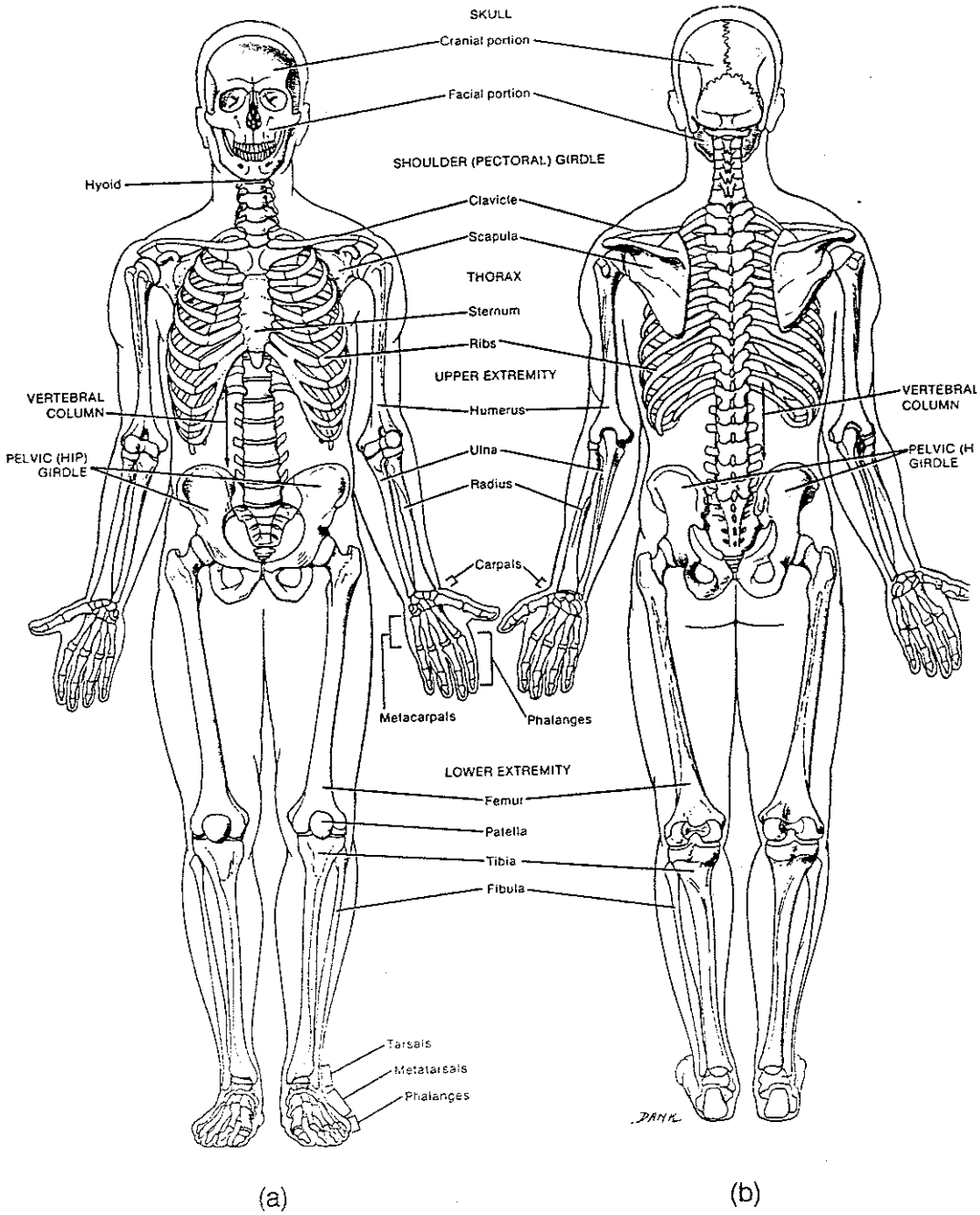

Figure 2.2 Whole skeletal system: (a) anterior view; (b) posterior view (from Tortora and Anagnostakos, 1990).

2.2.3 Structure of vertebral column

The vertebral column (spine), together with the sternum and ribs, constitutes the skeleton of the trunk of the body. The adult vertebral column consists of 24 separate vertebrae (i.e. 7 cervical vertebrae, 12 thoracic vertebrae and 5 lumbar vertebrae) with five fused vertebrae which form the sacrum, and usually four fused vertebrae which form the coccyx

(Figure 2.3). When viewed from the side, the vertebral column displays five curves in the upright posture: two cervical curves from the occiput to the axis (the second cervical vertebra) (concave forwards) and from the axis to the second thoracic vertebra (convex forwards), one thoracic curve (concave forwards) and one lumbar curve (convex forwards). The vertebral column has principal functions of supporting the human body in the upright posture, allowing movement and also protecting the spinal cord.

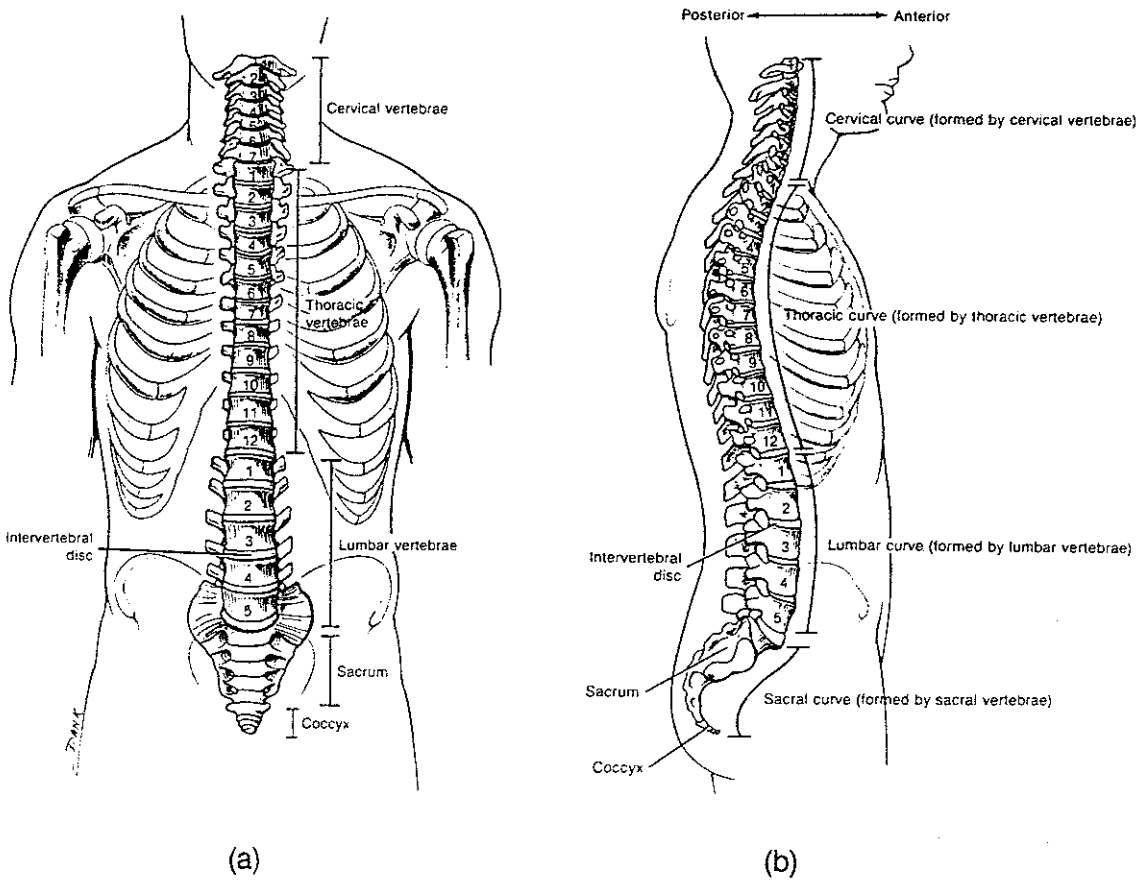

Figure 2.3 Vertebral column: (a) anterior view; (b) right lateral view (from Tortora and Anagnostakos, 1990).

2.2.4. Structure of each vertebra

Typical vertebral structure

Although there are variations in size, shape and detail in the vertebrae in different regions of the column, all the vertebrae are basically similar in structure (Figure 2.4). A typical vertebra consists of the vertebral body, vertebral arch and processes. The vertebral body

is a bony, thick, disc-shaped anterior portion which is the weight-bearing part of a vertebra. Its superior and inferior surfaces are roughened for the attachment of intervertebral discs. The vertebral arch extends posteriorly from the body. It is formed by two short and thick processes which are the pedicles and the laminae. The space between the vertebral arch and the body is named vertebral foramen and contains the spinal cord. The vertebral foramina of all the vertebrae together form the vertebral (spinal) canal. Seven processes arise from the vertebral arch. A transverse process extends laterally on each side. A single spinous process projects posteriorly and inferiorly from the junction of the laminae. These three processes serve points of attachment for the connective ligaments. The remaining four processes form joints with other vertebrae. The two superior articular processes articulate with the vertebra next superior to them. The two inferior articular processes articulate with the vertebra next inferior to them. The articulating surfaces of the articular processes are referred to as facets.

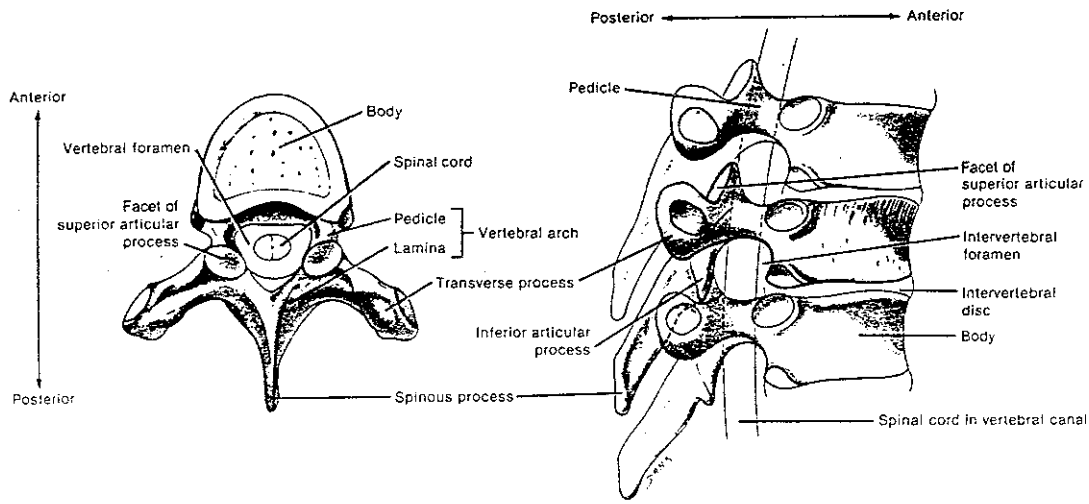

Figure 2.4 Typical vertebra: (a) superior view; (b) right lateral view (from Tortora and Anagnostakos, 1990).

Cervical vertebrae

The bodies of the cervical vertebrae are smaller than those of the thoracic vertebrae. However, the vertebral arches are larger. The first two cervical vertebrae differ considerably from the others. The first cervical vertebra is named atlas and supports the head. The atlas is a ring bone lacking in the body and the spinous process. The superior surface is named superior articular facets and articulates with the occipital bone of the skull. This articulation permits nodding of the head. The inferior surface is named inferior

articular facets and articulates with the second cervical vertebra. The second cervical vertebra is named axis which has the body. A peglike process called dens projects superiorly through the ring of the atlas. The dens makes a pivot on which the atlas and the head rotate. This articulation permits shaking of the head. The cervical vertebrae from the third to the seventh correspond to the structural pattern of the typical vertebra.

Thoracic vertebrae

The thoracic vertebrae are larger and stronger than the cervical vertebrae. The spinous processes are longer and directed inferiorly. The thoracic vertebrae also have longer and heavier transverse processes than the cervical vertebrae. Except for the eleventh and the twelfth thoracic vertebrae, the transverse processes have facets for articulating with the tubercles of the ribs, and the bodies have whole facets or half facets for articulating with the heads of the ribs.

Lumbar vertebrae

The lumbar vertebrae are the largest and the strongest column. Their various projections are shorter and thicker. The superior articular processes are directed medially instead of superiorly and the inferior articular processes are directed laterally instead of inferiorly. The spinous processes are thick and broad and project almost straight posteriorly.

Sacrum and coccyx

The sacrum is a triangular bone formed by union of five fused sacral vertebrae. The sacrum serves a strong foundation for the pelvic girdle. It is located at the posterior portion of the pelvic cavity between the two coxal (hip) bones. The coccyx is also triangular in shape and is formed by fusion of coccygeal vertebrae, usually the last four. The coccyx articulates superiorly with the sacrum.

2.2.5 Vertebral joints

Intervertebral disc

Adjacent vertebral bodies from the second cervical to the sacrum are linked by fibrocartilaginous intervertebral discs. Each disc consists of an outer fibrous ring made of

fibrocartilage called the annulus fibrosus and an inner soft, pulpy, highly elastic structure called the nucleus pulposus (Figure 2.5). The cross-section of a disc is similar to an ellipse with the anterior-posterior axis being the minor axis. Disc hight varies in different parts of the same disc. In the cervical and the lumbar regions, the discs are wedge-shaped, being deeper anteriorly than posteriorly to form their lordotic curves. The lumbo-sacral disc shows the greatest wedging. In the thoracic region, the discs are of almost uniform thickness. The discs are thickest at the lumbar region to bear a greater proportion of the body weight, and thinnest in the upper thoracic region. The hight of the disc is an important factor controlling movement of the spinal column: thicker discs allow more movement. The ratios of the disc height to the vertebral body height are 2:5 in the most mobile cervical region, 1:3 in the second most mobile lumbar region and 1:5 in the least mobile thoracic region. The discs form strong joints permitting various movements of the vertebral column such as flexion (bending motion to increase the distance between adjacent spinous processes), extension (bending motion in the opposite direction to flexion), lateral flexion (sideway bending) and axial rotation (torsion). Deformation of the disc accompanies bulging as shown in Figure 2.5.

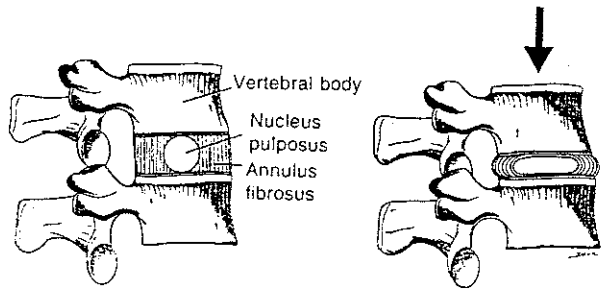

Figure 2.5 Intervertebral disc: (a) in normal state; (b) in compression (from Tortora and Anagnostakos, 1990).

Articular facets

The pair of the inferior articular facets of a vertebra forms plane joints with the pair of the superior articular facets of the next inferior vertebra. The articular cartilage lines the joint surfaces. In flexion-extension, lateral flexion and axial rotation, the facing articular facets slide each other in the direction determined by the facet orientation which determines the

direction of the relative motion of the adjacent vertebral bodies and sometimes the locking position of motion. In the cervical region, the articular facet joints bear some part of the weight of the head. However, in the thoracic and lumbar regions, they are not involved in weight bearing in the normal posture.

Connective ligaments

The typical group of main ligaments which connect adjacent vertebrae through the cervical and the thoraco-lumbar regions includes the anterior and posterior longitudinal ligaments, a pair of the capsular ligaments, a pair of the ligamenta flava, interspinous and supraspinous ligaments and a pair of the intertransverse ligaments (Figure 2.6). The anterior longitudinal ligament is a strong band lying attached anteriorly to the vertebral bodies and discs which works to prevent anterior separation of the vertebral bodies during flexion and to stabilise the lordosis. The posterior longitudinal ligament is lying posterior to the vertebral bodies and discs in the vertebral canal. Separation of the posterior ends of the vertebral bodies is restricted by this ligament. The capsular ligaments are attached to the margins of the articular facets. They are thin and loose, allowing freedom of sliding movement of the articular facets. Adjacent laminae are connected by the ligamenta flava which are short and thick ligaments fusing at the midline. These ligaments normally have a high proportion of elastic fibres, allowing separation of the laminae in flexion. They protect the discs by graduating the separation of the laminae so that an abrupt limit is not reached. They also assist the return movement from flexion to the natural position by their elasticity. The interspinous ligament connects adjacent spinous processes and they are continuous with the ligamenta flava anteriorly and the supraspinous ligament posteriorly. The supraspinous ligament connects adjacent spinous process tips. Both the interspinous and supraspinous ligaments resist separation of the spinous processes during flexion. However, they do not come into work until about half full flexion and they are slack at small angles of flexion. Adjacent transverse processes are connected by the intertransverse ligaments, which separate the anterior spinal muscles from the posterior spinal muscles.

In the cervical region, the anterior longitudinal ligament is attached to the occipital bone of the skull from which it extends inferiorly to the tubercle of the atlas and, then, it attaches to the front of the vertebral bodies. The posterior longitudinal ligament extends inferiorly from the body of the axis. The ligamentum nuchae is a membrane which is connected to the occipital bone and extends to all the cervical vertebrae. It is homologous with the

interspinous and supraspinous ligaments in the thoraco-lumbar region. The rest of the ligaments are the same as those in the typical connections.

In the thoracic region, all the ligament connections follow the typical pattern with a feature that the anterior longitudinal ligament and the ligamenta flava are the thickest in this region. In the lumbar region, the supraspinous ligament ends between the fourth and the fifth lumbar vertebrae. The iliolumbar ligaments connect the transverse processes of the fifth lumbar vertebra to the ilium. They include the anterior, posterior, superior, inferior and vertical iliolumbar ligaments which are powerful and complex, and provide stability at the lumbo-sacral junction, preventing the fifth lumbar vertebra from being displaced forwards. The rest of the ligaments are the same as those in the typical connections.

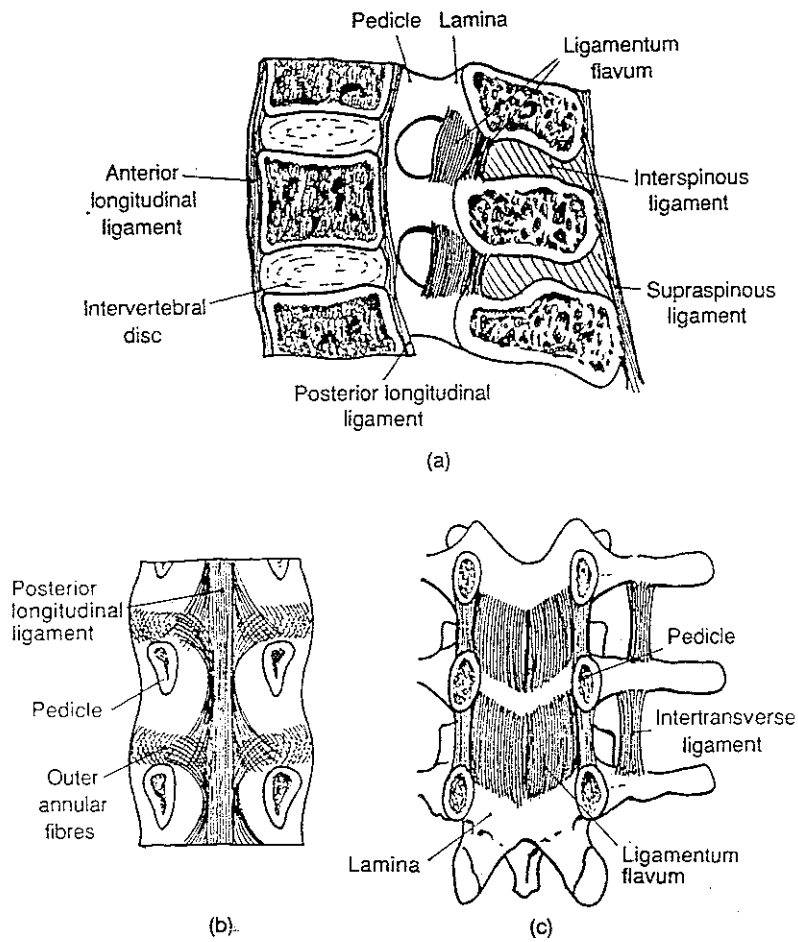

Figure 2.6 Connective ligaments (in lumbar region): (a) lateral view; (b) posterior longitudinal ligament; (c) anterior view of ligamenta flava (from Oliver and Middleditch, 1991).

2.2.6 Body cavities

Spaces within the body which contains internal organs are called body cavities. Various body cavities are separated by structures such as bones, muscles and ligaments (Figure 2.7). The dorsal body cavity is located near the posterior (dorsal) surface of the body. It is further subdivided into the cranial cavity and the vertebral (spinal) canal. The cranial cavity is a bony cavity formed by the cranial (skull) bones and contains the brain. The vertebral canal is also a bony cavity formed by the vertebrae and contains the spinal cord. The other principal body cavity is the ventral body cavity located on the anterior (ventral) aspect of the body. Its walls are composed of skin, connective tissue, bone, muscle and a membrane called the serous membrane. The organs inside the ventral body cavity are called the viscera. The ventral body cavity is divided into two subdivisions by the diaphragm. The upper portion is called the thoracic cavity and the lower portion is called the abdominopelvic cavity. The thoracic cavity contains several divisions. There are two pleural cavities, each surrounding the lung. The mediastinum is a broad, median partition between the lungs which extends from the sternum to the vertebral column. The mediastinum contains the heart, thymus gland, esophagus, trachea, bronchi, and many

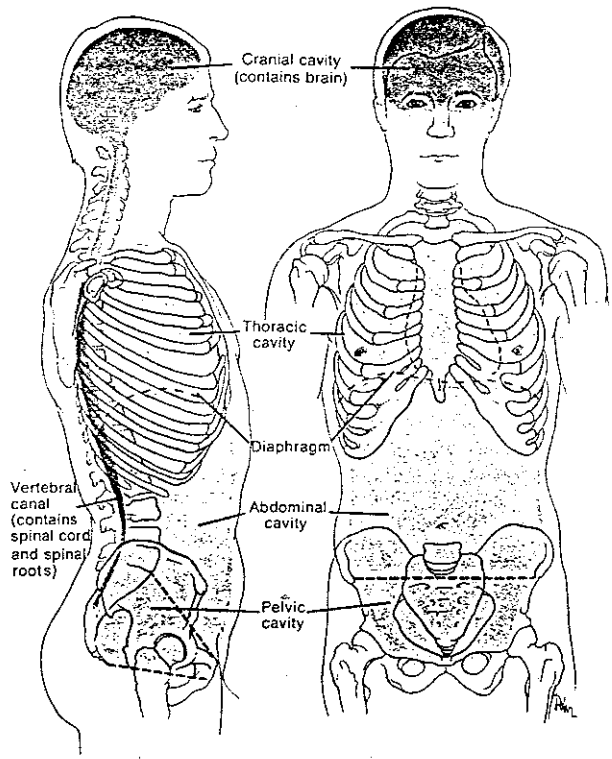

Figure 2.7 Body cavities: (a) right lateral view; (b) anterior view (from Tortora and Anagnostakos, 1990).

large blood and lymphatic vessels. The abdominopelvic cavity is divided into the upper abdominal cavity and the lower pelvic cavity although no wall separates them. The abdominal cavity contains the stomach, spleen, liver, gallbladder, pancreas, small intestine and most of the large intestine. The pelvic cavity includes the urinary bladder, cecum, appendix, sigmoid colon, rectum and internal male or female reproductive organs. The pelvic cavity is the region between the two imaginary planes. The top plane extends from the superior border of the sacrum to the upper margin of the symphysis pubis. The bottom plane extends from the end of the coccyx to the pelvic arch.

2.3 MEASUREMENT OF MECHANICAL RESPONSES TO WHOLE-BODY VIBRATION

2.3.1 Introduction

Mechanical responses of the human body to vibration have been measured at various parts of the body. Driving point responses, such as the driving point mechanical impedance and apparent mass, are widely measured responses. They are measured at the seat-buttocks interface while a subject is sitting on a seat mounted on a vibrator. The driving point responses are easy to measure and indicate the total response of the body. Another widely measured response is the acceleration transmissibility from the seat to the head. The transmissibility to the head is influenced by the vibration travelling from the bottom to the top through the body. Both the driving point responses and the transmissibility to the head are important because they are total responses at the lowest and highest ends of the body. Responses on other parts of the body, such as the spine and the viscera, have also been measured by some workers. However, difficulty of mounting transducers on the body has restricted the number of investigations and reliability of data.

It is a reasonable hypothesis, from an analogy to mechanical structures, that responses of the body vary depending on posture, muscle tension and body construction. Changing posture corresponds to changing the geometry of the body structure. Changing muscle tension corresponds to changing material properties. Different body constructions of different subjects possibly include both different geometry and different material properties. Responses of soft materials, such as rubber and foam, are known to reveal amplitude dependency. There will be such non-linearity of the body structure, if motion of soft tissue is dominant in responses.

This section summarises the theory concerning the transfer function, then reviews literature on measurements of the driving point mechanical impedance and apparent mass, transmissibility to the head, transmissibility to the spine, and other responses of the body. Some subsections concern factors affecting the responses. Only measurements on seated subjects exposed to vertical excitation will be reviewed.

2.3.2 Description and calculation of transfer functions

All the relationships between the input and the output of a system are termed transfer functions. Figure 2.8 shows a simple example of the input-output relationship of a system.

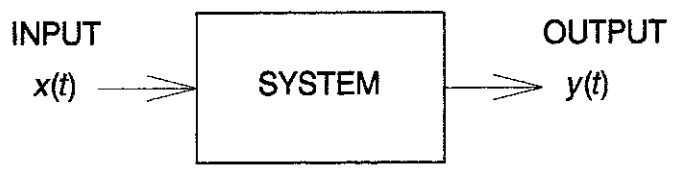

Figure 2.8 Input-output relationship

In vibration problems, the system is a structure and the input and the output may be force, acceleration, velocity, displacement and so on. The transfer function is defined as the ratio of the output to the input and usually described in the frequency domain. Transfer functions are mathematically complex and quite often described by the combination of modulus and phase. When excitation of the structure is sinusoidal, the modulus and phase can be directly obtained from the amplitude ratio and phase difference between the input and the output at each excitation frequency, by observing the signal waveforms acquired by transducers. This method of estimating transfer functions does not require computer based equipment and has been employed in many studies, although the estimated transfer functions are not very accurate. Modern computer technology and signal processing techniques have enabled the calculation of transfer functions to be obtained more quickly and more accurately, with random excitation. The input and the output are transferred into the frequency domain using a Fourier transform, then the ratio is calculated. A mathematical description of the transfer function of the system shown in Figure 2.8 is:

$$H(f) = \frac{Y(f)}{X(f)} \qquad \textbf{(2.1)}$$

where: f is the frequency; $H(f)$ is the transfer function; $X(f)$ is the Fourier transform of the input $x(t)$; $Y(f)$ is the Fourier transform of the output $y(t)$. In practice, signals acquired by transducers always contain some noise which reduces the accuracy of transfer functions calculated directly by equation (2.1). Therefore, the cross power spectrum and the auto power spectrum of the input and the output, including appropriate filtering in the measurement and averaging procedure, are often used to calculate the transfer function so as to minimise the effect of noise:

$$H(f) = \frac{G_{yy}(f)}{G_{yx}(f)} \tag{2.2}$$

$$H(f) = \frac{G_{xy}(f)}{G_{xx}(f)} \tag{2.3}$$

where: $G_{xx}(f)$ and $G_{yy}(f)$ are the auto power spectra of the input and the output; $G_{xy}(f)$ is the cross power spectrum from the input to the output; $G_{yx}(f)$ is the cross power spectrum from the output to the input. When the input contains noise, equation (2.2) is more appropriate, and when the output contains noise, equation (2.3) is more appropriate to minimise the effect of noise on the transfer function. In measurements of whole-body vibration, the input is usually measured on a vibrator or on a seat mounted on a vibrator, and the output is measured on the body. Therefore, equation (2.3) is more appropriate. This method of estimating transfer functions has been used in recent studies.

Another function often estimated with the transfer function is the coherence function. The coherence function is a frequency function which takes a value between 0 and 1. The coherency reflects the contribution of the input to the output. When the coherency is low, the contribution is low, and when the coherency equals to 0, there is no correlation between the input and the output. When the coherency is high, the contribution is high, and when the coherency equals to 1, the output is caused only by the input measured. Factors which reduce coherency are the presence of other inputs, noise and non-linearity of the structure. The coherence function, $\gamma^2(f)$, is calculated by equation (2.4):

$$\gamma^2(f) = \frac{|G_{xy}(f)|^2}{G_{xx}(f)G_{yy}(f)} \tag{2.4}$$

2.3.3 Driving point mechanical impedance and apparent mass

The mechanical impedance and the apparent mass are the most widely measured driving point responses for whole-body vibration. The mechanical impedance and the apparent mass are transfer functions, defined as the ratio of the force to the velocity and the ratio of the force to the acceleration, respectively. When the excitation point and the response point are different, they are termed transfer mechanical impedance and the transfer apparent mass. When the response point is the same as the excitation point, they are termed driving point mechanical impedance and the driving point apparent mass. The driving point (excitation point) of whole-body vibration is the buttocks when a subject is sitting on a seat. When measuring the driving point responses of a seated subject, the subject sits on a seat mounted on a vibrator. Excitation and measurement are usually all in the vertical direction. The excitation velocity or acceleration is measured on the seat. Velocity is sometimes integrated from acceleration measured by an accelerometer. The response force is measured by a force transducer placed between the seat and the buttocks of the subject. Mathematical descriptions of the driving point impedance and the apparent mass are obtained by replacing the output by force and the input by velocity or acceleration in equation (2.1):

$$Z(f) = \frac{F(f)}{V(f)} \tag{2.5}$$

$$M(f) = \frac{F(f)}{A(f)} \tag{2.6}$$

where: f is the frequency; $Z(f)$ is the driving point impedance; $M(f)$ is the driving point apparent mass; $F(f)$ is the Fourier transform of the response force measured beneath the buttocks; $V(f)$ is the Fourier transform of the excitation velocity measured on the seat; $A(f)$ is the Fourier transform of the excitation acceleration measured on the seat. In practice, equation (2.3) is used in estimation of the driving point impedance and the apparent mass so as to minimise the effect of noise. The impedance and the apparent mass have a relationship shown in equation (2.7) and they are easily transferred between each other.

$$M(f) = \frac{Z(f)}{i\omega} \tag{2.7}$$

where: $i^2=-1$; ω is the angular frequency ($\omega=2\pi f$).

Another consideration which should be taken into account when measuring the driving point responses is the effect of the mass of a force transducer. Some part of a force

transducer is excited and its inertial force affects the measured driving point responses. The effective mass of a force transducer can be measured by exciting the force transducer alone or with a known mass placed on it. The modulus of the apparent mass of a rigid mass is constant through all frequencies and corresponds to the static mass. Therefore, the modulus of the apparent mass of the force transducer alone indicates its effective mass. When a known mass is excited on the force transducer, the modulus of the apparent mass corresponds to the summation of the known mass and the effective mass of the force transducer. With the effective mass of the force transducer known, the true force is obtained by subtracting the inertial force of the effective mass of the force transducer from the measured force, using equation (2.8):

$$f(t) = f_m(t) - m_e\ddot{x}(t) \qquad \textbf{(2.8)}$$

where: $f(t)$ is the true response force; $f_m(t)$ is the measured force; m_e is the effective mass of the force transducer; $\ddot{x}(t)$ is the excitation acceleration. The alternative method is to subtract the impedance or apparent mass of the effective mass from the measured impedance or apparent mass in the frequency domain, using equation (2.9) or (2.10):

$$Z(f) = Z_m(f) - im_e\omega \qquad \textbf{(2.9)}$$

$$M(f) = M_m(f) - m_e \qquad \textbf{(2.10)}$$

where: $Z(f)$ and $M(f)$ are the true impedance and the apparent mass; $Z_m(f)$ and $M_m(f)$ are the measured impedance and apparent mass.

The driving point responses are easy to measure and indicate the total responses of the body. A substantial amount of research has been conducted on the measurement of the driving point responses of the human body. This section is divided into five subsections according to factors which might affect the driving point responses: effect of posture, effect of muscle tension, effect of constraint, inter-subject variability, and non-linearity.

2.3.3.1 Effect of posture

The effect of posture on the driving point responses have been investigated by several workers. Coermann (1962) investigated the effect of posture on the driving point impedance. A subject was exposed to vertical discrete sinusoidal vibration in the frequency range from 1 to 20 Hz with a magnitude of 0.1 g, in erect and relaxed postures. The first resonance frequency at about 5 Hz in the relaxed posture was shifted to about 6 Hz by the erect posture. The erect posture also increased the modulus of the

impedance above the first resonance: the modulus increased from $5x10^3$ to $6.8x10^3$ Ns/m at the first resonance. The effect of posture on a second resonance at about 11 Hz was not clear. The authors also measured the mean impedance of eight subjects in the erect posture. The modulus of the mean impedance is shown in Figure 2.9.

Miwa (1975) used vertical sinusoidal swept excitation with a magnitude of 0.1 g to measure the driving point impedance. He compared the driving point impedances of a subject in erect and relaxed postures. Changing posture affected neither the first resonance at about 7 Hz nor the second resonance at about 12 Hz. He also measured the impedances of eight subjects whose mean modulus is shown in Figure 2.9.

Fairley and Griffin (1989) compared the apparent masses of subjects in several postures. Vertical random vibration with a magnitude of 1.0 m/s^2 r.m.s. was used to excite eight subjects. The subjects adopted erect and normal postures. The first resonance frequency located between 4 and 5 Hz in the normal posture was increased by the erect posture in some subjects. The largest resonance shift was about 2.2 Hz. However, there were also other subjects who did not show any effect of the change of posture. The effect on the second resonance located around 10 Hz was not clear. Further investigation was conducted using one of the subjects. The subject adopted five different postures, slouched, normal, slightly erect, erect and very erect postures. In this study, a clear trend for the resonance frequency to shift from the slouched posture to the very erect posture was observed. The largest shift between the two extreme postures was about 1.5 Hz. The authors also measured the mean apparent masses of 60 subjects. The modulus of the mean normalised apparent mass is shown in Figure 2.10 (normalised apparent mass will be defined below).

2.3.3.2 Effect of muscle tension

The effect of muscle tension on the apparent mass was also investigated by Fairley and Griffin (1989). The same eight subjects were told to tense their muscles in the normal posture during the vibration exposure. Tensing muscles increased the first resonance frequency in some subjects. The largest resonance shift was about 3.5 Hz. Both the amount of the resonance shift and the number of subjects who showed the resonance shift were larger than those affected by the change of posture.

2.3.3.3 Effect of constraint

There are a few investigations in which some constraints were applied to some parts of the body so as to estimate the contributions of the body parts to the driving point responses. Coermann (1962) also investigated the effects of two types of body constraint on the driving point impedance. Firstly, a subject wore a semi-rigid envelope around the pelvis and the abdomen. The envelope covered the body from the symphysis-coccyx line to the level of the diaphragm and it was tight enough to impede the subject's breathing and venous blood flow slightly. The envelope decreased the modulus of the impedance at the first resonance both in the erect and relaxed postures: the modulus decreased from 4.5 to 3.5 in the erect posture and from 4.0 to 3.0 in the relaxed posture. The effect on the first resonance frequency located between 4 and 5 Hz was not clear. The envelope also appeared to have emphasized the second resonance peak found between 9 and 10 Hz. Secondly, the subject wore a pressure suit which constrained the whole body by air pressure tubes along the arms, back and legs and also by a bladder in front of the suit pressurising the abdominal wall and the lower part of the chest. The pressure suit increased the first resonance frequency as well as the modulus of the impedance at the first resonance both in the erect and relaxed postures: the first resonance frequency increased from 4.0 to 5.5 Hz in the erect posture and from 3.5 to 5.5 Hz in the relaxed posture; the modulus of the impedance at the first resonance increased from 4.5 to 6.0 in the erect posture and from 2.5 to 5.0 in the relaxed posture. The pressure suit also appeared to have emphasized the second resonance peak located around 10 Hz.

Sandover (1978) investigated the effects of two types of constraint on the apparent mass. Firstly, a subject sat on two wooden blocks with 2.5 cm dimension which were placed beneath the ischial tuberosities. Secondly, the subject wore a visceral support which was made of 4 cm wide webbing belt. He exposed the subject to vertical random vibration with a magnitude of 2 m/s^2 r.m.s.. The wooden blocks increased the first resonance frequency from 4 to 5 Hz and decreased the modulus of the normalised apparent mass (see below) at the first resonance from 1.6 to 1.4. The visceral support did not affect the first resonance but created a second resonance at about 8 Hz.

2.3.3.4 Inter-subject variability

Variability between subjects, inter-subject variability, can be explained partly by different postures and different muscle tension mentioned above. Another effect of anthropometric

parameters on the impedance was investigated by Donati and Bonthoux (1983). They exposed 15 subjects to vertical swept sinusoidal and vertical random vibration in the frequency range between 1 and 10 Hz with a magnitude of 1.6 m/s^2 r.m.s.. They found a significant positive correlation between the body weights of the subjects and the moduli of the impedance in the frequency range from 1.5 to 4 Hz.

Fairley and Griffin (1989) found that considerable inter-subject variability was accounted for by different static body weights on the force transducer. They proposed normalising the apparent mass by dividing it by the static weight on the force transducer. The normalised apparent mass reduced variability remarkably even between men, women and children. They also calculated correlation coefficients between various anthropometric parameters of 60 people and the first major resonance frequencies at about 5 Hz, the moduli of the normalised apparent mass at the first resonance and the moduli of the normalised apparent mass at 10 Hz (around the second resonance). The static weights on the force transducer divided by sitting heights had the most significant negative correlation with the first resonance frequencies. However, the moduli of the normalised apparent mass at the first resonance had the most significant positive correlation with the total body weights. The moduli of the normalised apparent mass at 10 Hz did not have significant correlation with any anthropometric parameter.

2.3.3.5 Non-linearity

There are various kinds of non-linearities in the responses of a structure to vibration. Excitation magnitude dependency is the most important non-linearity when application of laboratory data to various practical situations is considered. Some workers have investigated the non-linearity of the driving point responses. Wittmann and Phillips (1969) used a vertical drop tower to measure the transient driving point impedance. Four subjects participated in the experiment. Two types of vertical impacts with peak acceleration magnitudes of 6-7 g and 12-14 g were compared. The effect of acceleration profile was also investigated, using impacts with a 55 msec duration and a 120 msec duration. The obtained impedances showed differences between the four conditions. The authors also exposed a subject to sinusoidal acceleration so as to investigate the waveforms of the response force. They found that the positive phase of the force had a larger peak level and a shorter duration than the negative phase.

Miwa (1975) compared the driving point impedances of a kneeling subject exposed to

vertical vibration with two excitation magnitudes of 0.1 and 0.3 g. The higher magnitude shifted the first resonance frequency from about 5 Hz to about 4.5 Hz.

Sandover (1978) also investigated the non-linearity in the driving point apparent mass. He exposed two subjects to vertical random vibration with two different magnitudes of 1 and 2 m/s^2 r.m.s. and two different frequency spectra with -3 and +3 dB/octave slopes (i.e. the -3 dB/octave spectrum had more energy at lower frequencies and the +3 dB/oct spectrum had more energy at higher frequencies). The author concluded from the results that the effects of the non-linearities were small, although the largest resonance shift was from about 4.8 Hz with 1 m/s^2 magnitude and +3 dB/octave slope to 4.2 Hz with 2 m/s^2 magnitude and -3 dB/octave slope. The modulus of the apparent mass measured with 2 m/s^2 magnitude and -3 dB/octave slope was normalised as proposed by Fairley and Griffin, which is shown in Figure 2.10.

Donati and Bonthoux (1983) compared the driving point impedances in response to vertical swept sinusoidal and random vibration. The magnitude was 1.6 m/s^2 r.m.s. and the frequency range was from 1 to 10 Hz for both excitation. A total of 15 subjects was used. The result showed that the random excitation produced smaller modulus of the impedance below 5 Hz and larger modulus above 5 Hz, although the first resonance frequency at about 4 Hz did not shift: the moduli were $1.8x10^3$ and $1.9x10^3$ Ns/m at the first resonance and at 8 Hz with the random excitation, whereas they were $2.0x10^3$ and $1.8x10^3$ Ns/m with the sinusoidal excitation. The second resonance found at about 8 Hz with the random excitation was not clear with the sinusoidal excitation. The modulus of the mean impedance with the random excitation is shown in Figure 2.9.

Hinz and Seidel (1987) compared the apparent masses with two different excitation magnitudes of 1.5 and 3.0 m/s^2 r.m.s.. They used vertical discrete sinusoidal vibration in the frequency range from 2 to 12 Hz to excite four subjects. It was found that the first resonance frequency at about 4 Hz with the larger magnitude was increased to 4.5 Hz by the smaller magnitude. The authors also compared the apparent mass calculated from the r.m.s. values of the input and the output signals and the apparent masses calculated from the maximum values and the minimum values of the two signals. The apparent masses calculated by the three different methods resulted in three different values in the frequency range up to 5.5 Hz, due to the wave deformation of the output. The mean apparent mass calculated by the r.m.s. values with the magnitude of 1.5 m/s^2 r.m.s. was normalised as proposed by Fairley and Griffin, which is shown in Figure 2.10.

Fairley and Griffin (1989) exposed eight subjects to vertical random vibration with four different magnitudes of 0.25, 0.5, 1.0, 2.0 m/s^2 r.m.s.. All the eight subjects showed a significant effect of the magnitude on the resonance frequencies, in contrast to the effects of posture and muscle tension which were largely dependent on the subject. They found that doubling the magnitude generally reduced the resonance frequency more at the lower magnitudes. The mean first resonance frequency decreased from 6 to 4 Hz when the magnitude was increased from 0.25 to 2.0 m/s^2 r.m.s. (i.e. a factor of eight.). The second resonance frequency at about 10 Hz also appeared to have decreased with the increment of the magnitude.

A different type of non-linearity was found by Vogt *et al.* (1968). The authors measured the driving point impedances under static accelerations. A vibrator was mounted on a centrifuge which produced static accelerations along the spine of a subject sitting on the vibrator. A total of ten subjects were exposed to vertical discrete sinusoidal vibration with a magnitude of 0.5 g under the normal gravity, 2 g and 3 g static accelerations. The static accelerations shifted the first resonance frequency of the impedance from 5 Hz with the normal gravity to 7 Hz with 2 g and from 5 Hz to 8 Hz with 3 g respectively. The modulus of the mean impedance with the normal gravity is shown in Figure 2.9. The authors

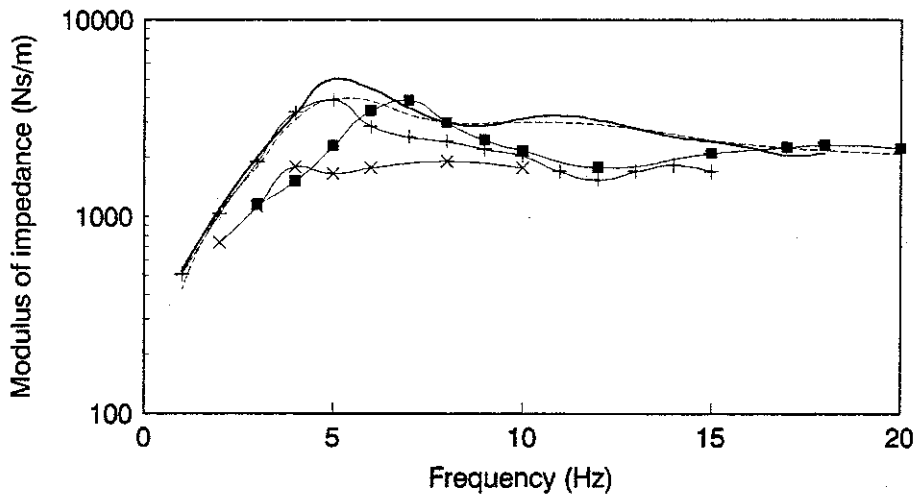

Figure 2.9 Moduli of the impedance: mean values of 8 subjects by Coermann *et al.* (——); mean values of 8 subjects by Miwa (—▪—); mean values of 10 subjects by Vogt *et al.* (—+—); mean values of 15 subjects by Donati and Bonthoux (—x—); International Standard 5982 (- - - -).

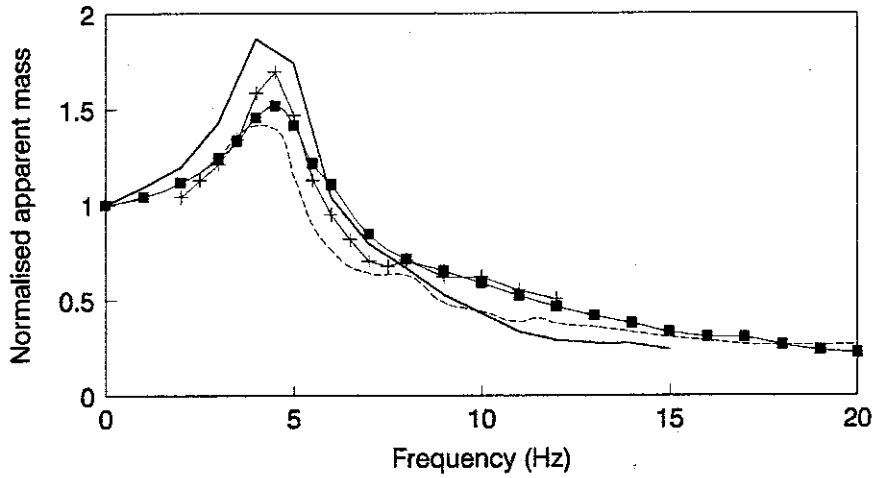

Figure 2.10 Normalised apparent masses: mean values of 10 subjects by Vogt *et al.* (——); mean values of two subjects by Sandover (- - - -); mean values of four subjects by Hinz and Seidel (—+—); mean values of 60 subjects by Fairley and Griffin (—■—).

also calculated the transmission factor which was defined as the ratio of the modulus of the impedance to the $m\omega$-value, where m is the static mass and ω is the angular frequency. The transmission factor is equivalent to the normalised apparent mass proposed by Fairley and Griffin (see above) which is shown in Figure 2.10.

2.3.4 Transmissibility to the head

The acceleration transmissibility from the seat to the head has been measured by many workers. The transmissibility is the modulus part of the transfer function which indicates attenuation or amplification of the excitation vibration through a structure. When measuring the transmissibility to the head of a seated subject, the subject sits on a seat mounted on a vibrator. The excitation acceleration is measured on the seat. The response acceleration is measured by an accelerometer attached on top of the head or bitten by the subject. The majority of research has been conducted with vertical excitation of subjects. A mathematical description of the acceleration transfer function from the seat to the head is obtained by replacing the output by acceleration of the head and the input by acceleration of the seat in equation (2.1):

$$T(f) = \frac{A_h(f)}{A_s(f)} \qquad \textbf{(2.11)}$$

where: $T(f)$ is the transfer function from the seat to the head; $A_h(f)$ is the Fourier transform of the acceleration measured at the head; $A_s(f)$ is the Fourier transform of the acceleration of the seat. The transmissibility, $|T(f)|$, is given by equation (2.12):

$$|T(f)| = \left|\frac{A_h(f)}{A_s(f)}\right| \qquad \textbf{(2.12)}$$

In practice, equation (2.3) is used to minimise the effect of noise.

The analogy of the human body to a mechanical structure may represent the head by a mass on a spinal beam which deforms in all the six directions. Therefore, vertical excitation of a subject induces motion of the head in the six axes due to the spinal deformation. The mass centre of the head has an anterior eccentricity from the cervical spine (Williams and Belytschko, 1981) so the flexible cervical spine and the atlanto-occipital joint allow a large pitching motion of the head. A few workers have measured multi-axis motion of the head. Paddan and Griffin (1988,1993) measured the head motion in all the six axes, using a bite-bar equipped with six accelerometers. A total of 12 sitting subjects were exposed to vertical random vibration in the frequency range from 0.2 to 31.5 Hz with a magnitude of 1.75 m/s^2 r.m.s.. The median and inter-quartile transmissibilities from vertical seat motion to motion of the head in the six axes are shown in Figure 2.11.

The transmissibility from the seat to the head is easy to measure and contains all information on vibration travelling from the bottom to the top through the body. This section is divided into four sections according to factors which might affect the transmissibility: effect of posture, effect of muscle tension, inter-subject variability, and non-linearity.

2.3.4.1 Effect of posture

Coermann (1962) investigated the effect of posture on the transmissibility from vertical seat motion to vertical head motion. A subject was exposed to vertical discrete sinusoidal vibration in the frequency range from 1 to 20 Hz with a magnitude of 0.1 g, adopting erect and relaxed postures. Vertical motion of the head was measured by an accelerometer mounted on top of the head using an elastic bandage. The erect posture increased the first resonance frequency at about 4.6 Hz in the relaxed posture to about 5.2 Hz and produced another resonance at about 3.2 Hz. The second resonance like peak in the relaxed posture at about 10 Hz also increased to 11 Hz by the erect posture. The fourth resonance appeared at about 15 Hz in the erect posture, whereas it was not seen in

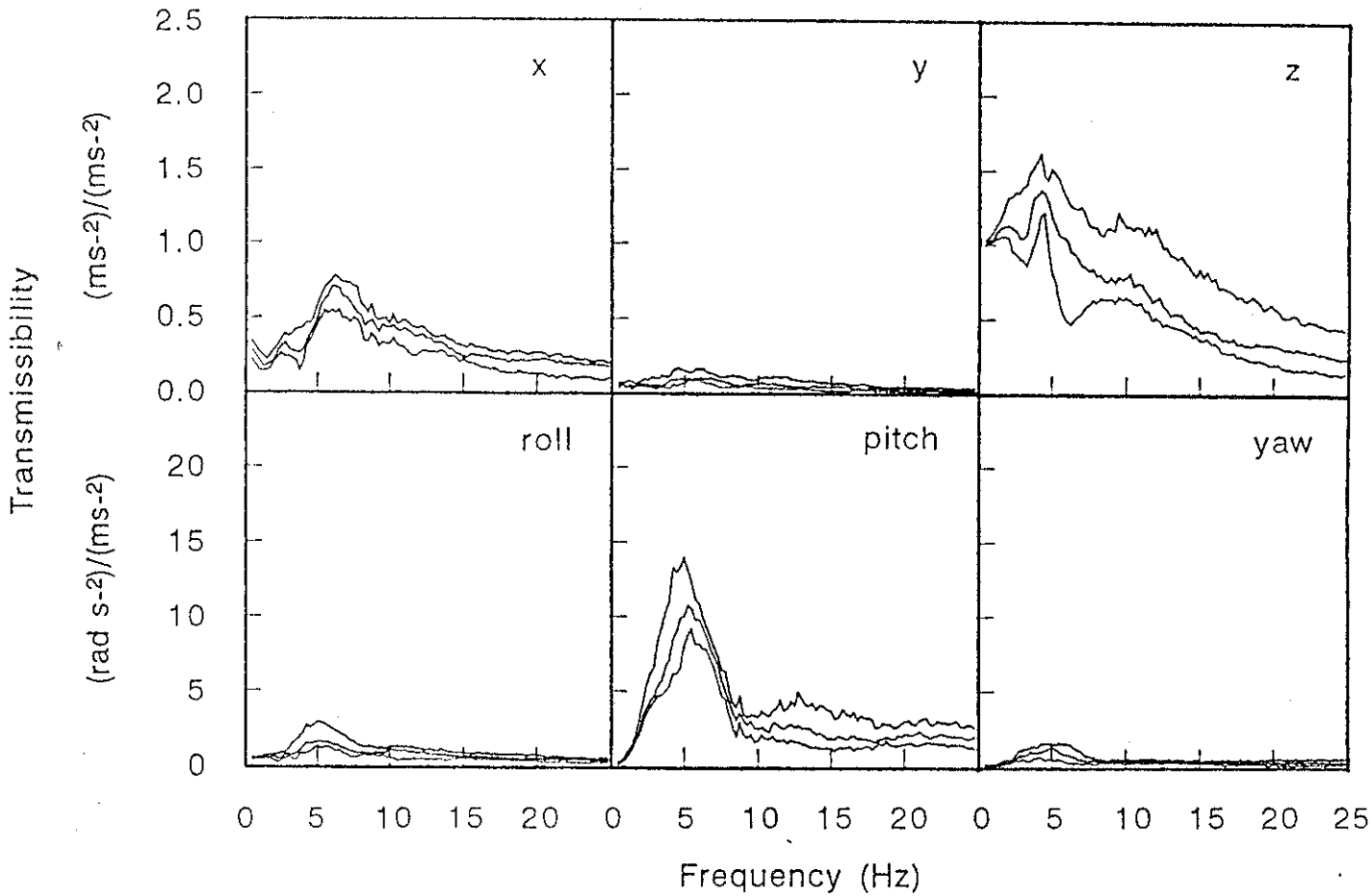

Figure 2.11 Transmissibilities from vertical seat acceleration to head acceleration in six axes (median and inter-quartile values of 12 subjects) by Paddan and Griffin (1993).

the relaxed posture. The erect posture also decreased the transmissibility below about 5.2 Hz but increased the transmissibility above 5.2 Hz: the erect posture decreased the transmissibility from 2.2 to 1.7 at the resonance around 5 Hz and increased the transmissibility from 0.5 to 1.1 at the resonance around 10 Hz. The transmissibility in the relaxed posture is shown in Figure 2.12.

Griffin (1975) exposed 12 subjects to vertical discrete sinusoidal vibration in the frequency range from 7 to 75 Hz with six magnitudes from 0.2 to 4.0 m/s^2 r.m.s.. Each subject adopted the most severe posture and the least severe posture in the sitting position. A bite-bar was used to measure acceleration at the head in the vertical, fore-and-aft, lateral and pitch directions. The transmissibilities from the seat to the head were calculated and compared between the two postures. It was found that the vertical transmissibility in the most severe posture was reduced by the least severe posture at all the frequencies measured. The largest reduction ratio was about 6:1 in the frequency range from 35 to 50 Hz. The transmissibility to the lateral head motion also showed the same trend as that observed in the vertical transmissibility, although the effect of posture appeared small in the transmissibility to the fore-and-aft and pitching motion of the head.

The transmissibilities in three different postures of 'normal upright', 'relaxed' and 'stiff' were compared by Griffin *et al.* (1978). A group of 18 men and a group of 12 boys were exposed to vertical discrete sinusoidal vibration in the frequency range from 1 to 100 Hz. The vertical acceleration at the head was measured using a bite-bar. The results from both groups showed that below about 5 Hz a relaxed posture produced the highest transmissibility and the stiff posture produced the lowest transmissibility, whereas above 5 Hz the trend was reversed: the largest differences of the transmissibilities for men were between 1.5 and 1.2 at 2.5 Hz and between 0.9 and 0.5 at 15 Hz. Further investigation was conducted, using one of the subjects. The subject changed the posture from a slouched posture to an erect posture in seven steps. The result showed the same trend as that found in the initial three postures. The effect of posture on the resonance frequency, which was observed in the driving point responses, was not clear in this study. The mean transmissibility of 18 men measured in the normal upright posture is shown in Figure 2.12.

Pope *et al.* (1987) developed an impact excitation method for whole-body vibration so as to save experimental time. Subjects sat on a platform suspended by rubber springs. The platform had a natural frequency at 1.8 Hz which was below the frequency range of

interest. A vertical impact excitation was given to the lower side of the platform by an impact pendulum. They measured the acceleration transmissibility from the platform to the head of 10 subjects in erect and relaxed postures, using a bite-bar. The transmissibility in the relaxed posture was decreased by the erect posture below 4 Hz, whereas the trend was reversed above 4 Hz: the largest differences were between 1.6 and 1.1 at 3 Hz and between 1.8 and 0.5 at 7 Hz.

Messenger (1987) investigated the effect of pelvic angle on the transmissibility to the head. A total of eight subjects was exposed to vertical random vibration in the frequency range from 0.5 to 40 Hz with a magnitude of 1 m/s^2 r.m.s.. The subjects adopted a normal posture and three additional postures which were defined by three different pelvic angles. The pelvic angle was measured by a goniometer. The pivot of the goniometer was placed at the head of the right great trochanter with one arm oriented along the femur and the other arm oriented towards the highest point on the right side of the iliac crest. The pelvic angle was controlled at 105, 95 and 85 degrees. The normal posture resulted in the posture between the pelvic angles of 105 and 95 degrees. Acceleration was measured at the head using a bite-bar in the vertical, fore-and-aft, lateral and the pitch directions. The transmissibilities from vertical seat motion to head motion in the four directions were calculated.

The largest effect of posture was found in the transmissibility to the vertical motion of the head. Decreasing the pelvic angle decreased the transmissibility below 4 Hz, whereas it increased the transmissibility above 6 Hz: the differences in the two extreme postures were between 1.2 and 1.5 at the first resonance around 2 Hz and between 0.9 and 1.5 at the third resonance around 12 Hz. Although the resonances were found at about 2, 4 and 12 Hz in the three postures, the effect on the resonance frequencies appeared small. The pitching motion of the head also showed a large effect. Decreasing the pelvic angle decreased the transmissibility below about 6 Hz, whereas the trend was reversed above 8 Hz: the differences in the two extreme postures were between 5.5 and 9.5 $rads^{-2}/ms^{-2}$ at the second resonance around 5 Hz and between 2.5 and 3.5 $rads^{-2}/ms^{-2}$ at the third resonance around 12 Hz. The second resonance frequency appeared to have increased with decreasing the pelvic angle: the second resonance frequency at 5.3 Hz with the largest pelvic angle was increased to about 6.5 Hz by the smallest pelvic angle. The effects on the first and the third resonance frequencies, which were about 3 and 12 Hz, were not clear. Changing pelvic angle also altered the transmissibility to the fore-and-aft motion of the head. Decreasing the pelvic angle increased the transmissibility in the entire

frequency range with the largest increment from 0.5 with the largest pelvic angle to 0.8 with the smallest pelvic angle at the first resonance at about 6 Hz. The effect on the transmissibility to the lateral motion of the head appeared small. The mean transmissibility to the vertical motion of the head in the normal posture is shown in Figure 2.12.

Further investigation was conducted by Messenger (1989). The correlation between the spinal curvatures and the transmissibilities to the head was studied. The spinal curvature was measured in terms of six angles (inclination) including the head, pelvis and four levels on the spine at the vertebrae C6, T5, T10, and L2. A total of 12 subjects was exposed to vertical random vibration in the frequency range from 0.5 to 25 Hz with a magnitude of 1.0 m/s^2 r.m.s.. Acceleration was measured at the head in the vertical, fore-and-aft, and the pitch directions, using a bite-bar. The correlation between the angles of the back and the transmissibilities were calculated. Increasing anterior tilting of the pelvis accompanied by increasing straightening of the lumbar spine decreased the transmissibilities at 4 Hz and increased the transmissibilities above 10 Hz in the vertical and fore-and-aft directions with statistic significance. On the other hand, increasing forward inclination of the upper spine increased the transmissibilities at 4 Hz and decreased the transmissibilities above 10 Hz in the same two directions with statistic significance.

2.3.4.2 Effect of muscle tension

Griffin *et al.* (1978) measured the transmissibility from vertical seat motion to vertical head motion of a subject with the muscles tensed as much as possible and with the muscles relaxed. The subject kept a normal sitting posture in both conditions. It was found that the tensed muscles increased the transmissibility at most frequencies up to 100 Hz with the largest increment from 1.0 to 1.4 at 5 Hz. The first resonance at about 4 Hz with the relaxed muscles also shifted to about 5 Hz by tensing the muscles. However, the effect of muscle tension appeared smaller than the effect of changing posture.

2.3.4.3 Inter-subject variability

Variability between subjects, inter-subject variability, can be explained partly by different postures and different muscle tension mentioned above. The effect of anthropometric parameters on the transmissibility from vertical seat motion to vertical head motion was investigated by Griffin *et al.* (1978). The authors calculated correlations between the transmissibilities of 18 men and their weights, heights, hip sizes, thigh sizes, and leg sizes.

A significant negative correlation was found between the transmissibilities at 16 Hz and the weights of the subjects. There was also a significant negative correlation between the transmissibilities at 4 Hz and the transmissibilities at 16 Hz. They also compared the transmissibilities of 18 women and 12 boys. The mean transmissibility of the men was found to be larger than that of the women below 4 Hz, whereas the trend was reversed above 5 Hz: the largest differences were between 1.1 and 1.4 at 2.5 Hz and between 0.7 and 0.9 at 12.5 Hz. The mean transmissibility of the boys was found to be smaller than that of the men above 10 Hz: the transmissibility of the boys was about half of the transmissibility of the men above 40 Hz.

2.3.4.4 Non-linearity

Griffin (1975) investigated the non-linearity by exposing his 12 subjects to vertical discrete sinusoidal vibration with six different magnitudes from 0.2 to 4.0 m/s^2 r.m.s.. He found a significant effect of the magnitude on the transmissibility from vertical seat motion to vertical head motion. The effect appeared to be larger at lower frequencies.

The effect of seven different magnitudes from 0.4 to 2.8 m/s^2 r.m.s. on the transmissibility from vertical seat motion to vertical head motion was investigated by Griffin *et al.* (1978). A subject was exposed to vertical sinusoidal swept vibration in the frequency range from 1 to 50 Hz. The authors concluded that the effect was insignificant compared with the variability caused by other factors, although the lower magnitude appeared to have increased the first resonance frequency around 4 Hz and reduced the transmissibility at the first resonance. They also compared the transmissibilities in response to vertical random vibration with three different frequency spectra. The results showed that decreasing the amount of the low frequency energy increased the first resonance frequency around 4 Hz.

Hintz and Seidel (1987) exposed four subjects to vertical discrete sinusoidal vibration in the frequency range between 2 and 12 Hz with two different magnitudes of 1.5 and 3.0 m/s^2 r.m.s.. The vertical head acceleration was measured using a bite-bar. The transmissibilities from vertical seat motion to vertical head motion showed that the resonance frequency at about 4 Hz with the higher magnitude increased to about 4.5 Hz with the lower magnitude. The authors also compared the transmissibility calculated from the r.m.s. values of the input and the output signals and the transmissibilities calculated from the maximum values and minimum values of the two signals. The transmissibilities

calculated by the three different methods resulted in three different values in the frequency range up to 5.5 Hz, due to the wave deformation of the output. The mean transmissibility with the lower magnitude is shown in Figure 2.12.

Pope *et al.* (1987) also compared the transmissibilities from vertical seat motion to vertical head motion in response to the vertical impact excitation and the conventional sinusoidal vibration excitation with a magnitude of 1.0 m/s^2 r.m.s. It was found that both in erect and relaxed postures, the vibration excitation produced higher transmissibility below 8 Hz, whereas the trend was reversed above 8 Hz, although the transmissibility curves were qualitatively similar: the largest differences were between 1.0 and 1.4 at 4 Hz and between 0.9 and 1.3 at 10 Hz in the erect posture.

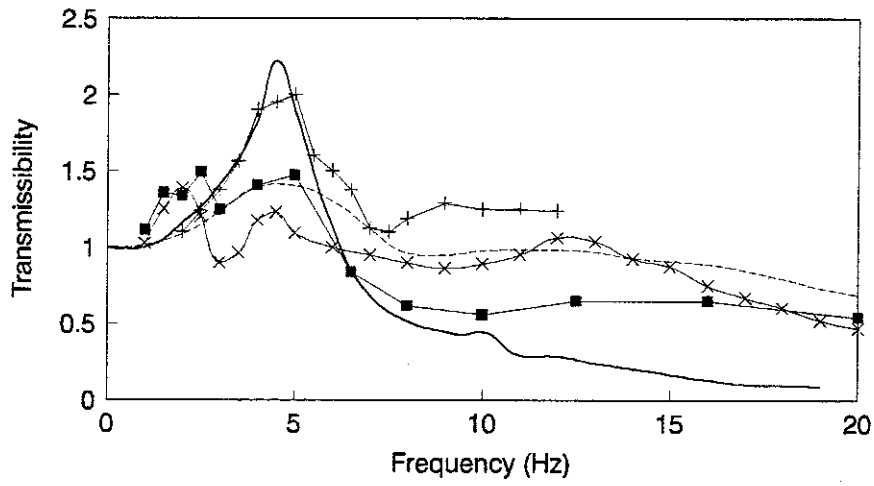

Figure 2.12 Acceleration transmissibilities from vertical seat motion to vertical head motion: values of a single subject by Coermann (——); mean values of 18 subjects by Griffin *et al.* (—■—); mean values of eight subjects by Messenger (—X—); mean values of four subjects by Hinz and Seidel (—+—); International Standard 7962 (- - - -).

2.3.5 Transmissibility to the spine

The acceleration or displacement transmissibility from seat motion to spinal motion has been investigated by some workers. When measuring the transmissibility to the spine of a sitting subject, the subject sits on a seat mounted on a vibrator. The excitation is measured on the seat. The response should be the response of a specific vertebra which

is not easy to measure. One of the ways to measure the spinal responses is to mount transducers on the body-surface above the spine. However, the mass of the transducers and tissue around the contact area form a local vibration system with the stiffness and damping of tissue. Therefore, the responses measured on the body-surface are filtered and different from the responses of the spine. An alternative way to measure spinal responses accurately is to mount transducers on a pin (e.g. Kirschner wire) inserted into the spine with local anaesthesia. This direct measurement has been employed by some workers, although the method restricts the number of measuring sites and the number of subjects.

The acceleration transfer function and the displacement transfer function are theoretically the same if the structure is linear. A mathematical description of the acceleration or displacement transfer function from seat motion to spinal motion is obtained by replacing the output by acceleration or displacement of a specific vertebra and the input by acceleration or displacement of the seat in equation (2.1):

$$T(f)=\frac{A_v(f)}{A_s(f)}=\frac{D_v(f)}{D_s(f)} \qquad \textbf{(2.13)}$$

where: $T(f)$ is the acceleration or displacement transfer function from seat motion to motion of a vertebra; $A_v(f)$ and $D_v(f)$ are the Fourier transforms of the acceleration and the displacement of a vertebra; $A_s(f)$ and $D_s(f)$ are the Fourier transforms of the acceleration and the displacement of the seat. The transmissibility, $|T(f)|$, is the modulus part of the transfer function as shown in equation (2.14):

$$|T(f)|=\frac{|A_v(f)|}{|A_s(f)|}=\frac{|D_v(f)|}{|D_s(f)|} \qquad \textbf{(2.14)}$$

In practice, equation (2.3) is used to minimise the effect of noise. There are some investigations in which the transfer functions or transmissibilities between two vertebrae are calculated to estimate relative motion within the spine. In this case, the Fourier transforms of the acceleration or displacement of two vertebrae are used in equations (2.13) and (2.14).

The spinal column is the principal vibration path from the seat to the head of a sitting subject. It consists of seven cervical vertebrae, from C1 to C7, twelve thoracic vertebrae, from T1 to T12, and five lumbar vertebrae, from L1 to L5. Since adjacent vertebrae are connected by deformable intervertebral disc, ligaments and muscles, the whole spinal

column deforms in all six directions like a beam. The transmissibility to the spine has been investigated so as to identify frequencies and levels of vibration which may cause spinal injuries. However, difficulty of mounting transducers on the spine has restricted the number of investigations and reliability of data. This section is divided into four sections: general responses of the spine, effect of posture, effect of muscle tension, and non-linearity.

2.3.5.1 General responses of the spine

Christ and Dupuis (1963) used a X-ray cinematography technique to visualise the motion of the cervical and the lumbar spine. The subjects were exposed to vertical sinusoidal vibration of 2 Hz, sitting on a good seat and a poor seat. They found that on the poor seat, the cervical spine moved vertically about 40 mm which was about the height of one vertebra, whereas it moved about 20 mm on the good seat. The lumbar spine was found to move vertically about 20 mm on both poor and good seats. The authors (1966) subsequently exposed a subject with pins inserted into the vertebrae T12, L2 and L4 to vertical discrete sinusoidal vibration in the frequency range from 0.5 to 8 Hz with an amplitude of 10 mm peak to peak. They used the cinematography technique for targets attached to the ends of the pins to estimate the spinal displacement responses: the motion of the targets were plotted in the sagittal plane at each frequency. The lower thoracic and the lumbar spine showed a resonance in the vertical direction at 4 Hz with a displacement transmissibility of 3.0, which was also accompanied by fore-and-aft motion of the spine.

Panjabi *et al.* (1986) measured acceleration of the vertebrae L1 and L3 in the vertical, fore-and-aft and rotational directions in the sagittal plane, using Kirschner wires. They exposed five subjects in a sitting posture to vertical discrete sinusoidal vibration with a magnitude of 0.1 g in the frequency range from 2 to 15 Hz. Transmissibilities from vertical seat acceleration to acceleration of the vertebrae in the three directions were estimated. They found no difference between the responses of the two vertebrae. The vertical transmissibility showed a resonance at 4.4 Hz with a transmissibility of 1.6, whereas the fore-and-aft transmissibility appeared to have simply increased from about 0.2 at 2 Hz to about 0.8 at 15 Hz and did not show any clear resonances. The rotational transmissibility had a large variability between the subjects and it was not possible to find a trend. The mean transmissibilities to the vertebra L3 in the vertical and fore-and-aft directions are shown in Figures 2.13 and 2.14 respectively.

Sandover and Dupuis (1987) reanalysed the X-ray cinematography data of Christ and Dupuis (1966), using more advanced techniques based on a computer. A subject with pins inserted into the vertebrae T12, L2 and L4 was exposed to vertical discrete sinusoidal vibration in the frequency range from 2 to 7 Hz with an amplitude of 10 mm peak to peak. Targets were attached to the ends of the pins and the displacement responses of the targets in the sagittal plane were recorded, using the cinematography technique. The targets displacement data were transferred to displacements at the vertebral body centroids. They also estimated the noise level and minimised it. The displacement spectra of the three vertebrae in the vertical direction showed little difference between them and had a resonance at 4 Hz with a resonance peak of 20 mm. The phase lags of the three vertebrae almost coincided at about 0 degree in the observed frequency range. The relative displacement between the three vertebrae in the vertical direction was so small that the data was not reliable due to noise. The displacement spectra in the fore-and-aft and rotational directions appeared to show peaks at 3 and 4 Hz with large relative displacements and phase differences between the three vertebrae. The relative displacement spectra in the fore-and-aft and rotational directions appeared to have peaks between 3 and 4 Hz. The authors found that the relative displacement between the vertebrae L2 and L4 was greater than that between the vertebrae T12 and L2 both in the fore-and-aft and rotational directions. They interpreted this finding as the result of rotational vibration of the pelvis around the ischial tuberosities. It was concluded that the response of the lumbar spine contained large bending deformation but small axial deformation in the observed frequency range. They also pointed out that rotational motion of the vertebrae caused translational motion at posterior measuring points which were distant from the centroids of the vertebrae and that care should be taken to avoid misinterpretation. The displacement transmissibilities to the vertebra L4 in the vertical and fore-and aft directions are shown in Figures 2.13 and 2.14 respectively.

Hinz *et al.* (1988a) measured vertical and fore-and-aft acceleration of the vertebrae L3 and L4 on the body surface. They estimated transfer functions of tissue between the spine and the body surface and the spinal acceleration was predicted from the surface measurement, using the estimated tissue transfer functions. A total of three subjects was exposed to vertical discrete sinusoidal vibration at 4.5 and 8 Hz with magnitudes of 1.5 and 3.0 m/s^2 r.m.s. The acceleration time histories of the vertebrae in the two directions were investigated. They found substantial bending motion of the spine and interpreted the motion of the lumbar spine as flexion (bending motion where the distance between adjacent spinous processes increases) during downwards and extension (bending motion

apposite to flexion) during upwards motion of the body both at 4.5 and 8 Hz. A detailed analysis measuring motion of the head, shoulder and the vertebra T5 reached the finding that downwards and upwards motion of the lumbar spine was also accompanied by the motion of those body parts in the same direction in phase. It was predicted that the vertical motion of the body parts above the lumbar spine might be the main cause of the bending motion of the lumbar spine.

Pope *et al.* (1991) investigated the displacement responses of the vertebrae L3, L4 and L5, using transducers mounted on pins inserted into the spinous processes. They exposed three subjects to vertical sinusoidal vibration at 5 and 8 Hz with a magnitude of 1.0 m/s^2 r.m.s.. It was found from the time history analysis that the vertebrae exhibited coupled motion of translational and rotational vibration and that both the translational and rotational vibration were greater at 5 Hz than at 8 Hz.

2.3.5.2. Effect of posture

Pope *et al.* (1986) exposed a subject with a Kirschner wire inserted into the spinous process of the vertebra L3 to vertical discrete sinusoidal vibration at 2, 4, 5 and 6 Hz with a magnitude of 0.2 g. The subject adopted erect and relaxed postures. The displacement transmissibilities from vertical seat motion to vertical motion of the vertebrae were calculated. They found a resonance at 4 Hz in both of the two postures. The transmissibilities in the relaxed posture at 4 and 5 Hz were decreased by the erect posture, whereas the trend was reversed at 6 Hz: the transmissibilities were decreased from 1.4 to 1.0 at 4 Hz, from 1.2 to 0.7 at 5 Hz and increased from 0.5 to 0.7 at 6 Hz. They also compared the obtained results with surface measurements and found a significant difference. The transmissibility in the relaxed posture is shown in Figure 2.13.

Broman *et al.* (1991) measured the acceleration transmissibility from vertical seat motion to motion of the vertebra L3, using the vertical impact excitation method which Pope *et al.* (1987) developed to measure the seat-to-head transmissibility. Kirschner wires were inserted into the spinous processes of three subjects. An accelerometer was mounted on the wire, being oriented in the vertical direction. The subjects adopted erect and relaxed postures. The transmissibilities generally showed a major resonance between 5 and 6.5 Hz and a small resonance at about 8 Hz. It was found that the major resonance at 6.3 Hz (mean) in the erect posture was shifted to 5.0 Hz (mean) by the relaxed posture. The resonance transmissibility was increased from 3 to 3.8 (mean) also by the erect posture.

The effect of posture on the second resonance at 8 Hz was not clear.

Magnusson *et al.* (1993) investigated the effect of backrest inclination on the responses of the vertebra L3 to the impact excitation, using the same apparatus Pope *et al.* (1987) used. A pair of accelerometers was mounted on a Kirschner wire inserted into the spinous process of the vertebra L3. The accelerometers were oriented in the directions along the spine and perpendicular to the spine. The backrest was located below the scapulae level to avoid the constraint in the lumbar region. A total of three subjects was exposed to the vertical impact excitation in four different postures: forward flexion at 80 degrees unsupported, upright at 90 degrees unsupported, leaning backwards at 110 degrees against the backrest and leaning backwards at 120 degrees against the backrest. The acceleration transfer functions from motion of the platform to motion of the vertebra L3 in the two directions were calculated. In general, the transmissibilities in the direction along the spine showed a major resonance between 4 and 8 Hz, whereas the transmissibilities in the direction perpendicular to the spine did not show clear resonances below 16 Hz and they stayed below unit at most frequencies. The transmissibilities in the direction perpendicular to the spine had a large variability between the subjects. No clear effects of the backrest inclination were found. The mean transmissibilities to motion of the vertebra L3 in the vertical and fore-and-aft directions in the unsupported upright posture are shown in Figures 2.13 and 2.14 respectively.

2.3.5.3. Effect of muscle tension

Hagena *et al.* (1985,1986) inserted Kirschner wires into the spinous processes of the vertebrae C7, T6, L1, L4, L5, and the sacrum so as to measure the acceleration responses of the spine directly. Vertical acceleration was measured on the Kirschner wires as well as on top of the head. A total of 11 subjects was exposed to vertical discrete sinusoidal vibration in the frequency range from 3 to 40 Hz with a magnitude of 0.2 g in sitting and standing postures with the muscles tensed and relaxed. The transmissibilities from vertical motion of the sacrum to vertical motion of the vertebrae and the head were calculated. There was no effect of muscle tension on the transmissibilities found both in the sitting and standing postures.

Broman *et al.* (1991) also investigated the effect of muscle tension on the spinal response to the impact excitation. The subjects pressurised the abdomen voluntarily. The acceleration transmissibility to vertical motion of the vertebra L3 showed that the major

resonance frequency at 5 Hz (mean) with the normal muscle tension in the relaxed posture was increased to 6.2 Hz (mean) by the pressurised abdomen. The pressurised abdomen also increased the transmissibility of the major resonance from 3.8 to 4.2 (mean). The small resonance which was shown at about 8 Hz with the normal muscle tension was not clear with the pressurised abdomen.

2.3.5.4. Non-linearity

Panjabi *et al.* (1986) also compared the spinal responses to two magnitudes of 0.1 and 0.3 g. However, the acceleration transmissibilities from vertical seat motion to motion of the vertebrae L1 and L3 in the vertical, fore-and-aft and rotational directions did not show any difference between the two magnitudes.

Hinz and Seidel (1987) measured vertical acceleration at the vertebra T5, using a miniature accelerometer weighing 0.5 g attached on the body surface. They exposed four subjects to vertical discrete sinusoidal vibration in the frequency range from 2 to 12 Hz with magnitudes of 1.5 and 3.0 m/s^2 r.m.s.. The acceleration transmissibilities from

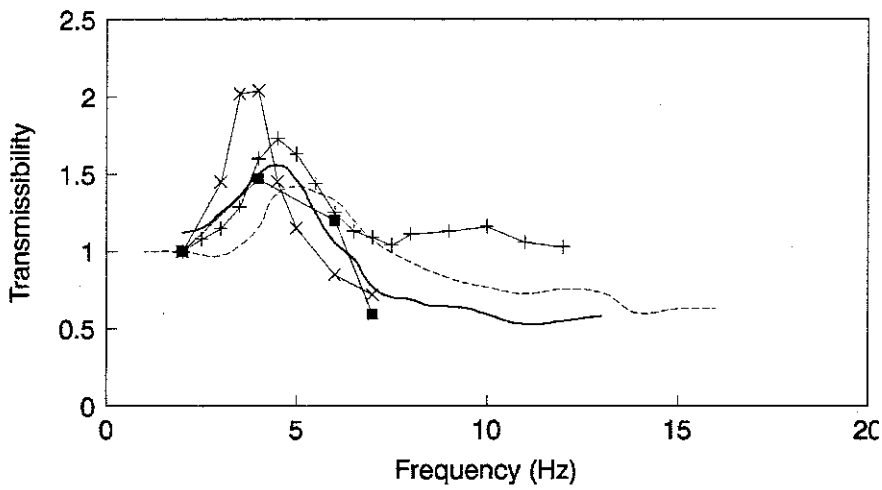

Figure 2.13 Transmissibilities from vertical seat motion to vertical spinal motion: mean acceleration transmissibility to the vertebra L3 of five subjects by Panjabi *et al.* (——); displacement transmissibility to the vertebra L3 of a single subject by Pope *et al.* (—■—); displacement transmissibility to the vertebra L4 of a single subject by Sandover and Dupuis (—x—); mean acceleration transmissibility to the vertebra T5 of four subjects by Hinz and Seidel (—+—); mean acceleration transmissibility to the vertebra L3 of three subjects by Magnusson *et al.* (- - - -).

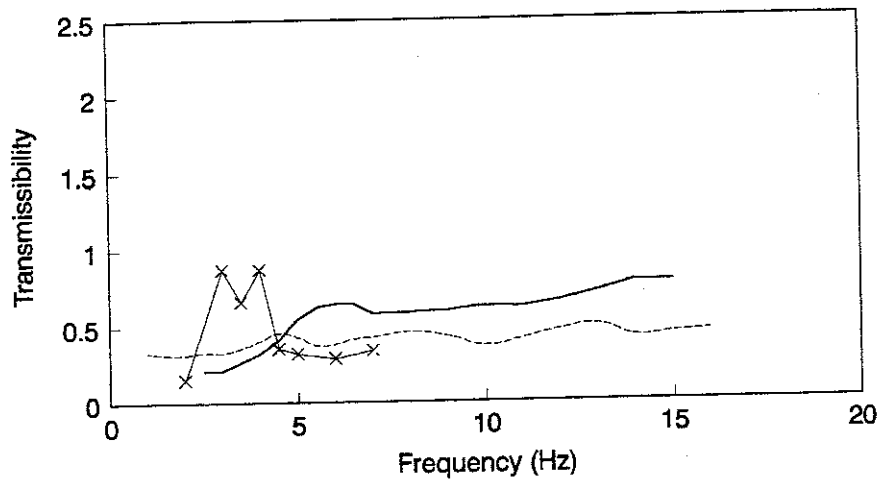

Figure 2.14 Transmissibilities from vertical seat motion to fore-and-aft spinal motion: mean acceleration transmissibility to the vertebra L3 of five subjects by Panjabi *et al.* (——); displacement transmissibility to the vertebra L4 of a single subject by Sandover and Dupuis (—x—); mean acceleration transmissibility to the vertebra L3 of three subjects by Magnusson *et al.* (- - - -).

vertical seat motion to vertical motion of the vertebra T5 were estimated. It was found that the resonance frequency at 4.5 Hz with the lower magnitude decreased to 4 Hz with the higher magnitude. They also demonstrated the wave distortion in the time history responses. The mean transmissibility with the magnitude of 1.5 m/s^2 r.m.s. is shown in Figure 2.13.

Broman *et al.* (1991) also compared the responses of the vertebra L3 to vertical impacts with two different energies and fond no significant differences. The authors concluded that the system could be regarded as linear.

2.3.6 Other responses of the body

There are some workers who measured other responses of the body so as to understand whole-body vibration more comprehensively. However, the difficulty of mounting transducers has restricted the number of such investigations. This section is divided into three sections: response of the viscera, response of the pelvis and response of the upper torso.

2.3.6.1 Response of the viscera

The visceral response to vibration has been measured by a few workers. The body cavity is divided into upper and lower cavities by the diaphragm located below the lung. The upper cavity, which is called thoracic cavity, contains the lung and the heart. The lower cavity, abdominopelvic cavity, is the region between the diaphragm and the pelvis, which contains the rest of the viscera. The visceral mass is concentrated below the diaphragm, which is about 80 % of the lower torso mass. It is obvious that the viscera has much lower stiffness than that of the spinal column: the stiffness of tissue is of the order of 10^4N/m, whereas the stiffness of the intervertebral discs is of the order of 10^6N/m (Belytschko and Privitzer, 1978). Therefore, the viscera in the abdominopelvic cavity forms a local vibration system, whose vertical motion pushes the lung via the diaphragm and may affect the respiration. Visceral vibration is also considered to contribute to psychological discomfort.

Coermann *et al.* (1960) investigated the abdominal wall displacement, the chest circumference (thorax expansion) and respiration air flow of a subject in the supine position in response to longitudinal discrete sinusoidal vibration in the frequency range from 1 to 20 Hz with a magnitude of 0.1 g. The abdominal wall displacement response was measured using accelerometers attached to the abdominal wall. The response of the chest circumference was measured using a pneumograph. The respiration response was measured using a breathing head. The results showed that all three responses had a major resonance between 3 and 1.5 Hz. The measured responses are shown in Figure 2.15

White *et al.* (1962) measure the colon pressure response. The pressure probe was placed at the rectal end of the colon sigmoideum. A total of eight subjects was exposed to vertical discrete sinusoidal vibration in the frequency range from 1 to 20 Hz with a magnitude of 1 g in sitting erect and sitting relaxed postures. The measured pressure was plotted against the frequency. It was found that the colon pressure curve had a resonance at about 4 Hz. Changing posture from relaxed to erect increased the resonance frequency from 4 to 4.5 Hz. The pressure in the erect posture was also found to be higher than that in the relaxed posture below 10 Hz, although the peaks at the resonance were the same at 56 mmHg/g both in the erect and relaxed postures. The mean pressure curve in the relaxed posture is shown in Figure 2.16.

Christ and Dupuis (1963) also visualised motion of the stomach during vibration exposure.

A subject was exposed to vertical sinusoidal vibration at 2 Hz in a sitting position. The motion of the stomach was observed, using a X-ray cinematography technique. They found that the motion of the stomach was larger than that of the rest of the body (by a factor of 2 at the bottom of the stomach), which indicated the presence of the local vibration system of the viscera.

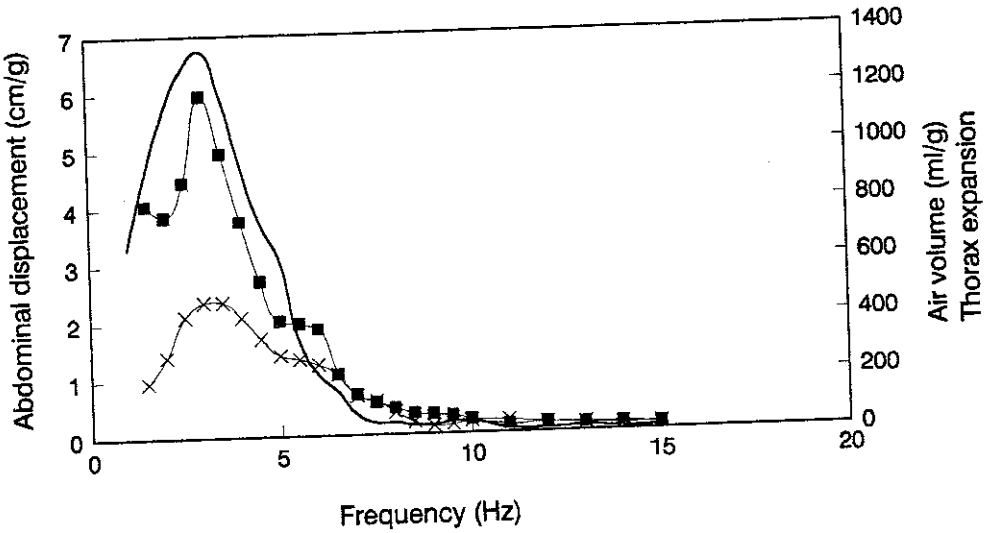

Figure 2.15 Abdominal wall displacement (——), respiration air volume (—■—) and thorax expansion (—X—) of a single subject measured by Coermann *et al.*.

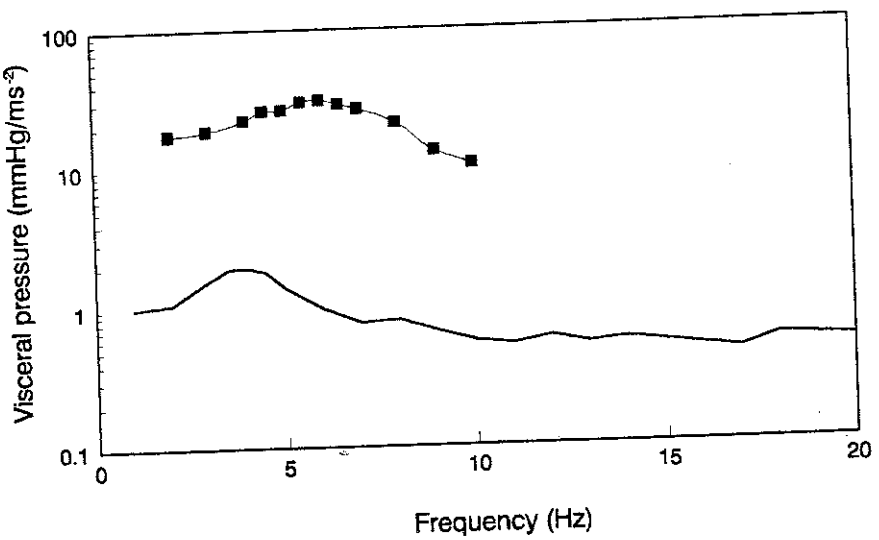

Figure 2.16 Mean colon pressure of eight subjects by White *et al.* (——) and intraabdominal pressure of a single subject by Sandover (—■—).

Sandover (1978) also measured the intraabdominal pressure, placing a probe in the lower intestine of a subject. The subject was exposed to vertical random vibration with a magnitude of 2 m/s^2 r.m.s. in a sitting position. The pressure was plotted against the frequency with the driving point apparent mass and the seat-to-head transmissibility. The result showed that all the three responses had a major resonance at the same frequency of 6 Hz. The pressure curve is shown in Figure 2.16.

2.3.6.2 Response of the pelvis

There is soft buttocks tissue beneath the pelvis supporting the whole upper body when a subject is in a sitting position. The pelvis on the buttocks tissue may contribute to the body responses by rotational (pitching) motion or by vertical translational motion. There are a few workers who measured the pelvic motion.

Coermann (1962) exposed a subject to vertical discrete sinusoidal vibration in the frequency range from 1 to 20 Hz with a magnitude of 0.1 g in a sitting position. He measured the vertical displacement responses of the hip bones and the neck, using light weight accelerometers attached on the body surface. The relative displacement between the seat and the hip bones divided by the acceleration on the seat showed two resonances at 5 and 9 Hz. The relative displacement between the hip bones and the neck divided by the acceleration on the seat also showed two resonances at the same frequencies. However, the relative displacement between the hip bones and the neck divided by the acceleration on the pelvis showed only one resonance at 5 Hz. He concluded that the pelvis had two resonances at 5 and 9 Hz, whereas the spinal column had only one resonance at 5 Hz. The vertical displacement response of the pelvis with respect to the seat acceleration is shown in Figure 2.17.

Hagena *et al.* (1985,1986) inserted Kirschner wires into the spinous processes of the vertebrae C7, T6, L1, L4, L5, and the sacrum so as to measure the acceleration responses of the spine directly. Vertical acceleration was measured on the Kirschner wires as well as on top of the head. A total of 11 subjects was exposed to vertical discrete sinusoidal vibration in sitting and standing postures in the frequency range from 3 to 40 Hz with a magnitude of 0.2 g. The transmissibilities from vertical motion of the sacrum to vertical motion of the vertebrae and the head were calculated. They found three resonances at about 4, 9, and 18 Hz in all the transmissibilities both in the standing and sitting postures. All the transmissibilities at the 4 Hz resonance in the range between 1.1 and 1.35 in the

standing posture were decreased to the range between 0.9 and 1.1 by the sitting posture. The transmissibilities to the vertebrae C7, T6 and L1 at the 18 Hz resonance in the range between 0.9 and 1.2 in the standing posture were increased to the range between 1.3 and 1.6 also by the sitting posture. The transmissibilities in the range between 1.1 and 1.3 at the 9 Hz resonance showed no difference between the two postures. The authors predicted from the results that the mode at 4 Hz might be the entire body mode, whereas the mode at 9 Hz might be the spinal mode.

Panjabi *et al.* (1986) measured vertical acceleration of the sacrum, using a Kirschner wire. They exposed five subjects in a sitting posture to vertical discrete sinusoidal vibration with a magnitude of 0.1 g in the frequency range from 2 to 15 Hz. The transmissibility from vertical seat acceleration to vertical sacral acceleration was estimated. The transmissibility showed a clear resonance at 4.8 Hz with a resonance transmissibility of 1.8, which is shown in Figure 2.17. Both the frequency and the transmissibility of the resonance of the seat-to-sacrum transmissibility were higher than those of the seat-to-lumbar transmissibilities with a statistic significance: the frequency and the transmissibility of the resonance of the seat-to-lumbar transmissibilities were 4.4 Hz and 1.6.

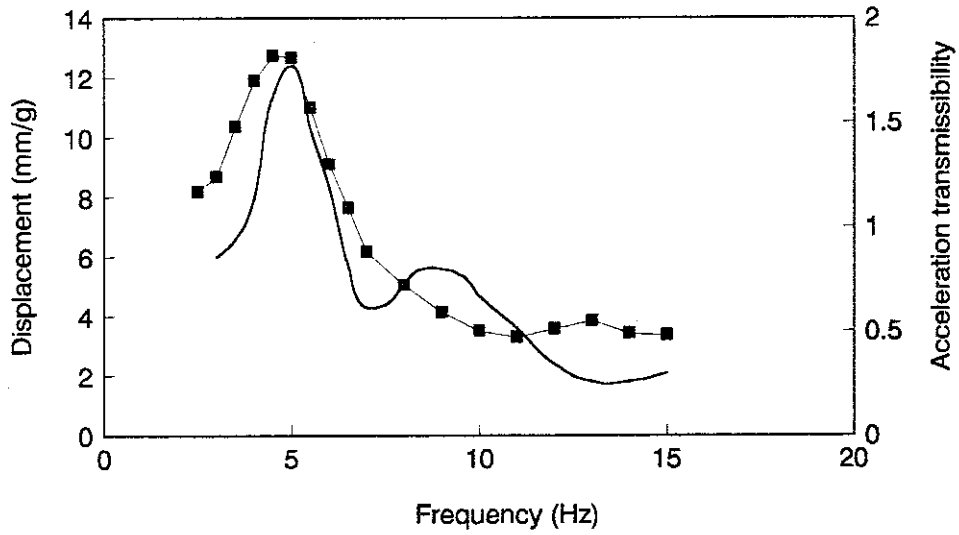

Figure 2.17 Vertical displacement response of the pelvis with respect to the vertical seat acceleration of a single subject by Coermann (——) and the mean transmissibility from vertical seat acceleration to vertical acceleration of the pelvis of four subjects by Panjabi *et al.* (—■—).

2.3.6.3. Response of the upper torso

There are several investigations in which the response of the upper torso to vibration was measured. Donati and Bonthoux (1983) measured vertical motion of the thorax. An accelerometer was attached to the body surface on the xiphoidian using a harness, being oriented in the vertical direction. A total of 15 subjects was exposed to vertical swept sinusoidal and vertical random vibration in the frequency range between 1 and 10 Hz with a magnitude of 1.6 m/s^2 r.m.s.. The transfer functions from vertical seat acceleration to vertical thorax acceleration were calculated. There was little difference between the transfer functions in response to the two excitation methods. The transmissibilities showed a resonance at 4 Hz with a transmissibility of 2.3. They also compared the results with the driving point impedance and found that the resonances coincided. The xiphoidian is a bone attached to the lowest end of the sternum. Because the sternum is connected to the thoracic spine via the ribs, the response measured in this investigation seemed to correspond to the response of the entire thoracic spine. The mean transmissibility in response to vertical random vibration is shown in Figure 2.18.

Woods (1967) measured vertical acceleration on the shoulder. A total of three subjects was exposed to vertical discrete sinusoidal vibration in the frequency range from 1 to 10 Hz with magnitudes of 0.07, 0.14 and 0.21 g r.m.s. The transmissibilities from vertical seat acceleration to vertical shoulder acceleration were calculated. The transmissibility with a magnitude of 0.07 g r.m.s. showed a resonance at 5 Hz with a resonance transmissibility of 2.2. The transmissibilities with magnitudes of 0.14 and 0.21 g r.m.s. showed a resonance at 4.5 Hz with a resonance transmissibility of 2.5. The mean transmissibility of the three subjects with the magnitude of 0.14 g r.m.s. is shown in Figure 2.18.

Vertical shoulder motion was also measured by Hinz and Seidel (1987), using a miniature accelerometer weighing 0.5 g attached on the body surface. They exposed four subjects to vertical discrete sinusoidal vibration in the frequency range from 2 to 12 Hz with magnitudes of 1.5 and 3.0 m/s^2 r.m.s.. The acceleration transmissibilities from vertical seat motion to vertical shoulder motion were calculated. The resonance frequencies were found at 4.5 Hz with the lower magnitude and at 4 Hz with the higher magnitude. They also measured the driving point apparent mass, the transmissibility to the head and the transmissibility to the vertebra T5. The responses at the different parts of the body were found to show the resonance at the same frequency. The mean transmissibility to the shoulder of four subjects with the lower magnitude is shown in Figure 2.18.

The shoulder consists of two main bones which are the clavicle and the scapula. The clavicle is connected to the arm (humerus) at one end and connected to the sternum at the other end. Therefore, the arm is suspended from the body via the clavicle, sternum, ribs and the thoracic spine. The shoulder contains five joints which allow the shoulder and the arm to move in a wide range. The responses of the shoulder measured by Woods, and Hinz and Seidel were possibly measured on the clavicle. Because of the suspended structure, the shoulder and the arm may construct a local vibration system. The results of Hinz and Seidel showed that vertical motion of the shoulder had a resonance at the same frequency as that of the rest of the body. However, the resonance transmissibility to the shoulder was larger than those to the head and to the vertebra T5: the resonance transmissibilities to the shoulder, to the head and to the vertebra T5 were 3.0, 2.0 and 1.7 respectively. Therefore, the transmissibility to the shoulder seemed to be amplified by the suspended structure.

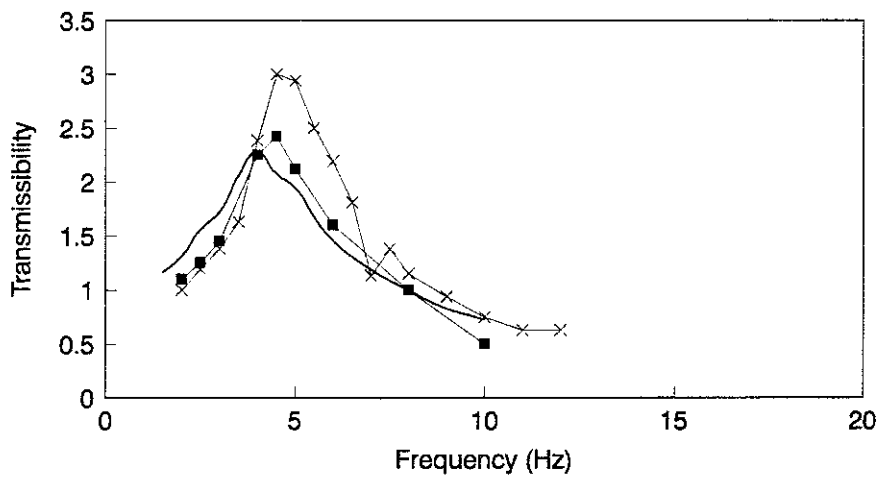

Figure 2.18 The mean transmissibility to the thorax of 15 subjects by Donati and Bonthoux (——), the mean transmissibility to the shoulder of three subjects by Woods (—■—) and the mean transmissibility to the shoulder of four subjects by Hinz and Seidel (—x—).

2.3.7 Discussion

2.3.7.1 General responses of the human body

There were some common findings in the various responses of the human body to

vibration. The major vertical resonance of the human body was located between 4 and 6 Hz. This resonance was always found in the driving point responses, the seat-to-head transmissibilities, the seat-to-spine transmissibilities at any vertebra, the visceral responses, the seat-to-pelvis transmissibilities and others. In most cases this major resonance was the first resonance found except the seat-to-head transmissibilities measured by Griffin *et al.* (1978) and Messenger (1987) where there was further lower resonance at about 2 Hz. Another vertical resonance was found between 8 and 12 Hz in some investigations regardless of body parts, although it was not as clear as the major resonance. The variabilities of the frequency of this resonance both between investigations and between subjects were larger than those of the frequency of the major resonance. Resonances were found occasionally above 12 Hz. However, they were ambiguous. The coincidence of the major resonance frequency between 4 and 6 Hz in all the vertical responses of the various body parts seems to indicate that the entire body is moving in the vertical direction rigidly at this resonance.

The workers who measured the spinal responses in other directions found that the vertical spinal motion was also accompanied by the fore-and-aft and rotational motion at most frequencies, although the seat-to-spine transmissibilities in these directions did not show clear resonances. Hinz *et al.* (1988a) interpreted the relation between the vertical body motion and the bending spinal motion as flexion of the spine during downwards motion of the body. The seat-to-head transmissibilities also showed fore-and-aft and rotational (pitching) resonances between 4 and 6 Hz.

Hagena *et al.* (1985,1986) found a large decrement in the transmissibilities from vertical motion of the sacrum to vertical motion of the spine and the head at the 4 Hz resonance from the standing posture to the sitting posture. Sandover (1978) found that constraining the pelvic motion using blocks placed beneath the ischial tuberosities affected the major resonance of the driving point apparent mass. The major resonance of the human body seems to follow the pelvis-buttocks behaviour. However there is no evidence found whether it is pelvic rotation or buttocks tissue deformation.

The visceral responses also showed a major resonance between 3 and 6 Hz. The resonance of the visceral pressure response in this frequency range indicates the presence of the local resonance which includes relative motion between the viscera and the rest of the body. The finding of Coermann (1962) of the effects of the abdomen constraint and the pressure suit on the major resonance of the driving point impedance

also implies the existence of the relative motion of the viscera to the spine and the contribution of the visceral local resonance to the major resonance of the human body.

To summarise, there are at least two resonances of the human body, the major resonance located between 4 and 6 Hz and the second major resonance between 8 and 12 Hz. The major resonance of the human body seems to consist of vertical entire body motion accompanied by pelvic rotation or buttocks tissue deformation, bending motion of the lumbar spine accompanied by fore-and-aft and pitching motion of the head, and relative vertical motion of the viscera to the rest of the body. The second major resonance also seems to contain vertical motion of some parts of the body and bending motion of the spine. However, the vibration mode is not clear.

2.3.7.2 Effect of posture

The effect of posture was found in some cases in the driving point responses, the seat-to-head transmissibility and the seat-to-spine transmissibility. The common trend of the effect on the driving point responses was for an erect posture to increase the major resonance frequency. However, there were also some subjects who did not show any effect of the change of posture. The effect on the second resonance was not clear. The seat-to-head and the seat-to-spine transmissibilities were found to show the effect of posture more consistently. The common trend was that either an erect posture increased the major resonance frequency or an erect posture decreased the major resonance transmissibility and increased the transmissibility at higher frequencies which appeared similar to the effect of increasing damping at the major resonance. The effect on the second resonance was not clear. There was only one investigation where the effect of posture on the visceral response was studied. The colon pressure showed that an erect posture increased the major resonance frequency and the pressure below 10 Hz. The effect on the other responses is not known.

From an analogy of the human body to a mechanical structure, changing posture corresponds to changing geometry of the structure which usually produces different responses. The most comparisons in the literature were between erect and relaxed postures which could be defined by the spinal curvature and the pelvic angle as Messenger (1987,1989) proposed. Therefore, the differences in responses between the two postures correspond to the differences in responses of structures possessing different spinal beam shapes and different boundary conditions at the bottom of the beam. The

different spinal curvature and the pelvic angle may affect the natural frequency and the mode shape of the bending mode of the spine contained in the major resonance. However, the pelvic angle may affect the entire body mode more directly by changing the contact condition between the pelvis and the seat surface with buttocks tissue between them, because the entire body mode may be caused by the pelvic rotation or buttocks tissue deformation.

There are several factors which may have caused variability of the effect of posture between subjects especially in the driving point responses. In most investigations, subjects were told to adopt erect and relaxed postures and the postures were not controlled or measured, except the investigations conducted by Messenger where the postures were defined by the pelvic angle and the spinal curvature. Therefore, the postures in the experiments may have had a wide variety. If some subjects might not rotate the pelvis forward when they pushed the lumbar spine forward to take an erect posture, the change would not have affected the entire body mode largely. Some subjects also may have tensed the muscles involuntarily when they adopted the erect posture that may have changed the stiffness as well as the geometry of the body.

2.3.7.3 Effect of muscle tension

There were few investigations into the effect of muscle tension on the responses of the human body. Tensing muscles was found to increase the major resonance frequency of the driving point apparent mass, the seat-to-head transmissibility and the seat-to-spine transmissibility in some subjects, although there were also some other subjects who did not show any effect of tensing muscles. The resonance shift appeared similar to the effect of posture. However, tensing muscles also increased the major resonance transmissibilities to the head and to the spine, that was opposite to the trend with an erect posture. The effect on the second resonance was not clear and the effect on the other responses is not known.

Changing muscle tension of the body corresponds to changing material properties of a structure. Tensing muscles increases stiffness of the muscles. The variability of the effect of muscle tension between subjects may be explained if some subjects tensed muscles involved in the resonance behaviour (i.e. vibration mode) more efficiently than other subjects. The muscles involved in the major resonance behaviour may be the muscles of the buttocks, muscles on the spine and the abdominal muscles.

Both the effect of posture and the effect of muscle tension seem to be dependent on the subject. It is also difficult to distinguish clearly between the effect of posture and the effect of muscle tension, because changing posture may involve an involuntary change in muscle tension. The quantitative relationships between posture, muscle tension and the dynamic responses are difficult to obtain due to the difficulty of measuring posture and muscle tension precisely.

2.3.7.4 Inter-subject variability

The variability in the dynamic responses between subjects can be explained partly by different postures and different muscle tension. Significant correlations were found in a few investigations between some anthropometric parameters and the vibration responses. The moduli of the driving point impedance and the normalised apparent mass, and the seat-to-head transmissibilities below the major resonance had a positive correlation with the total body weights of subjects. The major resonance frequencies of the apparent mass had the most significant negative correlation with the parameter obtained by dividing the sitting weight by the sitting height.

If the entire body motion due to buttocks tissue deformation is dominant in the major resonance, the major mode can be simplified by the response of a single degree-of-freedom model shown in Figure 2.19 with an assumption that the mass of the buttocks tissue is negligible compared with the rest of the body mass, where m_{bod} is the entire body mass (i.e. sitting weight), k_{but} is the stiffness of the buttocks tissue, c_{but} is the damping coefficient of the buttocks tissue, $x_b(t)$ is the displacement response of the entire body, $x_s(t)$ is the excitation displacement at the seat, and $f_s(t)$ is the reaction force from the seat surface.

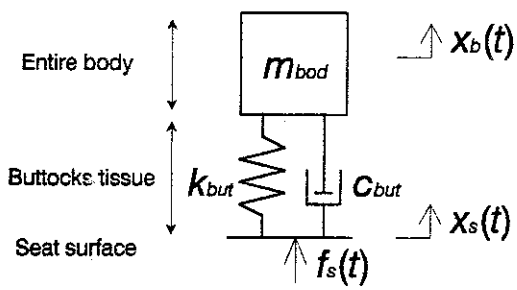

Figure 2.19 Equivalent model for the entire body mode.

From the solutions of the single degree-of-freedom model, the major resonance frequency, f_{mr}, of the driving point impedance, driving point apparent mass and the seat-to-head transmissibility can be approximated as (see Appendix 1):

$$f_{mr} \cong \frac{1}{2\pi}\sqrt{\frac{k_{but}}{m_{bod}}} \qquad \textbf{(2.15)}$$

The moduli of the driving point impedance, $|Z|_{mr}$, and the driving point apparent mass, $|M|_{mr}$, and the seat-to-head transmissibility, $|T_h|_{mr}$, at the major resonance are:

$$|Z|_{mr} \cong m_{bod}\ \omega_0 \frac{1}{2\zeta} \qquad \textbf{(2.16)}$$

$$|M|_{mr} \cong m_{bod}\ \frac{1}{2\zeta} \qquad \textbf{(2.17)}$$

$$|T_h|_{mr} \cong \frac{1}{2\zeta} \qquad \textbf{(2.18)}$$

with the relationships:

$$\omega_0 = \sqrt{\frac{k_{but}}{m_{bod}}} = 2\pi f_0 \qquad \textbf{(2.19)}$$

$$\zeta = \frac{c_{but}}{2\sqrt{m_{bod}\ k_{but}}} \qquad \textbf{(2.20)}$$

where: ω_0 is the natural angular frequency; f_0 is the natural frequency; ζ is the damping ratio. Therefore, the positive correlation between the moduli of the driving point impedance at the major resonance and the body weights can be explained by equation (2.16) if the major resonance is dominated by the entire body mode due to buttocks tissue deformation. The normalised apparent mass obtained by dividing the apparent mass by the sitting weight as proposed by Fairley and Griffin (1989) will be the same as the seat-to-head transmissibility around the major resonance if the major resonance corresponds to the entire body mode. In this case, equations (2.17), (2.18) and (2.20) can explain the positive correlations between the normalised apparent masses at the major resonance and the body weights and between the seat-to-head transmissibilities at the major resonance and the body weights. A negative correlation between the major resonance frequencies and the body weights are expected from equation (2.15). If the parameter defined as the sitting weight divided by the sitting height reflects the body construction and the buttocks tissue stiffness as well as the body weight in such a way that a thinner person may have smaller value for this parameter and may have stiffer buttocks tissue, the more significant negative correlation between this parameter and the major resonance frequencies can be

explained.

Although there were a few correlations found between some anthropometric parameters and the vibration responses, the investigations did not appear to have controlled other factors affecting the responses. If the posture and the muscle tension of the subjects had been controlled, more correlations might have been found.

2.3.7.5 Non-linearity

The non-linearity, excitation magnitude dependency, was found consistently in the behaviour of the major resonance frequency of the driving point responses, the seat-to-head transmissibility and the seat-to-shoulder transmissibility. The common trend was that decreasing magnitude increased the major resonance frequency although the trend for the second resonance was not clear. It was also found by some investigations that the major resonance shifted more by changes of magnitude in the lower magnitude range than by changes in the higher magnitude range, which looked as if an exponential decay relationship between the excitation magnitudes and the major resonance frequencies. There were also some investigations in which distortion of the response waveform to sinusoidal excitation was presented. The non-linearity in the seat-to-spine transmissibility is not clear: one investigation found the non-linearity of the major resonance shift and two investigations did not find any non-linearity. The non-linearity in the visceral responses is not known.

The exponential decay like relationship between excitation magnitudes and the resonance frequencies is a common non-linearity among soft materials such as rubber and foam. This dynamic non-linearity may be related to the static non-linearities which are seen in the force-deflection relationship of the material as the hysteresis and the upward concave curvature. The non-linearity in the responses could be the indicator to show how much soft material is involved in the resonance behaviour (i.e. vibration mode). Tissue of the human body is known to have more static non-linearity than intervertebral discs have. Therefore, the non-linearity found in the behaviour of the major resonance seems to indicate more contribution to the major resonance from tissue motion such as buttocks tissue deformation and visceral motion than from spinal motion such as spinal bending and axial deformation.

The increase of the major resonance frequency of the driving point impedance under

static acceleration investigated by Vogt *et al.* (1968) could be explained if all the deformable elements of the body such as muscles, viscera and the intervertebral discs of the spine were compressed downwards by the static acceleration and increased their stiffness due to non-linearity (i.e. the static non-linearity which is the curvature in the force-deflection relationship). However, the stiffness of the intervertebral discs is of the order of 10^6 N/m, whereas the stiffness of tissue is of the order of 10^4 N/m. Therefore, the static acceleration probably deformed and stiffened tissue more than the intervertebral discs. The result suggested that the entire body mode due to buttocks tissue deformation or the visceral mode might be more dominant than the bending mode of the lumbar spine at the major resonance.

There is also another explanation for the cause of the non-linearity that high magnitude vibration might force subjects to change the posture and the muscle tension so as to reduce discomfort. However, this explanation can not explain the exponential decay like relationship between excitation magnitudes and major resonance frequencies: the amount of resonance shift should be larger due to changes in the higher magnitude range (i.e. negative exponential like relationship) to be explained by the change of posture or muscle tension to reduce discomfort. The explanation is also contradictory to the result of Vogt *et al.*.

2.4 MODELLING MECHANICAL RESPONSES TO WHOLE-BODY VIBRATION

2.4.1 Introduction

The mechanical responses to whole-body vibration have been modelled using various approaches and techniques. Models are developed so as to interpret the measured responses with a physical and theoretical understanding, to predict the responses which are not easy to measure, and to predict the responses in various conditions which would require vast conditions in a experiment. The dynamic models for the human body can be categorised into three types, which are lumped parameter models, continuum models and discrete models. The lumped parameter models are the models where masses of the human body structure are concentrated into a few lumped masses interconnected by springs and dampers. Configuration of the models does not necessarily correspond to the anatomy and a large idealisation is required to simplify the body structure. The models are usually one dimensional and different models may be constructed for the responses of the same anatomical part in different directions. Although there are quite a lot of limitations,

the lumped parameter models are useful to interpret measured data with a physical and theoretical understanding so that underlying phenomena or mechanism may be found, by focusing only on the phenomena of interest. Calculation of the model responses does not require much computation and model parameters are usually determined, comparing the model responses with experimental data with a limited consideration for the anatomy.

The continuum models and the discrete models may be summarised as distributed parameter models in contrast to the lumped parameter models. The continuum models treat the spine as a homogeneous rod or beam, whereas the discrete models treat the spine as a layered structure of rigid elements representing the vertebral bodies and deformable elements representing the intervertebral discs. Internal stress or strain within the spine in response to vibration or shock may be predicted, using the models, so as to investigate the process of spinal injuries. Both types of model are developed principally based on the anatomy including the geometry of the human body such as the spinal curvature, although idealisations are still required to simplify the real structure. Usually material properties are obtained from cadavers. The recent computer based techniques such as the finite element method have made it possible to create more accurate models in geometry and also to calculate three dimensional responses. However, the more accurate the models become, the more lack of data of the material properties is found. There are also some material properties which are not easy to obtain such as stiffness of live tissue. Therefore, interpolation or extrapolation procedures for unknown parameters are required.

Experimental investigations showed that the vibration responses of the human body such as the driving point responses and the seat-to-head transmissibility revealed non-linear behaviour which was, for example, the resonance shift due to change in an excitation magnitude. Some anatomical components of the human body are also known to show non-linearities: the intervertebral discs are stiffer in compression than in tension and their force-deflection relationships reveal curvature; muscles have stiffness in tension only. Although inclusion of non-linear subsystems or elements in a model made calculation of the responses much more complicated and time consuming, some models incorporated the non-linearities directly. An alternative approach was also taken in some other models by including the effect of non-linearities in linearised model parameters.

This section reviews literature on modelling mechanical responses to whole-body vibration, being divided into four subsections for lumped parameter models, continuum

models, discrete models and discussion. Only the models for the human body exposed to vertical vibration or shock will be reviewed.

2.4.2 Lumped parameter models

Latham (1957) is cited as the first investigator who developed a lumped parameter model for the dynamic response of the spine in the pilot ejection environment. The human body on a seat was modelled by two masses interconnected by a spring (Figure 2.20). The upper mass was regarded as the body mass and the lower mass as the seat mass. The spring represented the combined stiffness of the body and the seat. Latham used the model to explain the behaviour of a pilot on an ejection seat, including the overshoot acceleration phenomenon, and also to analyse the effect of the seat stiffness on the body response in ejection. A similar single degree-of-freedom model for the human body was proposed by Payne (1965) which consisted of a mass representing the head and the upper torso, and a spring and a damper located in parallel representing the spinal column (Figure 2.21). The stiffness and damping of the spinal column were determined based on driving point impedance data. He proposed a dynamic response index (DRI) to predict the peak stress occurring within the spine and probability of spinal injury in pilot ejection. The DRI commences with the idea that the peak stress within the spine is given by:

$$\text{peak stress} = \frac{\text{peak force}}{\text{area}} \qquad \textbf{(2.21)}$$

where: area is that of the cross-section of the spine. It is assumed that the area is proportional to the effective mass of the subject. Therefore:

$$\text{peak stress} \propto \frac{\text{peak force}}{\text{effective mass}} \qquad \textbf{(2.22)}$$

The peak force within the spine is given by the spring stiffness of the spine, k, multiplied by the maximum spring deflection, δ_{max}, such that:

$$\text{peak stress} \propto \frac{k}{m}\delta_{max} \qquad \textbf{(2.23)}$$

Using the natural angular frequency, ω_n, of a single degree-of-freedom system:

$$\text{peak stress} \propto \omega_n^2 \delta_{max} \qquad \textbf{(2.24)}$$

where:

$$\omega_n = \sqrt{\frac{k}{m}} \tag{2.25}$$

The DRI is defined by:

$$\text{DRI} = \frac{\omega_n^2 \delta_{max}}{G} \tag{2.26}$$

where: ω_n=52.9 rad/s (8.42 Hz) is used from a consideration for driving point impedance data; δ_{max} is the response to an input profile given to the base of the model and it is calculated using the damping ratio of 0.225; G is the acceleration due to the gravity.

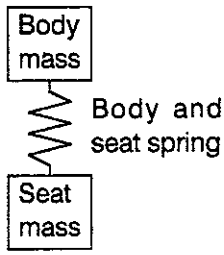

Figure 2.20 A man-seat model for pilot ejection developed by Latham.

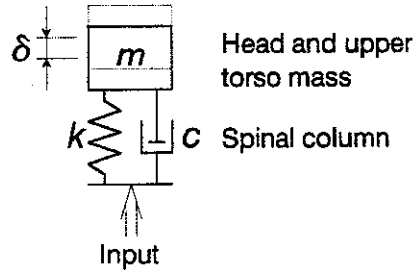

Figure 2.21 A single degree-of-freedom model for DRI developed by Payne.

Suggs *et al.* (1969) found two resonances at about 5 and 8 Hz in the driving point impedance of a sitting subject and, therefore, developed a two degree-of-freedom model. The model had a common rigid frame, from which two uncoupled masses were

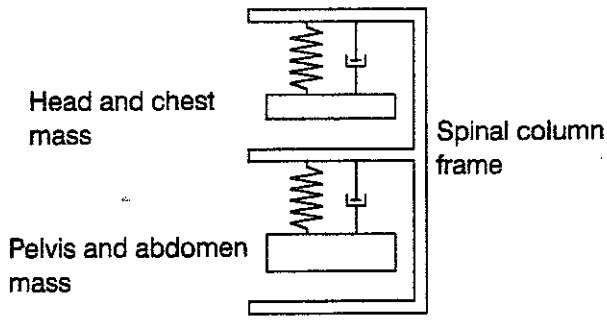

Figure 2.22 A two degree-of-freedom model for seat test developed by Suggs *et al.*.

suspended by springs and dampers (Figure 2.22). The lower mass was larger and represented the pelvis and the abdomen, while the smaller upper mass represented the head and the chest. The frame was analogous to the spinal column. The resonances of the lower and the upper masses corresponded to the 5 Hz and 8 Hz resonances respectively and the model parameters were determined so that the driving point impedance at the base of the rigid frame coincided with the measured impedance of the human body. The authors also transferred the mathematical model to a seat testing dummy which simulated the human loading on a seat to measure the seat transmissibility.

Payne and Band (1971) developed a four degree-of-freedom model. The model consisted of the pelvic mass, visceral mass, upper torso mass and the head mass with springs and dampers interconnecting between the masses (Figure 2.23). The mass distribution of the model was based on the anthropometry and the anatomy. Initial values for stiffnesses were based on data reported in the literature such as *in vivo* force-deflection relationship of the buttocks, the abdominal wall displacement response, *in vitro* force-deflection relationship of the vertebrae and the shoulder-to-head transmissibility. The stiffnesses and the damping ratios were adjusted, comparing the driving point impedance of the model with experimental data. The linear four degree-of-freedom model achieved a good agreement in the driving point impedance with the experimental data below 8 Hz and demonstrated that the major resonance of the driving point impedance at about 5 Hz was dominated by the buttocks stiffness and damping. They finally modified the model by replacing the linear springs for the spine and the buttocks by non-linear springs which possessed polynomial force-deflection relationships similar to the experimental data. It was

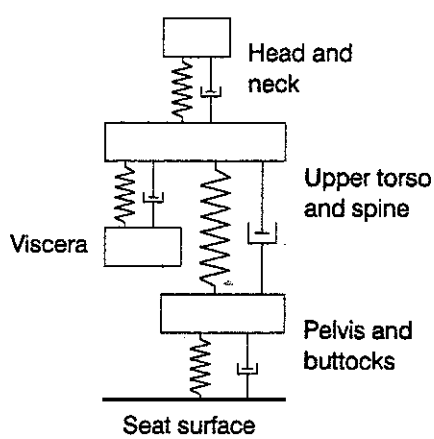

Figure 2.23 A four degree-of-freedom model developed by Payne and Band.

also concluded that the driving point impedance data reflected only the motion of the lower part of the body such as the pelvis and the buttocks, and more data on the response of each body segment would be required to develop a more validated whole body model.

Hopkins (1971) took a consideration for the non-linear behaviour of the abdominal viscera into his three degree-of-freedom non-linear model (Figure 2.24). The model consisted of the upper torso mass, lower torso mass, visceral mass, and springs and dampers interconnecting the masses. Also included in the model was a piston in a cylinder with an orifice interconnecting the upper torso mass and the visceral mass which represented the lungs. The model possessed tension cut-off non-linear connections between the visceral mass and the abdominal wall spring and between the visceral mass and the lung piston, assuming that vertical visceral motion would neither pull down the diaphragm nor pull up the pelvis. The equation of state of air inside the lung cylinder was incorporated into the equation of motion of the model. The model parameters were determined from a consideration for the anthropometry and the anatomy, and also from comparisons of the dynamic responses of the model with corresponding experimental data reported in the literature such as the driving point impedance, the seat-to-head transmissibility, and the abdominal strain and pressure responses. The model produced the non-linear excitation magnitude dependency in the driving point impedance, in which a higher magnitude decreased the modulus of the impedance at most frequencies.

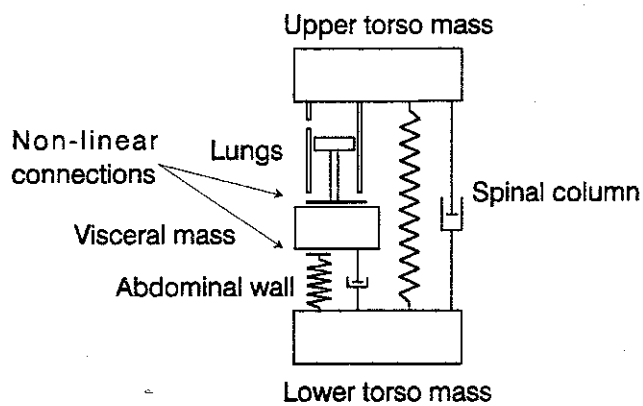

Figure 2.24 A three degree-of-freedom non-linear model developed by Hopkins.

Muksian and Nash Jr. (1974) developed a seven degree-of-freedom non-linear model which included masses for the head, torso, thorax, diaphragm, abdomen, back and the pelvis (Figure 2.25). The mass distribution was based on the anthropometry and the anatomy. The springs and the dampers interconnecting the masses possessed the non-linear polynomial force-deflection and force-velocity relationships except the spinal springs and dampers which were linear. The stiffnesses and damping ratios were determined, comparing the driving point impedance and the seat-to-head transmissibility of the model with experimental data. The model also included the ballistocardiographic force, F_b, and the diaphragm muscle force caused by respiration, F_d, which were modelled by half-sinusoidal pulses and step pulses respectively. The interaction between the ribs and the vertebrae was modelled by coulomb friction force, F_c. The calculated seat-to-head transmissibility of the model had a good agreement with experimental data.

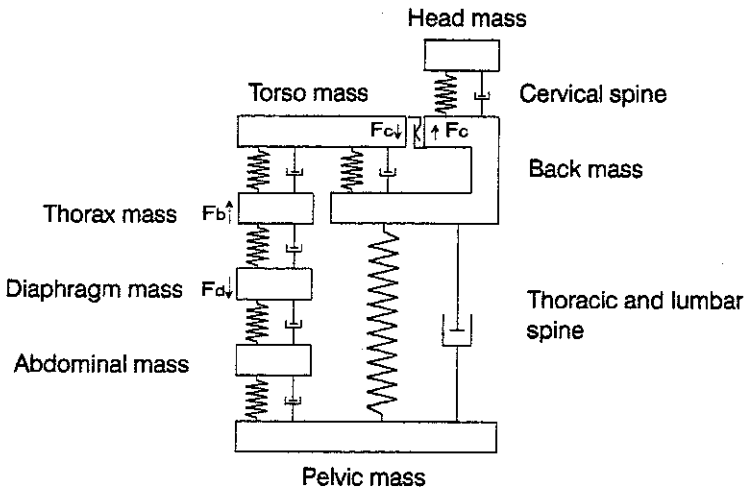

Figure 2.25 A seven degree-of-freedom non-linear model developed by Muksian and Nash Jr..

Mertens and Vogt (1978) proposed a five degree-of-freedom model (Figure 2.26). The model consisted of masses for the head, chest, abdomen, buttocks and some part of the legs. The mass distribution was based on the anthropometry and the anatomy. The stiffnesses for the spinal springs were chosen from the static and dynamic measurements of the spinal responses, and the stiffness for the abdominal spring was chosen from the abdominal pressure response data reported in the literature. The stiffnesses for the remaining parts and all the damping coefficients were estimated, comparing the driving

point impedance and the seat-to-head transmissibility of the model with experimental data. Parameter sets for the stiffnesses and the damping coefficients were estimated separately for the conditions with static vertical acceleration from 1 to 4 g, considering the non-linearity. The model was used to predict the internal force, acceleration and displacement of the various body parts in response to various input acceleration profiles.

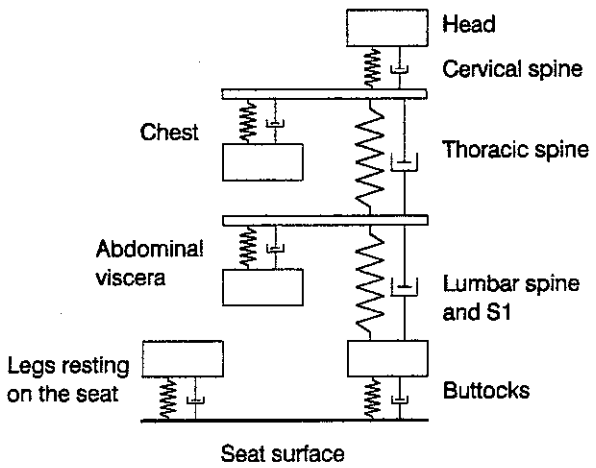

Figure 2.26 A five degree-of-freedom model developed by Mertens and Vogt.

Nigam and Malik (1987) developed a fifteen degree-of-freedom model for a standing human which included masses for the head, neck, upper torso, central torso, lower

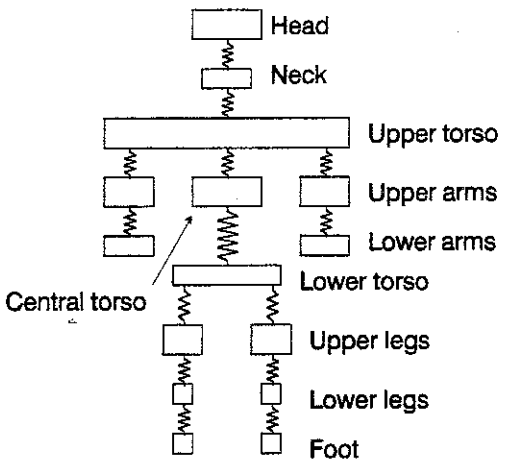

Figure 2.27 A fifteen degree-of-freedom model developed by Nigam and Malik.

torso, upper arms, lower arms, upper legs, lower legs and the feet (Figure 2.27). The whole body was segmented first based on an anthropomorphic model. The mass distribution was estimated from the volume of each segment with an assumption of equal density. The stiffness distribution was determined from geometric mean of the elastic moduli of bones and tissue at each segment. The modal analysis was conducted to estimate the natural frequencies. A total of eleven modes was calculated with the lowest natural frequency at 13.82 Hz. No comparison of the model responses with experimental data was made.

Amirouche and Ider (1988) developed a three dimensional model which consisted of 13 rigid and flexible segments interconnected to one another by spherical, revolve and free joints (Figure 2.28). The geometrical data were based on those of the Part 572 and Hybrid III dummies for car crash testing. The stiffnesses and dampings were adjusted, comparing the calculated driving point impedance with experimental data. The natural frequencies were found at 2.2, 4.9, 13.8 and 16.7 Hz below 20 Hz. The model succeeded to produce close driving point impedance and seat-to-head transmissibility to experimental data.

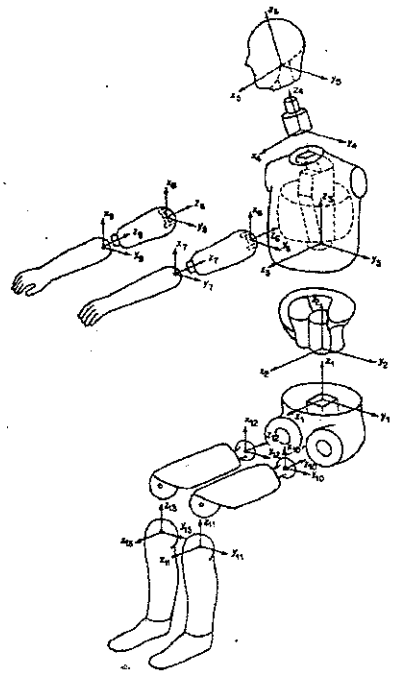

Figure 2.28 A three dimensional human model with 13 body segments developed by Amirouche and Ider.

The International Standard 5982 (1981) includes a two degree-of-freedom model for calculating the driving point impedance of the human body in sitting and standing positions (Figure 2.29). The International Standard 7962 (1987) includes a four degree-of-freedom model for calculating the seat-to-head transmissibility of the human body in sitting and standing positions (Figure 2.30).

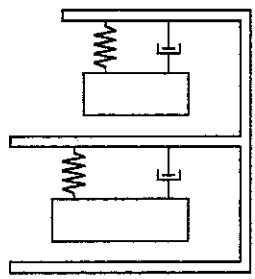

Figure 2.29 A two degree-of-freedom model for calculating the driving point impedance of the human body in sitting and standing positions given in International Standard 5982.

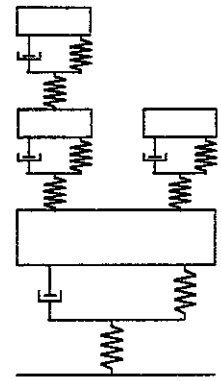

Figure 2.30 A four degree-of-freedom model for calculating the seat-to-head transmissibility of the human body in sitting and standing positions given in International Standard 7962.

2.4.3 Continuum models

Hess and Lombard (1958) are considered to be the first investigators who studied the longitudinal wave propagation in the spine. They modelled the head and the trunk by an uniform homogeneous elastic rod (Figure 2.31). Vertical accelerations at the head and a seat in ejection were measured in an experiment. Model parameters were determined comparing the measured acceleration responses at the head with calculated acceleration time histories at the free upper end of the rod in response to measured seat acceleration profiles which were given to the lower end of the rod. The model produced similar responses at the head to the experimental data within a short period of time after ejection. The discrepancy between the model responses and the measured responses at later times was explained by lack of damping in the model. A problem of the common maximum acceleration criterion for spinal injuries was raised and a maximum stress criterion was established in terms of acceleration rise time at an ejection seat.

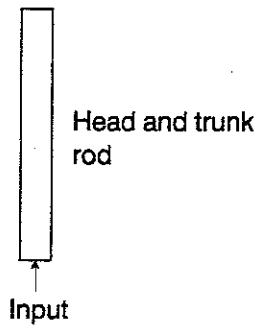

Figure 2.31 An uniform homogeneous elastic rod for the head and the trunk developed by Hess and Lombard.

Liu and Murray (1966) modified the model of Hess and Lombard by adding a head mass at the upper end of the uniform homogeneous elastic rod (Figure 2.32). The rod represented the human torso from the lumbar to the neck. The study was concentrated on theoretical formulation of the model response and the model parameters seemed to have been chosen arbitrarily. They investigated the longitudinal wave propagation and calculated the stress distribution in response to an axial step acceleration input. The effect of damping was studied. However, inclusion of the damping term did not affect the response largely except that it increased the stress in the lumbar region slightly. The authors also considered a non-linear effect by treating the speed of wave propagation as dependent on the displacement, and found that the non-linear term increased the stress significantly. It was concluded that the stress and the acceleration in the spine were

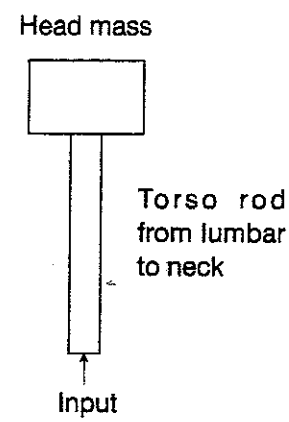

Figure 2.32 An uniform homogeneous elastic rod for the torso with a head mass developed by Liu and Murray.

different and the maximum acceleration criterion for spinal injuries should be replaced by the maximum stress criterion. The authors additionally demonstrated the applicability of the model to the whiplash problem associated with car collisions. The longitudinal rod of the model would be replaced by a two dimensional beam possessing the bending stiffness of the torso for that purpose.

Li *et al.* (1971) took a consideration for the spinal curvature in their continuum model so as to investigate both the axial and bending responses of the spine in the mid-sagittal plane. The model consisted of a sinusoidally curved beam, representing the spine from the upper lumbar region to the cervical region, with the upper end fixed to a head mass (Figure 2.33). The spinal beam possessed a constant cross section which was determined, considering the additional contribution of the supporting vertebral structure. The torso mass was uniformly distributed along the length of the beam. The material properties and the geometrical data were chosen from the literature on measurement of compressive wave propagation in the spine, measurement of the natural frequency of the spine, and compression and bending tests of the intervertebral discs. The elastic moduli for the spinal beam was adjusted to be larger than the reported static values so as to take account of the body weight preload and the non-linear curvature in the force-deflection relationships of the isolated intervertebral discs. The calculated undamped compressive wave velocity and the axial natural frequency were 36.6 m/s and 13.5 Hz respectively. The force and stress caused by the axial and bending deformation of the spine were calculated in response to an axial step acceleration given to the lower end of the spinal beam. It was predicted that the axial force was reduced by 25 % due to the presence of the initial spinal curvature and that the axial force and stress distribution were

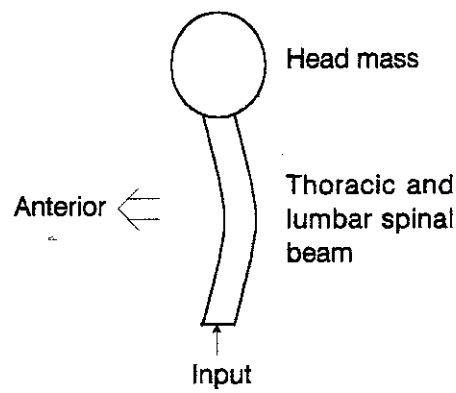

Figure 2.33 A curved spinal beam with a head mass developed by Li *et al.* .

significantly influenced by the bending deformation of the spine. The model was also used by Moffatt *et al.* (1971) with more reliable flexural rigidity data for the thoraco-lumbar spinal beam measured by the authors themselves. It was concluded that the flexure was an essential factor in assessing spinal injuries.

Krause and Shirazi (1971) modelled the lumbar spine by a curved beam with a thoracic mass placed at the upper end so as to investigate the bending responses of the spine in the mid-sagittal plane to an axial force input given to the lower end of the spinal beam (Figure 2.34). Experimental observations showed that the amplitude of the second derivative of the transverse displacement of the thoracic spine of a sitting subject in response to vertical vibration in the frequency range from 10 to 40 Hz was almost zero. This finding indicated that bending deformation hardly existed in the thoracic spine and, therefore, only the lumbar spine was modelled. No transverse displacement and no bending moment was assumed at the lower end of the spinal beam which corresponded to the pelvis. The spinal curvature was represented by a Fourier sine series. Only a theoretical investigation was conducted without substituting material properties and geometrical data into the formulation. They demonstrated that both the initial spinal curvature and the initial axial load due to the thoracic mass affected the natural frequencies and the bending deformations of the lumbar spine. It was also found that the bending moment distribution along the spine (i.e. the second derivative of the deformation) coincided with the statistic incidence curves for injuries along the spine.

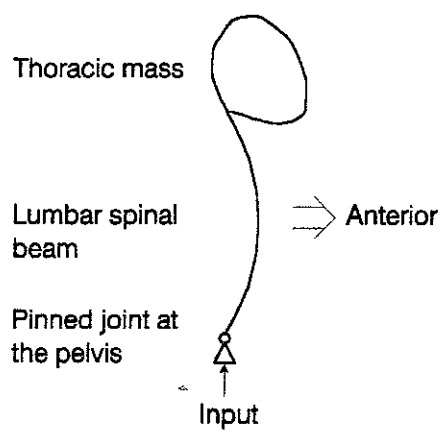

Figure 2.34 A curved spinal beam with a thoracic mass developed by Krause and Shirazi.

Mass centres of the torso segments are located anterior to the spine due to the presence of the rib cage and the viscera. Cramer *et al.* (1976) took a consideration for the distributed eccentric inertial loading of the torso into their curved spinal beam representing the vertebrae from L5 to C1 so as to investigate both the axial and bending responses of the spine in the mid-sagittal plane (Figure 2.35). The upper end of the spinal beam was connected to a head mass and the lower end was constrained by a pinned joint representing the lumbosacral junction. The geometrical data and the inertial properties were derived from an earlier experimental work of the authors in which a frozen cadaver was sliced at each vertebral level so as to measure the inertial properties of each torso segment. The area of the cross-section and the flexural rigidity of the spinal beam were treated as functions of the spinal height so as to take account of stiffness distribution along the spine. The stiffness data were chosen from *in vitro* measurements in the literature. The time histories for the spinal deformation, axial force, shear force and bending moment were calculated in response to an axial acceleration input given to the bottom of the spine for the pilot ejection problem. The bending moment distribution along the spine was found to coincide well with the statistic incidence curves for injuries along the spine.

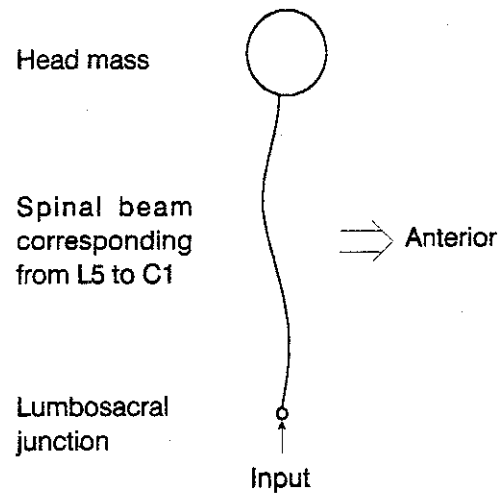

Figure 2.35 A curved spinal beam with a head mass and a distributed eccentric inertial loading of the torso developed by Cramer *et al.*.

2.4.4. Discrete models

Toth (1966) was the first investigator who modelled each vertebra separately. His eight degree-of-freedom non-linear model consisted of masses for the vertebrae from T12 to L5 and masses for the body above T12 and below L5 placed on a seat mass (Figure 2.36). The springs and dampers interconnecting masses represented the intervertebral discs except the lowest ones which represented the buttocks tissue. The stiffnesses and dampings were based on anatomical data and the non-linearity was incorporated into the intervertebral disc springs. The model was used to predict the force response at each vertebra to various input acceleration profiles so as to simulate the pilot ejection environment. It was concluded that the failure of an upper lumbar and/or thoracic vertebra was theoretically possible without vertebral column bending.

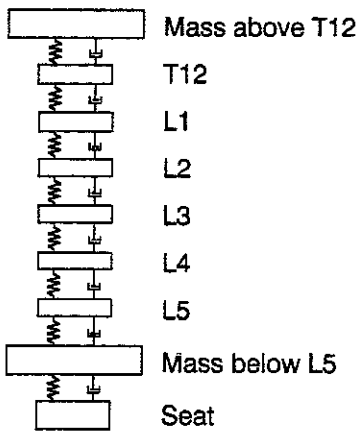

Figure 2.36 An eight degree-of-freedom non-linear model developed by Toth.

Orne and Liu (1971) developed a model which included the initial curvature of the spine and the eccentric inertial loading caused by the head and the trunk. The model consisted of all the vertebrae from L5 to C1 and a head mass fixed to the upper end of the spine (Figure 2.37). The spine was modelled by a layered structure of rigid links representing the vertebral bodies and deformable beams representing the intervertebral discs. Each disc beam could deform in the axial, shear and bending directions so as to simulate complete two dimensional response of the spine in the mid-sagittal plane. Each vertebra was assumed to support a distributed slice of the torso mass located at some eccentricity. Therefore, the spinal links and beams were massless and the mass centres of the torso

segments were located anterior to the spine. The angle of the spine at the bottom was assumed to be determined by the pelvic angle and a typical value was used. A large part of the material properties and geometrical data was unknown and the model construction had to be simplified, including uniform torso mass distribution and constant mass eccentricities along the spine. Time histories for the spinal deformation, axial force, shear force and bending moment at several spinal levels were calculated in response to vertical acceleration input so as to study the pilot ejection problem. It was concluded that the effect of bending deformation due to the presence of the spinal curvature was appreciable.

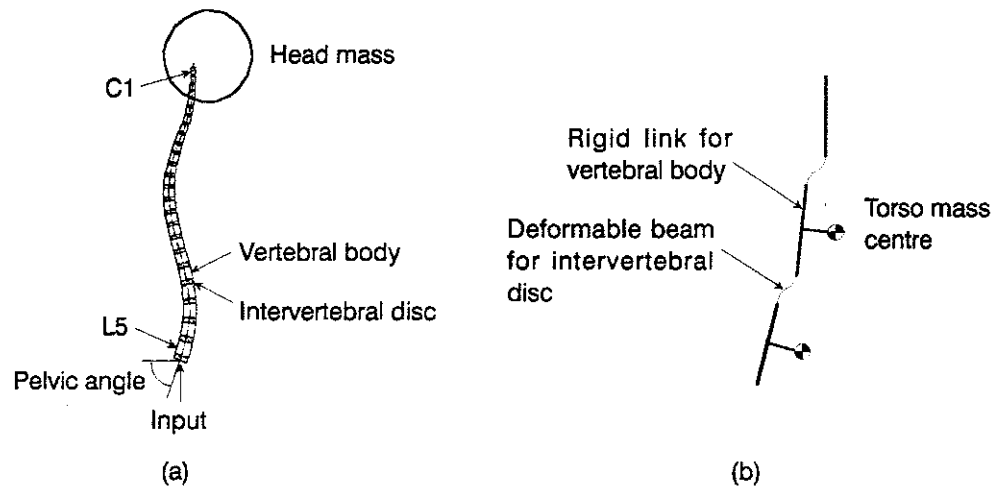

Figure 2.37 A discrete spine model with a head mass developed by Orne and Liu; (a) entire configuration; (b) connection between adjacent vertebrae.

Prasad and King (1974) extended the model of Orne and Liu by including the articular facet interaction in their discrete spine model as an additional load path in the spine in parallel with the main load path through the intervertebral discs. The articular facet interaction was modelled by two springs connected to the adjacent vertebral bodies via massless rigid links, one limiting relative rotation and the other limiting relative sliding of the vertebrae caused by bending and shear deformations of the intervertebral disc (Figure 2.38). Geometrical data were adopted from X-ray observations of cadavers. At the end of the experiment, the cadavers were frozen and sliced so as to measure the inertial properties of the torso segments. The stiffnesses for the intervertebral discs and the articular facets were based on the literature and missing data were assumed. The stiffnesses for the discs were increased from the reported data of the isolated intervertebral discs so as to take account of the non-linear force-deflection relationships of the discs and the additional resistance due to the presence of the rib cage for the

thoracic spine. The cadavers were exposed to vertical acceleration input given to the pelvis so as to simulate the pilot ejection environment. The response forces between adjacent vertebral bodies were measured to be compared with the model predictions. The effect of posture (i.e. spinal curvature) was also investigated by comparing the responses in erect and hyperextended postures and found to be significant. The predictions coincided well with the measurements.

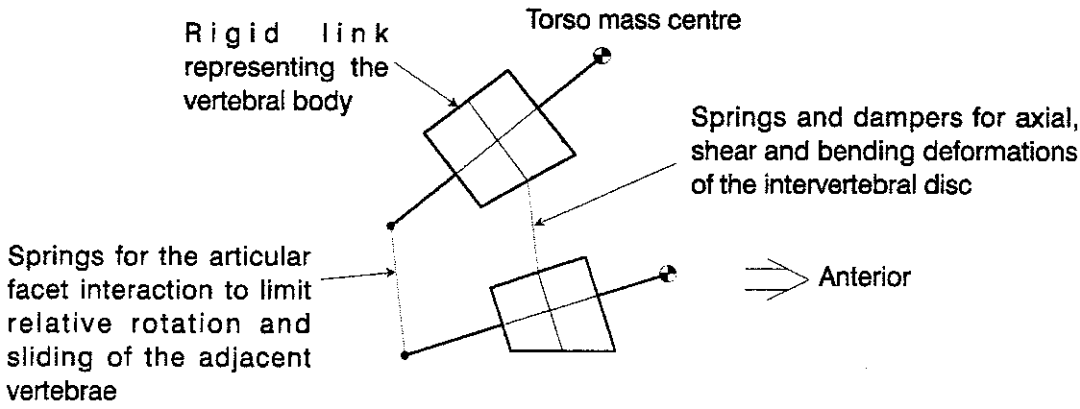

Figure 2.38 Configuration of adjacent vertebrae in a discrete spine model with head and pelvic masses developed by Prasad and King.

Belytschko *et al.* (1976) developed a highly anatomical three dimensional discrete model which consisted of the spine, ribs, head, pelvis and the viscera (Figure 2.39). The vertebral bodies from L5 to C2 were modelled by massless rigid bodies. Adjacent vertebral bodies were connected by a massless beam representing the intervertebral disc and five springs representing the connective ligaments (i.e. a pair of the intertransverse ligaments, a combination of the inter- and supra-spinous ligaments and a pair of the ligamenta flava) and a pair of springs representing the articular facet interaction in the thoracolumbar spine, whereas each pair was connected by a intervertebral disc beam, a single spring representing the interspinous ligament and a pair of hydrodynamic elements representing the articular facet interaction in the cervical spine. The intervertebral disc beams were given axial, bending and torsional stiffnesses. The ligament springs were non-linear featured by no resistance in compression. The model included the eccentric inertial loading of the torso by locating corresponding torso segmental masses anterior to the vertebral bodies following the model of Orne and Liu. A stack of the hydrodynamic elements, possessing axial stiffness only, was used to model the viscera. The bottom of

the viscera was connected to the pelvis and the top was connected to the lowest ribs at the level of the vertebra T10. Each rib was modelled by a rigid body and connected to the rigid sternum and to two vertebral bodies via deformable elements. The head and the pelvis were modelled by rigid bodies possessing all four inertial properties. Geometry and material properties were derived from the literature and missing data were interpolated, using geometrical scales. The bulk modulus of the hydrodynamic element for the viscera was determined so that the wave speed would coincide with the experimental value. The model was developed to analyse the pilot ejection problem. The modal analysis was also conducted for the modes in the mid-sagittal plane. It was found that the dominant mode in the low frequency range below 20 Hz was the bending mode of the spine: a total of seven bending modes was extracted below 20 Hz, whereas only one axial mode was found at 17 Hz. The authors also predicted that the major peak seen in the driving point impedance data at about 5 Hz corresponded to the fourth bending mode of the spine. The vibration mode shapes were not shown.

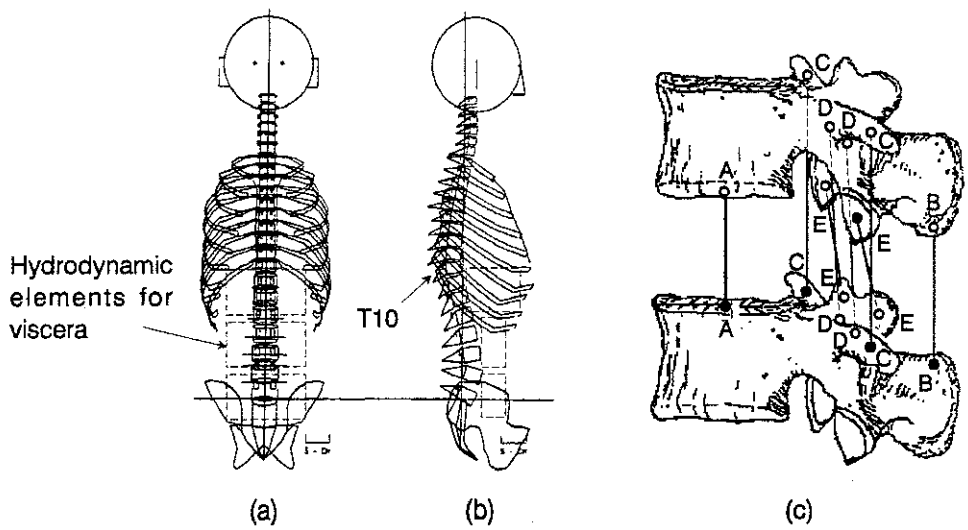

Figure 2.39 A discrete spine model with the ribs, head, pelvis and the viscera developed by Belytschko *et al.*; (a) front view; (b) side view; (c) connection between adjacent vertebrae in the thoraco-lumbar region (distance is exaggerated) (A-A; intervertebral disc beam, B-B; interspinous and supraspinous ligaments spring, C-C; intertransverse ligament springs, D-D; ligamentum flavum springs, E-E; articular facet interaction springs).

Belytschko *et al.* (1978) and Belytschko and Privitzer (1978a) subsequently modified the model into series of models with wide range of complexity. The material properties were also revised. The stiffnesses for the intervertebral discs in the lumbar spine were increased

so as to account for the effect of body weight preload acting on the discs which possessed non-linear force-deflection relationships. The visceral subsystem was totally reestablished (Figure 2.40). The torso segmental masses were divided into the spinal masses and visceral masses in the region below the level of the vertebra T10 (i.e. corresponding to the diaphragm level), using the graphical data of the torso cross-sections with an assumption of a uniform density. The visceral masses were restricted to move only in the longitudinal direction and interconnected by springs with the top connected to the vertebra T10 via a rigid link and the bottom connected to the pelvis. Each visceral mass was also connected to the corresponding torso mass with a horizontal spring to represent the viscera-spine interaction. The stiffnesses for the visceral interconnecting springs were determined so that the visceral resonance would be produced at 3.5 Hz. The stiffnesses for the viscera-spine horizontal springs were adjusted, comparing the driving point impedance of the model with experimental data. Validation of the models was conducted comparing the driving point impedance of the models with experimental data in successive papers (Belytschko and Privitzer (1978a,b) and Privitzer and Belytschko(1980)).

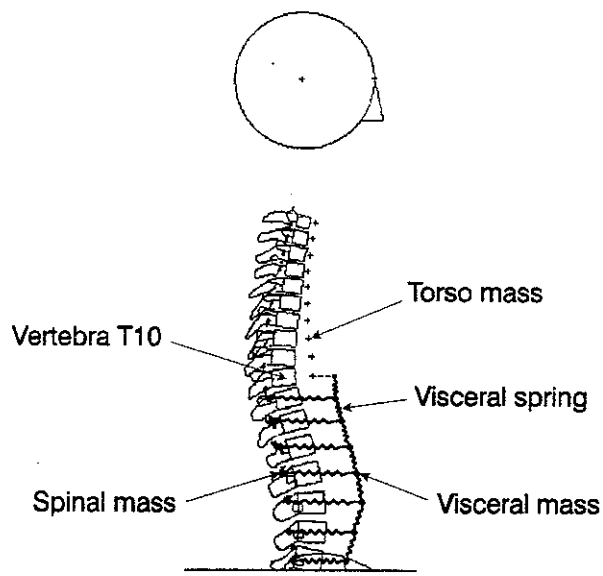

Figure 2.40 A discrete spine model with the modified viscera developed by Belytschko and Privitzer.

A simplified model was developed by Belytschko and Privitzer (1978b) as the last of the series of models for the whole body dynamics so as to save computation time. The model may be classified as a continuum model from the treatment of the spine. However, it is

cited here in sequence of the developing history. The spine was divided into four segments, for the vertebrae from C2 to T1, from T1 to T10, from T10 to L3 and from L3 to S1, and beam elements were assigned to the four spinal segments (Figure 2.41). The visceral masses were lumped into three masses and they were interconnected by springs between the pelvis and a rigid link placed at the T10 level. The visceral masses were also connected to the spinal beams by horizontal springs. All the geometrical data and the material properties were transformed from those for the previous precise models. The model was validated comparing the calculated driving point impedance with experimental data. The comparison reached a finding of necessity for an additional spring for the buttocks tissue and a vertical spring was placed beneath the pelvic mass. The driving point impedance produced by the simplified model with the buttocks spring coincided well with the experimental data. It was concluded that the major resonance of the impedance at about 5 Hz corresponded to a combination of the rigid body mode of the spine caused by axial buttocks deformation, the first axial mode of the viscera and the third bending mode of the spine. It was also found that the first axial mode of the spine occurred at about 13 Hz and the second visceral mode at about 9 Hz. Subsequently an intensive effort was made to refine the cervical spine by Williams and Belytschko (1981, 1983) and Belytschko *et al.* (1985) so as to analyse the pilot ejection injuries. The geometry and the material properties were revised and the articular facet interaction and connective ligaments and muscles were modelled more precisely in the cervical region.

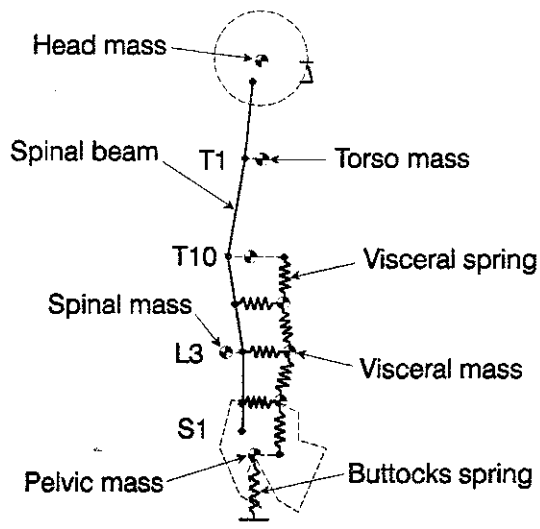

Figure 2.41 A simplified spine model with the head, pelvis, viscera and the buttocks developed by Belytschko and Privitzer.

2.4.5 Discussion

A large number of biodynamic models have been developed and this literature review does not include everything. However, the main developing histories of the three types of biodynamic models have been reviewed. The lumped parameter models were developed so as to investigate the responses of the human body to vibration with low magnitudes as well as to high acceleration shock such as pilot ejection. Choice of model configuration was rather arbitrary depending on the type and the degree of idealisation of the human body and an infinite number of models could be proposed. Considerations for the anatomy and anthropometry were limited and model parameters were determined, principally comparing the model responses such as the driving point impedance and the seat-to-head transmissibility with experimental data. However, because the model parameters were not equally sensitive to the body responses as Payne and Band (1971) suggested, they did not always seem to be optimal values indicating the anatomical parameters especially in the later models with many degrees of freedom.

The lumped parameter models are useful when they are developed, focusing on a few phenomena of interest. The seat testing dummy developed by Suggs *et al.* (1969) was a good example. The model, which was transferred to the dummy finally, was developed only to simulate the driving point behaviour at the seat-buttocks interface and the degrees of freedom were chosen to be necessary and sufficient from observation of the experimental data. Although anatomical interpretation for the model configuration was stated by the authors, the model was principally based on the experimental data and quite useful in a dynamic seat test to avoid inter-subjective variability of human subjects to load seats. The later lumped parameter models tended to have much more degrees of freedom. However, there were not always justification and validation for the model configuration and the model parameters. The models tended to lose the original advantages of the approach and it seemed that such models should be replaced by the continuum or discrete models based on the anatomy.

The obvious disadvantage of the lumped parameter models lay in the fact that the models were mainly one dimensional except some. Investigations using the continuum and discrete models reached a conclusion that the bending deformation of the spine played an important role in the total response of the human body as well as the axial deformation. However, it was not easy to model the coupled responses of the axial and bending deformations of the spine with the lumped parameter models and majority of the models

were developed for the axial response only.

The continuum models and the discrete models were developed mainly for predicting spinal injuries caused by pilot ejection with high acceleration shock. The development for those two types of model followed the same history at the early stage, beginning with a consideration for only the axial deformation of the spine and successively featured by inclusion of the spinal curvature, bending deformation of the spine and eccentric inertial loading of the torso. The discrete models progressed further by including the articular facet interaction, intervertebral ligaments and other subsystems such as the viscera which were difficult to be treated in the continuum models. The continuum models required more idealisations, such as homogeneity for the spinal beam, than the discrete models but their responses were easier to calculate. The development of the models also has been dependant on the development of mathematical methods to construct governing equations of motion for the spine-like structures and to solve those equations. There were some investigators who developed mathematical methods for calculating the responses of the spinal structure which was constructed in the discrete manner (Schultz and Galante (1970) and Panjabi (1973)). The recent computer based techniques, including the finite element method, have enabled the models to include more accurate geometry and, as a result, more degrees of freedom in the two dimensional or even in the three dimensional space.

One of the advantages of the discrete models was that the material properties could be chosen directly from the anatomical data. The models were constructed by assembling the anatomical parts with material and geometrical properties piece by piece. This process was quite different from that for the lumped parameter models in which the model parameters were usually identified by comparing the responses with experimental data. However, as the models became more accurate in geometry, they tended to include more anatomical parts separately and lack of data for the material properties became an obstacle for further development. Belytschko *et al.* (1978) interpolated the unknown stiffness data for some intervertebral discs from known data for others using the geometrical scales. They also estimated the stiffness for the visceral subsystem so that its natural frequency coincided with experimental data of the torso wall. These approaches will be required unless the material properties of all the necessary anatomical parts were obtained.

The driving point impedance was used to validate majority of the lumped parameter

models and some of the continuum and the discrete models. However, as Payne and Band (1971) pointed out, the driving point impedance at the seat-buttocks interface hardly reflected the motion of the upper body parts, due to the heavy damping of the human body structure, and its major resonance at about 5 Hz might be dominated by the buttocks tissue spring. Therefore, the validation using the driving point impedance was not exhaustive. Some continuum and discrete models were validated, comparing the model responses with the acceleration responses on the body of subjects or cadavers in ejection. The statistic incidence curves for injuries along the spine in ejection were also compared with the force or bending moment distribution along the spine predicted by some models. The responses of the human body to vibration with low acceleration magnitudes may be different from those to high acceleration shock. Because the human responses are usually non-linear and large deformation caused by shock may include additional deformation or resistance of some other subsystems such as the ribs and the articular processes. A sufficiently validated model for low magnitude vibration was not found.

Non-linear elements or components were incorporated in quite a few lumped parameter models, such as the non-linear force-deflection relationships of the intervertebral discs and tissue, the tension cut-off behaviour of the viscera between the pelvis and the diaphragm, the coulomb friction between the ribs and the vertebrae and the air flow caused by the diaphragm and the lungs. However, the effectiveness of incorporation of the non-linear elements were not clear. Some of the continuum models and the discrete models also included the non-linear force-deflection relationships. Majority of the models incorporated it into the increased (linearised) stiffnesses to account for the increment due to the non-linear force-deflection relationships and the body weight preload. Although the recent sophisticated computer based techniques can cope with inclusion of non-linear elements, this linearisation approach is still useful to save computation time and the number of necessary material properties.

The biodynamic modelling approach has proven its tremendous value to uncover underlying mechanisms in responses of the human body to vibration or shock, which may not be possible to be found through experiments. However, at the same time, it still has much more potential for discovering further and deeper understandings in this field through more sophisticated and more validated models. There are also other types of models such as anthropometric models, car crash models, micro-component finite element models for vertebrae, models of animals and so on. Models can be different

depending on the purpose of use and it is not necessary to develop a fully comprehensive model. An idealistic model should be well validated and should include necessary and sufficient complexity to investigate the problem of interest. Such a model may be a hybrid model of the lumped parameter, continuum and discrete types.

2.5 CONCLUSIONS FROM LITERATURE REVIEW

Because of the difficulty of measuring the dynamic responses of the human body accurately at the desired body parts and the complexity of the human body structure with unknown material properties and geometry, the two approaches of measurement and modelling will be complementary and achieve a fundamental understanding of the mechanical responses to whole-body vibration. Five questions have been raised from the literature review on measurement. The first question is what the vibration mode shapes for the major resonance (between 4 and 6 Hz) and the second resonance (between 8 and 12 Hz) of the human body are. Because those two resonances produce large response magnitudes, their adverse effects on health, activities and comfort may be large. It is the primary interest to find how the body responds (deforms) at the resonances. The major resonance was hypothesised as a combination of vertical entire body motion caused by pelvic rotation or buttocks tissue deformation, bending motion of the lumbar spine, fore-and-aft and pitching motion of the head, and vertical motion of the viscera. The second resonance was not as clear as the major resonance in most cases but hypothesised to contain vertical motion of some parts of the body and bending motion of the spine. However, there is no data proving the hypotheses. The second question is how changes in posture affect the vibration mode shapes and how they shift the major resonance of the body. The third question is how changes in muscle tension affect the vibration mode shapes and how they shift the major resonance of the body. It is also important to understand the effect of posture so that the adverse effects of whole-body vibration may be minimised by optimising the posture. The effects of posture and muscle tension on the responses appeared similar and both effects were largely dependent on the subject. The mechanism for the resonance shifts has not yet been known. The fourth question is how the anthropometric parameters correlate with the vibration responses. Although a few correlations were found, more correlations should be expected to explain the inter-subject variability in the vibration responses. Finally, the fifth question is how changes in excitation magnitude shift the major resonance of the body (i.e. a non-linearity). The excitation magnitude dependency of the responses is important when the laboratory data are

applied to practical situations. Although the effect of excitation magnitude was found consistently, the mechanism for the resonance shift has not yet been known.

The literature review on modelling has concluded that a distributed parameter model such as a continuum model and a discrete model or maybe a hybrid model is required to answer the above questions and there is no such a model with sufficient validation available. The desired model also should be based on reliable anatomical data for its material properties and the geometry. Validation should be conducted, using dynamic responses at various body parts, because the energy of distant body parts from a measuring site of a response tends to be dissipated by the heavy damping of the body and the measured response does not contain information of motion of such body parts. The driving point impedance and the seat-to-head transmissibility have been commonly used for validation of the models. However, it should be noted that those validations were limited for the body parts around the pelvis and around the head-neck region respectively. Some investigations into the spinal responses through both measurement and modelling found that bending mode of the spine was an important factor in the total body response. Therefore, experimental data for bending modes of the whole spine, if it is possible to obtain, will be quite useful to validate the biodynamic models.

The following research will be concentrated on the first and the second questions mentioned above as a first step. Answering the third and the fourth questions will require modelling muscles and tissue of the body, whose material properties are most difficult to obtain, and it may be possible to answer the first and the second questions, avoiding incorporating those elements separately into the model. Although the recent computer based modelling techniques can cope with some non-linearities, inclusion of non-linear elements require more computation time and more material properties. The non-linear material properties with preload dependence caused by the cubic force-deflection relationships will be treated through the linearising procedure by increasing stiffnesses for some elements. However, the non-linear excitation magnitude dependency of the responses is difficult to handle. If it is related to the hysteresis of the force-deflection relationships (N.B. not the linearised hysteretic damping) as discussed in section 2.3.7.5, there is no theory available to incorporate its effect yet. This non-linearity can be linearised when considering the responses of the human body to limited excitation magnitude range.

CHAPTER 3

MODELLING MECHANICAL RESPONSES TO WHOLE-BODY VIBRATION: PART 1

3.1 INTRODUCTION

From the literature review, several questions were raised. The research was started with modelling work. The literature review concluded that a model required to answer the questions would be a distributed parameter model such as a continuum model, a discrete model, and a hybrid model of those two types. The simplified model developed by Belytschko and Privitzer (1978b) was chosen as a model with which the modelling work would be started, because it was based on the most reliable geometrical data and material properties, and most reasonable assumptions. The simplified model also allowed a large freedom for theoretical modifications. In this chapter, the theoretical fundamentals are summarised first, then, more dynamic responses of the simplified model are calculated. Subsequently, two models are developed, comparing predicted responses with experimental data reported in the literature.

3.2 THEORY

3.2.1 The finite element method and Ansys

The finite element method treats a structure as an assemblage of components of simple elements such as rods, beams, plates and shells, and the matrices involved in the equations of motion for individual elements are derived based on the energy equations. The matrices for the equations of motion for the complete structure can be simply formed by assembling obtained matrices for individual elements, considering the geometrical boundary conditions (see Appendix 2).

There are a number of computer programs for the finite element method which construct the matrices for the equations of motion automatically and then calculate the responses, solving the equation. In such programs the geometry of the structure is defined by the locations of nodes which also divide the structure into elements. The programs usually include an element library from which users can simply choose desired types of elements

with specific material properties. In this research the biodynamic models are constructed, using Ansys-PC/Linear 4.4 (Swanson Analysis Systems, Inc.) on a PC computer.

3.2.2 Modal analysis

When the equations of motion for a structure are constructed, the modal analysis is conducted to determine the natural frequencies and the vibration mode shapes in Ansys. The equations of motion for free vibration of an undamped system can be written in a matrix form:

$$[M]\{\ddot{x}(t)\} + [K]\{x(t)\} = 0 \qquad \textbf{(3.1)}$$

where: [*M*] is the *NxN* symmetric mass matrix; [*K*] is the *NxN* symmetric stiffness matrix; $\{\ddot{x}(t)\}$ and $\{x(t)\}$ are the *Nx1* nodal acceleration and displacement vectors; *N* is the number of degrees of freedom.

Since the motion is harmonic, the displacement can be assumed:

$$\{x(t)\} = \{\phi\} \sin \omega t \qquad \textbf{(3.2)}$$

Substituting equation (3.2) into (3.1):

$$[K - \omega^2 M]\{\phi\} = 0 \qquad \textbf{(3.3)}$$

Equation (3.3) describes a classical eigenvalue problem. The eigenvalues $\omega_1^2, \omega_2^2, \ldots, \omega_N^2$ are obtained by letting the determinant of the matrix in equation (3.3) equal zero:

$$|K - \omega^2 M| = 0 \qquad \textbf{(3.4)}$$

The quantities $\omega_1, \omega_2, \ldots, \omega_N$ correspond to the first *N* natural frequencies. Substituting an obtained eigenvalue, ω_r^2, into equation (3.3), an associated eigenvector $\{\phi\}_r$ is obtained. The eigenvector $\{\phi\}_r$ corresponds to the vibration mode shape vector for the *r*th mode.

The mode shape vectors possess the property of orthogonality such that:

$$[\Phi]^T[M][\Phi] = [m_R] \qquad \textbf{(3.5a)}$$

$$[\Phi]^T[K][\Phi] = [k_R] \qquad \textbf{(3.5b)}$$

where: [Φ] is the modal matrix whose columns are mode shape vectors ([Φ]=[$\{\phi\}_1$, $\{\phi\}_2, \ldots, \{\phi\}_N$]; [$m_R$] and [$k_R$] are diagonal matrices referred to as the modal mass and modal stiffness matrices respectively.

Since any arbitrarily scaled value of $\{\phi\}_r$ satisfies equation (3.3), mode shape vectors can

be mass-normalised so that the modal mass is unity for each mode:

$$[\Phi]^T[M][\Phi] = [I] \tag{3.6a}$$

$$[\Phi]^T[K][\Phi] = [\omega_r^2] \tag{3.6b}$$

where: [I] is the identity matrix; $[\omega_r^2]$ is the diagonal matrix of square of angular natural frequencies. Ansys employs the Householder-Bisection-Inverse iteration technique to solve equation (3.3), then calculates the mode shape vectors satisfying equation (3.6).

3.2.3 Harmonic Response Analysis

3.2.3.1. Mode-superposition method

The harmonic response analysis calculates various transfer functions of the human body such as the driving point impedance or apparent mass and the acceleration transfer functions from the seat to the head or from the seat to the spine. The equations of motion for the harmonic response analysis are:

$$[M]\{\ddot{x}(t)\} + [K]\{x(t)\} = \{F\}e^{i\omega t} \tag{3.7}$$

where: $\{F\}$ is the applied nodal force amplitude vector; ω is the angular excitation frequency. The solution of equation (3.7) is complicated by the presence of the off-diagonal terms within the mass and stiffness matrices which couple the equations of motion. Ansys uses the mode-superposition technique for the harmonic response analysis which requires the modal analysis to be performed in advance. The orthogonality of the mode shape vectors shown in equations (3.5) and (3.6) enables the mode shape vectors to construct a new coordinate system, termed modal coordinates. The mode-superposition technique transforms the equations of motion into modal coordinates using equation (3.8) so that the equations of motion may be decoupled:

$$\begin{aligned}\{x(t)\} &= \sum_{r=1}^{N} \{\phi\}_r y_r(t) \\ &= [\Phi]\{y(t)\}\end{aligned} \tag{3.8}$$

where: $\{y(t)\}$ is the modal generalised displacement vector; N is the total number of degrees of freedom or the number of modes.

Substituting equation (3.8) into equation (3.7), pre-multiplying by $[\Phi]^T$, and using equation (3.6), a set of decoupled equations (3.9) is obtained:

$$\{\ddot{y}(t)\} + [\omega_r^2]\{y(t)\} = [\Phi]^T\{F\}e^{i\omega t} \quad \textbf{(3.9)}$$

Although a viscous damping element is available in Ansys, there are no reliable damping data found for the human body. Therefore, the damping effect was included through the use of effective damping ratio (modal viscous damping) at each mode. In this case, equation (3.9) becomes equation (3.10) with a damping term:

$$\{\ddot{y}(t)\} + [C]\{\dot{y}(t)\} + [\omega_r^2]\{y(t)\} = [\Phi]^T\{F\}e^{i\omega t} \quad \textbf{(3.10)}$$

$$[C] = [2\omega_r\zeta_r] \quad \textbf{(3.11)}$$

where: $[C]$ is the diagonal matrix of $2\omega_r\zeta_r$; ω_r is the rth natural angular frequency; ζ_r is the effective damping ratio for the rth mode. Equation (3.10) can be separated into individual equations for each mode because they are decoupled:

$$\ddot{y}_r(t) + 2\omega_r\zeta_r\dot{y}_r(t) + \omega_r^2 y_r(t) = \{\phi\}_r^T\{F\}e^{i\omega t} \quad \textbf{(3.12)}$$

Equation (3.12) can be easily solved, by substituting $y_r(t)=Y_re^{i\omega t}$:

$$Y_r = \frac{\{\phi\}_r^T\{F\}}{\omega_r^2 - \omega^2 + 2i\zeta_r\omega_r\omega} \quad \textbf{(3.13)}$$

Substituting $y_r(t)$ into equation (3.8) and letting $\{x(t)\}=\{X\}e^{i\omega t}$, the nodal displacement is determined:

$$\{X\} = \sum_{r=1}^{N} \frac{\{\phi\}_r^T\{F\}\{\phi\}_r}{\omega_r^2 - \omega^2 + 2i\zeta_r\omega_r\omega} \quad \textbf{(3.14)}$$

Equation (3.14) describes that the nodal displacement is expressed by superposing the mode shape vectors.

3.2.3.2 Driving point impedance and apparent mass

The driving point impedance, Z_{jj}, is defined in the frequency domain as:

$$Z_{jj}(f) = \frac{F_j(f)}{V_j(f)} = \frac{F_j(f)}{i\omega X_j(f)} \quad \textbf{(3.15)}$$

where: $F_j(f)$ is the Fourier transform of the applied force at node j; $V_j(f)$, $X_j(f)$ are the Fourier transforms of the velocity and displacement at the force applied node j; ω is the angular excitation frequency ($\omega=2\pi f$). Therefore, the driving point impedance is calculated, substituting the displacement of the appropriate node determined by equation (3.14) into

equation (3.15).

The driving point apparent mass, $M_{jj}(f)$, is calculated from the impedance, $Z_{jj}(f)$, using the relationship (3.16):

$$M_{jj}(f) = \frac{F_j(f)}{A_j(f)} = \frac{Z_{jj}(f)}{i\omega} \tag{3.16}$$

where: $A_j(f)$ is the Fourier transform of the acceleration at the force applied node j.

3.2.3.3 Acceleration transfer function

The acceleration transfer function, $T_{jk}(f)$, is calculated from the displacements of two nodes, $X_j(f)$, and, $X_k(f)$, which are obtained from equation (3.14):

$$T_{jk}(f) = \frac{A_k(f)}{A_j(f)} = \frac{X_k(f)}{X_j(f)} \tag{3.17}$$

where: $A_j(f)$ and $A_k(f)$ are the Fourier transforms of the acceleration at two nodes j and k. Therefore, the acceleration transfer function is calculated, substituting the displacements of the appropriate nodes determined by equation (3.14) into equation (3.17).

3.2.4 Master degrees of freedom

In general, some of the degrees of freedom are very often only of secondary importance in modelling using the finite element method. The analysis can be conducted more efficiently if these unwanted degrees of freedom are eliminated. Ansys allows users to define only important degrees of freedom as the master degrees of freedom and reduce matrices by a technique known as Guyan reduction to save computation time.

3.2.5 Additional considerations for the human body structure

3.2.5.1 Modal analysis

A seated human has a contact with seat surface via the soft tissue of the buttocks. The mass of buttocks tissue may be negligible, compared with the mass of the rest of the whole body system. Therefore, a seated human is equivalent to a model shown in Figure 3.1.

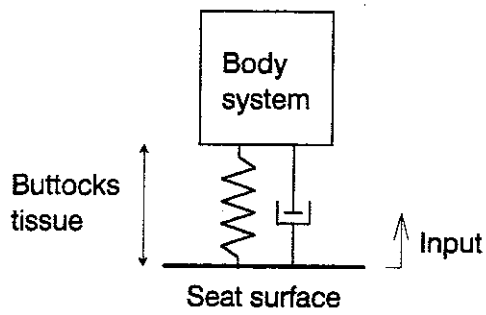

Figure 3.1 Equivalent model for a seated human.

In Ansys 'force applied nodes' must have masses and the directions of the forces must be defined as the master degrees of freedom. However, if a mass is placed at the seat-buttocks interface, the dynamic response will be different from the response of the model shown in Figure 3.1. This problem can be solved by locating an additional large mass at the force applied node. To make the problem easier, two simple systems, System 3.1 and System 3.2, in Figures 3.2 and 3.3 are considered.

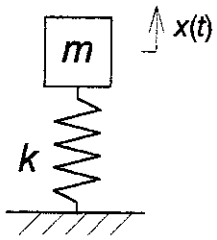

Figure 3.2 System 3.1 for modal analysis.

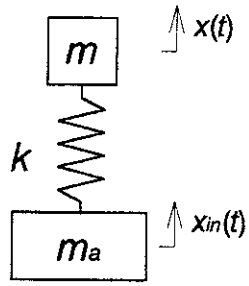

Figure 3.3 System 3.2 for modal analysis.

The equation of motion for System 3.1 is:

$$m\ddot{x}(t) + kx(t) = 0 \qquad \textbf{(3.18)}$$

Substituting $x(t)=Xe^{i\omega t}$, equation (3.19) is obtained:

$$(-\omega^2 m + k)X = 0 \qquad \textbf{(3.19)}$$

The eigenvalue of equation (3.19), $\omega^2_{sys3.1}$, is calculated by letting $(-\omega^2 m+k)=0$:

$$\omega^2_{sys\ 3.1} = \frac{k}{m} \tag{3.20}$$

The angular natural frequency of System 3.1, $\omega_{sys3.1}$, is:

$$\omega_{sys\ 3.1} = \sqrt{\frac{k}{m}} \tag{3.21}$$

On the other hand, the equations of motion for System 3.2 are:

$$m_a \ddot{x}_{in}(t) + k(x_{in}(t) - x(t)) = 0 \tag{3.22a}$$

$$m\ddot{x}(t) + k(x(t) - x_{in}(t)) = 0 \tag{3.22b}$$

Equation (3.22) can be written in a matrix form:

$$[M]\{\ddot{x}\} + [K]\{x\} = 0 \tag{3.23}$$

where:

$$[M] = \begin{bmatrix} m_a & 0 \\ 0 & m \end{bmatrix} \qquad [K] = \begin{bmatrix} k & -k \\ -k & k \end{bmatrix}$$

$$\{\ddot{x}\} = \begin{Bmatrix} \ddot{x}_{in}(t) \\ \ddot{x}(t) \end{Bmatrix} \qquad \{x\} = \begin{Bmatrix} x_{in}(t) \\ x(t) \end{Bmatrix} \tag{3.24}$$

Substituting $x_{in}(t)=X_{in}e^{i\omega t}$, $x(t)=Xe^{i\omega t}$ into equation (3.23), equation (3.25) is obtained:

$$([K] - \omega^2[M])\{X\} = 0 \tag{3.25}$$

where:

$$\{X\} = \begin{Bmatrix} X_{in} \\ X \end{Bmatrix} \tag{3.26}$$

The eigenvalues of equation (3.25), $\omega^2_{sys3.2}$, are calculated by letting the determinant of the matrix equal zero:

$$\left|[K] - \omega^2[M]\right| = 0 \tag{3.27}$$

Therefore:

$$\omega^2_{sys3.2} = \frac{(m_a + m)k}{m_a m}, \quad 0 \tag{3.28}$$

The angular natural frequencies of System 3.2, $\omega_{sys3.2,}$ are:

$$\omega_{sys\ 3.2} = \sqrt{\frac{(m_a + m)k}{m_a m}}, \quad 0 \tag{3.29}$$

System 3.2 has a zero-frequency mode because there is no constraint. The zero-frequency mode can be ignored.

When $m_a >> m$, the equation (3.29) yields:

$$\lim_{m_a \to \infty} \omega_{sys3.2} = \omega_{sys3.1} \tag{3.30}$$

Therefore, when the additional mass placed at the force applied node (i.e. the seat-buttocks interface) is large enough, compared with the total mass of the body, the natural frequencies will be close to those of the system without the additional mass. Validation of the method was conducted, comparing the natural frequencies of System 3.1 and System 3.2 calculated using Ansys and the theoretical solution for System 3.1. Used parameters and the results are shown in Table 3.1, where the error was evaluated using equation 3.31.

$$\text{Error of natural frequency} = \frac{|\text{calculated value} - \text{theoretical value}|}{\text{theoretical value}} \times 100 \tag{3.31}$$

When the additional mass is large enough, the calculated natural frequency of System 3.2 is close to the calculated natural frequency of System 3.1 and the theoretical solution.

Table 3.1 Validation for the effect of an additional large mass placed at the force applied node.

	Ansys calculation			Theory
Parameters	System 3.1	System 3.2		System 3.1
		case 1	case 2	
k (N/m)	3.5×10^4	3.5×10^4	3.5×10^4	3.5×10^4
m (kg)	50	50	50	50
m_a (kg)	0	1000	10000	0
Natural frequency (Hz)	4.211	4.315	4.221	4.213
Error (%)	0.05	2.4	0.2	——

3.2.5.2 Harmonic response analysis

In the harmonic response analysis, all the responses are calculated using equation (3.14), where mode shape vectors are obtained from the system with the additional mass at the load applied node due to the reason mentioned above. The effect of the additional mass

can be subtracted from the responses eventually. Systems 3.1 and 3.2 are considered again. They are shown in Figures 3.4 and 3.5 for the harmonic response analysis.

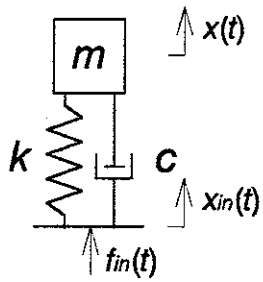

Figure 3.4 System 3.1 for harmonic response analysis.

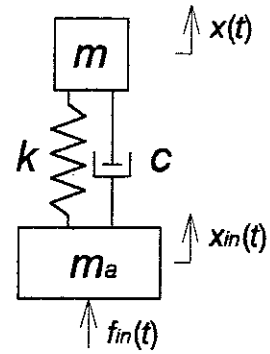

Figure 3.5 System 3.2 for harmonic response analysis.

For System 3.1, the force is simply in equilibrium with the reaction force from the spring and the damper. The equations of motion for System 3.1 are:

$$m\ddot{x}(t) + c(\dot{x}(t) - \dot{x}_{in}(t)) + k(x(t) - x_{in}(t)) = 0 \qquad \textbf{(3.32a)}$$

$$f_{in}(t) = c(\dot{x}_{in}(t) - \dot{x}(t)) + k(x_{in}(t) - x(t)) \qquad \textbf{(3.32b)}$$

Substituting $x(t)=Xe^{i\omega t}$, $x_{in}(t)=X_{in}e^{i\omega t}$ and $f_{in}(t)=F_{in}e^{i\omega t}$ into equation (3.32), equation (3.33) is obtained:

$$-\omega^2 mX + ic\omega(X - X_{in}) + k(X - X_{in}) = 0 \qquad \textbf{(3.33a)}$$

$$F_{in} = ic\omega(X_{in} - X) + k(X_{in} - X) \qquad \textbf{(3.33b)}$$

Solving equation (3.33), the driving point impedance for System 3.1, $Z_{sys3.1}$, is obtained:

$$Z_{sys\,3.1} = \frac{F_{in}}{i\omega X_{in}} = \frac{im\omega(ic\omega + k)}{-m\omega^2 + ic\omega + k} \qquad \textbf{(3.34)}$$

On the other hand, the equations of motion for System 3.2 are:

$$m_a\ddot{x}_{in}(t) + c(\dot{x}_{in}(t) - \dot{x}(t)) + k(x_{in}(t) - x(t)) = f_{in}(t) \qquad \textbf{(3.35a)}$$

$$m\ddot{x}(t) + c(\dot{x}(t) - \dot{x}_{in}(t)) + k(x(t) - x_{in}(t)) = 0 \qquad \textbf{(3.35b)}$$

Equations (3.35) can be written in a matrix form:

$$[M]\{\ddot{x}\} + [C]\{\dot{x}\} + [K]\{x\} = \{f\} \qquad \textbf{(3.36)}$$

where:

$$[M]=\begin{bmatrix} m_a & 0 \\ 0 & m \end{bmatrix} \quad [C]=\begin{bmatrix} c & -c \\ -c & c \end{bmatrix} \quad [K]=\begin{bmatrix} k & -k \\ -k & k \end{bmatrix}$$

$$\{\ddot{x}\}=\begin{Bmatrix} \ddot{x}_{in}(t) \\ \ddot{x}(t) \end{Bmatrix} \quad \{\dot{x}\}=\begin{Bmatrix} \dot{x}_{in}(t) \\ \dot{x}(t) \end{Bmatrix} \quad \{x\}=\begin{Bmatrix} x_{in}(t) \\ x(t) \end{Bmatrix} \tag{3.37}$$

Substituting $x(t)=Xe^{i\omega t}$, $x_{in}(t)=X_{in}e^{i\omega t}$, $f_{in}(t)=F_{in}e^{i\omega t}$ into equation (3.36), equation (3.38) is obtained:

$$(-\omega^2[M]+i\omega[C]+[K])\{X\}=\{F\} \tag{3.38}$$

where:

$$\{X\}=\begin{Bmatrix} X_{in} \\ X \end{Bmatrix} \quad \{F\}=\begin{Bmatrix} F_{in} \\ 0 \end{Bmatrix} \tag{3.39}$$

Solving equation (3.38), the driving point impedance for System 3.2, $Z_{sys3.2}$, is obtained:

$$Z_{sys\,3.2}=\frac{F_{in}}{i\omega X_{in}}=\frac{im\omega(ic\omega+k)}{-m\omega^2+ic\omega+k}+im_a\omega \tag{3.40}$$

The impedance of the additional mass, Z_{ma}, is:

$$Z_{m_a}=im_a\omega \tag{3.41}$$

The relationship of the driving point impedance between System 3.1 and System 3.2 is:

$$Z_{sys\,3.1}=Z_{sys\,3.2}-Z_{m_a} \tag{3.42}$$

Therefore, the driving point impedance of a system without the additional mass can be obtained by subtracting the impedance of the additional mass from the impedance of the system with the additional mass. The driving point apparent mass can be calculated using equation (3.16) after the subtraction. The modulus of the apparent mass can be normalized, by dividing it by the static mass (sitting weight) as proposed by Fairley and Griffin (1989).

The acceleration transfer functions of System 3.1 and System 3.2 are obtained from equations (3.33) and (3.36):

$$T_{sys3.1}=\frac{X}{X_{in}}=\frac{ic\omega+k}{-m\omega^2+ic\omega+k}=T_{sys3.2} \tag{3.43}$$

Therefore, the additional mass does not affect the acceleration transfer functions.

3.3 MODEL 1: SIMPLIFIED MODEL BASED ON BELYTSCHKO'S MODEL

3.3.1 Model description

The model was based on the simplified model developed by Belytschko and Privitzer (1978). Although their model was three dimensional, the model in this research was constructed in the two dimensional space of the mid-sagittal plane for the primary interest. Beam, spring and mass elements were used to model the spine, viscera, head, pelvis and buttocks tissue. The arms and the thighs were not directly modelled but the effects of their masses were considered. The simplified model was entirely linear although the real human structure had non-linear characteristics such as, cubic force-deflection curves of the lumbar discs, and tension cut-off of the intervertebral ligaments and muscles with no compression resistance. Belytschko *et al.* (1976) incorporated some of these non-linearities directly in their discrete models. However, in the simplified model, only the effect of the cubic force-deflection relationships of the discs and body-weight preload was included in the increased stiffness values for the lumbar spine. The model had only 18 nodes and 19 master degrees of freedom so that the response could be quickly calculated by a small computer and would be suitable for parametric study.

The spinal column was modelled by four beam elements representing the vertebrae from C2 to T1, T1 to T10, T10 to L3 and L3 to S1. The spinal beams were given axial and bending stiffnesses but no mass. Each vertebra was assumed to be embedded in the associated horizontal torso segment, therefore, the mass centre of each torso segment had an anterior eccentricity from the spinal column (Orne and Liu, 1970). The translational and rotational masses of the torso segments for the vertebral levels from T1 to T10 were lumped into mass elements at the T1 and T10 levels, which were connected to the spinal beam by horizontal massless rigid links. Below the T10 level (diaphragm level), the torso segmental masses were initially divided into the spinal masses and the visceral masses at each level. The spinal masses in this region were concentrated on a mass element placed at the L3 level, whereas the visceral masses were lumped into three mass elements at the levels of L1, L3 and L5.

The motion of the viscera was assumed to occur only in the axial direction. The visceral column was modelled by three mass elements with translational and rotational inertia at the L1, L3 and L5 levels interconnected by spring elements. The bottom of the visceral column was connected to the pelvic mass by a massless rigid link, and the top connected

to the spinal beam at the T10 level also by a massless rigid link representing the pair of the lowest complete ribs. The interaction between the viscera and the spine was modelled by horizontal spring elements interconnecting the visceral masses and the spinal beams at the levels of L1, L3 and L5.

The head and the pelvis were simply replaced by mass elements with translational and rotational inertia and connected to the top of the spinal column at the C2 level and to the bottom of the spinal column at the S1 level by massless rigid links. Buttocks tissue was modelled by a spring element and placed vertically beneath the pelvic mass. Figure 3.6 shows the simplified model. The outline of the skull and the pelvis are drawn in Figure 3.6 to assist interpretation.

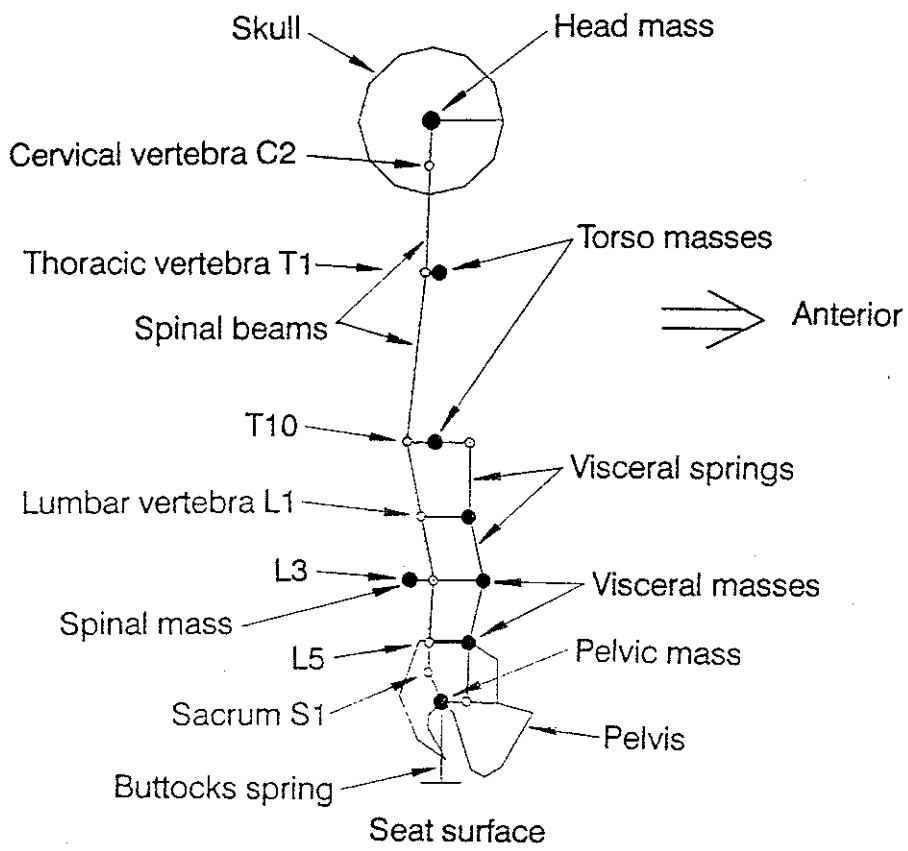

Figure 3.6 Model 1: Simplified model.

3.3.2 Geometry and material properties

Geometry

The geometry of the initial spinal curvature was based on the radiographic data of seated pilots obtained by Belytschko *et al.* (1976). This curvature was considered to be an almost erect posture. Node locations for the spinal beams corresponded to the geometrical centres of the vertebral bodies at the levels of C2, T1, T10, L3 and S1. The overall length of the thoraco-lumbar spine was 0.486 m (0.604 m for the whole spine from the vertebra C2 to the sacrum S1), which corresponded closely to that of an average American male.

Node locations for the torso masses above the T10 level coincided with the mass centres of the corresponding torso segments reported by Liu and Wickstrom (1973). Below the T10 level, the torso segmental masses were initially divided into the spinal masses and the visceral masses at each level and they were located so that the mass centres coincided with those of the corresponding torso segments. Only the node for the spinal mass at the L3 level and the three nodes for the visceral masses at the levels of L1, L3 and L5 were chosen for the simplified model. Table 3.2 shows the node locations.

Table 3.2 Node locations for the simplified model.

Level	Spinal column ($m \times 10^{-2}$)		Torso or spinal mass ($m \times 10^{-2}$)		Visceral column ($m \times 10^{-2}$)	
	x [1]	z	x	z	x	z
Head	-0.083	63.605	—	—	—	—
C2	-0.284	56.792	—	—	—	—
T1	-0.631	45.044	0.720	45.044	—	—
T10	-3.123	24.449	0.108	24.449	5.092	24.449
L1	-1.155	15.265	—	—	5.092	15.265
L3	0.461	7.726	-2.920	7.726	6.898	7.726
L5	0.0	0.0	—	—	4.984	0.0
S1	-0.189	-3.164	—	—	—	—
Pelvis	1.577	-7.195	—	—	4.984	-7.195

(1) The coordinate system has x-axis for the fore-and-aft and z-axis for the vertical directions.

Inertial data

Inertial properties of the torso were based on the data of Liu and Wickstrom (1973). In the region from the T1 to T10 levels, the translational and rotational masses of the torso segments were summed to two mass elements placed at the levels of T1 and T10, using the parallel axes theorem for the rotational masses. In the lower torso region below the T10 level (diaphragm level), the translational and rotational masses of the torso segments were divided into the visceral masses and the spinal masses at each level by Belytschko and Privitzer (1978) based on the graphical data of the torso cross-sections obtained by Eycleshymer and Shoemaker (1970), using an assumption of uniform density of 1 g/cm^3. The average percentage of the spinal mass associated with the mass of the corresponding torso segment was about 20 %. For the simplified model, the translational and the rotational spinal masses were summed to a single mass element placed at the L3 level, whereas the translational and the rotational visceral masses were lumped into three mass elements placed at the levels of L1, L3 and L5, using the parallel axes theorem for the rotational masses. The translational mass of the upper arms was added to the translational mass at the T1 level.

Inertial properties of the head and the pelvis were based on the data of Bartz (1972). A half of the translational mass of the thighs was added to the translational mass of the pelvis because vibration of some parts of the thighs will occur when exposed to vertical vibration in a sitting position. Table 3.3 shows the inertial data. The total mass of the simplified model was 68.8 kg, which corresponded to the total body weight of about 88 kg, 19.2 kg being for the legs not included in the model.

Stiffness data

The vertebral bodies were assumed to be rigid and, therefore, the spinal beams represented the elasticity of the intervertebral discs, intervertebral ligaments and the articular facet interaction. The axial and bending stiffness data for the intervertebral discs were primarily based on the data of Schultz *et al.* (1973) which summarised data from various investigations. The axial stiffness values for the intervertebral discs in the lumbar region were modified by Belytschko *et al.* (1978) to be increased to account for the effect of the cubic force-deflection relationships of the discs and body-weight preload. In the thoracic and the cervical region, the stiffness values were based on the data obtained from isolated spines, because a small non-linearity was seen in the force-deflection

Table 3.3 Inertial properties for the simplified model.

Level	Head, torso and pelvis		Viscera	
	Translational mass (kg)	Rotational mass[1] (kg m^2 x 10^{-2})	Translational mass (kg)	Rotational mass[1] (kg m^2 x 10^{-2})
Head	5.612	4.479	—	—
C2	—	—	—	—
T1	Torso 5.591 Arms 6.894	Torso 2.773	—	—
T10	6.846	5.328	—	—
L1	—	—	5.134	2.576
L3	1.660	0.400	3.368	1.203
L5	—	—	4.295	1.272
S1	—	—	—	—
Pelvis	Pelvis 16.20 Thighs/2 13.20	Pelvis 12.80	—	—

(1) Rotational mass around the mass centre.

relationships of the discs in this region. The stiffnesses for the intervertebral ligaments and the articular facet interaction seemed to be determined arbitrarily because no reliable data was found. The stiffnesses for the spinal beams of the simplified model were determined by summing series combinations of stiffnesses for the intervertebral discs, intervertebral ligaments and the articular facet interaction at each vertebral level.

In general, there are following relations between axial and bending stiffnesses of a beam, and its material property and geometry:

$$F = k_A \lambda \qquad k_A = \frac{EA}{L} \tag{3.44}$$

$$M = k_B \theta \qquad k_B = \frac{EI}{L} \tag{3.45}$$

where: F is the axial force; λ is the axial deflection; k_A is the axial stiffness; M is the moment in the sagittal plane; θ is the rotation in the sagittal plane; k_B is the bending stiffness; E is Young's modulus; A is the area of the cross-section; I is the second moment of area of the cross-section; L is the length. For the vibration response analysis of interest,

specification of the cross-sections would not affect the results. Therefore, the cross-sectional areas of the spinal beams were determined, assuming circles for the cross-sections with diameters shown in Table 3.4 which corresponded to approximate sizes of the intervertebral discs. The axial and bending stiffnesses for the spinal beams are shown in Table 3.5. Young's modulus, E, is calculated for each spinal beam by substituting the axial stiffness, k_A, in Table 3.5, cross-sectional area, A, and the length, L, of the beam in Table 3.4 into equation (3.44). The second moment of area of the cross-section, I, is obtained for each spinal beam by substituting the bending stiffness, k_B, in Table 3.5, calculated Young's modulus, E, and the length of the beam, L, in Table 3.4 into equation (3.45).

Table 3.4 Geometry of the spinal beam elements.

Spinal beams	Length (L) ($m \times 10^{-2}$)	Diameter ($m \times 10^{-2}$)	Area (A) ($m \times 10^{-4}$)
C2 - T1	11.76	2.0	3.142
T1 - T10	20.75	3.0	7.069
T10 - L3	17.10	4.0	12.57
L3 - S1	10.77	5.0	19.63

Because the spine is several orders of magnitude stiffer than the viscera, it is the primary path of vibration transmission from the seat to the upper torso and the head. However, the viscera in the abdominopelvic cavity transmits some of the vibration to the upper torso through the diaphragm located at the lowest pair of the complete ribs. The visceral vibration is also considered to contribute to the driving point responses. The visceral stiffness data were not based on the anatomy but largely on assumptions. Firstly, only the axial motion was assumed to transmit vibration through the viscera. Secondary, the stiffness was determined so that the visceral resonance would coincide with that measured by Coermann *et al.* (1960), assuming the viscera-abdominal wall system as a one-dimensional uniform rod (Belytschko and Privitzer 1978).

The relation between the resonance frequency and the natural frequency of a damped single degree-of-freedom system is:

$$f_r = f_n \sqrt{1 - 2\zeta^2} \qquad \textbf{(3.46)}$$

where: f_r is the resonance frequency, f_n is the natural frequency, ζ is the damping ratio. Using the value of 0.5 for the damping ratio of the viscera, the resonance frequency of the

abdominal wall displacement response at 3.5 Hz measured by Coermann *et al.* is transferred to the natural frequency at 5 Hz. If the viscera-abdominal wall system is assumed as a one-dimensional uniform rod fixed to the pelvis and the diaphragm at the both ends, the fundamental natural frequency is given by:

$$f_n = \frac{c}{2L} \tag{3.47}$$

where: L is the length of the visceral rod; c is the longitudinal wave speed through the viscera. The longitudinal wave speed is given by:

$$c = \sqrt{\frac{B}{\rho}} \tag{3.48}$$

where: B is the effective bulk modulus of the viscera; ρ is the density (1 g/cm^3). Substituting equation (3.48) into (3.47) yields:

$$B = (2Lf_n)^2 \rho \tag{3.49}$$

With the length of the visceral column (L=0.3164 m), the density of the viscera (ρ=1.0 x 10^3 kg/m^3) and the natural frequency (f_n=5 Hz), the bulk modulus B yields 1.0 x 10^4 N/m^2. Therefore, the stiffness of the visceral element is determined by the relationship:

$$k_v = \frac{AB}{L} \tag{3.50}$$

where: A is the cross-sectional area of the viscera. The visceral stiffness at each vertebral level was calculated, substituting area of the torso cross-sections, A, (Eycleshymer and Shoemaker, 1970), the obtained bulk modulus, B, and the height of the segment, L, into equation (3.50), and they were summed to four springs for the simplified model. Stiffness value for the horizontal springs was determined by Belytschko and Privitzer (1978), comparing the driving point impedance of the model with the experimental data of Vogt *et al.* (1968). Stiffness for buttocks tissue was based on the data of Payne (1971). Table 3.5 shows the stiffness data.

Damping data

Although a viscous damping element was available in Ansys, it was not directly used in the model because no reliable damping data were found. The effect of damping on the transfer functions was included through the use of the effective damping ratio (modal viscous damping) at each mode (see section 3.2.3.1). The effective damping ratios used

were 0.35 for the third and the fifth modes and 0.25 for all the remaining modes.

Table 3.5 Stiffness data for the simplified model.

Spine			Viscera	
Level	Axial stiffness ($N/m \times 10^4$)	Bending stiffness (Nm)	Level	Axial stiffness ($N/m \times 10^4$)
C2-T1	14.40	68.9	—	—
T1-T10	15.40	6.70	—	—
T10-L3	34.70	21.5	T10-L1	0.88
			L1-L3	1.03
L3-S1	56.80	34.3	L3-L5	0.83
			L5-Pelvis	0.54

For all the viscera-spine interconnecting springs:
stiffness = 1.0×10^4 N/m.
For buttocks spring: stiffness = 6.55×10^4 N/m.

3.3.3 Calculation conditions

A large mass of 1000 kg was placed at the lower end of the buttocks tissue spring (seat-buttocks interface) for the vertical excitation force to be applied at this node, according to the consideration mentioned in section 3.2.5.1. The master degrees of freedom were defined as the vertical, fore-and-aft and rotational (sagittal plane) directions at the nodes for the mass elements for the head, torso masses, spinal mass and the pelvis. They were defined as only the vertical direction at the nodes for the visceral masses and the large mass placed at the lower end of the buttocks tissue spring. In the harmonic response analysis, all the extracted modes below 50 Hz were used for the mode-superposition method (see section 3.2.3.1) and the applied vertical force was with a magnitude of 1 N at every 0.1 Hz increment up to 50 Hz. The magnitude was chosen to make the calculation of various transfer functions easier, because it would not affect the transfer functions in linear systems. The same calculation conditions will be used for all the following models in this chapter.

3.3.4 Results and discussion

A total of eleven modes was calculated below 20 Hz in the modal analysis. The calculated natural frequencies and the mode shapes are shown in Table 3.6 and Figure 3.7. It was found that the vibration modes below 20 Hz were dominated by bending modes of the spine, visceral modes and a buttocks mode. The axial modes of the spine were calculated by constraining bending deformation of the spinal beams. The lowest axial mode of the spine was found at 14.69 Hz (Figure 3.8) which appeared to be included in the 9th mode at 12.57 Hz and the 10th mode at 13.35 Hz without the constraint in Figure 3.7.

Table 3.6 Natural frequencies of the simplified model.

Mode No.	Natural frequency (Hz)	Mode No.	Natural frequency (Hz)
1	0.83	7	8.69
2	2.41	8	10.78
3	3.88	9	12.57
4	4.30	10	13.35
5	5.78	11	18.54
6	7.17		

The response of the simplified model calculated using Ansys in this research was compared with the response calculated by Belytschko and Privitzer (1978). Some difference was seen between the two responses (Figure 3.9), which may have been caused by different calculation procedures, including incorporation of the damping effect. The calculated impedance curve was also compared with the experimental data of Vogt *et al.* (1968) in Figure 3.9. Although the model in this research produced a similar curve to the data above 7 Hz, the calculated frequency of the principal resonance of the impedance located between 3.5 and 4 Hz was smaller than the experimental result. The difference of the principal resonance frequency was seen more clearly in the comparison of the driving point apparent mass between the model calculation and the experimental data of Fairley and Griffin (1989) (Figure 3.10).

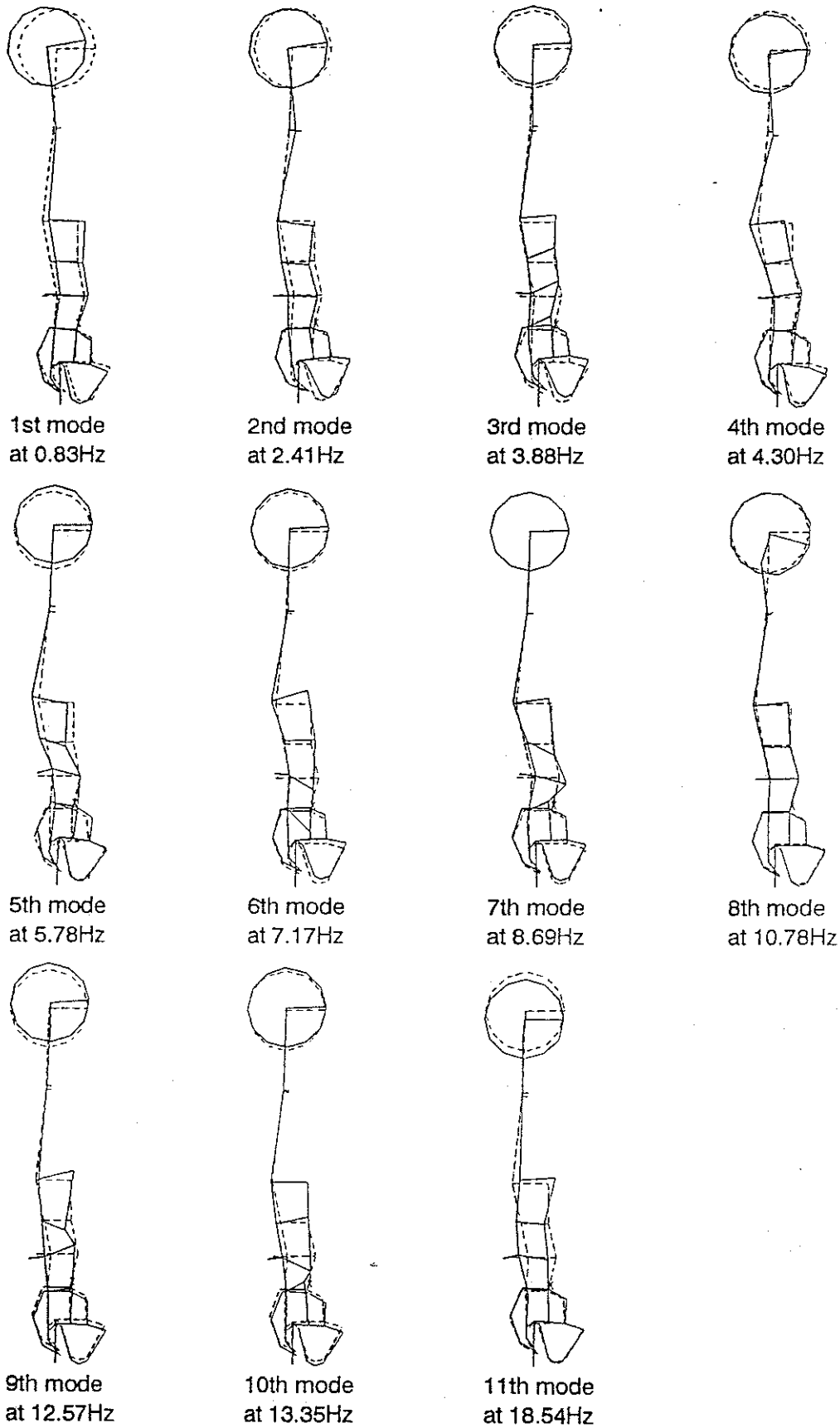

Figure 3.7 Calculated mode shapes of the simplified model (——) and the initial configuration (- - -).

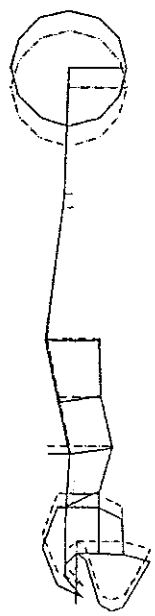

Figure 3.8 A mode shape of the simplified model for the lowest axial mode of the spine at 14.69 Hz calculated by constraining bending deformation of the spinal beams (——) and the initial configuration (- - -).

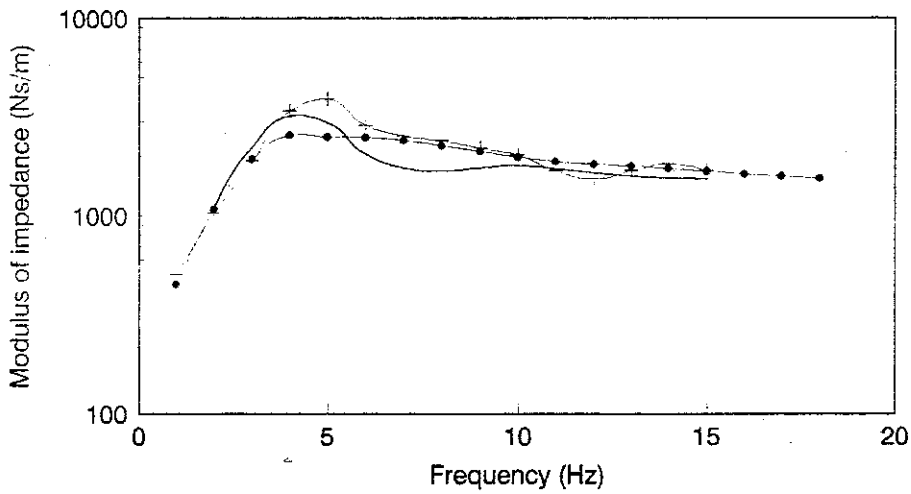

Figure 3.9 Moduli of the impedance of the simplified model calculated in this research (—•—), calculated by Belytschko and Privitzer (——) and experimental data of Vogt *et al.* (mean values of 10 subjects) (—+—).

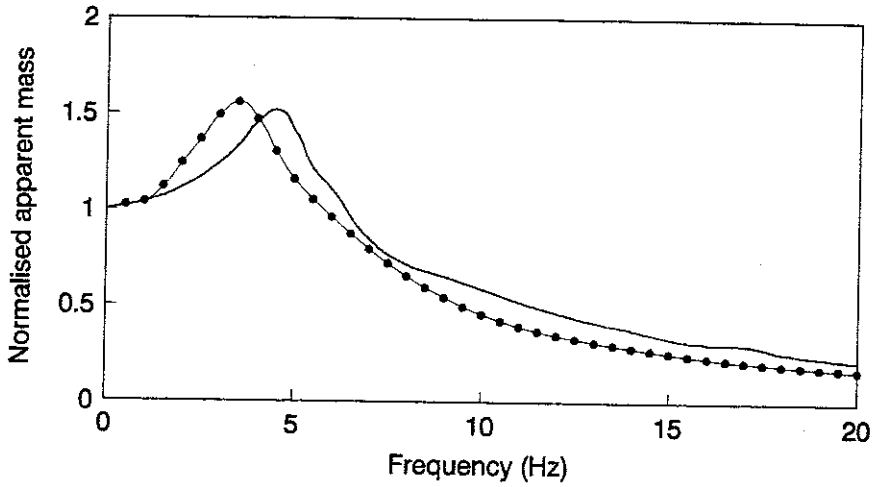

Figure 3.10 Normalised apparent mass of the simplified model in this research (—•—), and experimental data of Fairley and Griffin (mean values of 60 subjects) (——).

The driving point impedance was calculated with no damping so as to find modes corresponding to the principal resonances (Figure 3.11). It was found that the third mode at 3.88 Hz corresponded to the principal resonance of the driving point responses. The calculated mode shape shown in Figure 3.7 indicated that the third mode was dominated by an entire body mode caused by buttocks tissue deformation, a visceral mode with relative motion to the rest of the body and a small contribution of a bending mode of

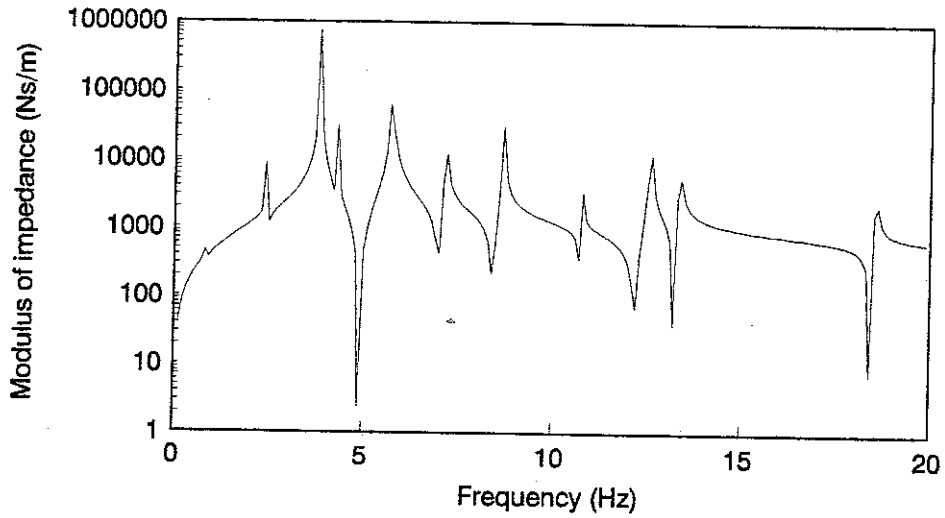

Figure 3.11 Modulus of the impedance of the simplified model with no damping.

the spine. Therefore, stiffnesses for the buttocks spring and the visceral springs of the simplified model were to be increased so as to achieve closer principal resonance frequency of the driving point responses to the experimental data. Although the impedance data also showed the second resonance at about 8 Hz in Figure 3.9, the corresponding mode was not clear in Figure 3.11 (the second resonance of the apparent mass was not clear in the average data shown in Figure 3.10 due to the inter-subject variability).

3.4 MODEL 2: MODIFIED SIMPLIFIED MODEL

3.4.1 Model description

A problem with the simplified model was the lower frequency of the principal resonance of the driving point responses than the experimental data. Material properties for the simplified model were modified. From the investigation into the mode shapes, changing parameters for either the visceral springs or the buttocks tissue spring might alter the principal resonance frequency of the driving point responses. This modification was reasonable as a first step, because the stiffness values for the viscera and the buttocks tissue were largely based on assumptions and, therefore, less reliable than other anatomically based values. The stiffness values for the visceral springs and the buttocks tissue spring were increased so as to shift the principal resonance frequency closer to the experimental data.

By means of trial and error, a combination of doubling visceral stiffness and a 50% increment in buttocks tissue stiffness achieved approximately the desired resonance frequency. In the modified simplified model, the inertial properties were also modified. The translational and the rotational masses for the head, pelvis and the thighs were derived from more reliable data of NASA (1978) and McConville *et al.* (1980). The translational mass of the arms was divided into a mass of the upper arms and masses of the forearms and the hands. The mass of the upper arms was added to the translational mass of the torso at the T1 level, whereas the masses of the forearms and the hands were added to the translational mass of the pelvis, because subjects put their hands on their thighs in many cases in the sitting position. The total mass of the modified simplified model was 59.124 kg.

3.4.2 Geometry and material properties

The node locations were the same as those for the simplified model shown in Table 3.3. The inertial data and the stiffness data for the modified simplified model are shown in Tables 3.7 and 3.8. The effective damping ratios used were the same as those for the simplified model, which were 0.35 for the third and the fifth modes and 0.25 for all the remaining modes.

Table 3.7 Inertial properties for the simplified model.

Level	Head, torso and pelvis		Viscera	
	Translational mass (kg)	Rotational mass[1] (kg m^2 x 10^{-2})	Translational mass (kg)	Rotational mass[1] (kg m^2 x 10^{-2})
Head	5.000*	2.000*	—	—
C2	—	—	—	—
T1	Torso 5.591 Upper arms 4.530*	Torso 2.773	—	—
T10	6.846	5.328	—	—
L1	—	—	5.134	2.576
L3	1.660	0.400	3.368	1.203
L5	—	—	4.295	1.272
S1	—	—	—	—
Pelvis	Pelvis 10.90* Thighs/2 8.1* Forearms 3.7*	Pelvis 9.42*	—	—

(1) Rotational mass around the mass centre.
* indicates the changed parameter from the simplified model.

Table 3.8 Stiffness data for the modified simplified model.

Spine			Viscera	
Level	Axial stiffness ($N/m \times 10^4$)	Bending stiffness (Nm)	Level	Axial stiffness ($N/m \times 10^4$)
C2-T1	14.40	68.9	—	—
T1-T10	15.40	6.70	—	—
T10-L3	34.70	21.5	T10-L1	1.76*
			L1-L3	2.06*
L3-S1	56.80	34.3	L3-L5	1.66*
			L5-Pelvis	1.08*

For all the viscera-spine interconnecting springs:
stiffness = 1.0×10^4 N/m.
For buttocks spring: stiffness = 9.825×10^4 N/m*.
* indicates the changed parameter from the simplified model.

3.4.3 Results and discussion

Calculated natural frequencies of the modified simplified model below 20 Hz are shown in Table 3.9. Various responses of the modified simplified model were compared with more experimental data reported in the literature. Comparisons in the driving point impedance, apparent mass, transmissibilities from vertical seat motion to vertical head motion, vertical seat motion to vertical and fore-and-aft motion of the spine, and visceral responses are shown in Figures from 3.12 to 3.17. The modified simplified model achieved similar driving point responses to the experimental data. The transmissibilities of the model also showed fairly good agreement with the data, except the seat-to-head transmissibility. In the transmissibility to vertical head motion, the discrepancy between the model response and the measurements was large above the principal resonance: some experimental data showed a wide peak above 10 Hz, whereas the model response did not show any noticeable peaks above 10 Hz. The measured transmissibilities to vertical head motion in Figure 3.14 possibly include both the translational and rotational (pitching) motion of the head except the transmissibility measured by Messenger (1987). In the simplified model and the modified simplified model, the head mass was connected to the cervical vertebra C2 by a massless rigid link and did not include the precise head-neck connection such as the atlanto-occipital joint. The head-neck region of the model needs to be modified to simulate more precise motion of the head.

Table 3.9 Natural frequencies of the modified simplified model.

Mode No.	Natural frequency (Hz)	Mode No.	Natural frequency (Hz)
1	0.91	7	10.80
2	2.87	8	11.75
3	4.69	9	14.67
4	4.81	10	16.73
5	6.60		
6	9.07		

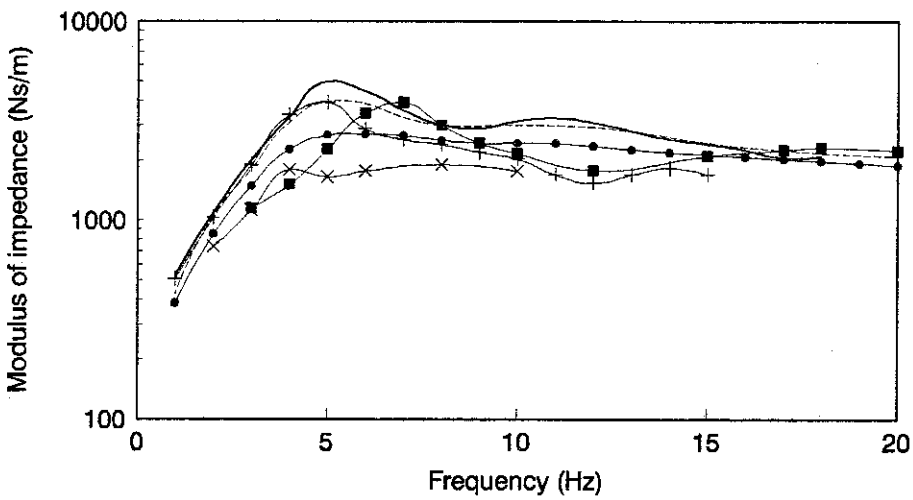

Figure 3.12 Moduli of the impedance: response of the modified simplified model (—•—); mean values of 8 subjects by Coermann *et al.* (——); mean values of 8 subjects by Miwa (—■—); mean values of 10 subjects by Vogt *et al.* (—+—); mean values of 15 subjects by Donati and Bonthoux (—x—); International Standard 5982 (- - - -).

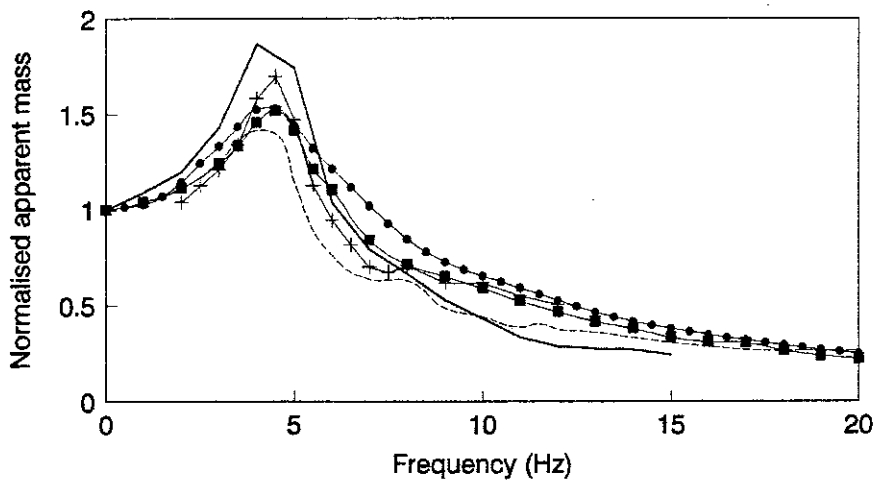

Figure 3.13 Normalised apparent masses: response of the modified simplified model (—•—); mean values of 10 subjects by Vogt *et al.* (——); mean values of two subjects by Sandover (- - - -); mean values of four subjects by Hinz and Seidel (—+—); mean values of 60 subjects by Fairley and Griffin (—■—).

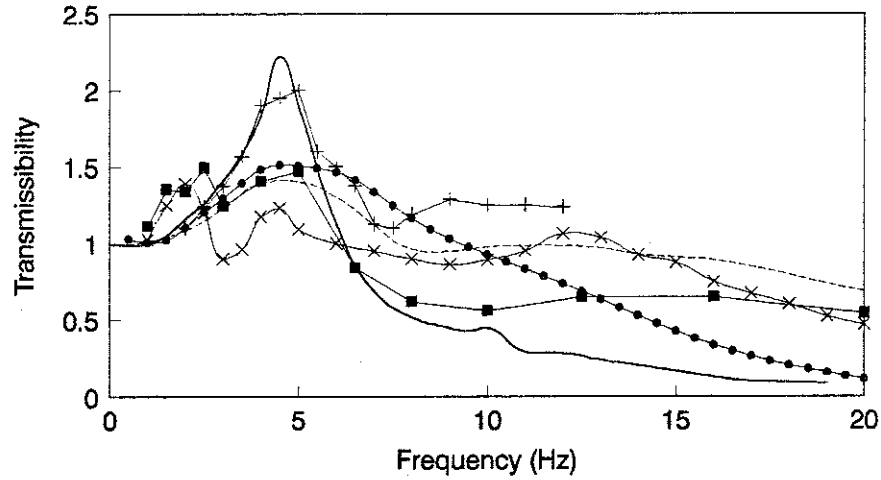

Figure 3.14 Acceleration transmissibilities from vertical seat motion to vertical head motion: response of the modified simplified model (—•—); values of a single subject by Coermann (——); mean values of 18 subjects by Griffin *et al.* (—■—); mean values of eight subjects by Messenger (—x—); mean values of four subjects by Hinz and Seidel (—+—); International Standard 7962 (- - - -).

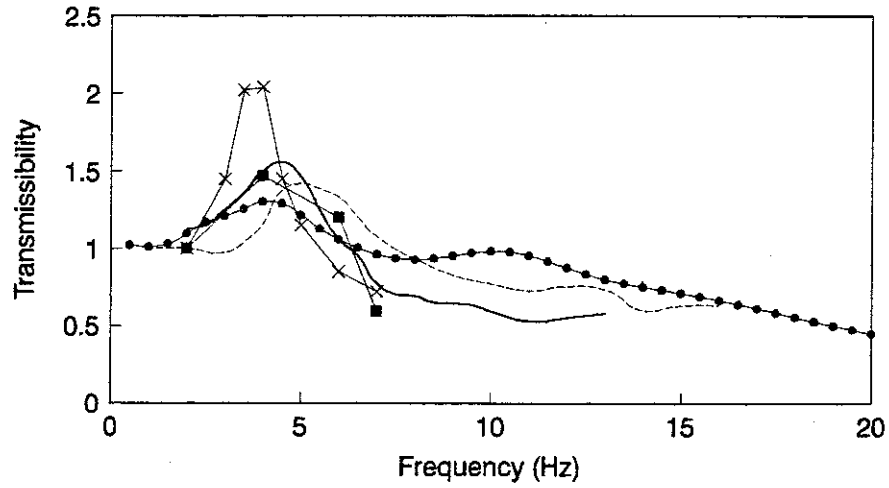

Figure 3.15 Transmissibilities from vertical seat motion to vertical spinal motion: acceleration (displacement) transmissibility to the vertebra L3 of the modified simplified model (—•—); mean acceleration transmissibility to the vertebra L3 of five subjects by Panjabi *et al.* (——); displacement transmissibility to the vertebra L3 of a single subject by Pope *et al.* (—■—); displacement transmissibility to the vertebra L4 of a single subject by Sandover and Dupuis (—x—); mean acceleration transmissibility to the vertebra L3 of three subjects by Magnusson *et al.* (- - - -).

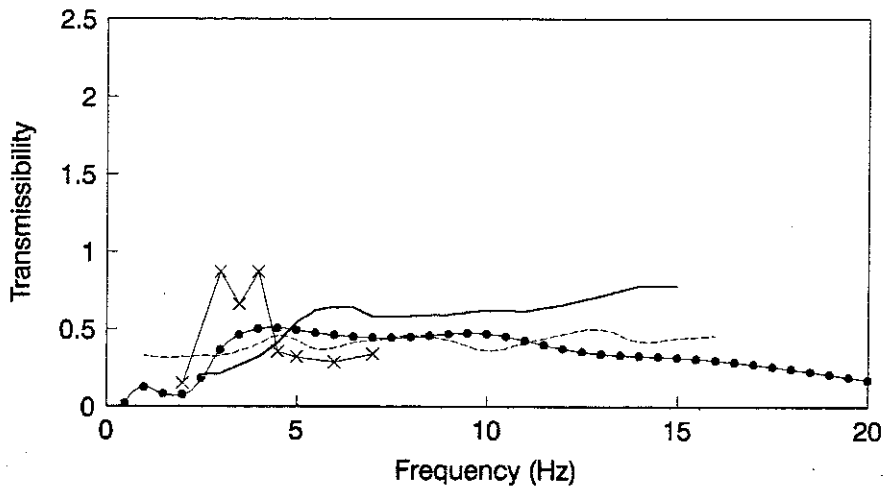

Figure 3.16 Transmissibilities from vertical seat motion to fore-and-aft spinal motion: acceleration (displacement) transmissibility to the vertebra L3 of the modified simplified model L3 (—•—); mean acceleration transmissibility to the vertebra L3 of five subjects by Panjabi *et al.* (——); displacement transmissibility to the vertebra L4 of a single subject by Sandover and Dupuis (—x—); mean acceleration transmissibility to the vertebra L3 of three subjects by Magnusson *et al.* (- - - -).

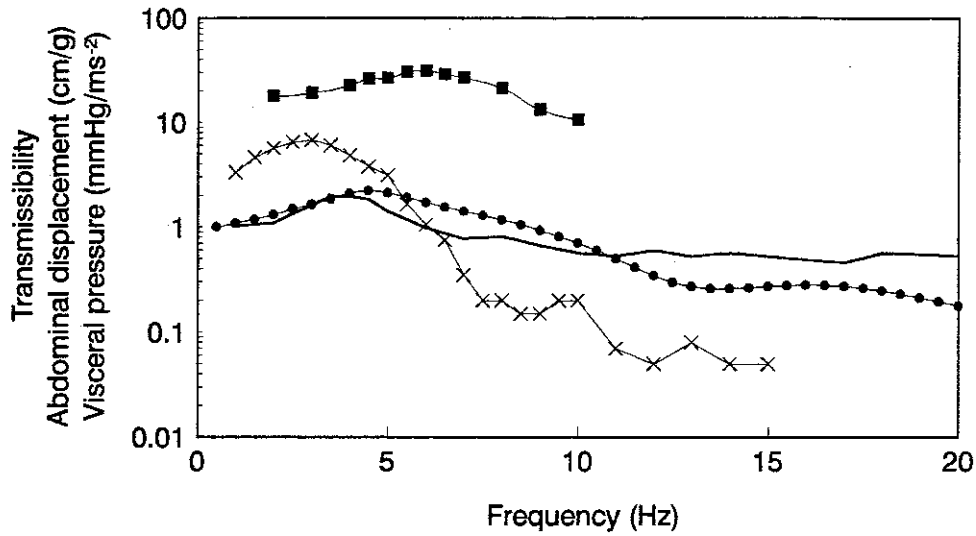

Figure 3.17 Acceleration (displacement) transmissibility from vertical seat motion to vertical visceral motion at the L3 level of the modified simplified model (—•—), abdominal wall displacement of a single subject by Coermann *et al.* (—x—), mean colon pressure of eight subjects by White *et al.* (——) and intraabdominal pressure of a single subject by Sandover (—■—).

Using the modified simplified model, the effect of changing posture was investigated. Responses in two postures, a slouched posture and the previously used erect posture (Figure 3.18), were compared. The comparisons are shown between the driving point apparent masses (Figure 3.19), transmissibilities from vertical seat motion to vertical head motion (Figure 3.20) and the transmissibilities from vertical seat motion to vertical spinal motion at the vertebra L3 (Figure 3.21). The slouched posture decreased the modulus of the apparent mass at the principal resonance. The slouched posture also decreased the seat-to-head transmissibility below 7 Hz around the principal resonance and increased the transmissibility above 7 Hz. The seat-to-spine transmissibility was decreased above 9 Hz by the slouched posture.

The common trends for the effect of posture on the responses found in the literature review (section 2.3) were for an erect posture to increase the principal resonance frequency of the driving point responses, and either to increase the principal resonance frequency or to decrease the principal resonance transmissibility and increase the transmissibility at higher frequencies of the seat-to-head and the seat-to-spine transmissibilities. Although the calculated effect of posture on the seat-to-head

transmissibility was similar to one of the common trends, the expected resonance shift was seen in none of the responses investigated. This result had illustrated the limitation of the modified simplified model. The calculated natural frequencies in the slouched posture are shown in Table 3.10.

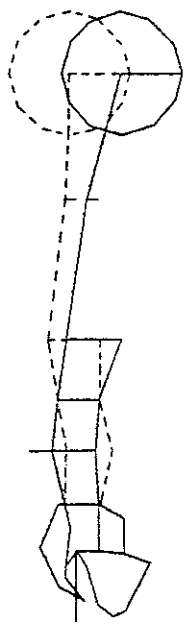

Figure 3.18 Two postures compared: slouched posture (——) and erect posture (- - -).

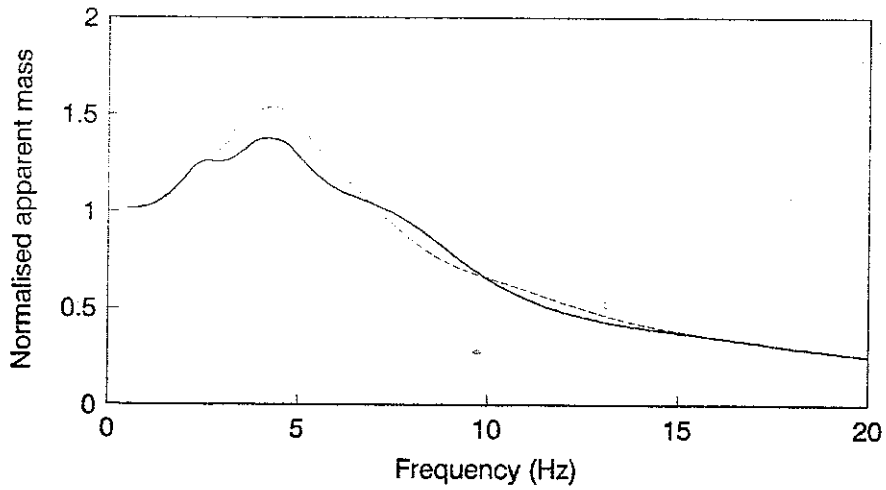

Figure 3.19 Normalised apparent masses of the modified simplified model in the slouched posture (——) and in the erect posture (- - -).

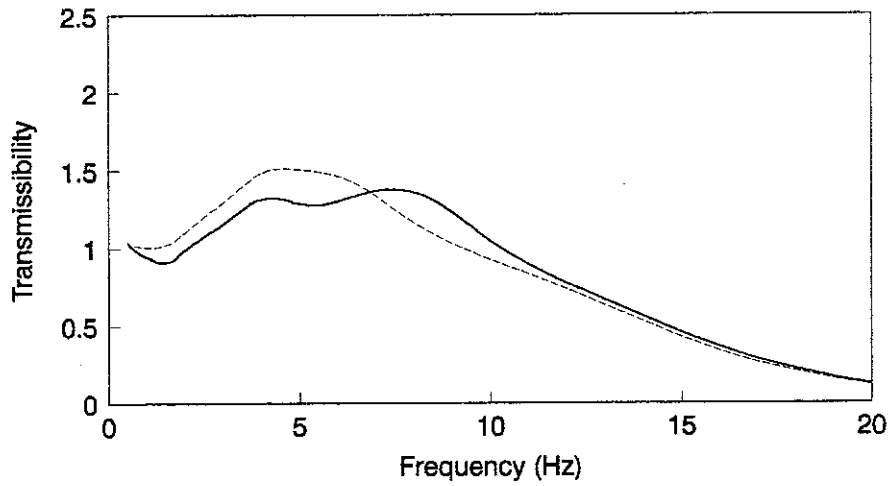

Figure 3.20 Transmissibilities from vertical seat motion to vertical head motion of the modified simplified model in the slouched posture (——) and in the erect posture (- - -).

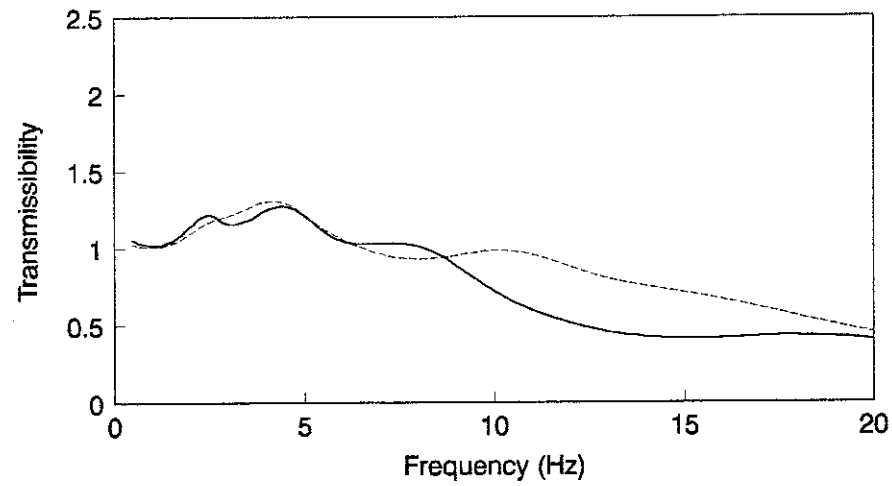

Figure 3.21 Transmissibilities from vertical seat motion to vertical motion of the vertebra L3 of the modified simplified model in the slouched posture (——) and in the erect posture (- - -).

Table 3.10 Natural frequencies of the modified simplified model in a slouched posture.

Mode No.	Natural frequency (Hz)	Mode No.	Natural frequency (Hz)
1	0.90	7	11.30
2	2.73	8	11.66
3	4.53	9	14.96
4	5.01	10	18.26
5	7.13	11	18.99
6	8.41		

3.5 MODEL 3: EXPANDED MODEL

3.5.1 Model description

For the simplified model and the modified simplified model, the whole spine was divided into four segments of the vertebrae from C2 to T1, T1 to T10, T10 to L3 and L3 to S1 based on the simplification of the spine by Belytschko and Privitzer (1978). However, the division was not necessarily appropriate from both dynamic and static view points (i.e. for determination of the vibration mode shapes and definition of postures). There were also unclear points in Belytschko's simplification procedure for the material properties and the geometry. The modified simplified model was expanded into a model in which all the nodes corresponding to the vertebrae from T1 to S1 were defined and all the intervertebral discs in this region were modeled by separate beam elements (Figure 3.22). The cervical spine was modelled by a single beam element representing the vertebrae from C2 to C7. The torso masses were also assigned to all the vertebral levels of the thoraco-lumbar spine separately and below the T10 level they were divided into the spinal masses and the visceral masses at each level.

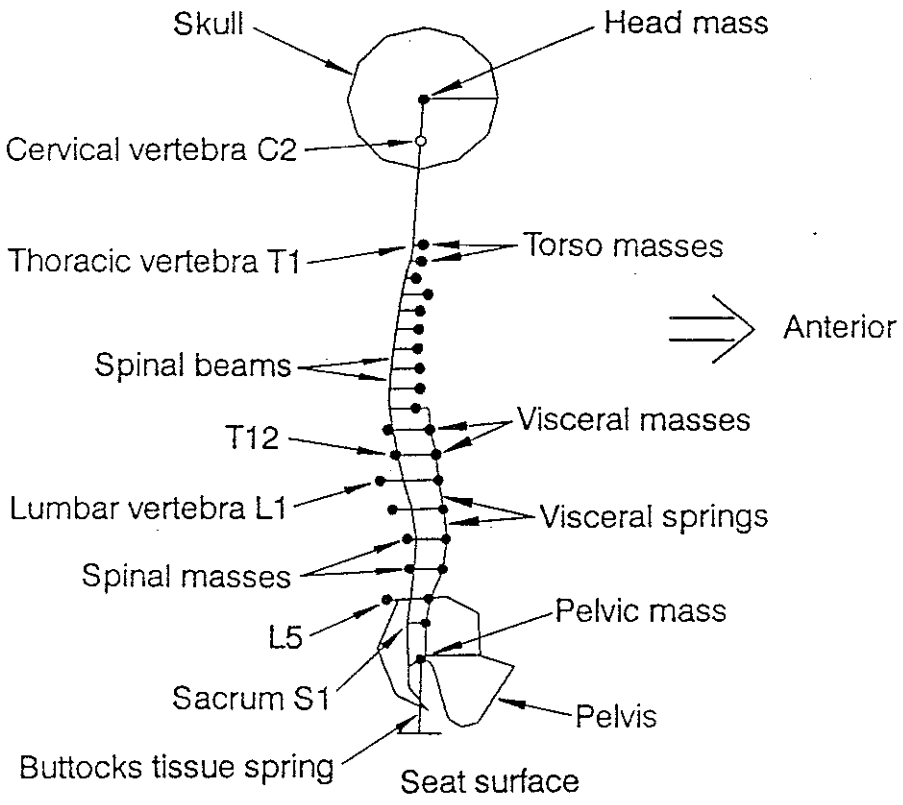

Figure 3.22 Model 3: Expanded model.

3.5.2 Geometry and material properties

The geometry and material properties were chosen directly from the anatomical data Belytschko used initially. The geometry of the initial spinal curvature was based on the radiographic data of seated pilots obtained by Belytschko *et al.* (1976). This curvature was considered to be an almost erect posture. The data provided coordinates of the inferior end-plate centres of the vertebral bodies, heights of the vertebral bodies and heights of the intervertebral discs as shown in Figure 3.23. The coordinates of the geometrical centres of the vertebral bodies were calculated from the provided data, using equation (3.51), so as to determine node locations for the spinal beams.

$$x_{ci} = x_i + \frac{H_i}{2(H_i + H_{Di})}(x_{i+1} - x_i) \qquad \textbf{(3.51a)}$$

$$y_{ci} = y_i + \frac{H_i}{2(H_i + H_{Di})}(y_{i+1} - y_i) \qquad \textbf{(3.51b)}$$

where: (x_{ci},y_{ci}) is the coordinate of the geometrical centre of the vertebral body i; (x_i,y_i) is the coordinate of the inferior end-plate of the vertebral body i; (x_{i+1},y_{i+1}) is the coordinate of the inferior end-plate of the adjacent vertebral body $i+1$; H_i is the height of the vertebral body i; H_{Di} is the height of the intervertebral disc i.

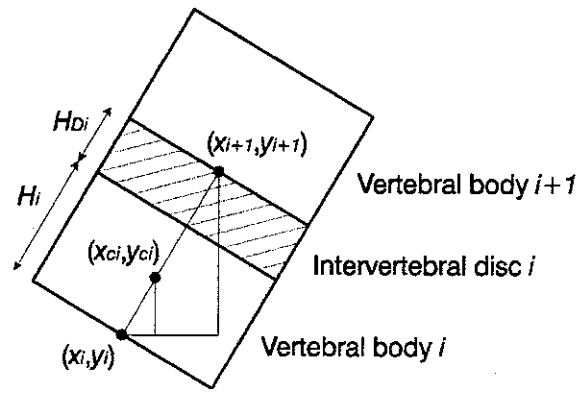

Figure 3.23 Estimation of the geometrical centre of the vertebral body.

For the cervical spine, only a single node corresponding to the vertebra C2 was defined for a single beam element representing the vertebrae between C2 and T1. The spinal beams were massless and mass elements representing the translational and rotational masses of the torso segments reported by Liu and Wickstrom (1973) (Table 3.11) were assigned to the mass centres of the segments in the region from the T1 to T10 levels. Below the T10 level, the torso segmental mass was divided into the spinal mass and the visceral mass at each vertebral level by Belytschko and Privitzer (1978) based on the graphical data of the torso cross-sections of Eycleshymer and Shoemaker (1970) with an assumption of uniform density for the torso. The ratios between the spinal masses and the visceral masses below the T10 level are shown in Table 3.12.

The spinal mass and the visceral mass were placed at each level so that the location of the mass centre, the total translational and rotational masses coincided with those of the corresponding torso segment (Figure 3.24). Horizontal distance of the visceral mass from the torso mass centre, L_v, was assumed to be constant and it was set to be 1.0×10^{-2} m. The translational mass, M_c, and the rotational mass, I_c, of the segment are known in Table 3.11. The translational masses of the spine and the viscera, M_s and M_v, are also known using the ratios shown in Table 3.12. Therefore, unknown values are the horizontal distance of the spinal mass from the mass centre, L_s, and the rotational masses of the

spine and the viscera, I_s and I_v. The equilibriums of the translational and rotational masses are given by:

$$M_s L_s = M_v L_v \quad \textbf{(3.52a)}$$

$$I_c = M_s L_s^2 + M_v L_v^2 + I_s + I_v \quad \textbf{(3.52b)}$$

The horizontal distance of the spinal mass from the mass centre, L_s, is obtained from equation (3.52a) and the location of the spinal mass is determined with the mass eccentricity from the spinal column, e, shown in Table 3.11. The sum of the rotational masses of the spine and the viscera, I_s+I_v are obtained from equation (3.52b) and it was divided into the spinal rotational mass, I_s, and the visceral rotational mass, I_v, with the ratio shown in Table 3.12. The torso, spinal and the visceral masses were connected to the spinal beams by massless rigid links.

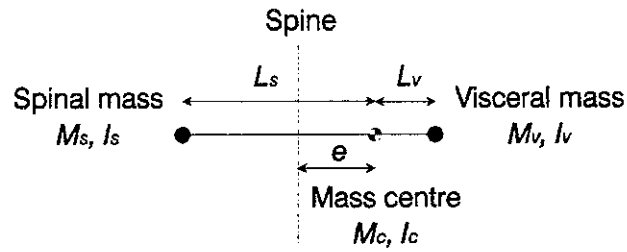

Figure 3.24 Mass distribution of a torso segment.

The translational mass on the pelvis included the translational masses of the pelvis, forearms, hands and a half of the thighs. The translational mass of the upper arms was added to the translational torso mass for the T2 level. The inertial properties for those components and for the head were based on the data of NASA (1978) and McConville *et al.* (1980). The total mass of the expanded model was 60.222 kg, including 12.796 kg for the total visceral mass. Tables 3.13 and 3.14 show the node locations and the inertial properties.

The spinal beams were given only the axial and bending stiffnesses of the intervertebral discs. No effects of the intervertebral ligaments and the articular facet interaction were included in the beams, since no reliable anatomical data were available. The stiffness data for the discs were originally based on the data of Schultz *et al.* (1973) and modified by Belytschko and Privitzer (1978) to be increased to account for the cubic force-deflection relationships and body-weight preload in the lumbar region. In the thoracic region,

Table 3.11 Geometry and inertial property distribution of the torso segments (mean values of 10 cadavers) measured by Liu and Wickstrom (1973).

Level	Anterior mass eccentricity[1] ($m \times 10^{-2}$)	Translational mass (kg)	Rotational mass[2] ($kg\ m^2 \times 10^{-2}$)
T1	—— [3]	1.36	0.0745
T2	——	1.07	0.208
T3	——	1.16	0.288
T4	3.08	1.06	0.314
T5	2.50	1.18	0.384
T6	2.88	1.19	0.443
T7	2.80	1.31	0.537
T8	3.22	1.33	0.554
T9	3.81	1.42	0.616
T10	3.64	1.35	0.603
T11	3.39	1.60	0.706
T12	3.47	1.68	0.702
L1	2.98	1.96	0.806
L2	2.65	2.01	0.835
L3	2.97	2.15	0.826
L4	2.24	2.19	0.808
L5	1.28	2.24	0.819

(1) Anterior horizontal distance from the geometrical centre of the vertebral body to the mass centre of the torso segment (the mass eccentricity, *e*, in Figure 3.24).
(2) Rotational mass around the mass centre in the sagittal plane.
(3) Data were not measured.

the stiffness values were based on the data obtained from isolated spines, because a small non-linearity was seen in the force-deflection relationships of the discs in this region. In the cervical region, the stiffness value for the single beam element, representing the vertebrae from C2 to T1, was based on the data for the simplified model. Precise definition

of the cross-sectional area of the spinal beams was not necessary for the vibration analysis of interest. The cross-sectional area of the spinal beams was assumed to be constant and the value of $1.0 \times 10^{-3}\ m^2$ (corresponding to a circle with a diameter of 3.5 cm) was used to estimate Young's modulus and the second moment of area of the cross-section, using equations (3.44) and (3.45).

Table 3.12 Mass distribution between the spinal mass and the visceral mass at each level obtained by Belytschko and Privitzer based on the graphical data of the torso cross-sections of Eycleshymer and Shoemaker.

Level	Spinal mass ratio (%)	Visceral mass ratio (%)
T11	19.9	80.1
T12	19.9	80.1
L1	14.5	85.5
L2	17.0	83.0
L3	20.1	79.9
L4	25.7	74.3
L5	20.8	79.2

Reliable stiffness data for the viscera and the buttocks tissue were also difficult to obtain. Belytschko and Privitzer determined the visceral stiffness so that the visceral resonance would coincide with that measured by Coermann *et al.* (1960), assuming the torso-wall system as a one-dimensional uniform rod. For the expanded model, the stiffnesses for the visceral springs were doubled and the stiffness for the buttocks tissue spring was increased by 50 % from the values used by Belytschko and Privitzer, considering the results of the modified simplified model. The stiffness data for the expanded model are shown in Table 3.15. The effective damping ratios used were 0.35 for the third and the fourth modes and 0.25 for all the remaining modes.

Table 3.13 Node locations for the expanded modal.

Level	Spinal column (m x 10^{-2})		Torso or spinal mass[2] (m x 10^{-2})	Visceral column[2] (m x 10^{-2})
	x[1]	z		
Head	-0.594	59.830	——	——
C2	-0.630	52.972	——	——
T1	-1.142	41.224	1.351	——
T2	-1.650	39.117	1.351	——
T3	-2.100	37.040	1.351	——
T4	-2.475	34.925	3.080	——
T5	-2.789	32.804	2.500	——
T6	-3.069	30.583	2.880	——
T7	-3.371	28.285	2.800	——
T8	-3.548	25.849	3.220	——
T9	-3.634	23.304	3.810	——
T10	-3.634	20.629	3.640	4.640
T11	-3.114	17.845	-0.636	4.390
T12	-2.288	14.810	-0.558	4.470
L1	-1.573	11.455	-2.917	3.980
L2	-0.564	7.799	-2.233	3.650
L3	-0.050	3.906	-1.007	3.970
L4	0.0	0.0	-0.651	3.340
L5	-0.511	-3.820	-2.528	2.280
S1	-0.700	-6.984	——	2.280
Pelvis	1.066	-11.015	——	1.214

(1) The coordinate system has x-axis for the fore-and-aft and z-axis for the vertical directions.
(2) Relative x coordinate with respect to the spinal column (vertebral body centre).

Table 3.14 Inertial properties for the expanded model.

Level	Torso or spinal mass		Visceral mass	
	Translational mass (kg)	Rotational mass[1] ($kgm^2 \times 10^{-2}$)	Translational mass (kg)	Rotational mass[1] ($kgm^2 \times 10^{-2}$)
Head	5.0	2.0	——	——
C2	——	——	——	——
T1	1.359	0.0745		
T2	Torso 1.074 Upper arms 4.530	Torso 0.2077	——	——
T3	1.160	0.2878	——	——
T4	1.064	0.3138	——	——
T5	1.175	0.3838	——	——
T6	1.193	0.4425	——	——
T7	1.308	0.5374	——	——
T8	1.326	0.5543	——	——
T9	1.417	0.6164	——	——
T10	1.352	0.6028	——	——
T11	0.3184	0.1283	1.282	0.5130
T12	0.3329	0.1270	1.341	0.5079
L1	0.2842	0.1036	1.676	0.5870
L2	0.3420	0.1253	1.670	0.6119
L3	0.4325	0.1482	1.720	0.5927
L4	0.5621	0.1937	1.625	0.5514
L5	0.4659	0.1540	1.774	0.5793
S1	——	——	1.708	0.1000
Pelvis	Pelvis 10.9 Thighs/2 8.1 Forearms 3.7	Pelvis 9.42	——	——

(1) Rotational mass around the mass centre.

Table 3.15 Stiffness data for the expanded model.

Level	Spine					Viscera
	Axial stiffness ($N/m \times 10^6$)	Bending stiffness ($Nm \times 10^2$)	Length ($m \times 10^{-2}$)	Young's modulus ($N/m^2 \times 10^7$)	Second moment [1] ($m^4 \times 10^{-8}$)	Axial stiffness ($N/m \times 10^4$)
C2-T1	0.14	0.69	11.76	1.646	49.30	——
T1-T2	0.70	0.20	2.167	1.517	2.857	——
T2-T3	1.20	0.40	2.184	2.621	3.333	——
T3-T4	1.50	0.60	2.148	3.222	4.000	——
T4-T5	2.10	1.00	2.144	4.502	4.762	——
T5-T6	1.90	1.00	2.239	4.254	5.263	——
T6-T7	1.80	1.00	2.318	4.172	5.556	——
T7-T8	1.50	1.00	2.442	3.663	6.667	——
T8-T9	1.50	1.10	2.546	3.819	7.333	——
T9-T10	1.50	1.10	2.675	4.013	7.332	——
T10-T11	1.50	1.20	2.827	4.241	7.999	5.72
T11-T12	1.50	1.00	3.145	4.718	6.666	5.24
T12-L1	1.80	0.90	3.430	6.174	5.000	4.84
L1-L2	2.13	0.90	3.793	8.079	4.225	4.48
L2-L3	2.00	0.90	3.927	7.854	4.500	3.82
L3-L4	2.00	0.90	3.906	7.812	4.500	3.28
L4-L5	1.87	0.80	3.854	7.207	4.278	3.36
L5-S1	1.47	0.70	3.170	4.660	4.762	2.58
S1-Pelvis	——	——	——	——	——	1.84

(1) Second moment of area of the cross-section. Area was assumed to be 1.0×10^{-3} m^2 and constant.
For all the viscera-spine interconnecting springs: axial stiffness=1.0×10^4 N/m.
For the buttocks spring: axial stiffness=9.825×10^4 N/m.

3.5.3 Results and discussion

The expanded model produced 12 modes below 20 Hz. The calculated natural frequencies are shown in Table 3.16. The driving point impedance and apparent mass of the expanded model were compared with the responses of the modified simplified model

(Figures 3.25 and 3.26). The driving point responses of the expanded model showed good agreements with those of the modified simplified model.

Calculated vibration mode shapes of the expanded model are shown in Figure 3.27. From an observation of the impedance with no damping (Figure 3.28), the fourth mode at 5.56 Hz was found to correspond to the principal resonance of the driving point responses. The fourth mode contained an entire body mode caused by buttocks tissue deformation in phase with a vertical visceral mode, and a small bending mode of the whole spine. The mode corresponding to the second principal resonance, which was generally found between 8 and 12 Hz, was not clear.

Table 3.16 Natural frequencies of the expanded model.

Mode No.	Natural frequency (Hz)	Mode No.	Natural frequency (Hz)
1	0.92	7	11.33
2	2.27	8	12.64
3	4.12	9	14.71
4	5.56	10	15.32
5	6.70	11	17.85
6	9.69	12	18.77

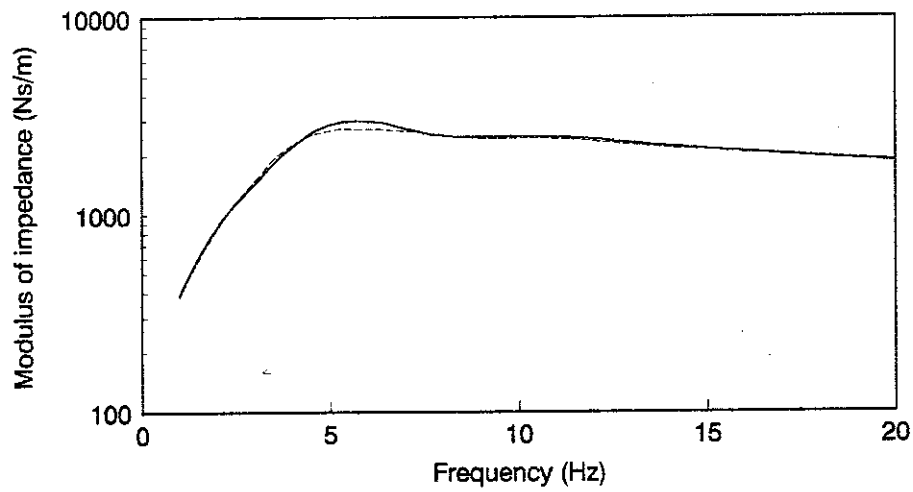

Figure 3.25 Moduli of the driving point impedance: the expanded model (——) and the modified simplified model (- - -).

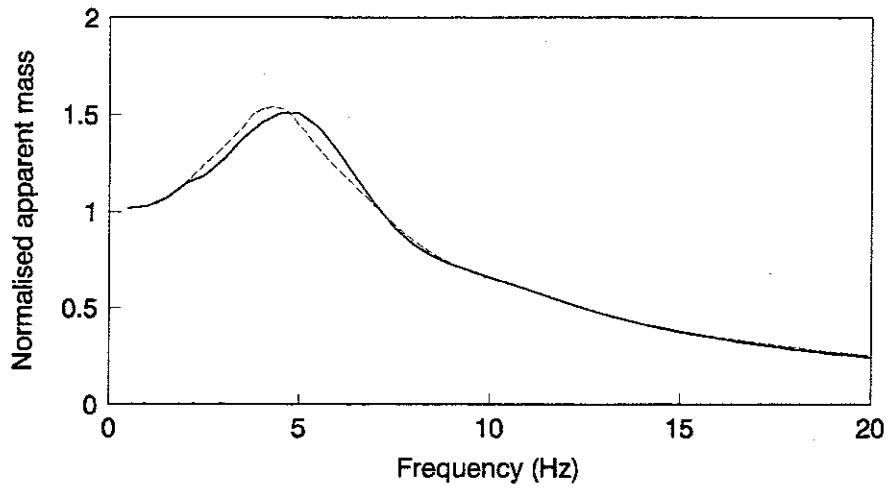

Figure 3.26 Normalised apparent masses: the expanded model (——) and the modified simplified model (- - -).

Figure 3.27 shows that the dominant modes in the frequency range below 20 Hz were bending modes of the spine which sometimes included a rotational mode of the pelvis, a buttocks mode and visceral modes. The axial modes of the spine were calculated by constraining bending deformation of the spinal beams. The lowest axial mode of the spine was found at 17.74 Hz (Figure 3.29) which appeared to be included in the tenth mode at 15.32 Hz without the constraint (Figure 3.27). Because many bending modes of the spine were found throughout the frequency range below 20 Hz, the model should be validated, comparing the bending responses of the spine with experimental data for further modification. However, such data are not available. The vibration mode shapes showed that when the fore-and-aft responses of the body were measured at the head, vertebrae T1, T6, T11, L3 and the sacrum S1, the bending modes of the spine might be determined below at least 10 Hz. The acceleration transmissibilities from vertical seat motion to vertical and fore-and-aft motion of the head, vertebrae and the pelvis were calculated, as well as the transmissibility from vertical seat motion to vertical visceral motion (Figure 3.30). The vertical responses were similar regardless of the body parts, suggesting that the vertical responses were dominated by the entire body mode and maybe the visceral mode. On the other hand, the fore-and-aft responses were distinctive that indicated the feasibility of extracting the bending modes of the spine from measured fore-and-aft responses.

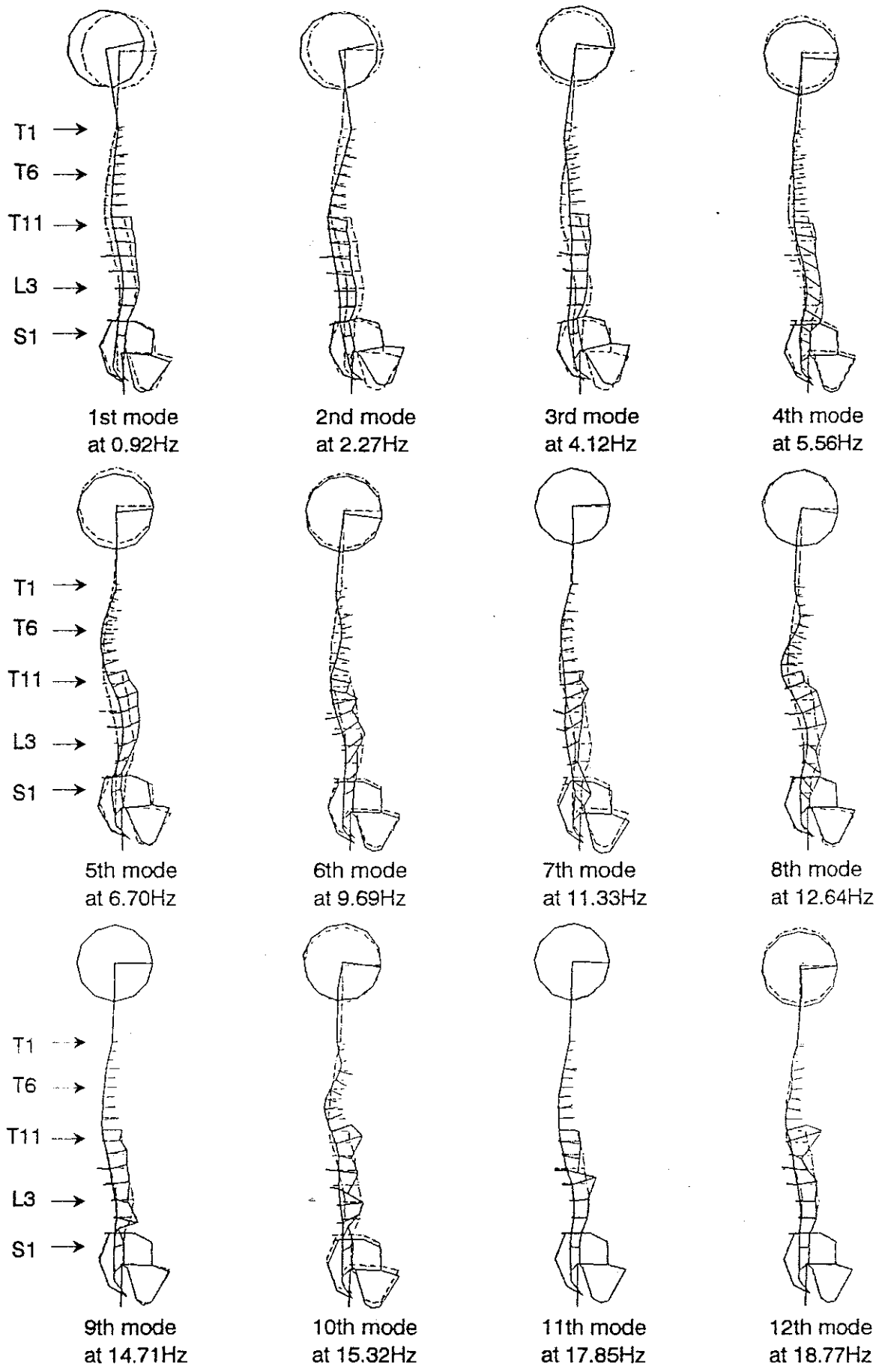

Figure 3.27 Calculated mode shapes of the expanded model (——) and the initial configuration (- - -).

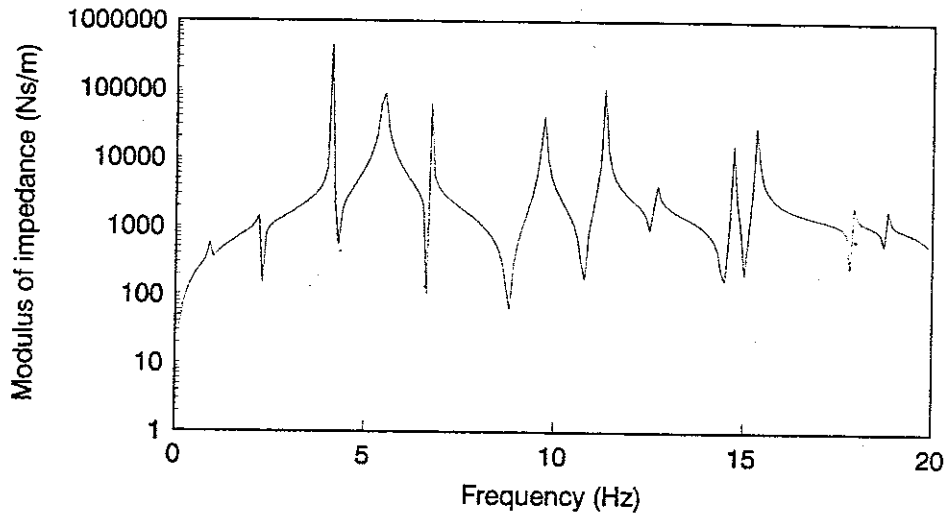

Figure 3.28 Modulus of the impedance of the expanded model with no damping.

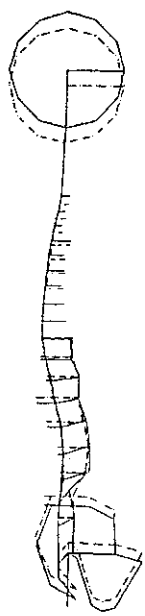

Figure 3.29 A mode shape of the expanded model for the lowest axial mode of the spine at 17.74 Hz, calculated by constraining bending deformation of the spinal beams (——) and the initial configuration (- - -).

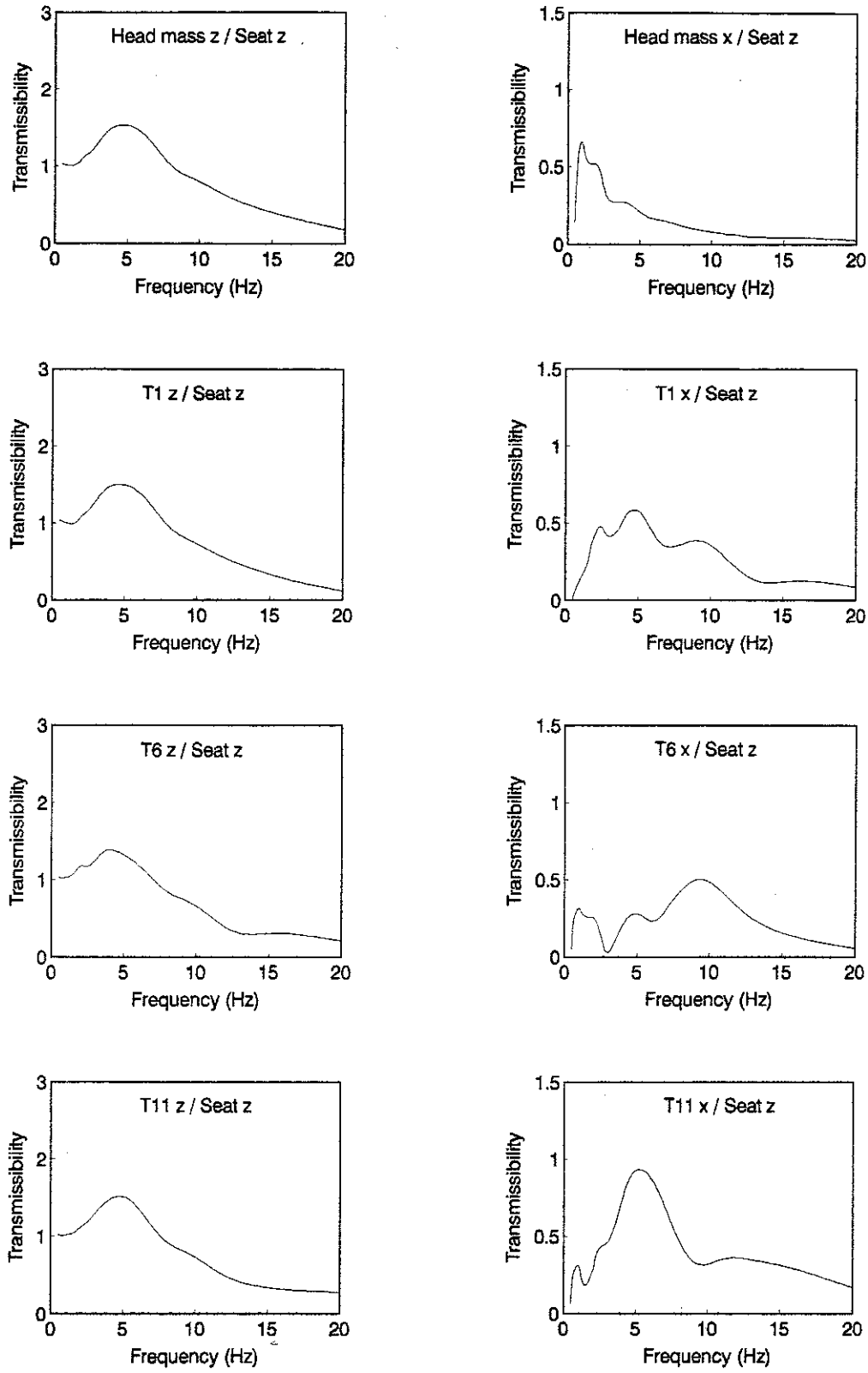

Figure 3.30 Calculated transmissibilities of the expanded model (z=vertical direction; x= fore-and-aft direction).

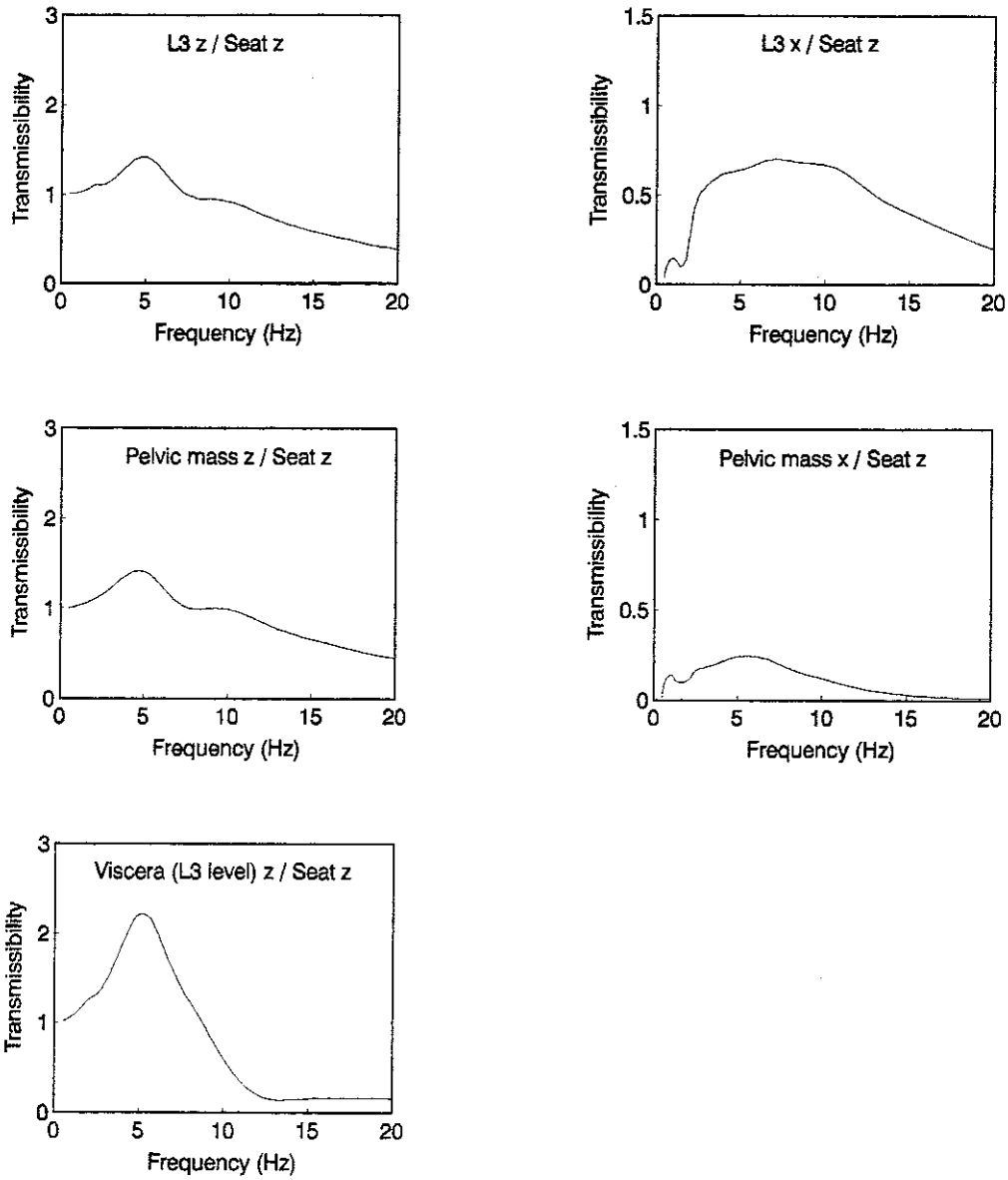

Figure 3.30 (Continued).

3.6 CONCLUSIONS FROM MODELLING: PART 1

The spinal column was modelled by four beam elements representing the vertebrae (intervertebral discs) from C2 to T1, T1 to T10, T10 to L3 and L3 to S1 for the simplified model and the modified simplified model. The principal resonance frequency of the driving point responses of the simplified model was found to be lower than the experimental results. The modified simplified model which was given increased stiffness values for the

visceral springs (100 % increment) and the buttocks tissue spring (50 % increment) achieved similar driving point responses to the experimental data. Changing the posture of the modified simplified model from erect to slouched did not shift the principal resonance frequency of the responses, although the modulus of the principal resonance was affected by the change.

For the expanded model, all the vertebrae in the thoraco-lumbar region were modelled by separate beam elements (the cervical spine was modelled by a single beam element) and the material properties and the geometry were based more directly on the anatomical data. The expanded model produced similar driving point responses to those of the modified simplified model. The vibration mode shapes of the expanded model showed that the principal resonance of the body at about 5 Hz consisted of an entire body mode caused by buttocks tissue deformation in phase with a vertical visceral mode, and a small bending mode of the entire spine. The dominant modes of the body in the frequency range below 20 Hz were bending modes of the spine which sometimes included a rotational mode of the pelvis, a buttocks mode and visceral modes. The lowest axial mode of the spine was included in the mode found at 15.32 Hz.

The models were validated, comparing the calculated driving point responses with the experimental data reported in the literature. However, the principal resonance at about 5 Hz in the driving point responses was found to be dominated by a buttocks mode (an entire body mode) and a visceral mode, and the validation of the responses of other body parts such as the spine was not exhaustive as pointed out by Payne and Band (1971). Many bending modes of the spine were calculated, by the expanded model, throughout the frequency range below 20 Hz. Therefore, the models should be validated comparing the bending responses of the spine with experimental data for further modification, nevertheless such data are not available. The predicted transmissibilities from vertical seat motion to vertical and fore-and-aft motion of the head, vertebrae T1, T6, T11, L3, pelvis and the viscera were distinctive that indicated the feasibility of extracting the vibration modes from measured transmissibilities.

CHAPTER 4

EXPERIMENTAL DETERMINATION OF MODE SHAPES OF WHOLE-BODY VIBRATION

4.1 INTRODUCTION

The calculation results shown in chapter 3 indicated that the vibration mode shapes of the human body below 20 Hz were dominated by bending modes of the spine, a buttocks mode and visceral modes. The models were validated, using the driving point responses whose principal resonance at about 5 Hz was dominated by a buttocks mode (an entire body mode) and a visceral mode. Because many bending modes of the spine were calculated, by the expanded model, throughout the frequency range below 20 Hz, the models should be validated, comparing the bending responses of the spine with experimental data for further modification. However, such data are not available. The predicted transmissibilities from vertical seat motion to vertical and fore-and-aft motion of the head, vertebrae T1, T6, T11, L3, pelvis and the viscera were distinctive that indicated the feasibility of extracting the vibration modes from measured transmissibilities.

Experimental modal analysis is one of the methods to characterise the dynamic behaviour of structures. In this chapter, experimental modal analysis is applied to whole-body vibration to extract the natural frequencies and the vibration mode shapes of the human body. The chapter includes three experimental studies. Firstly, a data correction method is developed to eliminate the effect of local tissue-accelerometer vibration from responses measured on the body surface. Secondly, experimental modal analysis is applied to whole-body vibration, using the developed correction method. Finally, a small experiment measuring the driving point apparent mass with constraints on subjects is conducted so as to support the results from the experimental modal analysis.

4.2 A DATA CORRECTION METHOD FOR SURFACE MEASUREMENT OF VIBRATION ON THE HUMAN BODY

4.2.1 Introduction

The dynamic responses of the spine to vibration have been investigated in various studies

so as to identify frequencies and levels of vibration which may cause spinal injuries. One of the easiest ways to measure spinal motion is surface measurement, where accelerometers are mounted on the skin. However, when accelerometers are attached on the body surface, local tissue-accelerometer vibration may result in a difference between the accelerometer measurement and the acceleration of the spine. An alternative way to measure spinal motion is direct measurement in which accelerometers are mounted on Kirschner wires inserted into the spine during local anaesthesia. Pope *et al.* (1986) compared displacement responses of the vertebra L3 by the surface measurement and the direct measurement and found a significant difference. The direct measurement has been employed in several studies. However, it requires medical skill and restricts the number of measuring sites and the number of subjects. Even when Kirschner wires are used, data may vary depending on the thickness of the wires and the depth of insertion (see Panjabi *et al.* 1986).

Various investigators have devised procedures to either minimize or correct for the effect of the local tissue-accelerometer vibration on surface measurements. A preload has been applied to surface-mounted accelerometers on the limbs by many workers so as to increase the stiffness of tissue and minimize its effects. There are some ways of preloading, such as mass preloading (Saha and Lakes, 1977; Nokes *et al.*, 1984), spring preloading (Saha and Lakes) and strap preloading (Ziegert and Lewis, 1979; Valiant *et al.*, 1987). However, the additional components required to preload accelerometers may result in additional resonant systems. Besides, the application of a preload by means of masses, springs or straps as used on the limbs is not practical for measuring vibration of the spine.

Mathematical correction methods for the effects of skin and other tissue on surface measurements have been proposed by some workers. Collier and Donarski (1987) developed a correction method based on an impedance technique. They measured the driving point impedance on the body surface of the tibia in the direction perpendicular to the bone. The correction frequency function was calculated by subtracting the impedance of the mass of the accelerometer from the measured impedance and assumed zero mass of tissue involved in the local vibration. This assumption is probably inappropriate when measuring spinal motion because some subjects have thick tissue between the spine and the body surface. No validation of the method was shown. Hinz *et al.* (1988b) and Smeathers (1989) assumed a single degree-of-freedom linear model for the local tissue-accelerometer system in the vertical direction on the spine. They proposed a free vibration test of the accelerometer attached on the body surface while a subject was sitting or

standing still so as to estimate the natural frequency and the damping ratio of the local system. The correction frequency function was calculated using the estimated natural frequency and damping. The method of Hinz *et al.* (1988b) and Smeathers (1989) for the estimation of the natural frequencies and the damping ratios was based on the time domain analysis and can be difficult to apply because heavy damping of tissue results in rapid decay of free vibration so that peaks are not always clear: the damping ratios the authors estimated ranged from 0.1 to 0.5. The effectiveness of the method for the fore-and-aft motion of the spine was not reported. No validation for the method was shown.

The objectives of this section are to (1) establish a data correction method with appropriate accuracy so as to eliminate the effect of local tissue-accelerometer vibration from surface measurements over the spine both in the vertical and the fore-and-aft directions, (2) apply the method to measuring the motion of the viscera, (3) validate the method without using direct measurement and clarify the limitation of the method, and (4) standardise the correction function if there is only a small variability between subjects and between measuring sites on the body.

4.2.2 Theory

4.2.2.1 Definition of the correction frequency function

The method assumed a single degree-of-freedom linear model, within the frequency range of interest, for the local tissue-accelerometer system on the spine in the vertical axis (shear direction of tissue) and in the fore-and-aft axis (normal direction of tissue) respectively. The assumption was the same as that Hinz *et al.* (1988b) and Smeathers (1989) made for the local system in the vertical axis only. The local system can be described by the mass of an accelerometer and tissue involved in the local vibration, m, the stiffness of tissue, k, and the viscous damping coefficient of tissue, c, attached to the body system which may have multi degrees of freedom as shown in Figure 4.1.

The input point of the body system is the buttocks, when the subject is sitting, and the feet, when the subject is standing. The input may be acceleration or force. The true acceleration of the spine is $\ddot{x}_t(t)$. However, the measured acceleration is $\ddot{x}_m(t)$, which is the response of the local system to the input, $\ddot{x}_t(t)$.

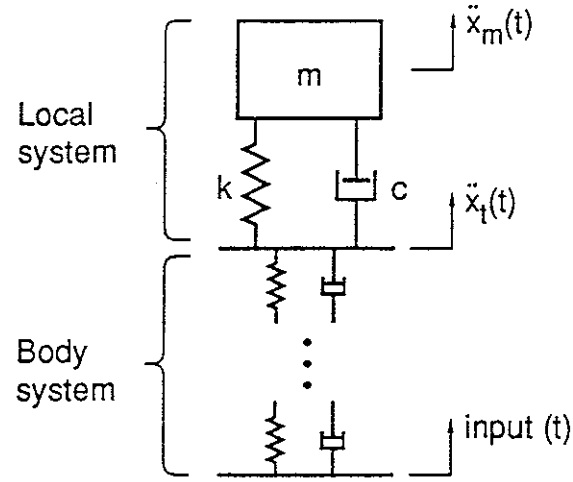

Figure 4.1 Equivalent model for the local system of an accelerometer mounted on the body surface.

The acceleration transfer function of the local system, $T_l(f)$, is the same as the displacement transfer function, which is given by:

$$T_l(f) = \frac{F\{\ddot{x}_m(t)\}}{F\{\ddot{x}_t(t)\}} = \frac{X_m(f)}{X_t(f)} \tag{4.1}$$

where: $\omega=2\pi f$; $F\{x(t)\}=X(f)$ means a Fourier transform from the time domain to the frequency domain. If the transfer function of the local system, $T_l(f)$, is determined, the Fourier transform of the true acceleration of the spine, $F\{\ddot{x}_t(t)\}$, can be obtained from the Fourier transform of the measured acceleration $F\{\ddot{x}_m(t)\}$:

$$F\{\ddot{x}_t(t)\} = F\{\ddot{x}_m(t)\}C(f) \tag{4.2}$$

where:

$$C(f) = \frac{1}{T_l(f)} \tag{4.3}$$

Therefore, $C(f)$ is the correction frequency function to eliminate the effect of the local tissue-accelerometer vibration from the measured acceleration. The time history of the true spinal acceleration, $\ddot{x}_t(t)$, is obtained by carrying out an inverse Fourier transform of equation (4.2).

When the true transfer function of the body system, $T_t(f)$, is to be estimated, it can be calculated from the measured transfer function, $T_m(f)$, and the correction frequency

function, $C(f)$:

$$T_t(f) = T_m(f)C(f) \tag{4.4}$$

where:

$$T_t(f) = \frac{F\{\ddot{x}_t(t)\}}{F\{input\ (t)\}} \tag{4.5}$$

$$T_m(f) = \frac{F\{\ddot{x}_m(t)\}}{F\{input\ (t)\}} \tag{4.6}$$

The input can be force or acceleration. When the input is force, the transfer functions, $T_t(f)$ and $T_m(f)$, are termed accelerances. When the input is acceleration, they are termed acceleration transfer functions.

4.2.2.2 Description of the correction frequency function

The equation of motion about the mass of the local system in Figure 4.1 is given by:

$$m\ddot{x}_m(t) + c(\dot{x}_m(t) - \dot{x}_t(t)) + k(x_m(t) - x_t(t)) = 0 \tag{4.7}$$

Solving equation (4.7) by substituting $x_t(t)=X_te^{i\omega t}$, $x_m(t)=X_me^{i\omega t}$, the theoretical acceleration, or displacement, transfer function of the local system, $T_l(f)$, is obtained:

$$T_l(f) = \frac{ic\omega + k}{-m\omega^2 + ic\omega + k} \tag{4.8}$$

Using the natural angular frequency, ω_o, damping ratio, ζ, and frequency ratio, β, equation (4.8) is simplified into equation (4.9):

$$T_l(\beta) = \frac{1 + 2i\zeta\beta}{1 - \beta^2 + 2i\zeta\beta} \tag{4.9}$$

where:

$$\omega_0 = 2\pi f_0 = \sqrt{\frac{k}{m}}$$

$$\zeta = \frac{c}{2\sqrt{mk}} \tag{4.10}$$

$$\beta = \frac{\omega}{\omega_0} = \frac{f}{f_0}$$

Therefore, the correction frequency function is:

$$C(\beta) = \frac{1-\beta^2 + 2i\zeta\beta}{1+2i\zeta\beta} \tag{4.11}$$

If the natural frequency, f_o, and the damping ratio, ζ, of the local system are found, the correction frequency function, $C(\beta)$, is determined.

4.2.2.3 Estimation of the natural frequency and damping ratio of the local system

The natural frequency and the damping ratio of the local system are estimated so as to determine the correction frequency function, using the spectral analysis of the free vibration response of the local system. Free vibration is caused by displacing the accelerometer on the body surface and releasing it while a subject is sitting or standing still. The equivalent model for the free vibration test is shown in Figure 4.2.

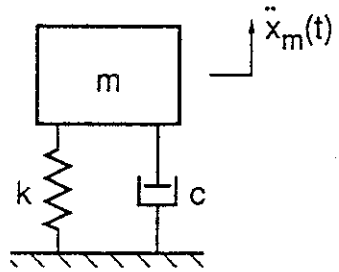

Figure 4.2 Equivalent model for the local system in free vibration.

The equation of motion about the mass of the local system in free vibration is:

$$m\ddot{x}_m(t) + c\dot{x}_m(t) + kx_m(t) = 0 \tag{4.12}$$

The initial conditions for the free vibration test are given by:

$$x_m(0) = x_0, \qquad \dot{x}_m(0) = 0 \tag{4.13}$$

To solve equations (4.12) and (4.13), a Laplace transform is more useful than a Fourier transform. In fact, a Laplace transform is the same as a Fourier transform, when letting s equal $i\omega$. By carrying out the Laplace transform of equation (4.12), with the initial conditions (4.13), a Laplace transform of the displacement response, $X_m(s)$, is obtained:

$$X_m(s) = \frac{(ms + c)x_0}{ms^2 + cs + k} \tag{4.14}$$

where: s is a Laplace operator. A Laplace transform of the acceleration response, $A_m(s)$, is calculated from equation (4.14) with the initial condition (4.13):

$$A_m(s) = -\frac{ksx_0}{ms^2 + cs + k} \tag{4.15}$$

Substituting $s=i\omega$ and using the relationship (4.10), equation (4.16) is obtained:

$$A_m(\beta) = -\frac{i\omega_0 x_0 \beta}{1-\beta^2 + 2i\zeta\beta} \tag{4.16}$$

where: $A_m(\beta)$ is the Fourier transform of the acceleration response to free vibration of the local system. The modulus of the free vibration response is:

$$|A_m(\beta)| = \frac{\omega_0 x_0 \beta}{\sqrt{(1-\beta^2)^2 + (2\zeta\beta)^2}} \tag{4.17}$$

Letting the derivative of equation (4.17) equal zero, the frequency corresponding to the peak modulus is obtained:

$$|A_m(\beta)|_{max} = \frac{\omega_0 x_0}{2\zeta} \qquad \text{at} \quad \beta = 1 \tag{4.18}$$

Therefore, the modulus of the free vibration response reaches a peak at the natural frequency.

Damping can be estimated from the width of the modulus curve around the peak. Letting equation (4.17) equal to half the power of the peak given by equation (4.18), equation (4.19) is obtained:

$$\zeta = \pm \frac{1-\beta^2}{2\beta} \tag{4.19}$$

Using the width of the curve, with Δf_- and Δf_+ in the lower and upper sides as shown in Figure 4.3, the frequency ratio corresponding to the half power points is obtained:

$$\beta = 1 \pm \frac{\Delta f_\pm}{f_0} \tag{4.20}$$

Substituting equation (4.20) into equation (4.19), the damping ratio is obtained:

$$\zeta_{\pm} = \mp \frac{1-(1\pm\frac{\Delta f_{\pm}}{f_0})^2}{2(1\pm\frac{\Delta f_{\pm}}{f_0})} \qquad (4.21)$$

When damping is quite small, equations (4.21) can be approximated to $\zeta_{\pm}=\Delta f_{\pm}/f_0$. However, the approximation is not appropriate for the heavy damping of the human body.

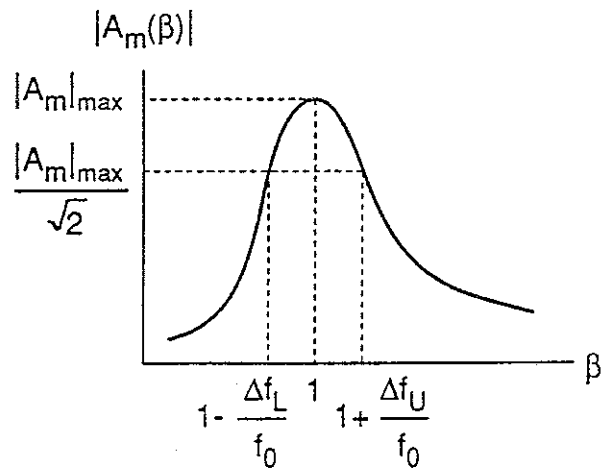

Figure 4.3 Estimation of the natural frequency and the damping ratio of the local system.

By the above means, a correction function is obtained by substituting the natural frequency and the damping ratio into equation (4.11). The advantage of this method is that correction works not only for the additional mass of the accelerometers but also for the mass of skin and shallow tissue around the contact area involved in the local vibration, because the method does not use the mass and the stiffness of the local system directly. The method may therefore be applied to the response on the abdominal wall so as to measure the motion of the viscera.

4.2.3 Experimental methods

The experimental validation of the method was conducted without using direct measurement. The transfer functions measured by accelerometers, with different masses, mounted on the body surface over the spine and on the abdominal wall were corrected separately and compared to find if they would coincide into the true transfer functions to the spine and the viscera. A pair of miniature accelerometers, Entran EGA-125-10D, weighing about 1 g were attached orthogonally to each other so as to measure acceleration both in the vertical and fore-and-aft directions at one site. The pair of accelerometers was attached on a stiff card which had dimensions of 35 mm (vertical) by 40 mm (horizontal) so as to increase the contact area at the body surface. Increasing the contact area would increase the stiffness of tissue and also stabilise the motion of the accelerometer. The effect of contact area was not investigated in this study and it was determined from a consideration of the approximate size of the vertebral bodies in the lumbar and thoracic region. The accelerometers were attached to the body surface over the spinous process of the vertebra L3 via the card using double-sided adhesive tape. The total mass of the accelerometers including the stiff card and adhesive tape was 6.3 g. Another pair of the same accelerometers were attached to the abdominal wall at about the level of the vertebra L2, using the same card. However, only vertical acceleration was measured on the abdominal wall. The total mass at each site was varied from 6.3 g to 15.8, 25.4 and 34.5 g, by attaching additional masses to the card.

Eight male subjects participated in the study. None of them had suffered back problems in the past. The free vibration test was conducted first. The subjects sat on a stationary rigid seat without a backrest in a normal relaxed posture. The stiff card was pulled up or down, using a thread connected to the card; the thread was cut to cause local free vibration. Free vibration time histories were recorded for 5 seconds with a sampling rate of 400 samples per second and low pass filtered at 100 Hz with a cut-off rate of 48 dB/octave. A total of 512 samples, corresponding to 1.28 seconds, around the actual response was extracted from each free vibration time history of 5 seconds so as to calculate a Fast Fourier Transform. An exponential window, defined by equation (4.22) and shown in Figure 4.4, was used for extraction so as to reduce the effect of noise:

$$W(t) = \begin{cases} e^{a(t-t_1)} & (t < t_1) \\ 1 & (t_1 \le t < t_2) \\ e^{-a(t-t_2)} & (t_2 \le t) \end{cases} \qquad \textbf{(4.22)}$$

where: t_1 and t_2 are the times of the beginning and the end of the visible response; the time constant of a=100 was used. The vertical and fore-and-aft accelerations were measured simultaneously for each excitation at the vertebra L3. The free vibration test was repeated four times at each site for each accelerometer mass. The effect of the initial displacement was also investigated to estimate any non-linearity of the local system.

The extracted time histories were transformed into the frequency domain, using a Fast Fourier Transform, and the moduli were calculated. The moduli were then normalised so that the peaks would coincide in magnitude. The most smooth modulus curves were chosen from the four repeated runs for the estimation of the natural frequencies and the damping ratios. The modulus curves sometimes showed more than one peak. In these situations, the first major peak and the width of the lower frequency side of the first peak were used. The natural frequencies and the damping ratios were estimated separately for each direction and for each accelerometer mass at each site. Then, the correction frequency functions were calculated, using the estimated natural frequencies and the damping ratios.

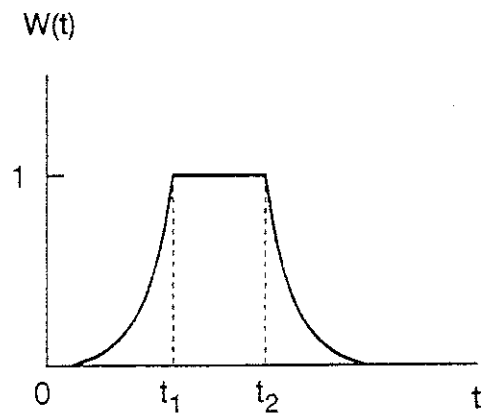

Figure 4.4 An exponential window for extraction of the free vibration response.

Following the free vibration test, a dynamic test was conducted. The subjects sat on a rigid seat without a backrest mounted on a vibrator and adopted the same posture as that for the free vibration test. A horizontal head position was measured and controlled before each experimental run to reduce the effects of changing posture between runs. The subjects were exposed to vertical random vibration with a magnitude of 2.0 m/s^2 r.m.s. in the frequency range from 0.5 to 35 Hz for 1 minute duration. The dynamic test consisted of four experimental runs: one for each of the four different accelerometer masses. During

each run, vertical and fore-and-aft acceleration over the vertebra L3 and vertical acceleration on the abdominal wall were measured as well as the input vertical acceleration on the rigid seat. The data were acquired with a sampling rate of 100 samples per second after low pass filtering at 35 Hz with a cut-off rate of 48 dB/octave. The acceleration transfer functions from the seat to each part of the body were calculated and then corrected by multiplication with the estimated correction frequency functions.

4.2.4 Results

The effect of the exponential window for extraction is shown in Figure 4.5. The noise in the time history resulted in ruggedness of the modulus curve (Figures 4.5a and 4.5b) but the exponential window eliminated the ruggedness from the modulus curve (Figures 4.5c and 4.5d). The modulus curves of the vertical acceleration over the L3 vertebra, corresponding to three different initial displacements during the free vibration test, are shown in Figure 4.6. The effect of initial displacement (i.e. non-linearity) on the natural frequency and the damping was small, as reported by Smeathers (1989).

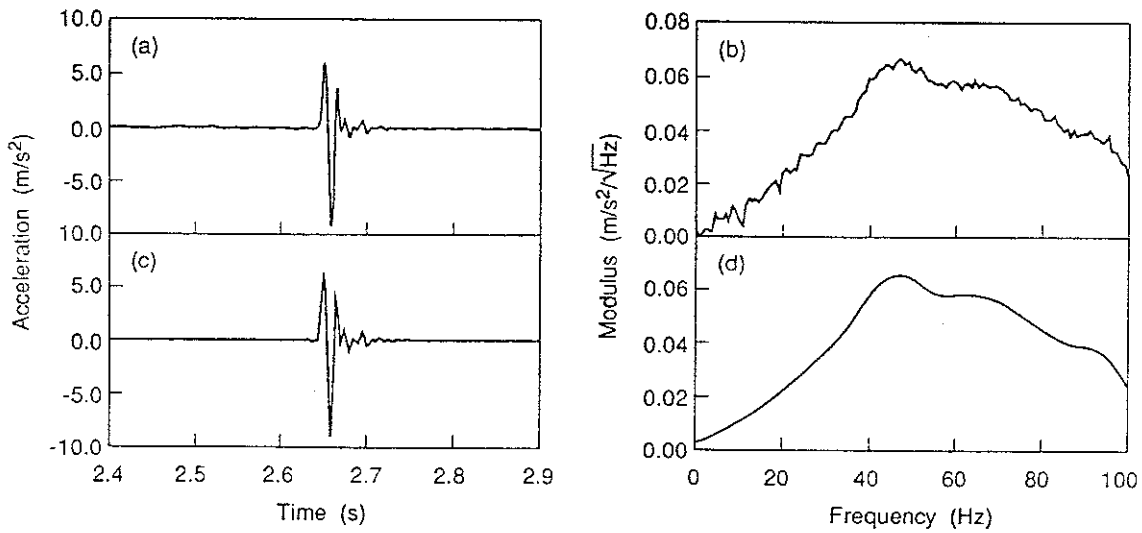

Figure 4.5 Effect of the exponential window to reduce noise: (a) free vibration time history extracted using a rectangular window; (b) modulus of the Fourier transform of the free vibration response extracted using a rectangular window; (c) free vibration time history extracted using the exponential window; (d) modulus of the Fourier transform of the free vibration response extracted using the exponential window.

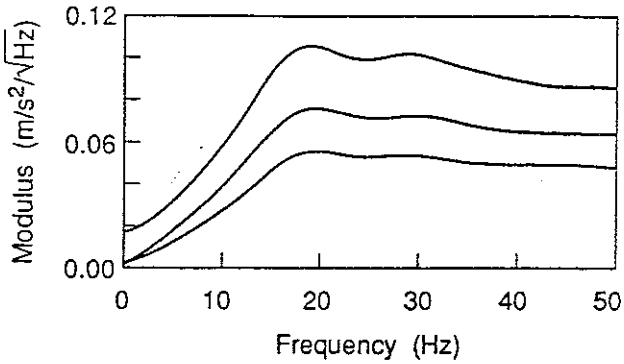

Figure 4.6 Modulus curves of the free vibration responses with different initial displacements measured over the L3 vertebra.

The modulus curves of the free vibration responses of four repeated runs showed that the repeatability of the free vibration test was satisfactory for the vertical responses over the vertebra L3 and on the abdominal wall (Figure 4.7). The modulus curves for the vertical responses with the four different accelerometer masses showed a systematic trend, where increased accelerometer masses decreased the natural frequencies as predicted by equation (4.10) (Figure 4.8). On the other hand, the repeatability was poor and the modulus curves with the four different accelerometer masses did not show any trend for the fore-and-aft responses over the vertebra L3 (Figures 4.7 and 4.8). The natural frequencies and the damping ratios were estimated only for the vertical responses (Tables 4.1 and 4.2). The results shown in Tables 1 and 2 may also be dependent on the contact area of the accelerometers. There were large differences found in the estimated natural frequencies and damping ratios between the subjects and between the sites.

The method was found to be effective for the vertical responses over the vertebra L3 and on the abdominal wall by the dynamic test. The transfer functions with the four different accelerometer masses before the correction and after the correction are shown in Figure 4.9 for one of the subjects, and in Figure 4.10 with the median transfer functions of the eight subjects. The four different accelerometer masses produced a systematic trend in the transfer functions from the seat to the vertebra L3 and to the abdominal wall in the vertical direction before the correction, where increased accelerometer masses increased the transmissibilities and the phase lags throughout the observed frequency range. The correction dramatically reduced the differences in the transmissibilities and the phase lags so that they became close to the identical ones which were the true transmissibility and

the true phase lag to the vertebra L3 and to the viscera in the vertical direction. The transfer functions from the seat to the vertebra L3 in the fore-and-aft direction appeared identical without the correction.

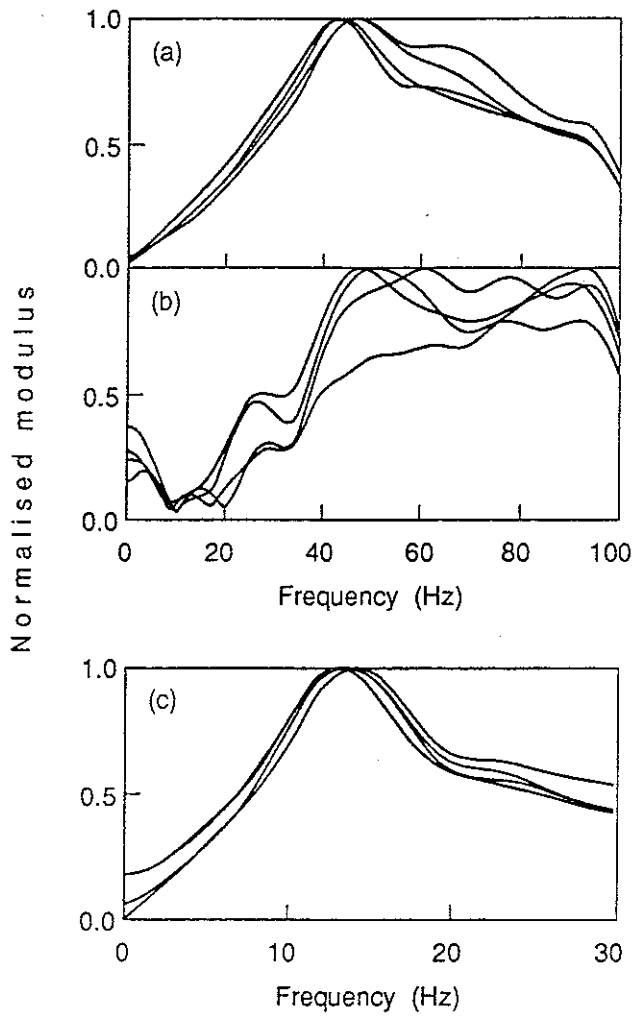

Figure 4.7 Typical normalised modulus curves of the free vibration responses of the four repeated runs to investigate the repeatability of the free vibration test: (a) vertical responses over the vertebra L3; (b) fore-and-aft responses over the vertebra L3; (c) vertical responses on the abdominal wall.

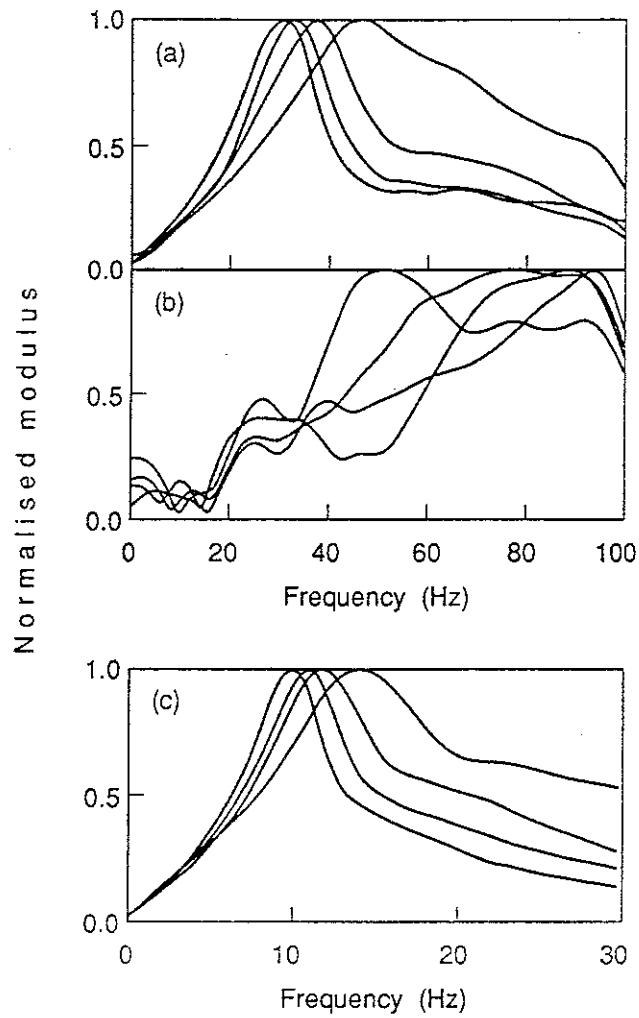

Figure 4.8 Typical normalised modulus curves of the free vibration responses with the four different masses: (a) vertical responses over the vertebra L3; (b) fore-and-aft responses over the vertebra L3; (c) vertical responses on the abdominal wall.

Table 4.1 Natural frequencies and damping ratios of the local tissue-accelerometer system over the vertebra L3 in the vertical direction estimated by the free vibration test.

Subject No.	Natural frequencies (Hz)				Damping ratios			
	Accelerometer mass (g)				Accelerometer mass (g)			
	6.4	15.8	25.4	34.5	6.4	15.8	25.4	34.5
1	46.1	37.6	33.0	30.9	0.31	0.30	0.29	0.32
2	14.7	15.1	14.5	—	0.39	0.34	0.31	—
3	36.0	26.6	23.8	21.4	0.42	0.28	0.26	0.25
4	19.6	19.1	18.2	19.5	0.41	0.37	0.32	0.27
5	33.5	30.3	29.1	21.6	0.39	0.37	0.20	0.18
6	33.1	28.4	26.2	21.5	0.35	0.26	0.26	0.23
7	22.3	19.9	17.9	17.4	0.51	0.40	0.38	0.30
8	34.0	30.0	26.1	23.9	0.57	0.43	0.35	0.29
Mean	29.9	25.9	23.6	22.3	0.42	0.34	0.30	0.26

(——); Not measured

Table 4.2 Natural frequencies and damping ratios of the local tissue-accelerometer system on the abdominal wall in the vertical direction estimated by the free vibration test.

Subject No.	Natural frequencies (Hz)				Damping ratios			
	Accelerometer mass (g)				Accelerometer mass (g)			
	6.4	15.8	25.4	34.5	6.4	15.8	25.4	34.5
1	14.2	11.8	10.9	10.0	0.34	0.27	0.26	0.26
2	7.23	7.30	7.07	7.09	0.27	0.23	0.23	0.20
3	11.0	11.0	10.1	9.08	0.36	0.34	0.30	0.30
4	7.87	7.44	7.38	7.42	0.26	0.24	0.24	0.17
5	9.50	10.1	10.9	10.9	0.48	0.40	0.44	0.45
6	12.6	12.2	11.7	10.9	0.45	0.39	0.35	0.36
7	15.6	14.8	13.8	11.8	0.52	0.40	0.40	0.34
8	10.6	10.2	9.93	9.57	0.31	0.29	0.23	0.19
Mean	11.1	10.6	10.2	9.60	0.37	0.32	0.31	0.28

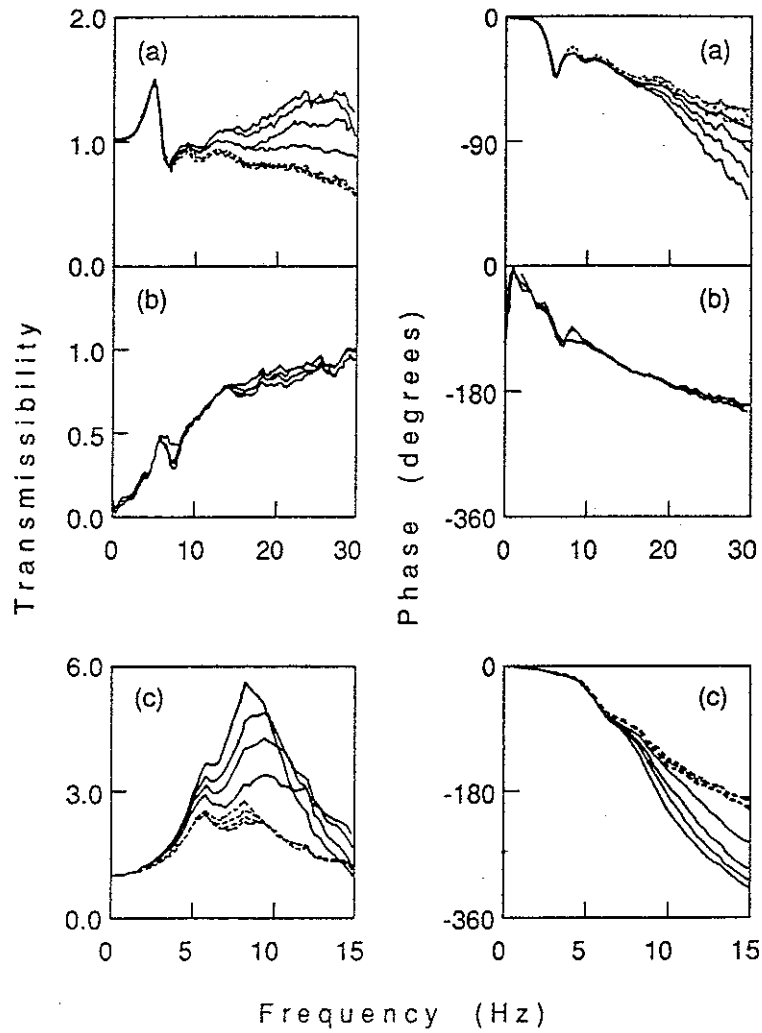

Figure 4.9 Transfer functions with the four different accelerometer masses on subject 1 before the correction (——) and after the correction (- - -): (a) from vertical seat acceleration to vertical acceleration of the vertebra L3; (b) from vertical seat acceleration to fore-and-aft acceleration of the vertebra L3; (c) from vertical seat acceleration to vertical acceleration of the abdominal wall (viscera).

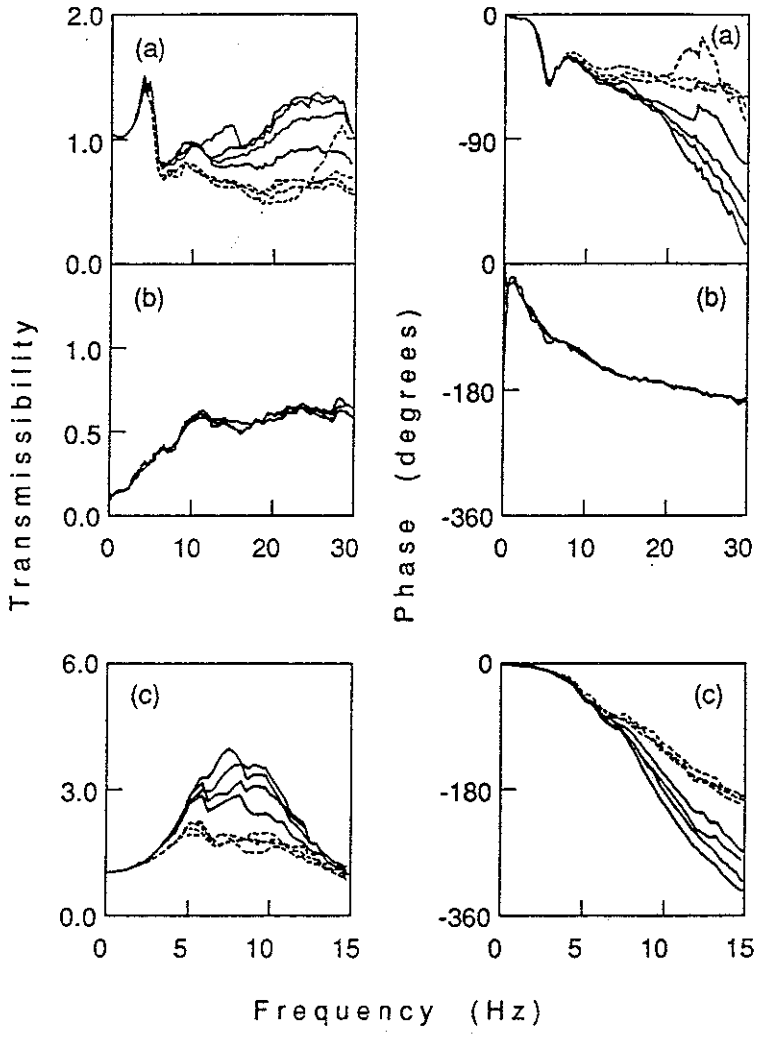

Figure 4.10 Median transfer functions of the eight subjects with the four different accelerometer masses before the correction (——) and after the correction (- - -): (a) from vertical seat acceleration to vertical acceleration of the vertebra L3; (b) from vertical seat acceleration to fore-and-aft acceleration of the vertebra L3; (c) from vertical seat acceleration to vertical acceleration of the abdominal wall (viscera).

4.2.5 Discussion

A correction method to eliminate the effect of local tissue-accelerometer vibration from surface measurement of motion of the spine was developed and it was also applied to measuring motion of the viscera. The method was validated without using direct measurement so as to clarify the limitation of the method. For the vertical responses over the vertebra L3 and on the abdominal wall, the correction worked satisfactorily except at the highest frequencies. The assumption of a single degree-of-freedom linear model

illustrated the limitation of the method both in the free vibration test and the dynamic test. The modulus curves of the free vibration responses generally showed deviations from the theoretical curves given by equation (4.17) above the natural frequencies corresponding to the first major peaks (Figure 4.11). In some cases there were more than one peak seen clearly. This finding indicated a multi degree-of-freedom response of the local system in each direction.

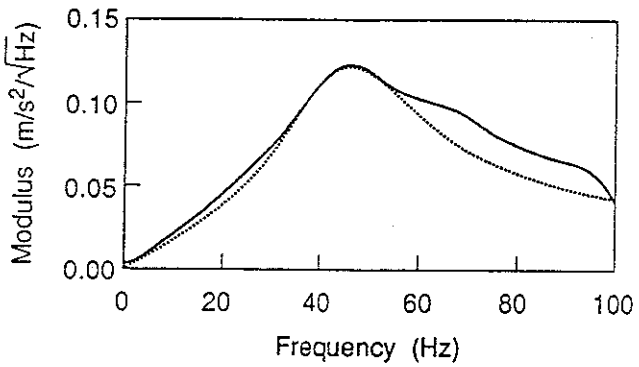

Figure 4.11 Comparison between the measured modulus curve (——) and the theoretical curve (- - -) of the vertical response to free vibration over the vertebra L3.

The deviation from a single degree-of-freedom model in the free vibration responses at the highest frequencies resulted in less effective correction of the transfer functions at those frequencies. Friedman two-way analysis of variance was used to investigate the statistical significance of differences between the transfer functions with the different accelerometer masses before and after the correction. The test was conducted separately on the transmissibilities and the phase lags at six frequencies (Tables 4.3, 4.4 and 4.5). The differences were not significant at the lowest frequencies either with or without correction for all the transfer functions, which suggested that the correction was not necessary at those frequencies. For the transfer functions to the vertebra L3 and the abdominal wall in the vertical direction, the differences reduced after the correction at frequencies below the estimated natural frequencies most significantly: the mean natural frequencies for the vertical responses with the heaviest accelerometer mass over the vertebra L3 and on the abdominal wall were 22.3 and 9.6 Hz respectively (Tables 4.1 and 4.2). It indicated that the correction was the most effective below the estimated natural frequency of the local system. This limitation of the method coincides with the limitation shown by Kim *et al.* (1993) who measured the transfer function of tissue using surface measurement and direct

measurement, and compared it with a theoretical transfer function of the same model for the local tissue-accelerometer system as used in this study. The estimated natural frequencies, which define the 'effective frequency range' of the correction, depended on the subject and the measuring site on the body. However, when using accelerometers weighing less than 30 g, the correction generally works up to about 20 Hz over the vertebra L3 and important responses of the spine occur within this frequency range.

For the transfer functions to the vertebra L3 in the fore-and-aft direction, Friedman analysis showed no statistically significant differences without the correction (Table 4.4). The results of the free vibration test and the dynamic test seemed to indicate that there was no clear mode of the local system occurring in this direction induced by the vertical excitation, and that the correction was not necessary for this direction at the frequencies considered. There were some workers who measured the natural frequency of tissue on the tibia using a preload in the direction perpendicular to the bone (Ziegert and Lewis, 1979; Collier and Donarski, 1987) and in the direction along the bone (Kim *et al.*, 1993; Valiant *et al.*, 1987). From these results, the stiffness of tissue on the tibia, neglecting the effect of preload and mass of tissue, ranged from 1.8×10^3 to 4.1×10^5 N/m for the normal direction, and 4.5×10^2 to 6.5×10^2 N/m for the shear direction. The stiffness of tissue in the normal direction was generally much higher than the stiffness in the shear direction. It is therefore reasonable to expect that the natural frequencies of the local system on the spine in the fore-and-aft direction were higher than the frequency range analyzed and they were high enough to make the correction unnecessary in the observed frequency range.

Table 4.3 Levels of statistical significance of differences, obtained using Friedman two-way analysis of variance, between the transfer functions to the vertebra L3 (vertical) with the four different accelerometer masses before and after the correction (*; $p<0.05$, †; $p<0.01$).

Transmissibility						
Freq.(Hz)	4.7	9.4	16.4	21.1	25.8	30.4
Before	0.856	0.100	0.001†	0.003†	0.020*	0.025*
After	0.478	0.392	0.774	0.692	0.018*	0.011*
Phase						
Freq.(Hz)	4.7	9.4	16.4	21.1	25.8	30.4
Before	0.100	0.429	0.478	0.034*	0.002†	0.004†
After	0.100	0.419	0.319	0.319	0.856	0.934

Table 4.4 Levels of statistical significance of differences, obtained using Friedman two-way analysis of variance, between the transfer functions to the vertebra L3 (fore-and-aft) with the four different accelerometer masses before the correction (*; p<0.05, †; p<0.01).

Transmissibility						
Freq.(Hz)	4.7	9.4	16.4	21.1	25.8	30.4
Before	0.692	0.392	0.086	0.116	0.054	0.001†
After	——	——	——	——	——	——
Phase						
Freq.(Hz)	4.7	9.4	16.4	21.1	25.8	30.4
Before	0.208	0.116	0.116	0.208	0.134	0.168
After	——	——	——	——	——	——

Table 4.5 Levels of statistical significance of differences, obtained using Friedman two-way analysis of variance, between the transfer functions to the abdominal wall (vertical) with the four different accelerometer masses before and after the correction (*; p<0.05, †; p<0.01).

Transmissibility						
Freq.(Hz)	2.3	4.7	7.0	9.4	11.7	14.1
Before	0.415	0.016*	0.004†	0.392	0.583	0.241
After	0.327	0.145	0.024*	0.861	0.583	0.789
Phase						
Freq.(Hz)	2.3	4.7	7.0	9.4	11.7	14.1
Before	0.930	0.615	0.018*	0.008†	0.005†	0.002†
After	0.648	0.348	0.290	0.062	0.024*	0.014*

Error functions between the transfer functions with the different accelerometer masses were calculated to investigate the effect of the correction at different frequencies. The error functions were defined for the vertical responses as follows:

For transmissibility

$$E_T(f) = \frac{T_{+j}(f)}{T_{+0}(f)} \qquad (j = 1,2,3) \tag{4.23a}$$

For phase

$$E_p(f) = P_{+j}(f) - P_{+0}(f) \qquad (j = 1,2,3) \tag{4.23b}$$

where: $E_T(f)$ and $E_P(f)$ are the error functions for the transmissibility and the phase; $T(f)$ and $P(f)$ are the transmissibility and the phase; subscript +0, +1, +2 and +3, represents the experimental conditions with the four accelerometer masses of 6.3, 15.8, 25.4 and 34.5

g respectively. Median error functions of the eight subjects before and after the correction are shown in Figures 4.12 and 4.13. The significance levels for differences between the error functions before and after the correction were calculated using the Wilcoxon matched pairs signed-ranks test and the results are shown in Tables 4.6 and 4.7. The errors (differences) between the transfer functions of the vertical responses with different accelerometer masses reduced, after the correction, by a statistically significant amount within the effective frequency range.

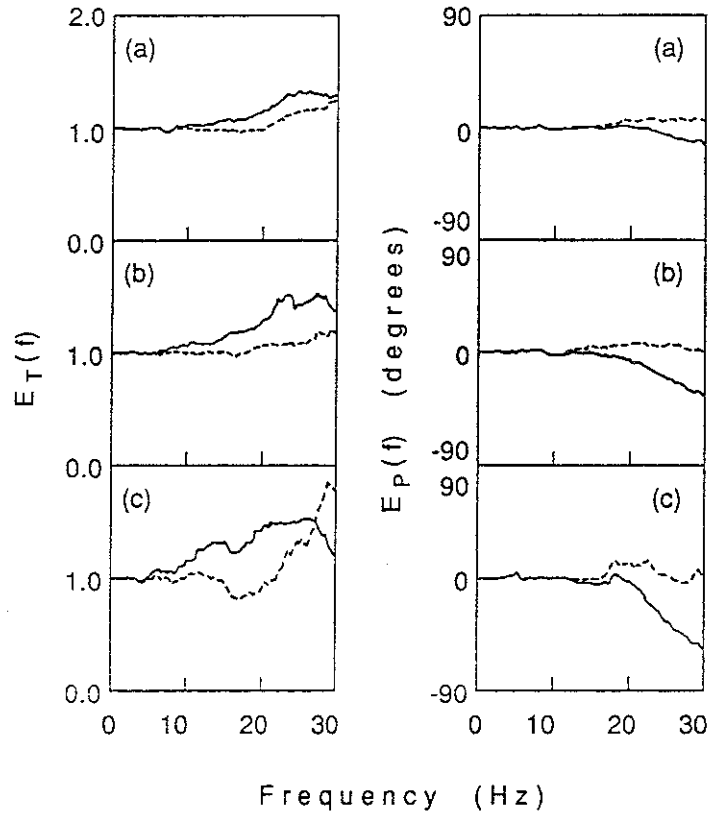

Figure 4.12 Median error functions of the transfer functions to the vertebra L3 (vertical) between different accelerometer masses, before the correction (——) and after the correction (- - -): (a) error between accelerometer masses 6.3 and 15.8 g; (b) error between 6.3 and 25.4 g; (c) error between 6.3 and 34.5 g.

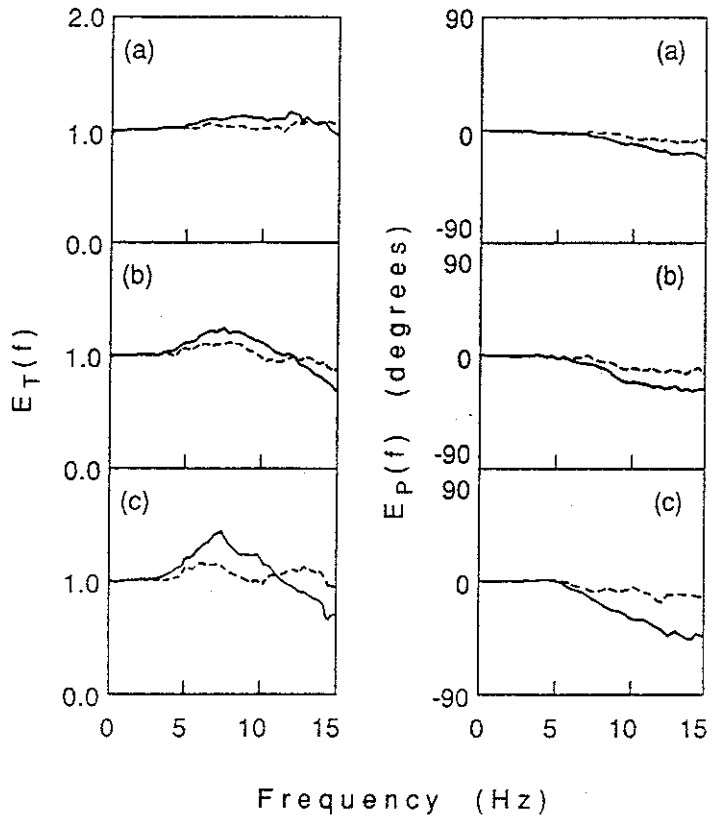

Figure 4.13 Median error functions of the transfer functions to the abdominal wall (vertical) between different accelerometer masses, before the correction (——) and after the correction (- - -): (a) error between accelerometer masses 6.3 and 15.8 g; (b) error between 6.3 and 25.4 g; (c) error between 6.3 and 34.5 g.

Table 4.6 Levels of statistical significance of differences, obtained using Wilcoxon matched pairs signed-ranks test, between the error functions for the transfer functions to the vertebra L3 (vertical) before and after the correction (*; $p<0.05$, †; $p<0.01$).

Error for transmissibility, E_T						
Freq.(Hz)	4.7	9.4	16.4	21.1	25.8	30.4
+0 - +1	0.021*	0.010†	0.010†	0.010†	0.080	0.624
+0 - +2	0.010†	0.010†	0.010†	0.059	0.080	0.624
+0 - +3	0.014*	0.014*	0.014*	0.022*	0.205	0.052
Error for phase, E_P						
Freq.(Hz)	4.7	9.4	16.4	21.1	25.8	30.4
+0 - +1	0.183	0.529	0.441	0.010†	0.010†	0.010†
+0 - +2	0.234	0.080	0.141	0.010†	0.010†	0.010†
+0 - +3	0.205	0.076	0.014*	0.204	0.014*	0.014*

+0 - +1; error between the accelerometer masses of 6.4 and 15.8 g
+0 - +2; error between the accelerometer masses of 6.4 and 25.4 g
+0 - +3; error between the accelerometer masses of 6.4 and 34.5 g

Table 4.7 Levels of statistical significance of differences, obtained using Wilcoxon matched pairs signed-ranks test, between the error functions for the transfer functions to the abdominal wall (vertical) before and after the correction (*; $p<0.05$, †; $p<0.01$).

Error for transmissibility, E_T						
Freq.(Hz)	2.3	4.7	7.0	9.4	11.7	14.1
+0 - +1	0.141	0.021*	0.010†	0.080	0.183	0.441
+0 - +2	0.107	0.030*	0.014*	0.080	0.528	0.141
+0 - +3	0.058	0.014*	0.014*	0.058	0.294	0.021*
Error for phase, E_P						
Freq.(Hz)	2.3	4.7	7.0	9.4	11.7	14.1
+0 - +1	0.624	0.624	0.726	0.030*	0.010†	0.010†
+0 - +2	0.441	0.059	0.080	0.042*	0.021*	0.014*
+0 - +3	0.726	0.834	0.042*	0.014*	0.014*	0.014*

+0 - +1; error between the accelerometer masses of 6.4 and 15.8 g
+0 - +2; error between the accelerometer masses of 6.4 and 25.4 g
+0 - +3; error between the accelerometer masses of 6.4 and 34.5 g

In order to validate the method further, the data were compared with direct measurements. Panjabi *et al.* (1986) measured the transmissibilities from vertical seat acceleration to vertical and fore-and-aft acceleration of the vertebra L3, using Kirschner wires. Five subjects were excited by vertical discrete sinusoidal vibration with a magnitude of 1.0 m/s^2 in the frequency range from 2 to 15 Hz. Magnusson *et al.* (1993) measured the same transmissibilities also using Kirschner wires. Three subjects were exposed to vertical impact excitation given to the seat. The mean corrected transmissibility to the vertebra L3 in the vertical direction and the mean uncorrected transmissibility to the vertebra L3 in the fore-and-aft direction appear to be in good agreement with the direct measurements (Figures 4.14 and 4.15).

Standard correction frequency functions could not be established because of a large variability in the natural frequencies and the damping ratios between subjects and between measuring sites. Increments in the accelerometer mass generally reduced both the natural frequencies and the damping ratios. However, for all the subjects, the shifts were smaller than calculated from the theory using the accelerometer masses and equation (4.10). This result seems to indicate that the mass of skin and other tissue involved in the local vibration reduced the effect of the additional masses. There were some subjects who showed large decrements in the natural frequency but small decrements in the damping ratio (see subject 1 in Table 4.1) while others showed the opposite trend (see subject 4 in Table 4.1). This result suggests that the stiffness and the damping coefficient of the local system changed when the mass was changed (i.e. a non-linearity), and that the change depended on the subject. Valiant *et al.* (1987) found that both the stiffness and the damping coefficient of the local system increased with increasing mass of the accelerometer.

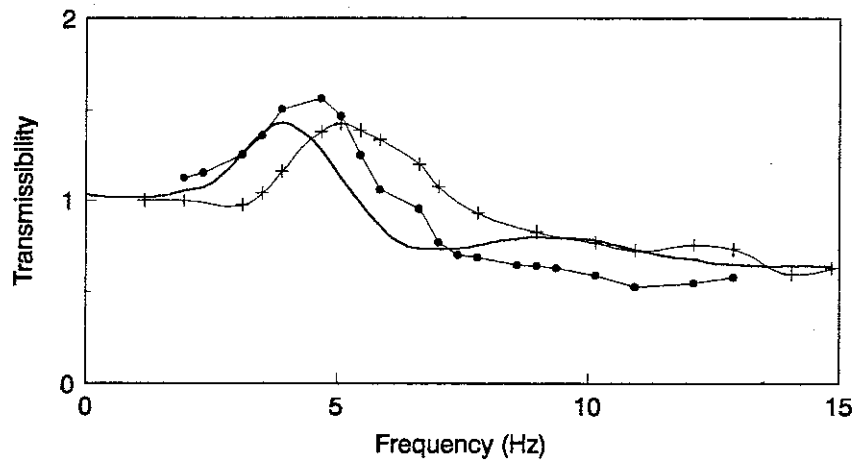

Figure 4.14 Comparison between the transmissibilities from vertical seat acceleration to vertical acceleration of the vertebra L3 in this study and direct measurements: mean corrected transmissibility of eight subjects in this study (——); mean transmissibility of five subjects measured using Kirschner wires by Panjabi *et al.* (—•—); mean transmissibility of three subjects measured using Kirschner wires by Magnusson *et al.* (—+—).

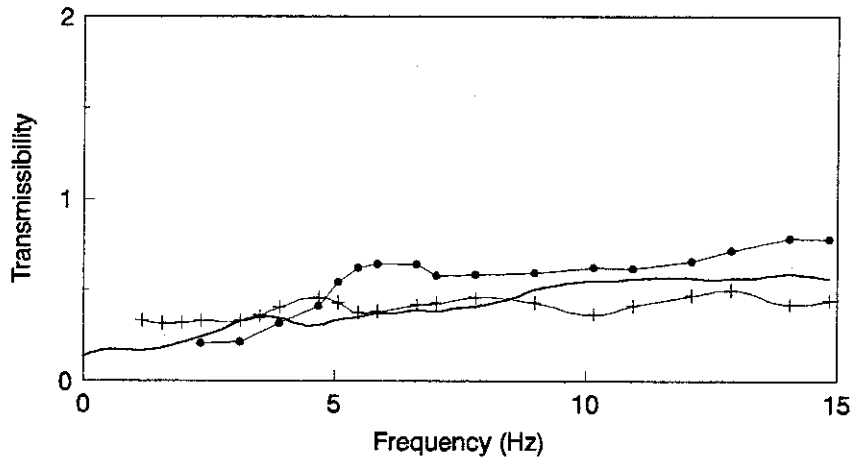

Figure 4.15 Comparison between the transmissibilities from vertical seat acceleration to fore-and-aft acceleration of the vertebra L3 in this study and direct measurements: mean uncorrected transmissibility of eight subjects in this study (——); mean transmissibility of five subjects measured using Kirschner wires by Panjabi *et al.* (—•—); mean transmissibility of three subjects measured using Kirschner wires by Magnusson *et al.* (—+—).

4.2.6 Conclusions

A correction method has been devised to eliminate the effect of local tissue-accelerometer vibration from surface measurements over the spine in the vertical direction. Fore-and-aft responses over the spine did not seem to require correction. The method is also suitable for the measurement of vertical responses of the viscera on the abdominal wall. The procedure is limited to frequencies below the estimated natural frequency of the local system. Variability in the natural frequencies and the damping ratios of the local system between subjects and measuring sites prevented the determination of standard correction frequency functions. It is concluded that responses of the spine and the viscera can be measured non-invasively using the method which has been developed.

4.3 EXPERIMENTAL MODAL ANALYSIS OF WHOLE-BODY VIBRATION

4.3.1 Introduction

Mechanical responses to whole-body vibration have been measured by many workers so as to investigate the effects of vibration on health, activities and comfort. However a theory to explain how human body responds to vibration has not yet been established. Experimental modal analysis is one of the methods that may be used to characterise the dynamic behaviour of structures. In this section, experimental modal analysis is applied to whole-body vibration to extract the natural frequencies and the vibration mode shapes of the human body. The objectives of this section are (1) to assess the applicability of experimental modal analysis to whole-body vibration, (2) to identify the vibration mode shape of the principal resonance of the human body at about 5 Hz, which was hypothesised as a combination of an entire body mode, a visceral mode and a bending mode of the spine, (3) to identify the vibration mode shape of the second principal resonance between 8 and 12 Hz, (4) to identify the effect of posture on the vibration mode shapes and (5) to provide vibration mode shape data to validate biodynamic models.

4.3.2 Theory

4.3.2.1 Fundamentals of the experimental modal analysis

Experimental modal analysis relies on the theory that the dynamic behaviour of a structure

can be described in terms of its modal properties of the natural frequencies, the mode shapes and the damping. The technique seeks to extract the modal properties from measured data, generally from transfer functions. There are some assumptions required to apply the experimental modal analysis technique to the human body structure. Firstly, the human body is assumed to be linear. Although non-linear responses have been found in the driving point responses and the seat-to-head transmissibilities, the assumption may be valid within the restricted range of magnitudes used in the study. Secondly, the hysteretic damping is assumed for the human body. There are no known data identifying whether the damping of the human body is viscous or hysteretic.

The equation of motion for a linear structure with *N* degrees of freedom and the hysteretic damping can be described by equation (4.24):

$$[M]\{\ddot{x}(t)\} + i[H]\{x(t)\} + [K]\{x(t)\} = \{f(t)\} \qquad \textbf{(4.24)}$$

where: [*M*] is the *N*x*N* mass matrix; [*H*] is the *N*x*N* hysteretic damping matrix; [*K*] is the *N*x*N* stiffness matrix; $\{\ddot{x}(t)\}$ and $\{x(t)\}$ are the *N*x1 acceleration and displacement response vectors; $\{f(t)\}$ is the *N*x1 applied force vector. The free response (i.e. $\{f(t)\}=0$) solution of equation (4.24) provides *N* eigenvalues; λ_1^2, λ_2^2,..., λ_N^2 and associated eigenvectors; $\{\phi_1\},\{\phi_2\},\cdots,\{\phi_N\}$. For this general case, both the eigenvalues and the eigenvectors are mathematically complex. The eigenvalues are of the form:

$$\lambda_r^2 = \omega_r^2(1+i\eta_r) \qquad \textbf{(4.25)}$$

where: ω_r is the undamped natural angular frequency for the *r*th mode; η_r is the damping loss factor for the *r*th mode. In the special case of the proportional damping where the damping matrix is described by equation (4.26), both the eigenvalues and the eigenvectors take real values and they are equal to those for an undamped system obtained in section 3.2.2:

$$[H] = \beta[M] + \gamma[K] \qquad \textbf{(4.26)}$$

The complex eigenvectors, which correspond to the complex mode shape vectors, can be scaled in such a way that the orthogonality properties may be expressed by the relationships:

$$[\phi]^T[M][\phi] = [I] \qquad \textbf{(4.27a)}$$

$$[\phi]^T[K][\phi] = [\omega_r^2] \qquad \textbf{(4.27b)}$$

$$[\phi]^T[H][\phi] = [\eta_r\omega_r^2] \qquad \textbf{(4.27c)}$$

where: $[\phi]$ is the modal matrix whose columns are mode shape vectors (i.e. $[\phi]=[\{\phi_1\},\{\phi_2\},\cdots,\{\phi_N\}]$; $[I]$ is the identity matrix; $[\omega_r^2]$ is the diagonal matrix of ω_r^2; $[\eta_r\omega_r^2]$ is the diagonal matrix of $\eta_r\omega_r^2$.

Transforming equation (4.24) into the form using the modal coordinates (see section 3.2.3.1) and letting $\{x(t)\}=\{X\}e^{i\omega t}$, $\{f(t)\}=\{F\}e^{i\omega t}$, the displacement response is obtained:

$$\{X\}=\sum_{r=1}^{N}\frac{\{\phi\}_r^T\{F\}\{\phi\}_r}{\omega_r^2-\omega^2+i\eta_r\omega_r^2} \tag{4.28}$$

The receptance (displacement/force) between the sites j and k, α_{jk}, can be written by a decoupled equation (4.29):

$$\frac{X_j}{F_k}=\alpha_{jk}=\sum_{r=1}^{N}\frac{A_{jkr}+iB_{jkr}}{\omega_r^2-\omega^2+i\eta_r\omega_r^2} \tag{4.29}$$

with:

$$A_{jkr}+iB_{jkr}=\phi_{jr}\phi_{kr} \tag{4.30}$$

where: X_j is the displacement response at the site j; F_k is the applied force at the site k; ϕ_{jr},ϕ_{kr} are the mode shapes for the rth mode at the sites j and k which correspond to deformation ratios for the rth mode; ω is the angular excitation frequency; A_{jkr} and B_{jkr} are termed the modal constants. Equation (4.29) indicates that the response is expressed by a summation of all the modes. Equation (4.29) can be approximated to a single term corresponding to the dominant rth mode with a constant and complex residual term representing the contributions of the remaining modes:

$$\alpha_{jk}\cong\frac{A_{jkr}+iB_{jkr}}{\omega_r^2-\omega^2+i\eta_r\omega_r^2}+residual \tag{4.31}$$

Experimental modal analysis extracts the modal properties of the natural frequencies, ω_r, the damping, η_r, and the modal constants, A_{jkr} and B_{jkr}, for each mode, generally based on equation (4.31). Finally, the modal matrix, $[\phi]$, is determined using the relationship (4.30) and the deformation of the structure can be plotted at each mode.

There are various methods for extracting the modal properties. A widely used single degree-of-freedom method is based on the fact that the frequency response around the resonance (equation 4.31) may be displayed as a circular locus when plotted on an Argand diagram (complex plane). The modal properties are extracted from the best fit circle based on equation (4.31). The method used in this study is based on a single

degree-of-freedom model classified as the dynamic stiffness (1/receptance) method. Reversing equation (4.31), equation (4.32) is obtained:

$$\frac{1}{\alpha^{*}_{jk}} = \frac{\omega_r^{\,2} - \omega^2 + i\eta_r\omega_r^{\,2}}{A_{jkr} + iB_{jkr}} \tag{4.32}$$

with:

$$\alpha^{*}_{jk} = \alpha_{jk} - residual \tag{4.33}$$

If the real and imaginary components of equation (4.32) are plotted against ω^2 with an assumption of the proportional damping for the structure (i.e. B_{jkr}=0), it is possible to extract the modal properties directly from slopes and intercepts of the straight lines. The method used in this study was the modified dynamic stiffness method developed by Dobson (1987) which can calculate the complex modal constants and does not require the calculation of the residual term in advance (see Appendix 3). A computer program also allowed iterative analysis around closely located modes so as to eliminate the effect of adjacent modes at each iteration so that closely located modes became well separated.

4.3.2.2 Additional considerations for the application of experimental modal analysis to whole-body vibration

The acceleration transfer functions were used for the experimental modal analysis instead of the receptances or accelerances due to the following reason. The body system of a seated human shown in Figure 3.1 may be expressed by a series of masses and springs as shown in Figure 4.16, where dampers are excluded to simplify the problem.

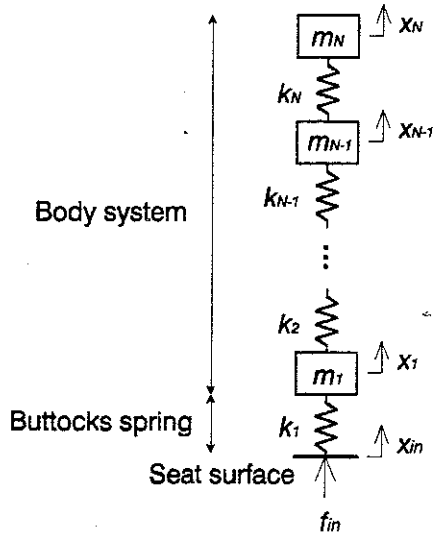

Figure 4.16 System 4.1: equivalent model for a seated human.

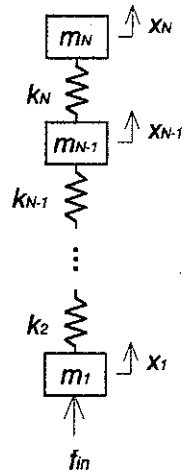

Figure 4.17 System 4.2.

The equation of motion for the lowest mass, m_1, of System 4.1 is:

$$m_1\ddot{x}_1(t) + k_1(x_1(t) - x_{in}(t)) + k_2(x_1(t) - x_2(t)) = 0 \quad \textbf{(4.34)}$$

The force measured at the seat-buttocks interface is in equilibrium with the reaction force from the spring, k_1:

$$f_{in}(t) = k_1(x_{in}(t) - x_1(t)) \quad \textbf{(4.35)}$$

Combining equations (4.34) and (4.35):

$$m_1\ddot{x}_1(t) + k_2(x_1(t) - x_2(t)) = f_{in}(t) \quad \textbf{(4.36)}$$

Equation (4.36) is the same as the equation of motion for the lowest mass, m_1, in System 4.2 shown in Figure 4.17. Therefore:

$$\text{System 4.1} = \text{System 4.2} \quad \textbf{(4.37)}$$

If the force at the seat-buttocks interface and the displacement or acceleration of the body are measured, receptances, α_j, or accelerances (inertances), A_j, are calculated and they might be used for the analysis based on equation (4.29) with the relationships:

$$\alpha_j = \frac{X_j(f)}{F_{in}(f)} \quad \textbf{(4.38)}$$

$$A_j = -\omega^2\alpha_j = \frac{-\omega^2 X_j(f)}{F_{in}(f)} \quad \textbf{(4.39)}$$

where: $X_j(f)$ and $F_j(f)$ are the Fourier transforms of the displacement, $x_j(t)$, and the force, $f_j(t)$ respectively.

However, if there is an entire body mode where the body system moves rigidly and only the buttocks spring, k_1, works, the system will be equivalent to System 4.3 in Figure 4.18.

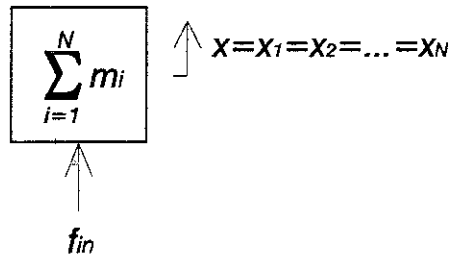

Figure 4.18 System 4.3: Entire body mode.

The equation of motion for System 4.3 is:

$$M\ddot{x}(t) = f_{in}(t) \tag{4.40}$$

where:

$$M = \sum_{i=1}^{N} m_i \tag{4.41a}$$

$$x(t) = x_1(t) = x_2(t) = \cdots = x_N(t) \tag{4.41b}$$

The Fourier transform of equation (4.40) yields:

$$-\omega^2 MX(f) = F_{in}(f) \tag{4.42}$$

Hence, the receptance, α_{ent}, and the accelerance, A_{ent}, for the entire body mode are obtained by substituting equation (4.42) into equations (4.38) and (4.39):

$$\alpha_{ent} = \frac{1}{-\omega^2 M} \tag{4.43}$$

$$A_{ent} = \frac{1}{M} \tag{4.44}$$

The modulus of the receptance for the entire body mode is simply proportional to 1/(frequency)^2 and the modulus of the accelerance is constant. Therefore, neither the receptance nor the accelerance detect the entire body mode.

The acceleration transfer functions are more appropriate to extract the vibration modes of the human body which may include an entire body mode. Equation (4.34) can be written in the other form with damping terms:

$$m_1\ddot{x}_1(t) + (i\eta_1 + k_1)x_1(t) + (i\eta_2 + k_2)(x_1(t) - x_2(t)) = f_1(t) \tag{4.45}$$

$$f_1(t) = (i\eta_1 + k_1)x_{in}(t) \tag{4.46}$$

Equation (4.45) is the same as the equation of motion for the lowest mass, m_1, in System 4.4 shown in Figure 4.19 with an assumption of equation (4.46).

Therefore, the displacement response is given by equation (4.28) with an assumption:

$$\{F\} = \begin{Bmatrix} (i\eta_1 + k_1)X_{in} \\ 0 \\ \vdots \\ 0 \end{Bmatrix} \tag{4.47}$$

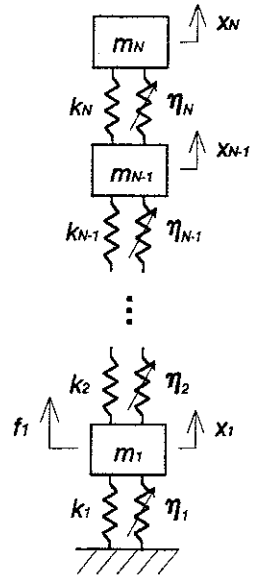

Figure 4.19 System 4.4.

The acceleration transfer function is obtained from equations (4.28) and (4.47):

$$\frac{X_j}{X_{in}} = \sum_{r=1}^{N} \frac{\phi_{jr}\phi_{1r}(i\eta_1 + k_1)}{\omega_r^{\,2} - \omega^2 + i\eta_r\omega_r^{\,2}} = \sum_{r=1}^{N} \frac{A_{j1r} + iB_{j1r}}{\omega_r^{\,2} - \omega^2 + i\eta_r\omega_r^{\,2}} \qquad \textbf{(4.48)}$$

The modal constants extracted from the acceleration transfer functions using the procedure based on equations from (4.31) to (4.33) are multiplied by the constant, $i\eta_1+k_1$. However, since the mode shapes merely mean the ratios of deformation between sites, the constant does not affect the results.

4.3.2.3 Modal assurance criteria

When the modal properties are extracted and corresponding mode shapes are determined, a 'modal assurance criterion' (MAC) can be used to find correlated mode shapes. The modal assurance criterion is defined by equation (4.49):

$$\mathrm{MAC}(a,b) = \frac{\left|\sum_{r=1}^{m} (\phi_a)_r (\phi_b)_r^*\right|^2}{\left\{\sum_{r=1}^{m} (\phi_a)_r (\phi_a)_r^*\right\}\left\{\sum_{r=1}^{m} (\phi_b)_r (\phi_b)_r^*\right\}} \qquad \textbf{(4.49)}$$

where: MAC(a,b) is the modal assurance criterion between two mode shapes, a and b; $(\phi_a)_r$ and $(\phi_b)_r$ are the elements of the rth row of the mode shape vectors, a and b; m is the number of rows in the mode shape vectors which corresponds to the number of measuring sites and directions; (* signifies the complex conjugate). The MAC takes a value between 0 and 1: when two modes are close together, MAC is closer to 1; if two modes are different, MAC becomes close to 0.

4.3.3 Methods

4.3.3.1 Experimental methods

The acceleration responses of the spine, pelvis, viscera and the head were measured so as to conduct the modal analysis of whole-body vibration. The spinal responses were measured at four vertebrae T1, T6, T11, L3 and at the sacrum S2. A pair of miniature accelerometers (Entran Model EGA-125-10D) weighing 1 g was attached perpendicularly to each other on a stiff card which had a dimension of 35 mm (vertical) x 40 mm (horizontal). The pairs of the accelerometers were attached to the body surface over the spinous processes via the cards using double-sided adhesive tape (Figure 4.20a) and they were oriented in the directions along the spine and perpendicular to the spine so as to measure the axial and bending responses in the mid-sagittal plane at each level of the spine. The total mass of the accelerometers on the card with adhesive tape was about 6 g. The same type of accelerometer was attached to the pelvis on the front-upper edge of the right side iliac crest (Figure 4.20b). It was oriented in the vertical direction so as to determine the rotational response of the pelvis with the responses measured at the sacrum S2, assuming that the pelvis was rigid and the sacrum was connected to the pelvis rigidly (see section 4.3.3.2). The vertical response of the viscera was measured by attaching the same type of accelerometer on the abdominal wall at the L2 level (Figure 4.20b). The responses of the head were measured by accelerometers (Entran Model EGCSY-240D-10D) which were mounted on a bite-bar 90 mm left and 100 mm behind the mouth (Figure 4.20b), and oriented in the directions along and perpendicular to the cervical spine. The accelerometers on the bite-bar was located behind the mouth so as to reduce acceleration measurement due to pitching motion of the head. The same type of accelerometer was used to measure the vertical excitation acceleration on a rigid seat. The vertical response force was also measured by a force platform (Kistler Type 9281B) placed between the rigid seat and the buttocks of the subjects.

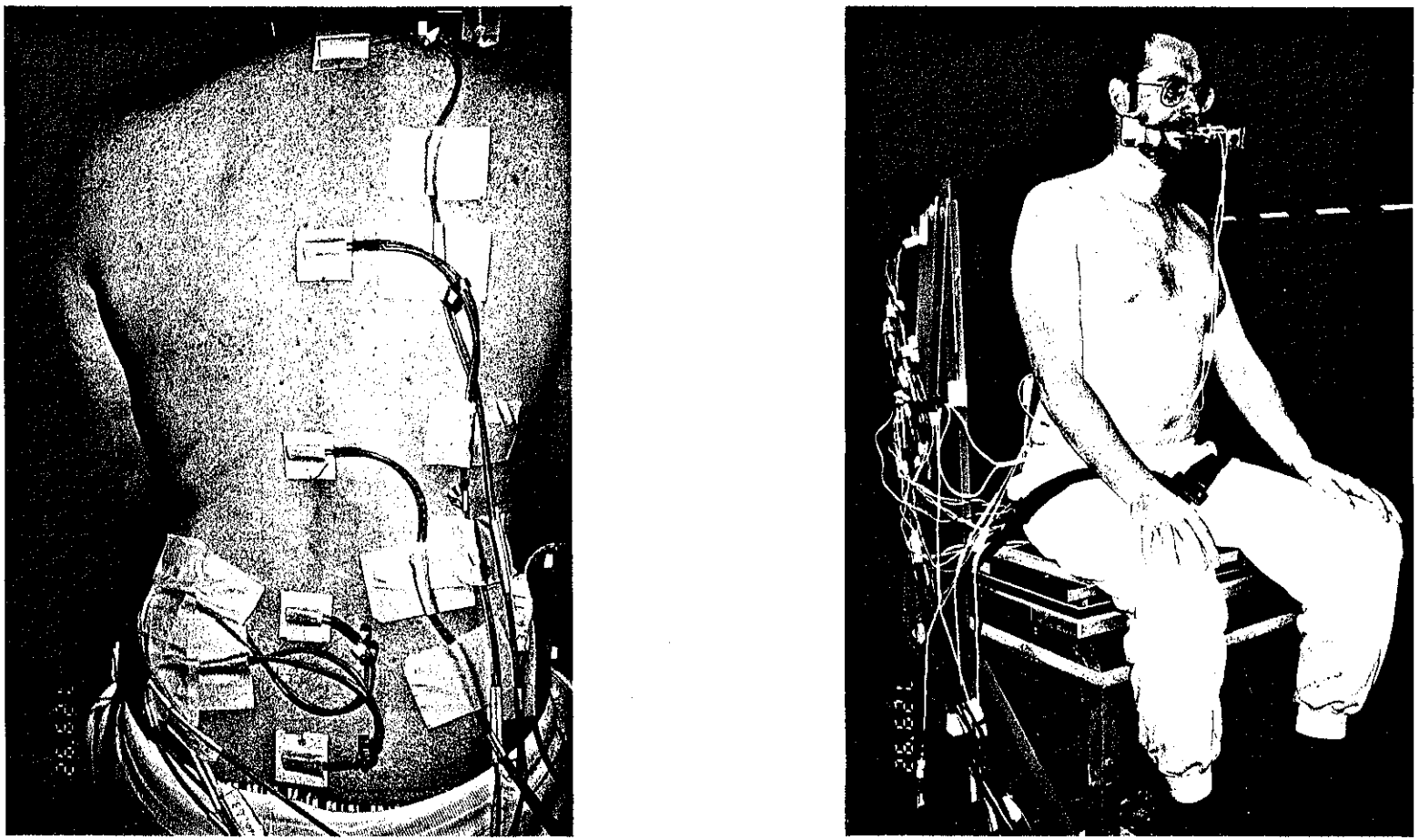

(a) (b)

Figure 4.20 Accelerometers attached to the body of a subject; (a) accelerometers over the spinous processes of the vertebrae T1, T6, T11, L3 and S2; (b) accelerometers on the abdominal wall (L2 level), front-upper edge of the right side iliac crest and on the bite-bar (90 mm left and 100 mm behind the mouth).

The subjects adopted erect, normal and slouched postures in a sitting position. The erect posture was defined as the position with the pelvis rotated most forward with maximally forward bent lumbar spine and the upright thoracic and cervical spine. The normal posture was the position with the pelvis rotated most backward with the straightened lumbar spine without moving the thoraco-cervical spine and the head from the erect position. The slouched posture was defined as the position with the thoraco-cervical spine and the head inclined forward about 25 degrees from the normal position with the same position of the pelvis and the lumbar spine as for the normal posture. The subjects sat on the force platform connected to a rigid seat without a backrest which was mounted on a vibrator, and adopted the required postures. The postures were measured using an anthropometric stand. The spinal curves of the vertebral body centres were estimated from the postural data measured on the posterior body surface of the subjects (see section 4.3.3.3) and the mean spinal curves were calculated. The thighs and lower legs were set to horizontal and vertical by adjusting the height of a footrest which moved with the vibrator platform. Subjects were told to tense their muscles moderately.

A total of eight subjects participated in the experiment. None of them had suffered back problems in the past. They were exposed to vertical random vibration with a magnitude of 1.7 m/s^2 r.m.s. in the frequency range from 0.5 to 35 Hz for 1 minute duration three times for the three postures. The posture was measured and controlled before each run. All the time histories of acceleration and force were acquired simultaneously into a computer with a sampling rate of 100 samples per second through anti-aliasing low pass filters at 35 Hz with a cut-off rate of 36 dB/octave. The longitudinal and vertical accelerations measured on the body surface were corrected to eliminate the effect of the local tissue-accelerometer vibration from the measurements, using the method developed in section 4.2. The transfer functions from vertical seat acceleration to acceleration on the body were calculated for the modal analysis. The accelerances were also calculated on one subject, dividing acceleration on the body by vertical force at the seat-buttocks interface so as to validate the investigation mentioned in section 4.3.2.2. The driving point apparent masses were calculated, dividing vertical force by vertical seat acceleration, and then normalised, dividing them by the sitting weights of the subjects, as proposed by Fairley and Griffin (1989).

The acceleration transfer functions were used for the modal analysis. The transfer functions were calculated using different frequency resolutions, 0.2, 0.4 and 0.8 Hz for the frequency ranges below 4.5 Hz, between 4.5 and 10 Hz and above 10 Hz respectively, so

as to obtain smooth circular loci or straight lines in the analysis referred to in equations (4.31) and (4.32). The modal properties were extracted from the transfer functions for each subject separately and also from the mean transfer functions of the eight subjects in the normal posture within the frequency range below 20 Hz. The modal assurance criteria were, then, calculated between the mode shapes extracted from the mean transfer functions and the mode shapes extracted from the transfer functions for each subject separately, so as to find modes highly correlated between the subjects. For the erect and the slouched postures, the modal properties were extracted from the mean transfer functions only. Although the extracted modal constants were generally mathematically complex, only the real parts were used to plot the vibration mode shapes except where noted.

4.3.3.2 Calculation of pelvic motion

Two directions of acceleration over the sacrum S2 and one direction over the front-upper edge of the iliac crest were measured on the pelvis. The pelvis was assumed to be rigid within the frequency range of investigation. Therefore, the mode shapes for the sites on the pelvis simply determine the displacements of the pelvis without deformation. At the *r*th mode, relationships between the displacements are:

$$x_{S2}' = x_{S2} + \phi_{S2x} \qquad \textbf{(4.50a)}$$

$$z_{S2}' = z_{S2} + \phi_{S2z} \qquad \textbf{(4.50b)}$$

$$z_{ic}' = z_{ic} + \phi_{icz} \qquad \textbf{(4.50c)}$$

where: (x_{S2}', z_{S2}') is the displaced location of the sacrum S2; z_{ic}' is the displaced vertical location of the iliac crest; (x_{S2}, z_{S2}) is the initial location of the sacrum S2; z_{ic} is the initial vertical location of the iliac crest; ϕ_{S2x} and ϕ_{S2z} are the extracted mode shapes for the sacrum S2 at the *r*th mode and transferred from the transverse and longitudinal directions of the spine to horizontal (fore-and-aft) and vertical directions of motion; ϕ_{icz} is the extracted mode shape for the vertical motion of the front-upper edge of the iliac crest at the *r*th mode. From the assumption of the rigidity of the pelvis, the distance between the two sites on the pelvis does not change:

$$(x_{S2} - x_{ic})^2 + (z_{S2} - z_{ic})^2 = (x_{S2}' - x_{ic}')^2 + (z_{S2}' - z_{ic}')^2 \qquad \textbf{(4.51)}$$

Substituting equations (4.50) into equation (4.51), the unknown displaced horizontal location of the iliac crest, x_{ic}', is obtained.

Any displacement of a rigid structure may be described by a combination of translational and rotational displacements. Therefore, the displacements of the sacrum S2 and the iliac crest can be written:

$$\begin{Bmatrix} x_{S2}' \\ z_{S2}' \end{Bmatrix} - \begin{Bmatrix} x_0 \\ z_0 \end{Bmatrix} = [R]\left[\begin{Bmatrix} x_{S2} \\ z_{S2} \end{Bmatrix} - \begin{Bmatrix} x_0 \\ z_0 \end{Bmatrix}\right] + \begin{Bmatrix} \Delta x_L \\ \Delta z_L \end{Bmatrix} \qquad \textbf{(4.52a)}$$

$$\begin{Bmatrix} x_{ic}' \\ z_{ic}' \end{Bmatrix} - \begin{Bmatrix} x_0 \\ z_0 \end{Bmatrix} = [R]\left[\begin{Bmatrix} x_{ic} \\ z_{ic} \end{Bmatrix} - \begin{Bmatrix} x_0 \\ z_0 \end{Bmatrix}\right] + \begin{Bmatrix} \Delta x_L \\ \Delta z_L \end{Bmatrix} \qquad \textbf{(4.52b)}$$

$$[R] = \begin{pmatrix} \cos\theta & -\sin\theta \\ \sin\theta & \cos\theta \end{pmatrix} \qquad \textbf{(4.52c)}$$

where: (x_0, z_0) is a location of the pivot of rotation; $(\Delta x_L, \Delta z_L)$ is a translational displacement; θ is a rotational angle. The pivot can be determined arbitrarily. Therefore, the translational displacement, $(\Delta x_L, \Delta z_L)$, and the rotational angle, θ, are calculated from equations (4.52). Finally, the displacement of the whole pelvis are determined by equation (4.53):

$$\begin{Bmatrix} x_p' \\ z_p' \end{Bmatrix} = [R]\left[\begin{Bmatrix} x_p \\ z_p \end{Bmatrix} - \begin{Bmatrix} x_0 \\ z_0 \end{Bmatrix}\right] + \begin{Bmatrix} \Delta x_L \\ \Delta z_L \end{Bmatrix} + \begin{Bmatrix} x_0 \\ z_0 \end{Bmatrix} \qquad \textbf{(4.53)}$$

where: (x_p, z_p) is an arbitrary point on the pelvis; (x_p', z_p') is the displaced point.

4.3.3.3 Estimation of spinal curves

The vertical and horizontal locations of the head and the spinous process tips of the vertebrae T1, T6, T11, L3 and the sacrum S2 were measured on the posterior body surface of the subjects, using an anthropometric stand. The measured postural data over the spine were transferred to the locations of the geometrical centres of the vertebral bodies. The horizontal distances between the posterior body surface and the vertebral body centres were based on the data measured by Liu and Wickstrom (1973) and the vertical distances between the spinous process tips and the vertebral body centres were based on the data used by Belytschko *et al.* (1976) (Table 4.8). The vertical distance data of Belytschko *et al.* were available only on the vertebra T6 in the thoracic region and the same value was used for the vertebrae T1 and T11. The data of Liu and Wickstrom did not include the horizontal distance for the sacrum S2. The horizontal distances between the posterior body surface and the centre of the sacrum and also between the posterior body surface and the head mass centre were estimated from the data of Singley III and Haley

(1978). Another postural landmark measured was the location of the ischial tuberosities. The initial pelvic angle was determined around the pivot at the ischial tuberosities with the relationship between the locations of the sacrum S2 and the ischial tuberosities.

Table 4.8 Horizontal and vertical distances for estimation of the spinal curves from the measured postural data on the posterior body surface.

Level	Horizontal distance[1] ($m \times 10^{-2}$)	Vertical distance[2] ($m \times 10^{-2}$)
Head	8.770	——
T1	6.456	1.400
T6	6.856	1.400
T11	7.293	1.400
L3	7.914	0.460
S2	4.000	0.000

(1) Horizontal distances between the posterior body surface and the head mass centre and between the posterior body surface and the vertebral body centres.
(2) Vertical distances between the spinous process tips and the vertebral body centres.

4.3.4 Results

The estimated natural frequencies and the damping ratios of the local tissue-accelerometer system (see section 4.2) are shown in Tables 4.9 and 4.10 for the eight subjects. The natural frequencies of the local system define 'the effective frequency ranges' for the correction, which are generally higher than 20 Hz over the spine and about 10 Hz for the abdominal wall. Therefore, the results of the analysis are valid below 20 Hz for the spinal motion and below 10 Hz for the visceral motion.

The accelerances and the acceleration transfer functions of the body were compared first so as to validate the investigation described in section 4.3.2.2. They are shown in Figures 4.21 and 4.22. It was found that the resonance at about 5 Hz seen in the acceleration transmissibilities did not appear in the moduli of the accelerances. This result indicated that the mode at about 5 Hz was dominated by the entire body mode as discussed in section 4.3.2.2.

Table 4.9 Estimated natural frequencies of the local tissue-accelerometer system.

	Subject No.								
Level	1	2	3	4	5	6	7	8	Mean
T1 z	30.5	22.4	34.0	22.0	14.5	14.6	46.8	28.0	26.6
T6 z	46.2	42.7	46.8	57.4	49.6	30.5	48.6	53.9	50.0
T11 z	50.4	40.0	63.1	48.9	33.7	20.4	30.0	53.9	42.6
L3 z	26.1	46.1	30.0	20.7	40.0	28.8	43.3	27.3	32.8
S2 z	21.0	14.8	13.1	18.6	15.4	11.0	37.2	12.8	18.0
AW(1)	14.8	8.8	13.7	10.3	7.4	7.1	16.3	8.9	10.9
FP(2)	17.0	13.5	68.8	22.7	20.0	46.3	22.7	40.0	31.4

(1) Abdominal wall z (2) Front pelvis z (z=longitudinal or vertical direction)

Table 4.10 Estimated damping ratios of the local tissue-accelerometer system.

	Subject No.								
Level	1	2	3	4	5	6	7	8	Mean
T1 z	0.40	0.34	0.49	0.43	0.25	0.28	0.57	0.47	0.40
T6 z	0.34	0.46	0.35	0.38	0.56	0.37	0.40	0.39	0.41
T11 z	0.34	0.54	0.34	0.34	0.48	0.31	0.43	0.32	0.39
L3 z	0.39	0.38	0.68	0.23	0.54	0.40	0.36	0.59	0.45
S2 z	0.49	0.50	0.26	0.50	0.35	0.32	0.78	0.30	0.44
AW(1)	0.59	0.62	0.56	0.25	0.21	0.50	0.41	0.57	0.46
FP(2)	0.55	0.43	0.55	0.52	0.45	0.73	0.37	0.39	0.50

(1) Abdominal wall z (2) Front pelvis z (z=longitudinal or vertical direction)

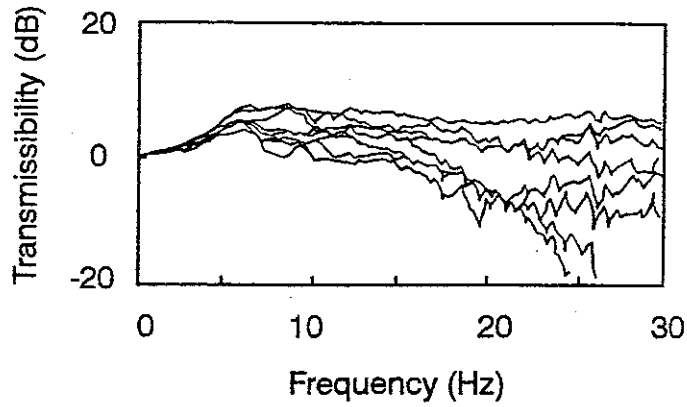

Figure 4.21 Transmissibilities between vertical seat acceleration and longitudinal spinal accelerations.

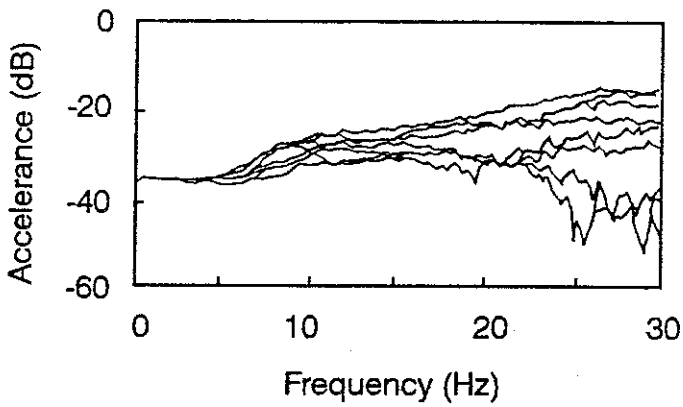

Figure 4.22 Moduli of accelerance between vertical force at the seat-buttocks interface and longitudinal spinal accelerations.

Experimental modal analysis was found to be applicable to whole-body vibration, using the acceleration transfer functions, although the heavy damping of the human body made the iteration procedure necessary for closely located modes. Good coherency for the transfer functions was a prerequisite for the following analysis. The coherencies for the transfer functions to the longitudinal responses were good within the required frequency range. The coherencies for the transfer functions to the transverse responses were fairly good, except some below 5 Hz and above 15 Hz, where the response levels of the bending modes of the spine were extremely low (Figure 4.23). The Argand diagrams in the analysis referred to by equation (4.31) showed clear circles corresponding to modes (Figure 4.24). The clear circles indicated the feasibility of extracting the modal properties, although they were not directly used for extraction in this study. Δ versus ω^2-curves (see Appendix 3) around specific resonances in Figure 4.24 are shown in Figures 4.25 and

4.26, which were used for extracting the modal properties. The straight lines indicated the high accuracy of the extraction. One of the methods to assess the accuracy of the extracted modal properties is to compare the measured transmissibilities and the synthesised transmissibilities calculated by synthesising the extracted modal properties by equation (4.29). The comparison generally showed good coincidence (Figure 4.27). A total of ten modes was extracted from the transfer functions for one of the subjects in the normal posture within the frequency range below 20 Hz (below 10 Hz for the visceral modes due to the limitation of the correction) (Table 4.11). The modal assurance criteria for the extracted ten mode shapes showed that they were generally well separated (Table 4.12).

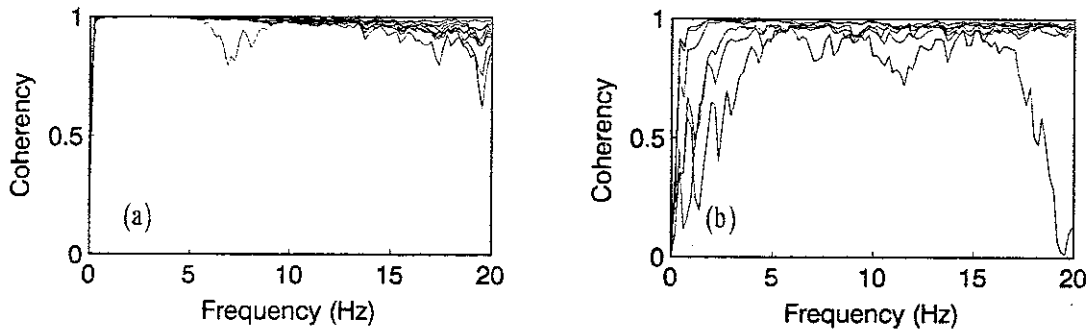

Figure 4.23 Typical coherence functions for the transfer functions for one of the subjects; (a) for the transfer functions from vertical seat motion to longitudinal body motion; (b) for the transfer functions from vertical seat motion to transverse body motion.

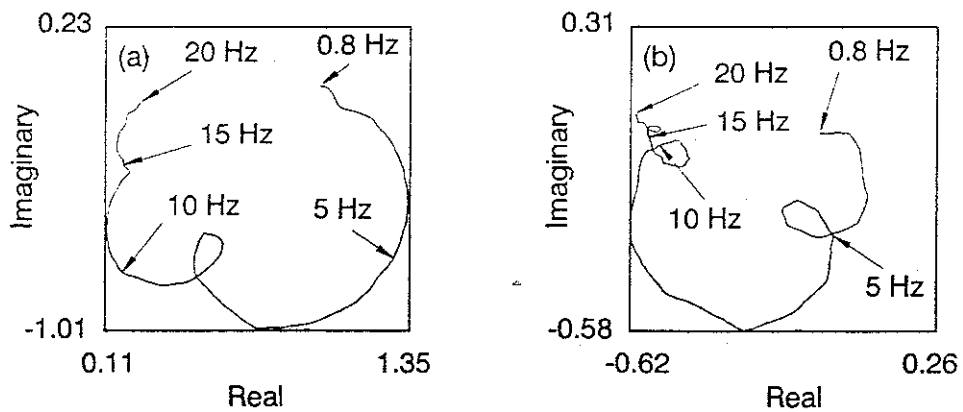

Figure 4.24 Typical Argand diagrams for one of the subjects; (a) for the transfer function from vertical seat motion to longitudinal motion of the vertebra L3; (b) for the transfer function from vertical seat motion to transverse motion of the vertebra L3.

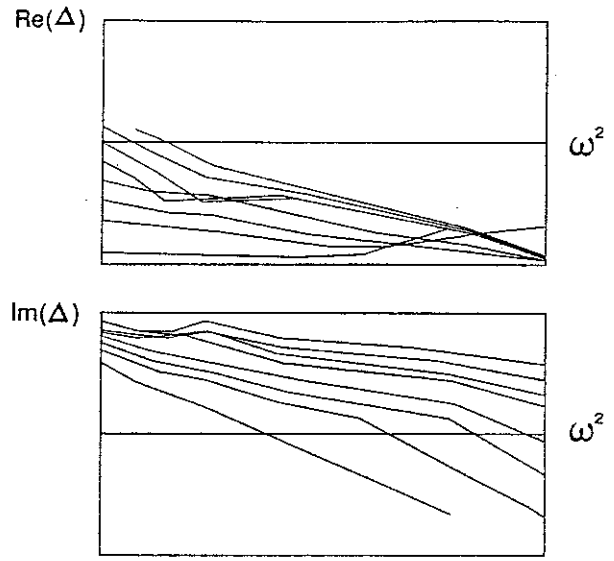

Figure 4.25 Re(Δ) and Im(Δ) versus ω^2-curves of the transfer function from vertical seat motion to longitudinal motion of the vertebra L3 around the resonance at about 5 Hz shown in Figure 4.24(a).

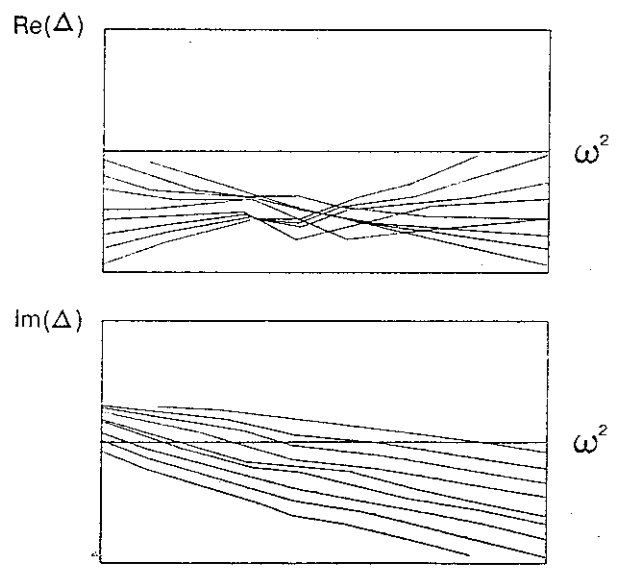

Figure 4.26 Re(Δ) and Im(Δ) versus ω^2-curves of the transfer function from vertical seat motion to transverse motion of the vertebra L3 around the resonance at about 6 Hz shown in Figure 4.24(b).

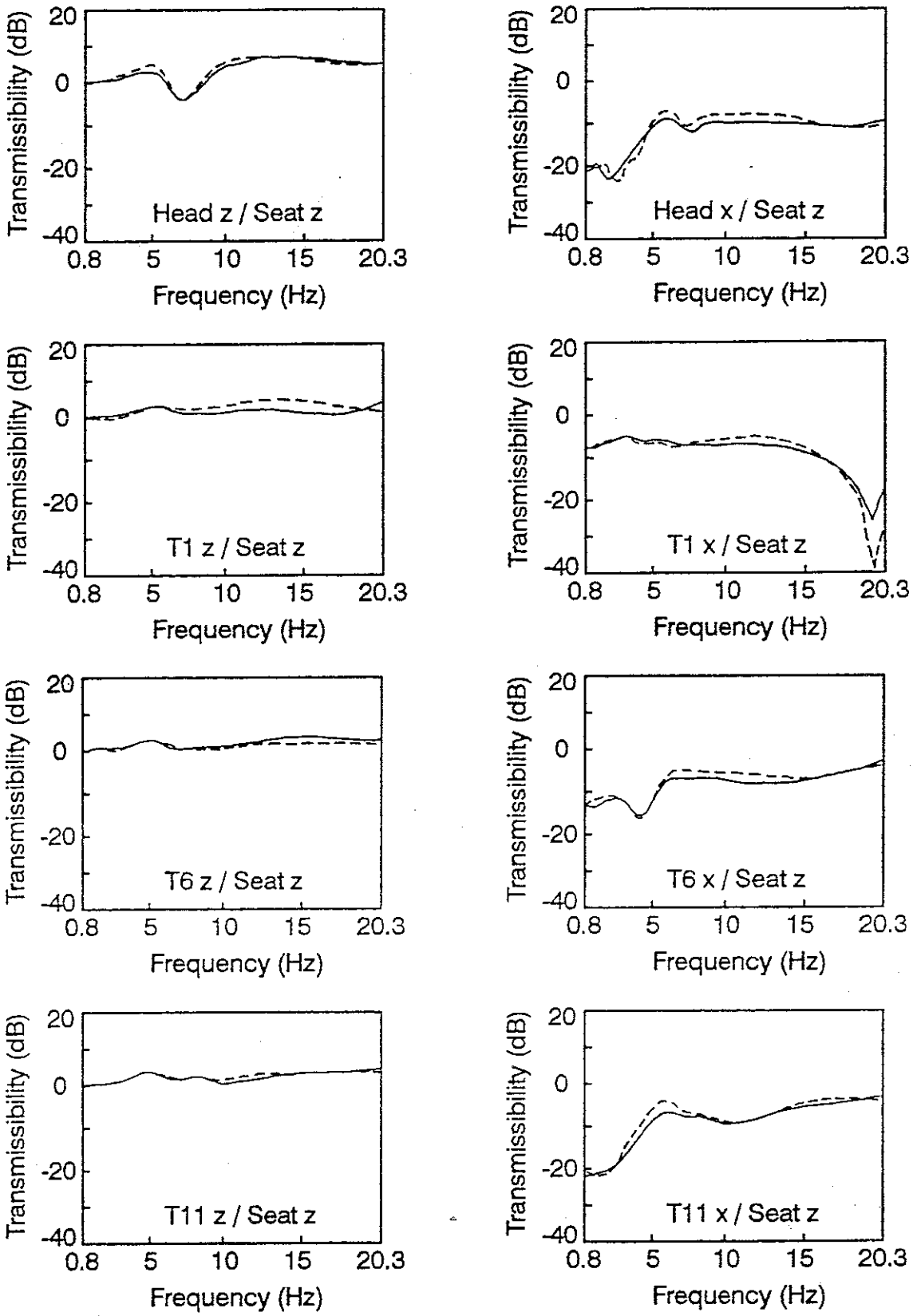

Figure 4.27 Typical comparisons between the synthesised transmissibilities (——) and the measured transmissibilities (- - - -) for one of the subjects in the normal posture (z=longitudinal or vertical direction; x=transverse or fore-and-aft direction).

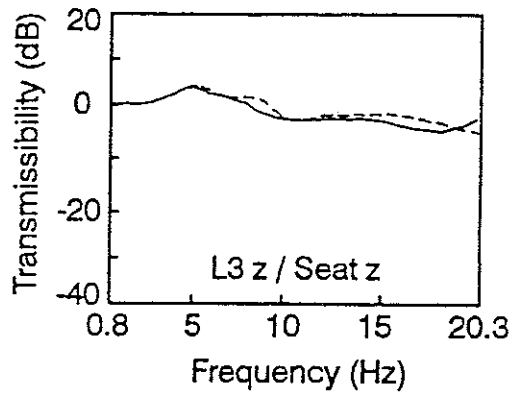

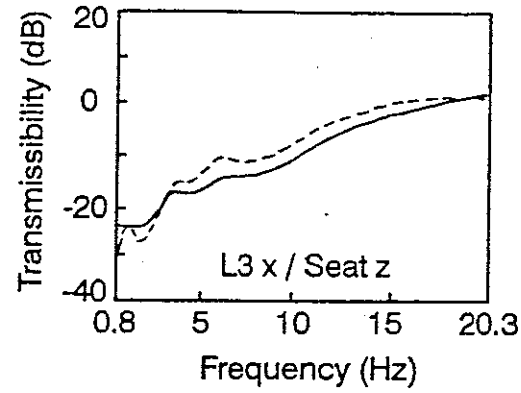

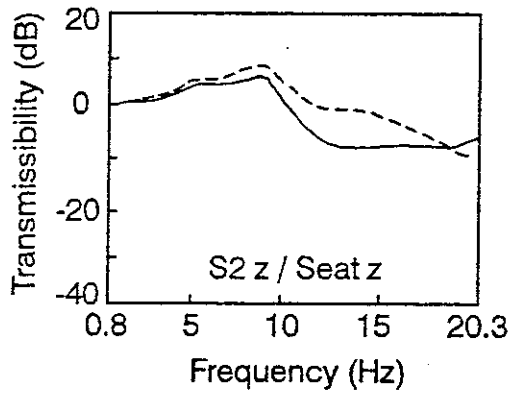

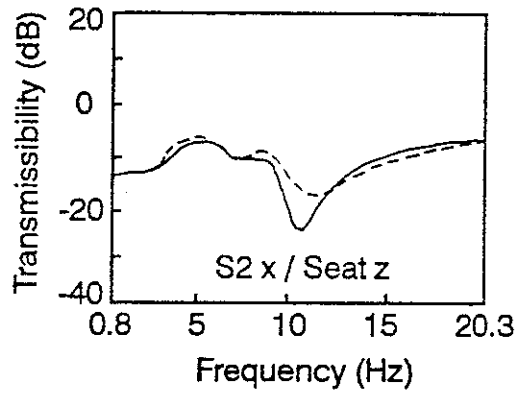

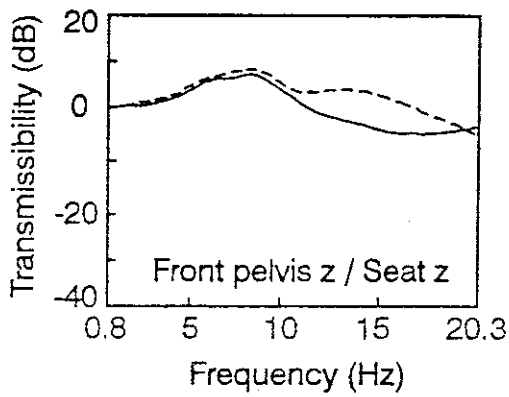

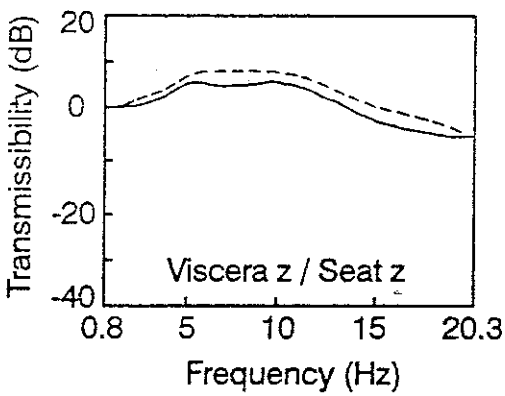

Figure 4.27 (Continued).

Table 4.11 Typical natural frequencies and damping loss factors extracted for one of the subjects in the normal posture.

Mode No.	Natural frequency (Hz)	Damping loss factor
1	1.8	0.45
2	3.3	0.43
3	4.1	0.36
4	5.3	0.47
5	6.2	0.36
6	8.5	0.29
7	9.2	0.24
8	10.3	0.48
9	12.4	0.66
10	15.2	0.63

Table 4.12 Typical modal assurance criteria between the complex mode shapes extracted for one of the subjects in the normal posture.

		Mode No.									
		1	2	3	4	5	6	7	8	9	10
	1	1.00	0.49	0.06	0.00	0.09	0.00	0.00	0.00	0.01	0.02
	2		1.00	0.00	0.00	0.03	0.00	0.00	0.00	0.00	0.05
	3			1.00	0.01	0.02	0.00	0.03	0.00	0.00	0.02
Mode	4				1.00	0.07	0.04	0.04	0.30	0.16	0.13
No.	5					1.00	0.42	0.01	0.00	0.19	0.09
	6						1.00	0.03	0.00	0.00	0.13
	7							1.00	0.00	0.07	0.04
	8								1.00	0.00	0.00
	9									1.00	0.00
	10										1.00

Estimated spinal curves of the eight subjects (see section 4.3.3.3) are shown in Figure 4.28. Variability between the subjects was minimised by the definitions of the three postures. The mean locations of the head, spine and the pelvis are listed in Table 4.13 and they are plotted in Figure 4.29. The mean transmissibilities of the eight subjects in the three postures are shown in Figure 4.30. A total of 14 modes were extracted from the mean transfer functions of the eight subjects in the normal posture within the frequency range below 20 Hz (below 10 Hz for the visceral modes due to the limitation of the correction). The extracted natural frequencies and the damping loss factors are listed in Table 4.14 and the vibration mode shapes are plotted in Figure 4.31 (see Appendix 4 for the modal matrix). The MAC values between the mode shapes extracted from the mean transfer functions and the mode shapes extracted from the transfer functions for each subject generally showed high correlations below 13 Hz and the highest correlations were found for the modes at 4.9 and 8.1 Hz (Table 4.15). Modes located above 13 Hz were unclear due to the heavy damping (Figure 4.30) and, therefore, the correlations were low. The model calculation also predicted the limitation of extracting modes at high frequencies at the used measuring sites due to short wavelength of the bending modes of the spine (see section 3.5). This limitation was possibly valid for the mode shapes in all the three postures.

Table 4.13 Mean locations of the head[(1)], spine[(2)] and the pelvis.

Level	Erect ($m \times 10^{-2}$)		Normal ($m \times 10^{-2}$)		Slouched ($m \times 10^{-2}$)	
	x	z	x	z	x	z
Head	2.98	80.86	2.57	80.25	14.86	78.16
T1	-0.69	66.28	-1.21	65.46	5.19	64.77
T6	-4.09	52.63	-5.86	52.33	-2.93	52.97
T11	-2.97	38.25	-6.50	38.31	-6.41	38.80
L3	-1.96	25.75	-6.12	24.51	-6.83	24.20
S2	-7.19	15.11	-9.49	13.24	-9.87	12.70
I.T.[(3)]	0.0	0.0	0.0	0.0	0.0	0.0
F.P.[(4)]	1.38	21.65	-0.93	19.78	-1.09	19.46

(1) Location of the head mass centre.
(2) Locations of the geometrical centres of the vertebral bodies.
(3) Location of the ischial tuberosities as the origin of the coordinates.
(4) Location of the front-upper edge of the right side iliac crest.

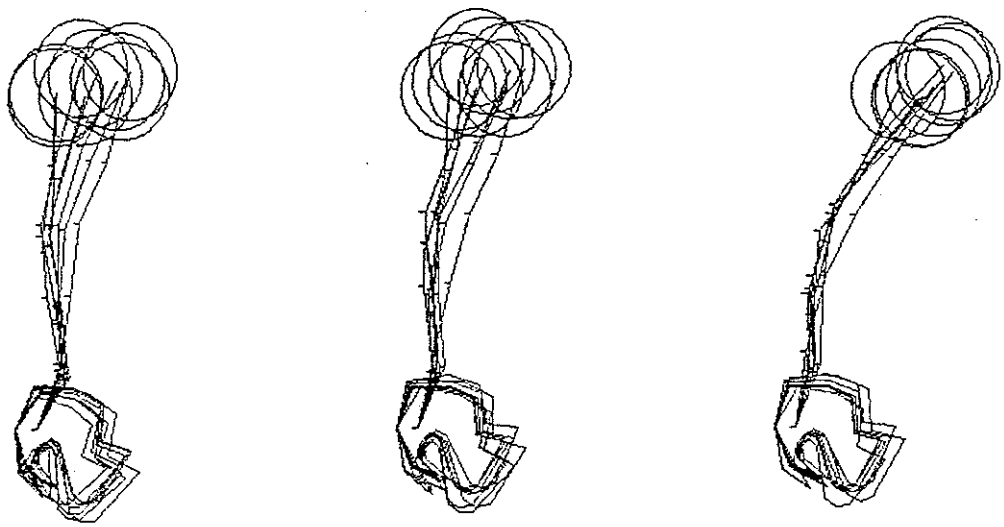

Figure 4.28 Estimated spinal curves of the eight subjects; (a) erect posture; (b) normal posture; (c) slouched posture.

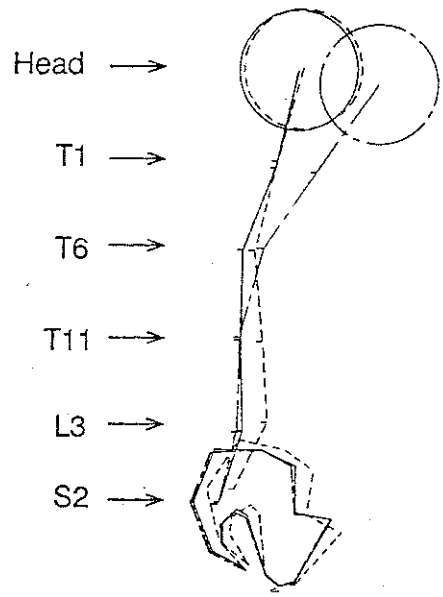

Figure 4.29 Mean spinal curves of the eight subjects; erect posture (- - - -); normal posture (——); slouched posture (— - —).

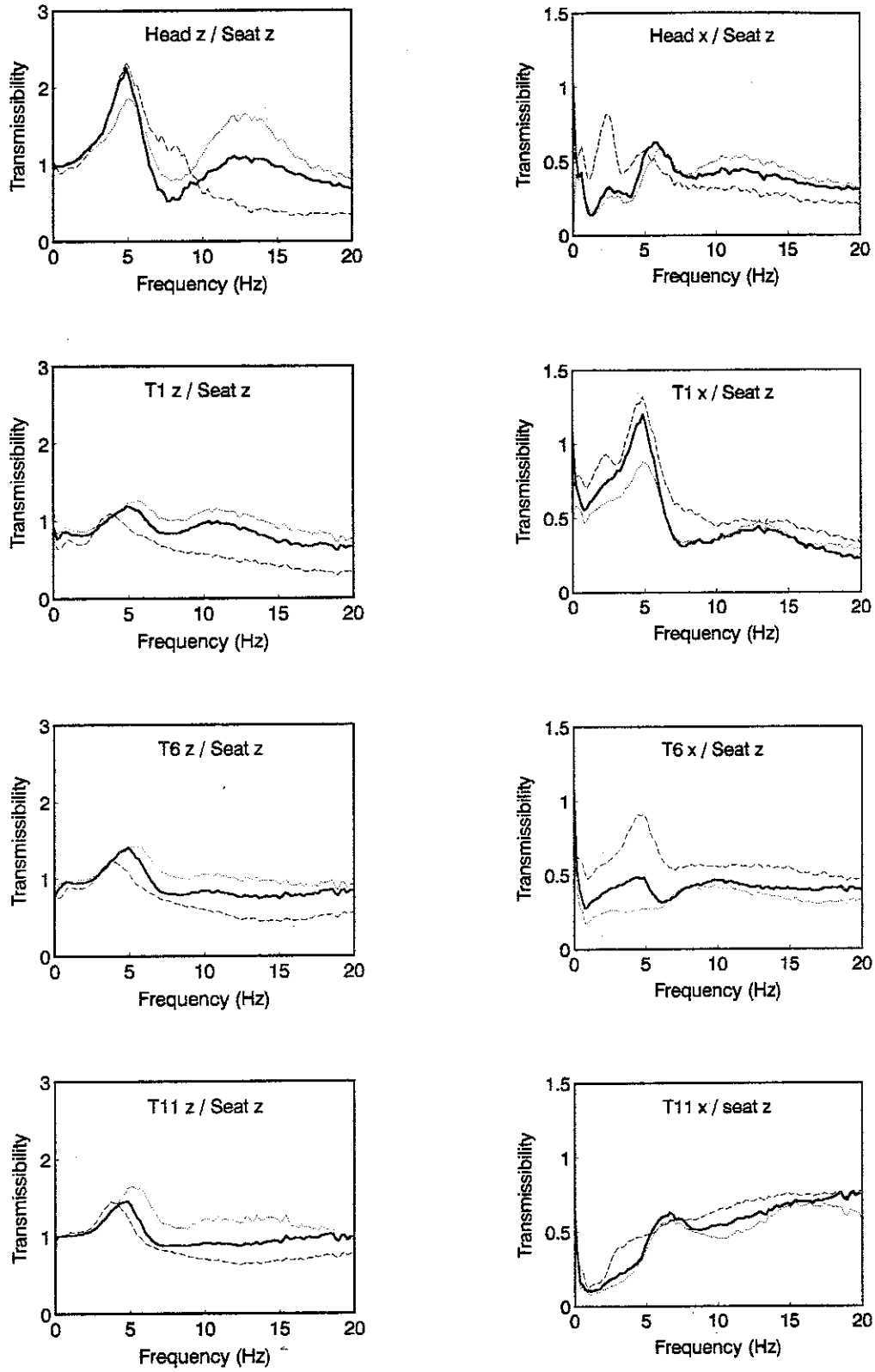

Figure 4.30 Mean transmissibilities of the eight subjects in the erect posture (.....), normal posture (——) and the slouched posture (- - - -) (z=longitudinal or vertical direction; x=transverse or for-and-aft direction).

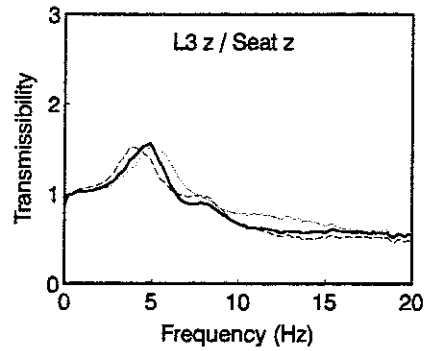

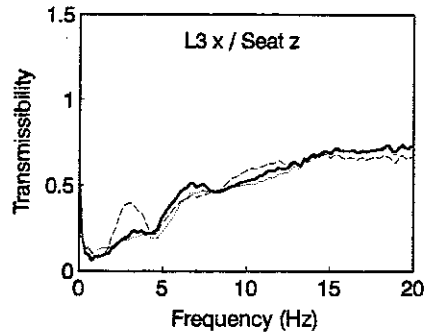

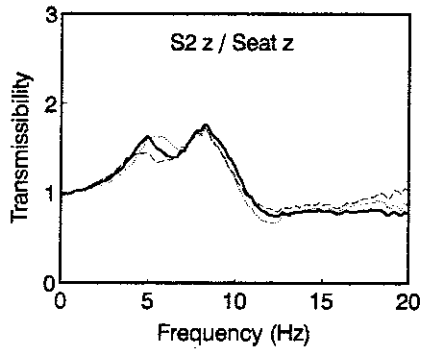

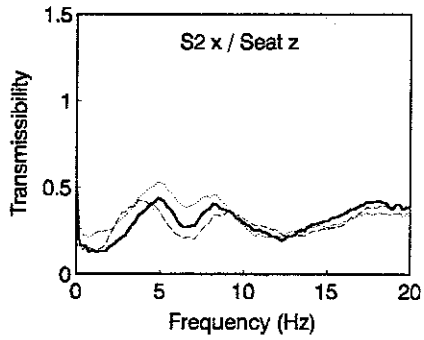

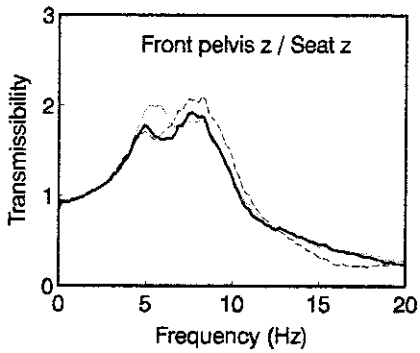

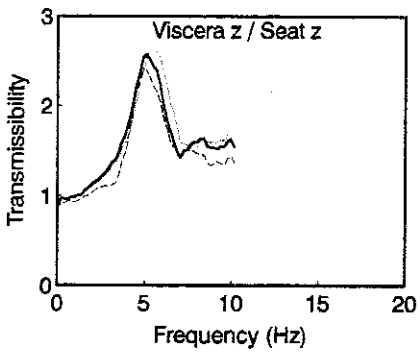

Figure 4.30 (Continued).

Table 4.14 Natural frequencies and damping loss factors extracted from the mean transfer functions in the three postures.

Mode No.	Erect		Normal		Slouched	
	Natural frequency (Hz)	Damping loss factor	Natural frequency (Hz)	Damping loss factor	Natural frequency (Hz)	Damping loss factor
1	1.5	0.65	1.1	1.59	0.97	1.59
2	2.2	0.38	2.2	0.58	2.4	0.56
3	3.3	0.19	3.4	0.42	3.3	0.41
4	4.4	0.35	4.9	0.46	4.0	0.66
5	5.2	0.45	5.6	0.45	4.9	0.43
6	5.7	0.41	7.0	0.43	6.0	0.41
7	6.7	0.30	8.1	0.38	7.3	0.28
8	8.4	0.36	8.7	0.32	8.3	0.37
9	9.2	0.34	9.3	0.46	9.2	0.18
10	10.4	0.53	10.4	0.56	10.6	0.75
11	12.2	0.60	12.5	0.67	13.0	0.33
12	14.3	0.33	14.0	0.32	14.1	0.32
13	17.1	0.26	16.5	0.35	16.5	0.63
14	18.8	0.22	19.2	0.28	17.8	0.32

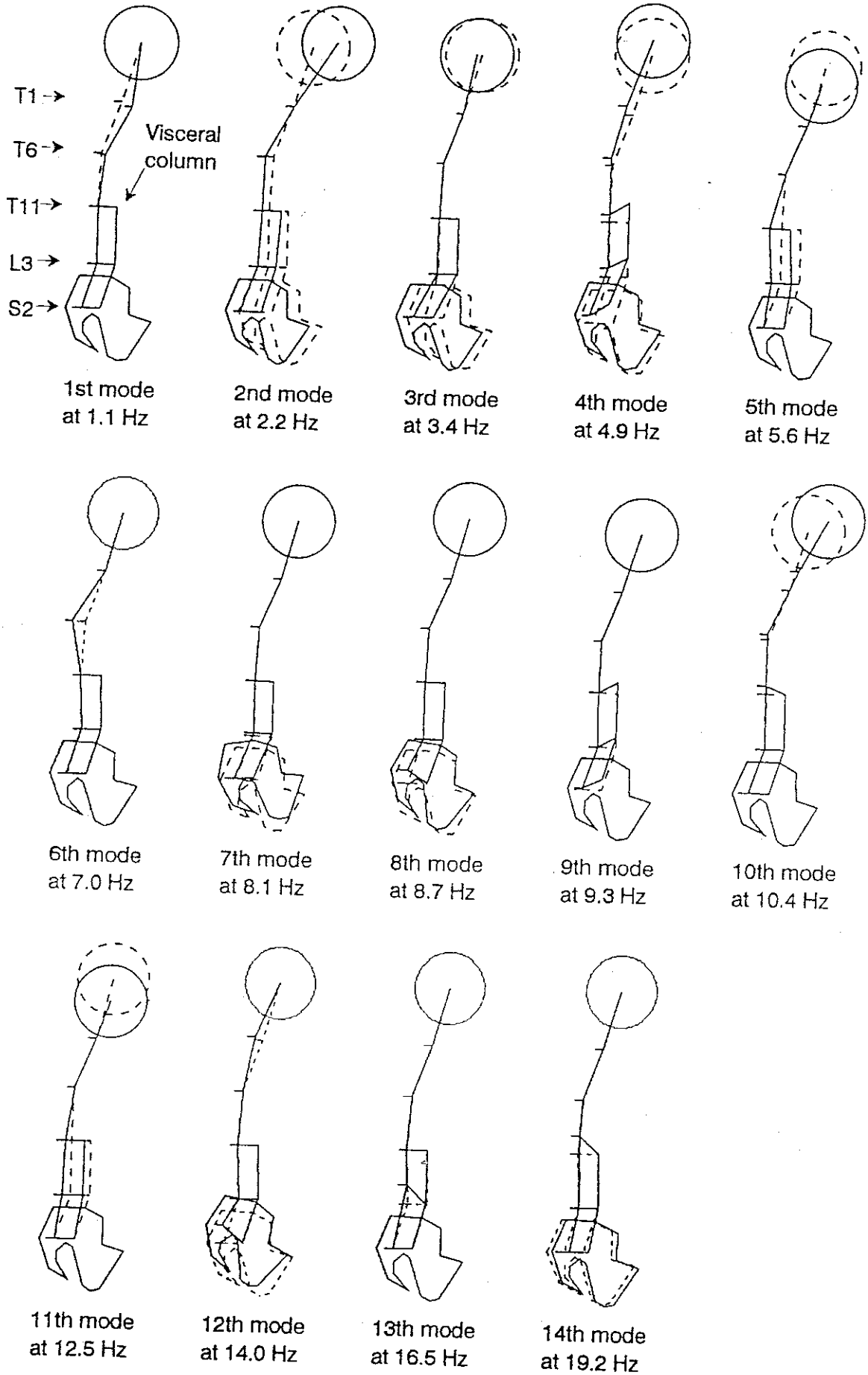

Figure 4.31 Vibration mode shapes in the normal posture extracted from the mean transfer functions of the eight subjects (———) and the initial configuration (- - - -).

Table 4.15 Modal assurance criteria between the complex mode shapes extracted from the mean transfer functions (reference) and the complex mode shapes extracted from the transfer functions for each subject (compared) in the normal posture. (MAC≥0.05) ((n); mode number, upper part; natural frequency (Hz), lower part; MAC, *; MAC>0.3, †; MAC>0.5, ——— ; no correlated mode was fond, upper part of the mean column; mean natural frequency (Hz), lower part of the mean column; mean MAC).

Reference	Compared subject No.								
	1	2	3	4	5	6	7	8	Mean
(1)1.1	(2)3.3	(2)3.5	(1)0.9	(1)1.7	(1)1.3	(1)1.5	(1)1.6	———	2.0
	0.61†	0.28	0.26	0.13	0.53*	0.96†	0.51†	———	0.47*
(2)2.2	(1)1.8	(1)2.0	(2)2.2	(1)1.7	(3)3.4	(3)3.4	(2)2.4	(1)1.1	2.3
	0.13	0.46*	0.33*	0.28	0.65†	0.41*	0.45*	0.46*	0.40*
(3)3.4	(3)4.1	(3)4.4	(2)2.2	(2)2.3	(3)3.4	(2)2.6	(2)2.4	(3)3.2	3.1
	0.67†	0.67†	0.06	0.23	0.09	0.19	0.31*	0.48*	0.34*
(4)4.9	(4)5.3	(4)5.6	(4)4.3	(5)5.1	(4)5.0	(4)4.6	(5)5.00	(5)5.1	5.0
	0.75†	0.52†	0.90†	0.83†	0.86†	0.51†	0.84†	0.63†	0.73†
(5)5.6	(5)6.2	(4)5.6	(5)5.2	(6)5.8	(6)6.7	(4)4.6	(4)4.3	(4)4.8	5.4
	0.42*	0.33*	0.53†	0.68†	0.60†	0.26	0.39*	0.59†	0.48*
(6)7.0	(5)6.2	———	(7)6.8	(7)7.0	———	———	(6)8.1	(6)6.2	7.0
	0.07	———	0.11	0.15	———	———	0.20	0.11	0.08
(7)8.1	(6)8.5	(7)8.6	(8)8.5	(9)9.4	(7)7.8	(6)7.0	(7)9.1	(7)7.4	8.3
	0.82†	0.18	0.76†	0.47*	0.73†	0.92†	0.45*	0.57†	0.61†
(8)8.7	(7)9.2	(7)8.6	(8)8.5	(9)9.4	(8)8.7	(7)7.6	(7)9.1	(7)7.4	8.6
	0.82†	0.68†	0.27	0.53†	0.54†	0.26	0.31*	0.27	0.46*
(9)9.3	(8)10.4	———	(10)12.5	(8)8.3	(7)7.8	(7)7.6	(6)8.1	———	9.1
	0.98†	———	0.75†	0.98†	0.06	0.47*	0.50†	———	0.47*
(10)10.4	(9)12.4	(8)10.3	(9)10.2	(11)12.4	(10)12.7	(9)10.3	(9)12.2	(8)8.3	11.1
	0.59†	0.44*	0.32*	0.81†	0.39*	0.50†	0.23	0.35*	0.45*
(11)12.5	(9)12.4	(10)14.5	(9)10.2	(11)12.4	(10)12.7	(9)10.3	(9)12.2	(12)14.6	12.4
	0.51†	0.58†	0.64†	0.38*	0.69†	0.38*	0.41*	0.69†	0.54†
(12)14.0	(10)15.2	(9)12.7	(12)18.8	(13)17.9	(11)14.1	———	(9)12.2	(11)12.5	14.8
	0.07	0.11	0.21	0.57†	0.07	———	0.25	0.19	0.19
(13)16.5	(10)15.2	———	(11)16.1	———	———	———	———	(11)12.5	15.3
	0.05	———	0.21	———	———	———	———	0.12	0.05
(14)19.2	(10)15.2	———	(12)18.8	———	(12)17.9	(11)15.1	(10)14.4	———	16.6
	0.42*	———	0.34	———	0.05	0.44	0.08	———	0.17

The natural frequencies corresponding to the principal and the second principal resonances of the apparent mass (Figure 4.32) were found to be 4.9 and 8.6 Hz for the normal posture which were extracted from the mean apparent mass using the same technique as for the modal analysis. Therefore, the mode at 4.9 Hz corresponded to the principal resonance and the modes at 8.1, 8.7 and 9.3 Hz (some or all) corresponded to the second principal resonance of the apparent mass: the second principal resonance was not as clear as the principal resonance both in Figure 4.32 and in the Argand diagram, and the tolerance for the extracted modal properties was larger. The mode at 4.9 Hz was found to contain an entire body mode with vertical and fore-and-aft pelvic motion due to buttocks tissue deformation in phase with a vertical visceral mode, and a bending mode of the upper thoracic and the cervical spine (Figure 4.31). A bending mode of the lumber and the lower thoracic spine was not found at this mode but found in the next higher mode at 5.6 Hz. The modes at 8.1 and 8.7 Hz contained rotational modes of the pelvis and the mode at 9.3 Hz was the second visceral mode.

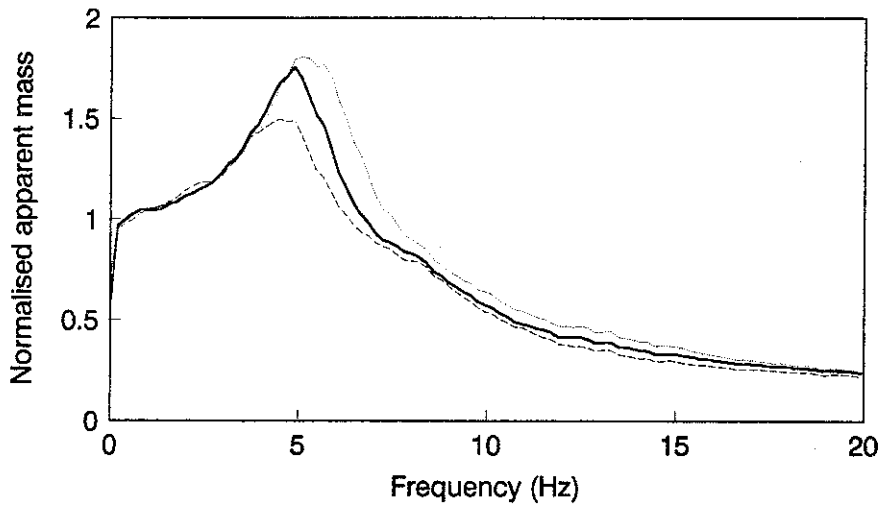

Figure 4.32 Mean normalised apparent masses of the eight subjects in the erect posture (.....), normal posture (——) and the slouched posture (- - - -).

The mean apparent masses showed that both the frequency and the modulus of the principal resonance decreased when the subjects changed posture from erect to slouched. The natural frequencies for the principal and the second principal resonances extracted from the mean apparent masses were 5.2 and 8.8 Hz for the erect posture, and 4.4 and 8.3 Hz for the slouched posture. The natural frequencies and the damping loss

factors extracted from the mean transfer functions in the erect and the slouched postures are listed in Table 4.14 and the vibration mode shapes are plotted in Figures 4.33 and 4.34 (see Appendix 4 for the modal matrices). The mode shapes corresponding to the principal resonance of the apparent masses in the three postures are compared in Figure 4.35. It was found that the natural frequency for the entire body mode decreased when changing posture from erect to slouched. In the slouched posture, the visceral mode was separated from the entire body mode and remained at 4.9 Hz whereas the entire body mode shifted to 4.0 Hz. Therefore, both modes at 4.0 and 4.9 Hz seemed to contribute to the principal resonance of the apparent mass at 4.4 Hz. It is also seen in Figure 4.35 that the fore-and-aft pelvic motion in the entire body mode, which possibly included shear deformation of buttocks tissue, increased from the erect posture to the slouched posture.

4.3.5 Discussion

A total of ten correlated modes between the subjects was extracted for the normal posture and they were dominated by bending modes of the spine, a buttocks mode, a visceral mode and rotational modes of the pelvis as predicted by the expanded model (section 3.5). The first three modes were bending modes of the spine. The first mode at 1.1 Hz might include substantial amount of error due to the low coherency for the bending responses at this frequency (Figure 4.23). The second mode at 2.2 Hz and the third mode at 3.4 Hz were similar to the first and the second bending modes of a beam with both ends free. The fourth mode at 4.9 Hz was the principal mode mentioned above. The fifth mode at 5.6 Hz contained a bending mode of the lumbar and the lower thoracic spine and motion of the head. Paddan and Griffin (1993) showed a resonance in the transmissibility from vertical seat motion to pitching motion of the head between 5 and 6 Hz which was higher than the resonance in the transmissibility to vertical translational motion of the head (Figure 2.11). Therefore, the accelerometers on the bite-bar possibly measured the pitching mode of the head in the fifth mode, although they were located behind the mouth. The fifth mode was located close to the fourth mode, and Sandover and Dupuis (1987) and Hinz *et al.* (1988) may have extracted the fourth mode and the fifth mode together. The sixth mode had a low correlation between the subjects and it was not reliable. The seventh mode at 8.1 Hz and the eighth mode at 8.7 Hz, corresponding to the second principal resonance of the apparent mass, contained rotational modes of the pelvis with what may be axial deformation of the lower lumbar spine. However, the lumbar spine at this level is located deep below the posterior body surface (Table 4.8) and bending motion of the spine might appear as axial motion on the body surface as pointed out by Sandover and

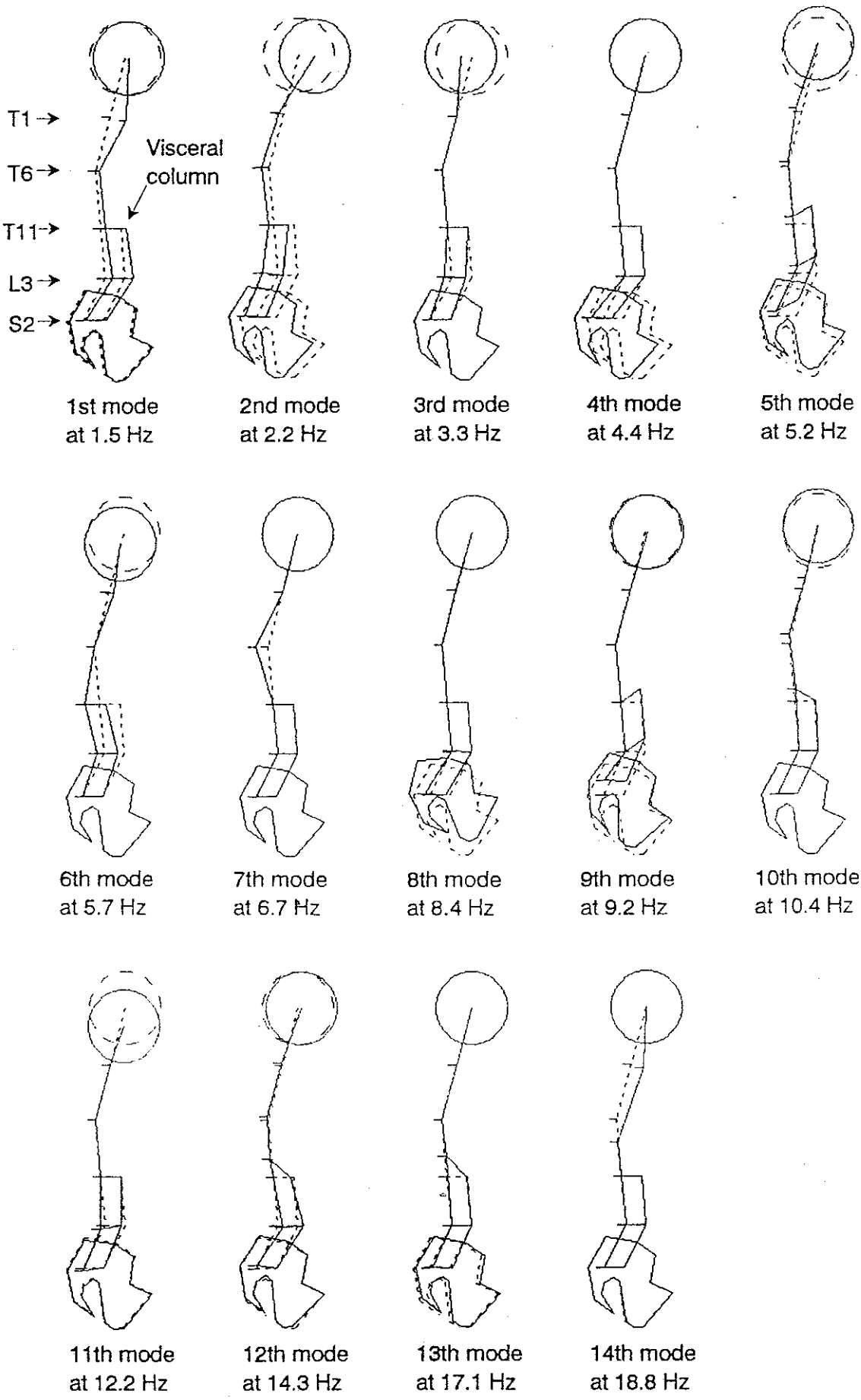

Figure 4.33 Vibration mode shapes in the erect posture extracted from the mean transfer functions of the eight subjects (——) and the initial configuration (- - - -).

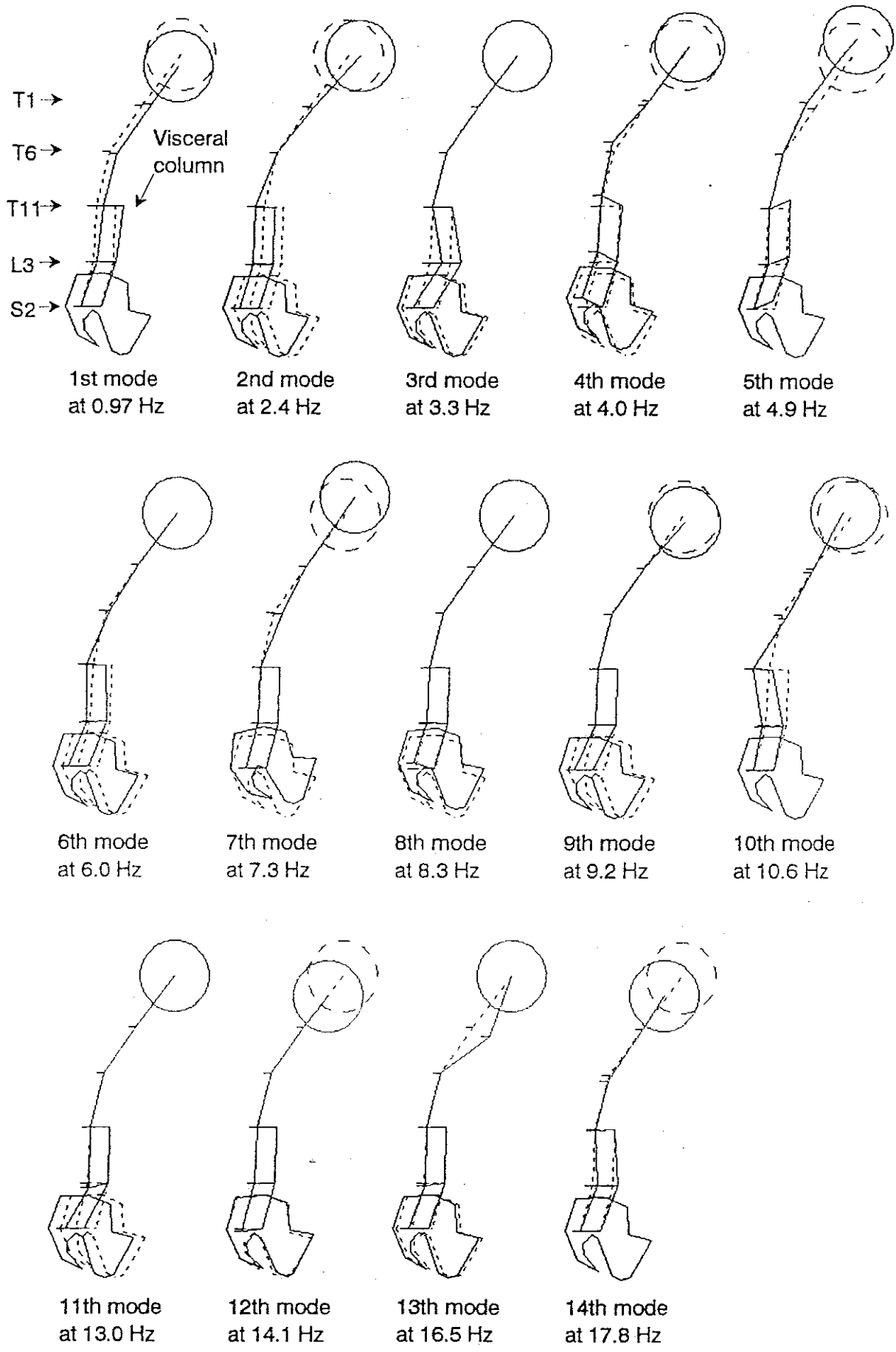

Figure 4.34 Vibration mode shapes in the slouched posture extracted from the mean transfer functions of the seven subjects (———) and the initial configuration (- - - -).

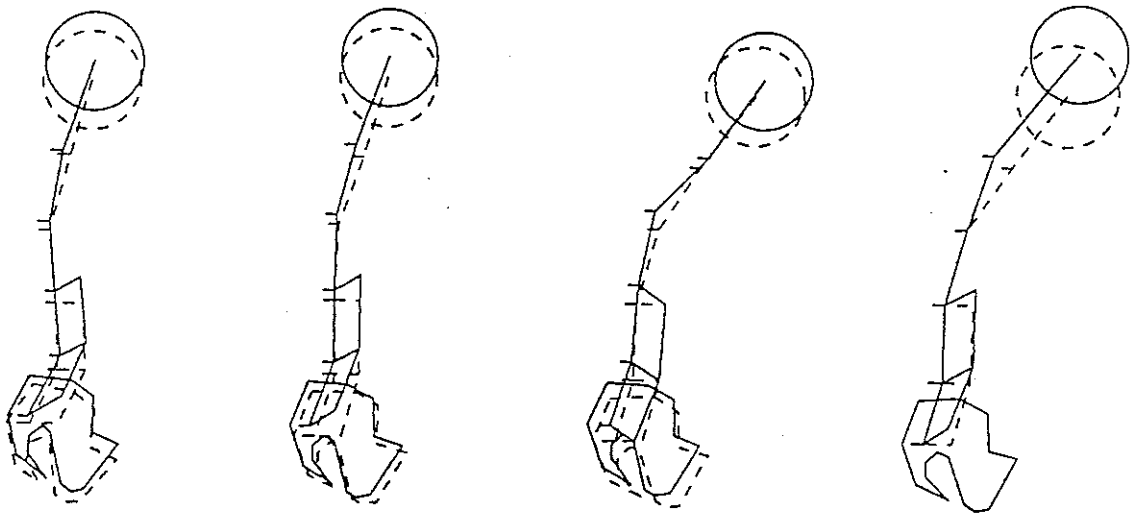

Figure 4.35 Vibration mode shapes corresponding to the principal resonance of the apparent mass (——) and the initial configuration (- - - -): (a) mode at 5.2 Hz in the erect posture; (b) mode at 4.9 Hz in the normal posture; (c) mode at 4.0 Hz in the slouched posture (d) mode at 4.9 Hz in the slouched posture.

Dupuis (1987). The ninth mode at 9.3 Hz was the second visceral mode and might have made some contribution to the second principal resonance of the apparent mass. The tenth mode at 10.4 Hz appeared to contain an axial mode of the thoracic and the cervical spine. The eleventh mode at 12.5 Hz appeared similar to the fifth mode at 5.6 Hz. However, the complex mode shapes for the two modes revealed a distinctive difference (Figure 4.36). The modes found above 13 Hz had low correlations between the subjects and they were not reliable.

Changing posture from erect to slouched decreased the principal resonance frequency of the apparent mass: the natural frequencies for the principal resonance extracted from the apparent masses were 5.2 Hz in the erect posture, 4.9 Hz in the normal posture and 4.4 Hz in the slouched posture. The natural frequency for the entire body mode also decreased due to the postural change, corresponding to the resonance shift: 5.2 Hz in the erect posture, 4.9 Hz in the normal posture and 4.0 Hz in the slouched posture. In the slouched posture, the visceral mode remained at 4.9 Hz and was separated from the entire body mode at 4.0 Hz, resulting in the resonance at 4.4 Hz. This result indicated that the resonance shift was caused by the shift of the entire body mode. Therefore, the

postural change must have changed some parameters involved in the entire body mode. It is a reasonable hypothesis that changing posture from erect to slouched increased the effective contact areas between the buttocks and the thighs and the seat surface, resulting in decrease of the total axial stiffness under the pelvis due to the non-linear force-deflection relationship of tissue. The resonance shift was larger from the normal posture to the slouched posture than from the erect posture to the normal posture, and it was explained if the backward rotation of the pelvis from the erect posture to the normal posture increased contact of some part of the buttocks posterior to the ischial tuberosities, and the forward inclination of the thoraco-cervical spine and the head from the normal posture to the slouched posture increased contact of the thighs.

The increase of the fore-and-aft pelvic motion in the entire body mode from the erect posture to the slouched posture also seemed to have contributed to the shift of the natural frequency. Changing posture from erect to slouched increased the horizontal distance between the excitation point at the buttocks and the mass centre of the entire body. This induced an excitation moment and fore-and-aft motion of the pelvis, involving shear deformation of buttocks tissue. The shear stiffness of tissue is generally much lower than the axial stiffness (see section 4.2) and so the natural frequency was decreased by the postural change towards the slouched posture. The decrease in the modulus of the apparent mass at the principal resonance from the erect posture to the slouched posture suggested that the axial reaction force from buttocks tissue decreased and the shear force might have increased, although it was not measured.

Changing posture also affected the second principal resonance of the apparent mass: the natural frequencies for the second principal resonance extracted from the apparent masses were 8.8 Hz in the erect posture, 8.6 Hz in the normal posture and 8.3 Hz in the slouched posture. The natural frequencies for the rotational modes of the pelvis also decreased due to the postural change, corresponding to the resonance shift: 9.2 and 8.4 Hz in the erect posture, 8.7 and 8.1 Hz in the normal posture, and 8.3 and 7.3 Hz in the slouched posture. The decreased axial stiffness and the increased contribution of shear deformation of buttocks tissue seemed to have decreased the natural frequencies for the rotational modes of the pelvis when changing posture from erect to slouched. The shift of the natural frequency for the second visceral mode was not clear: 9.2 Hz in the erect posture, 9.3 Hz in the normal posture and it was not found in the slouched posture. Therefore, the contribution of the second visceral mode to the second principal resonance of the apparent mass seemed to be smaller.

The effect of posture on the transmissibilities from vertical seat motion to longitudinal motion of the head and the spine coincided with the general trend (see section 2.3). The principal resonance frequency decreased when changing posture from erect to slouched, which was explained by the same mechanism as for the resonance shift in the apparent mass. The shift of the principal resonance in the seat-to-head transmissibility was smaller than the shift in the seat-to-spine transmissibilities, indicating the presence of relative motion of the head to the spine around the principal resonance which was possibly pitching motion of the head. The transmissibilities from vertical seat motion to longitudinal motion of the spine also decreased above the principal resonance due to the postural change, and the decrement was larger at the thoracic spine. The effect of posture on the transmissibilities from vertical seat motion to transverse motion of the body was large at the head and the thoracic spine. The transmissibilities to the thoracic spine increased at most frequencies below 20 Hz when changing posture from erect to slouched, indicating that the magnitude of the bending modes of the thoracic spine increased throughout the frequency range. The transmissibility to transverse motion of the head increased below 5 Hz due to the postural change, whereas the trend reversed above 5 Hz.

The mathematical complexities of the extracted modal constants were large for some modes. The real mode shapes (deformations) of sites on a structure are either in phase or in opposite phase (i.e. phase differences are either 0 or 180 degrees) to produce a standing wave at the corresponding natural frequency. The complex mode shapes have phase differences other than 0 or 180 degrees between sites on a structure with a travelling wave (Figure 4.36). The complex mode shapes are produced from the non-proportional damping, but there is no comprehensive theory to treat the complex mode shapes.

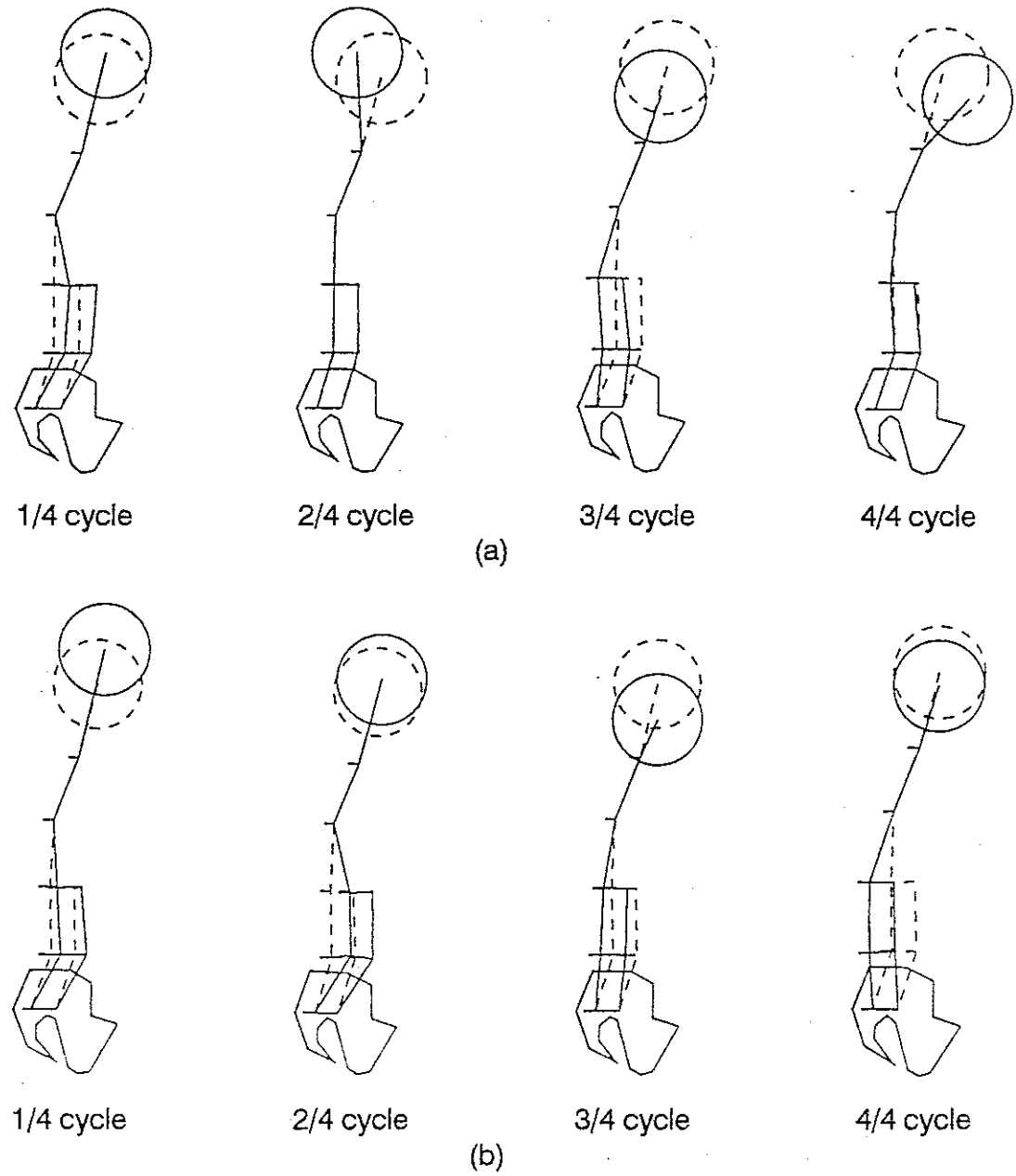

Figure 4.36 Complex mode shapes (——) and the initial configuration (- - - -) in the normal posture; (a) 5th mode at 5.6 Hz and (b) 11th mode at 12.5 Hz.

4.3.6 Conclusions

Experimental modal analysis was found to be applicable to whole-body vibration. A total of ten correlated modes between the subjects was extracted for the normal posture below 13 Hz. The principal resonance of the driving point responses at about 5 Hz corresponded to a combination of an entire body mode with vertical and fore-and-aft pelvic motion due to buttocks tissue deformation in phase with a vertical visceral mode, and a bending mode

of the upper thoracic and the cervical spine. A bending mode of the lumbar and the lower thoracic spine was found in the next higher mode which was located close to the principal mode. The second principal resonance of the driving point responses at about 8 Hz was found to correspond to rotational modes of the pelvis and might have some contribution of the second visceral mode. When a subject changed posture from erect to slouched, the natural frequencies for the entire body mode and the rotational modes of the pelvis decreased, resulting in the decrease in the frequencies for the principal and the second principal resonances of the driving point responses. The fore-and-aft motion of the pelvis, including shear deformation of buttocks tissue, was found to increase in the entire body mode due to the postural change towards the slouched posture. The effect of posture was found to be large in the transmissibilities to the head and to the thoracic spine throughout the frequency range below 20 Hz.

4.4 MEASUREMENT OF THE APPARENT MASS WITH CONSTRAINTS

4.4.1 Introduction

From the experimental modal analysis, the principal resonance of the driving point responses at about 5 Hz was found to correspond to a combination of an entire body mode with vertical and fore-and-aft pelvic motion due to buttocks tissue deformation in phase with a vertical visceral mode, and a bending mode of the upper thoracic and the cervical spine (see section 4.3). It was also found that the second principal resonance at about 8 Hz corresponded to rotational modes of the pelvis and might have some contribution of the second visceral mode. In order to support the results, the driving point apparent masses were measured with constraints applied to the buttocks (pelvis) and the viscera. The hypotheses were (1) if the principal resonance of the apparent mass is dominated by the buttocks mode (i.e. entire body mode) and the visceral mode, constraints to restrict motion of the buttocks and the viscera would affect the principal resonance, (2) if the second principal resonance is dominated by the rotational modes of the pelvis and the second visceral mode, constraints to restrict motion of the pelvis and the viscera would affect the second principal resonance.

4.4.2 Experimental methods

Vertical response force was measured by a force platform (Kistler Type 9281B) placed

beneath the buttocks of seated subjects so as to determine the driving point apparent mass with vertical excitation acceleration measured by an accelerometer (Entran Model EGCSY-240D-10D) attached to the vibrator platform. Subjects sat on the force platform mounted on a vibrator platform without a backrest, adopting an upright normal relaxed posture. The thighs and the lower legs were set to horizontal and vertical by adjusting the height of a stationary footrest placed outside the vibrator platform.

The experiment consisted of three conditions. For the first condition, the subjects were vibrated without constraint. For the second condition, the subjects sat on two wooden square blocks, which had a dimension of 5 cm (width) x 5 cm (length) x 1 cm (height), placed between the force platform and the ischial tuberosities of the subjects. The blocks reduced the contact area between the buttocks and the force platform and increased the stiffness of tissue, assuming a non-linear force-deflection relationship (buttocks constraint). The increased stiffness of the buttocks tissue also constrained the motion of the pelvis (pelvic constraint), including the rotational motion of the pelvis. For the third condition, the subjects wore a wide belt (about 15 cm height) around the abdomen. The belt was tight, impeding respiration of the subjects slightly, and constrained relative motion of the viscera to the spine (visceral constraint).

A total of seven subjects participated in the experiment. None of them had suffered back problems in the past. They were exposed to vertical random vibration with a magnitude of 1.6 m/s^2 r.m.s. in the frequency range below 50 Hz for 2 minutes duration three times for the three conditions. The time histories of force and acceleration were acquired simultaneously into a computer with a sampling rate of 100 samples per second through anti-aliasing low pass filters at 35 Hz with a cut-off rate of 30 dB/octave. The apparent masses were calculated, dividing vertical response force by vertical excitation acceleration in the frequency domain after Fast Fourier Transform. The effect of the mass of the force platform was subtracted (see section 2.3.3). The apparent masses were then normalised, dividing them by the sitting weights of the subjects as proposed by Fairley and Griffin (1989).

4.4.3 Results

The apparent masses of the seven subjects in the three conditions, and the mean apparent masses, are shown in Figure 4.37. The buttocks constraint and the visceral constraint generally affected the principal resonance of the apparent mass at about

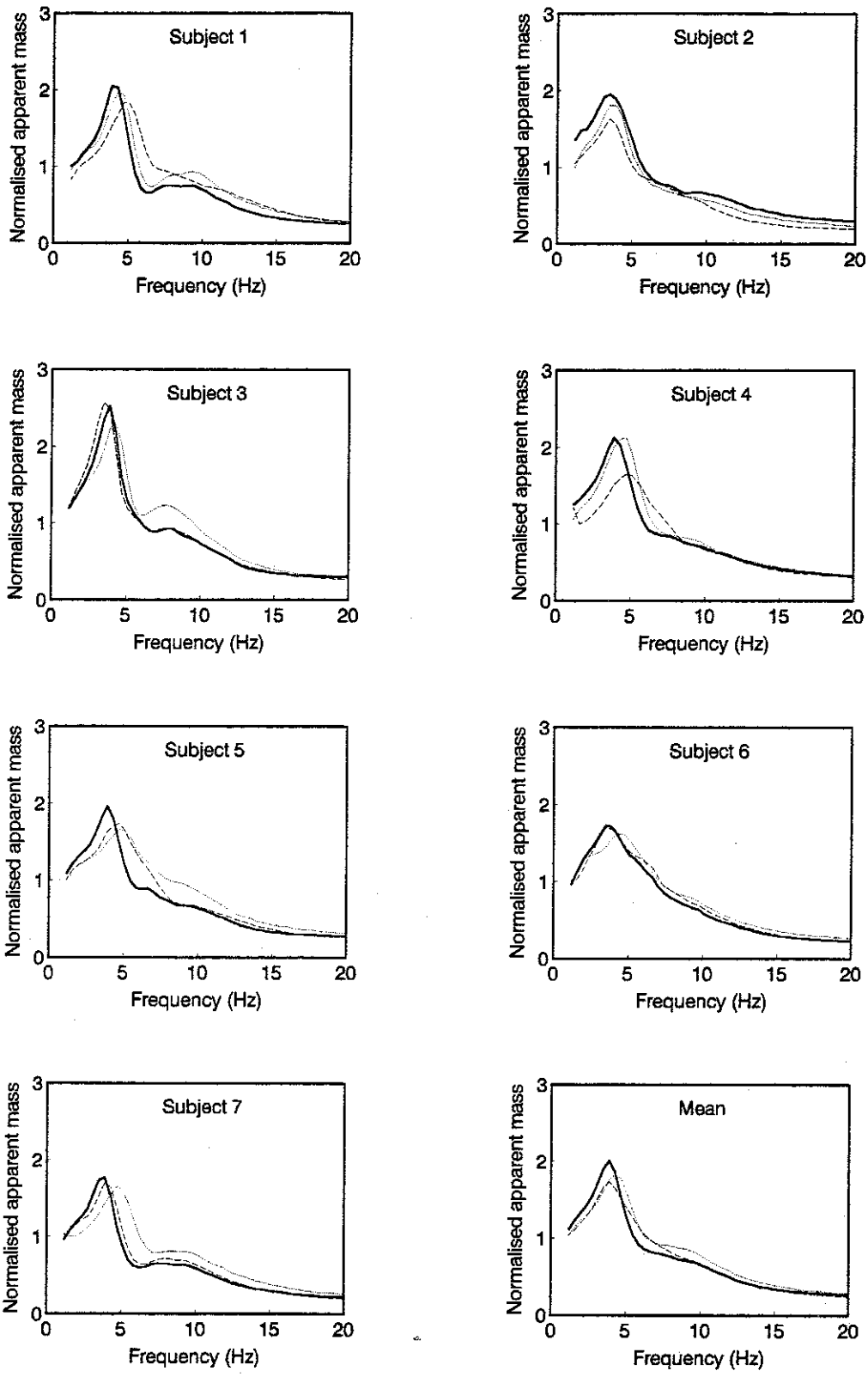

Figure 4.37 Normalised apparent masses of the seven subjects and the mean apparent masses without constraint (——), with the blocks beneath the ischial tuberosities (- - - -) and with the belt around the abdomen (.....).

5 Hz by increasing the frequency or decreasing the modulus, or both. There was no clear difference between the effects of the two types of constraint on the principal resonance. The magnitudes of the effects of the constraints were dependent on the subject. However, the effects appeared on subjects with approximately the same probability for the two constraints: the effect of the buttocks constraint was larger on subjects 1, 2 and 4, whereas the effect of the visceral constraint was larger on subjects 3, 6 and 7, both effects were approximately of the same magnitude on subject 5 and in the mean apparent mass. Therefore, the principal resonance of the apparent mass contained both the buttocks mode (the entire body mode) and the visceral mode, and the contributions of the two modes were about the same. The effect of the constraints on the second principal resonance at about 8 Hz was not clear. However, it appeared that the pelvic constraint flattened the second principal resonance on subjects 1, 4, 5 and in the mean apparent mass, and the visceral constraint enhanced the second principal resonance on subjects 1, 3 and 5.

4.4.4 Discussion

Coermann (1962) measured the impedance of a single subject with a tight envelope around the pelvis and the abdomen. The envelope decreased the modulus of the impedance at the principal resonance and enhanced the second principal resonance slightly. Sandover (1978) measured the apparent mass of a single subject with two wooden blocks (2.5 cm x 2.5 cm) placed beneath the ischial tuberosities and a webbing belt (4 cm width) around the abdomen. The blocks increased the frequency and decreased the modulus of the principal resonance, and appeared to have flattened the second principal resonance. The belt reduced the modulus of the principal resonance slightly and increased the modulus of the second principal resonance. Although these investigations used single subjects, the results were consistent with the results obtained in this study. The variation in the effects of the constraints depending on the subject may be explained if the buttocks constraint or the visceral constraint changed either the posture (spinal curve) or the muscle tension involuntarily. This could work to cancel some part of the effects of the constraints on some subjects.

A theoretical investigation of the vibration mode containing the entire body mode and the visceral mode was conducted. The mode may be simplified to the two degree-of-freedom model shown in Figure 4.38: where m_V and m_B are the mass of the viscera and the mass of the entire body excluding the viscera; k_V and k_B are the stiffnesses for the viscera and

the buttocks tissue; $x_V(t)$ and $x_B(t)$ are the displacements of the viscera and the entire body.

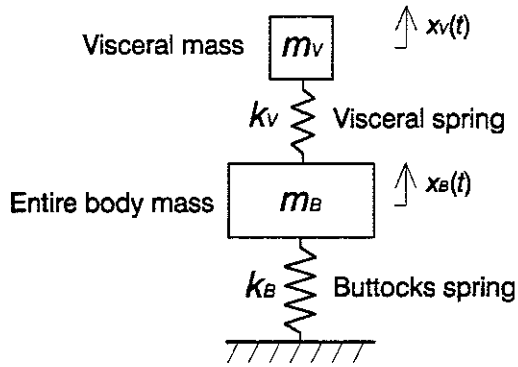

Figure 4.38 A two degree-of-freedom model equivalent to the mode containing the entire body mode and the visceral mode.

The equations of motion for the model shown in Figure 4.38 are:

$$m_B\ddot{x}_B(t) + k_B x_B(t) + k_V(x_B(t) - x_V(t)) = 0 \qquad \textbf{(4.54a)}$$

$$m_V\ddot{x}_V(t) + k_V(x_V(t) - x_B(t)) = 0 \qquad \textbf{(4.54b)}$$

Substituting $x_B(t)=X_Be^{i\omega t}$, $x_V(t)=X_Ve^{i\omega t}$ into equation (4.54), equation (4.55) is obtained in a matrix form:

$$\begin{bmatrix} -m_B\omega^2 + k_B + k_V & -k_V \\ -k_V & -m_V\omega^2 + k_V \end{bmatrix}\begin{Bmatrix} X_B \\ X_V \end{Bmatrix} = 0 \qquad \textbf{(4.55)}$$

The natural frequencies are obtained by letting the deteminant of the matrix in equation (4.55) equal zero:

$$\omega_1^2, \omega_2^2 = \frac{1}{2}\left\{\left(\frac{k_B + k_V}{m_B} + \frac{k_V}{m_V}\right) \mp \sqrt{\left(\frac{k_B + k_V}{m_B} + \frac{k_V}{m_V}\right)^2 - 4\frac{k_B k_V}{m_B m_V}}\right\} \qquad \textbf{(4.56)}$$

Associated mode shapes are obtained, substituting equation (4.56) into equation (4.55):

$$\phi_1 = \begin{Bmatrix} -m_B\omega_1^2 + k_B + k_V \\ k_V \end{Bmatrix} \qquad \textbf{(4.57a)}$$

$$\phi_2 = \begin{Bmatrix} -m_B\omega_2{}^2 + k_B + k_V \\ k_V \end{Bmatrix} \quad \textbf{(4.57b)}$$

where: ϕ_1 and ϕ_2 are the mode shape vectors for the first and the second modes (the upper row corresponds to the displacement of the visceral mass, m_V, and the lower row corresponds to the displacement of the entire body mass, m_B.

The driving point apparent mass of the two degree-of-freedom model is calculated based on the model shown in Figure 4.39, where c_V and c_B are the damping coefficients for the viscera and the buttocks tissue; $x_{in}(t)$ is the input displacement; $f_{in}(t)$ is the response force measured at the base. The equations of motion for the model shown in Figure 4.39 are:

$$m_B\ddot{x}_B(t) + c_B(\dot{x}_B(t) - \dot{x}_{in}(t)) + k_B(x_B(t) - x_{in}(t)) + c_V(\dot{x}_B(t) - \dot{x}_V(t)) + k_V(x_B(t) - x_V(t)) = 0 \quad \textbf{(4.58a)}$$

$$m_V\ddot{x}_V(t) + c_V(\dot{x}_V(t) - \dot{x}_B(t)) + k_V(x_V(t) - x_B(t)) = 0 \quad \textbf{(4.58b)}$$

$$f_{in}(t) = c_B(\dot{x}_{in}(t) - \dot{x}_B(t)) + k_B(x_{in}(t) - x_B(t)) \quad \textbf{(4.58c)}$$

Substituting $x_B(t)=X_Be^{i\omega t}$, $x_V(t)=X_Ve^{i\omega t}$ and $f_{in}(t)=F_{in}e^{i\omega t}$ into equation (4.58), the apparent mass $M(f)$ is obtained with the relationship (4.59):

$$M(f) = \frac{F_{in}}{-\omega^2 X_{in}} \quad \textbf{(4.59)}$$

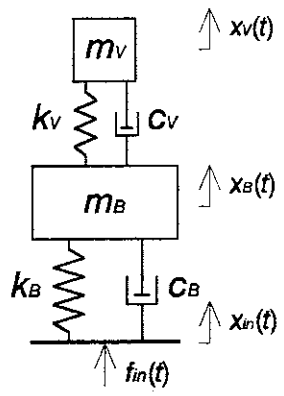

Figure 4.39 The two degree-of-freedom model to calculate the driving point responses.

Numerical simulation was conducted using parameters for the human body. The visceral mass and the entire body mass were obtained by summing corresponding masses used in the modified simplified model (see section 3.4). The buttocks stiffness was chosen also from the modified simplified model. The visceral stiffness was determined so that the visceral subsystem produced the natural frequency at about 5 Hz. The parameters employed in the model are shown below.

$$m_B=46 \text{ kg}, \quad k_B=9.8 \times 10^4 \text{ N/m}$$

$$m_V=13 \text{ kg}, \quad k_V=1.5 \times 10^4 \text{ N/m}$$

The calculated natural frequencies and the mode shapes are:

$$f_1 = 4.8\,\text{Hz}, \qquad \phi_1 = \begin{Bmatrix} 4.7 \\ 1 \end{Bmatrix}$$

$$f_2 = 8.2\,\text{Hz}, \qquad \phi_2 = \begin{Bmatrix} -0.6 \\ 1 \end{Bmatrix}$$

The mode shapes obtained are shown in Figure 4.40.

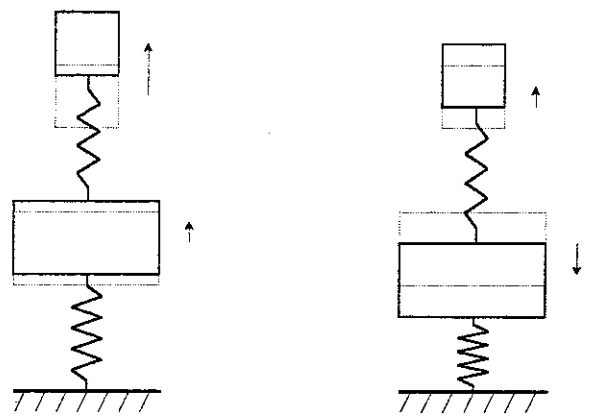

Figure 4.40 Calculated vibration mode shapes of the two degree-of-freedom model.

The calculated natural frequencies for the first and the second modes of the two degree-of-freedom model were close to the frequencies of the principal and the second principal resonances of the driving point apparent mass of the human body. The mode shape for the first mode at 4.8 Hz for the two degree-of-freedom model contained the buttocks deformation in phase with the visceral motion, corresponding to the principal mode of the

human body at 4.9 Hz extracted by the experimental modal analysis (Figure 4.31). A mode similar to the second mode of the two degree-of-freedom model was not found around 8 Hz in the measurements. The second visceral mode was found at 9.3 Hz on its own in the mode shapes extracted from the mean transfer functions of the eight subjects (Figure 4.31). However, there were some subjects who showed the second visceral mode between 7.5 and 8 Hz (Table 4.15). Their mode shapes contained the visceral motion in opposite phase with the buttocks deformation and they were similar to the second mode of the two degree-of-freedom model. Therefore, the second visceral mode in the measurements might have some error caused by the variability between the subjects and also by the fact that the acceleration was measured at only one site on the abdominal wall in the experiment.

The driving point apparent masses were calculated using three different sets of parameters, corresponding to the three conditions with constraints in the experiment, which are listed below.

The first parameter set for the condition without constraint

m_B=46 kg, k_B=9.8 x 10^4 N/m, c_B=0.1 x 10^4 Ns/m

m_V=13 kg, k_V=1.5 x 10^4 N/m, c_B=0.025 x 10^4 Ns/m

The second parameter set for the condition with the buttocks constraint

m_B=46 kg, k_B=14.7 x 10^4 N/m (50% increment), c_B=0.1 x 10^4 Ns/m

m_V=13 kg, k_V=1.5 x 10^4 N/m, c_B=0.025 x 10^4 Ns/m

The third parameter set for the condition with the visceral constraint

m_B=46 kg, k_B=9.8 x 10^4 N/m, c_B=0.1 x 10^4 Ns/m

m_V=13 kg, k_V=2.25 x 10^4 N/m (50% increment), c_B=0.025 x 10^4 Ns/m

The calculated apparent masses of the two degree-of-freedom model are shown in Figure 4.41. The increased stiffnesses for the buttocks and the viscera affected the first resonance located at about 5 Hz, which corresponded to the principal resonance of the driving point responses of the human body. Both increments of the stiffnesses increased the frequency of the first resonance, and the increased buttocks stiffness also reduced the modulus of the first resonance. However, the increased visceral stiffness increased the modulus of the first resonance which was not observed in the experiment. The increased stiffnesses for the buttocks and the viscera also increased the frequency of the second resonance at about 8 Hz which was located close to the second principal resonance of the driving point responses of the body. However, the effects on the modulus of the second resonance was opposite to the effects observed in the experiment: in the experiment, it appeared that the

buttocks constraint flattened and the visceral constraint enhanced the second principal resonance.

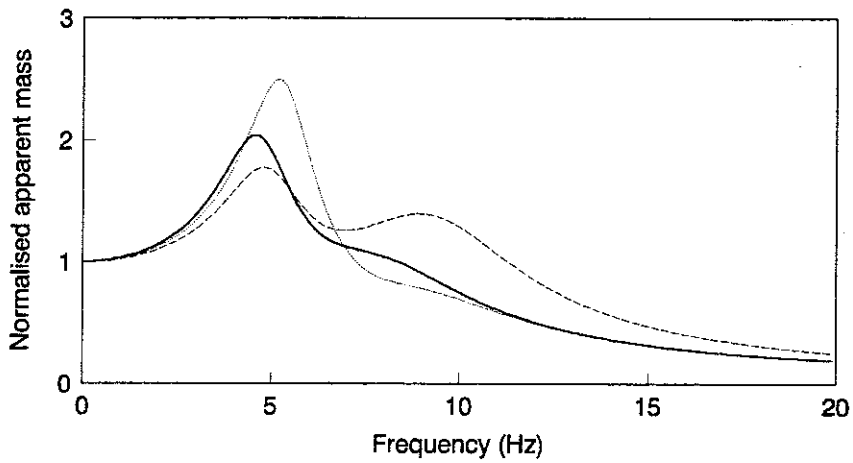

Figure 4.41 The apparent masses of the two degree-of-freedom model calculated using the first parameter set for the condition without constraint (——), the second set with the increased buttocks stiffness for the buttocks constraint (- - - -) and the third set with the increased visceral stiffness for the visceral constraint (·····).

The two degree-of-freedom model with parameters for the human body produced the natural frequencies at about 5 and 8 Hz. The mode shape for the principal mode of the human body at about 5 Hz was explained by the first mode of the two degree-of-freedom model and the model demonstrated the effects of the constraints on the principal resonance of the apparent mass. The model also suggested the effects of the constraints on the second mode at about 8 Hz, which was located close to the second principal resonance of the driving point responses of the body. However, the mode shape and the effects of the constraints were not entirely consistent with the measurements.

4.4.5 Conclusions

The buttocks constraint and the visceral constraint affected the principal resonance of the apparent mass at about 5 Hz by increasing the frequency or decreasing the modulus, or both. There was no clear difference between the effects of the two types of constraint on the principal resonance and the effects appeared on subjects with approximately the same probability for the two constraints. The result suggested that the buttocks mode (the entire body mode) and the visceral mode made equal contributions to the principal resonance.

The effect of the constraints on the second principal resonance at about 8 Hz was not clear.

4.5 CONCLUSIONS FROM EXPERIMENTAL WORK

A data correction method was developed to eliminated the effects of local tissue-accelerometer vibration from accelerations measured on the body surface. Experimental modal analysis was applied to whole-body vibration to extract the natural frequencies and the vibration mode shapes of the human body. The acceleration transfer functions from vertical seat motion to motion of the head, spine, pelvis and the viscera in the mid-sagittal plane were measured on the body surface, using the correction method. For the subject group, a total of ten correlated modes was extracted for the normal posture below 13 Hz. The principal resonance of the driving point responses at about 5 Hz was found to correspond to a combination of an entire body mode with vertical and fore-and-aft pelvic motion due to buttocks tissue deformation in phase with a vertical visceral mode, and a bending mode of the upper thoracic and cervical spine. A bending mode of the lumbar and the lower thoracic spine was found in the next higher mode which was located close to the principal mode. It was found by an additional experiment measuring the apparent mass with constraints on subjects that the entire body mode and the visceral mode made equal contributions to the principal resonance. The second principal resonance of the driving point responses at about 8 Hz seemed to correspond to rotational modes of the pelvis and might have some contribution of the second visceral mode. When a subject changed posture from erect to slouched, the natural frequencies for the entire body mode and the rotational modes of the pelvis decreased, resulting in decreases in the frequencies for the principal and the second principal resonances of the driving point responses. It was also found that the fore-and-aft motion of the pelvis, including shear deformation of buttocks tissue, increased in the entire body mode when changing posture from erect to slouched. This might also contribute to the resonance shift with the much lower shear stiffness of the buttocks tissue than the axial stiffness.

CHAPTER 5

MODELLING MECHANICAL RESPONSES TO WHOLE BODY VIBRATION: PART 2

5.1 INTRODUCTION

The models developed in chapter 3 produced similar driving point responses to the experimental data reported in the literature. However, the principal resonance at about 5 Hz in the driving point responses seemed to be dominated by a buttocks mode (an entire body mode) and a visceral mode, and the validation of the responses of other body parts such as the spine was not exhaustive. Another remaining problem of the models in chapter 3 was the effect of posture. The models did not show the resonance shift due to the change in posture which was reported consistently in the experimental data for the driving point responses, seat-to-head and seat-to-spine transmissibilities but whose mechanism was not known.

The expanded model in chapter 3 and the experimental modal analysis in chapter 4 predicted that the response of the human body contained many bending modes of the spine below 20 Hz. In this chapter, the expanded model is modified, comparing the vibration mode shapes of the model with the experimentally determined mode shapes of the human body. A mechanism for the resonance shift due to the change in posture was discussed in section 4.3 and is incorporated into the model.

5.2 MODEL 4: MODIFIED EXPANDED MODEL

5.2.1 Model description

The cervical vertebrae from C1 to C7 were newly incorporated into the modified expanded model based on the inertial and stiffness data for the neck estimated by Williams and Belytschko (1981). The modified expanded model finally included the spinal beams representing the stiffnesses of all the intervertebral discs (and possibly some part of connective tissue such as ligaments and muscles) between the vertebra C1 and the sacrum S1 and also the stiffness of the atlanto-occipital (C1-head) joint. The spinal curves were totally modified based on the measurements for the three postures of erect, normal

and slouched (section 4.3). The buttocks tissue spring for the expanded model was replaced by two beam elements placed in parallel (front and rear) beneath the pelvis for the modified expanded model so as to induce more pelvic rotation which was observed in the experiment (section 4.3). The inertial properties were principally based on those for the expanded model with minor modifications. The stiffness data were largely modified, comparing the calculated vibration mode shapes with the measurements.

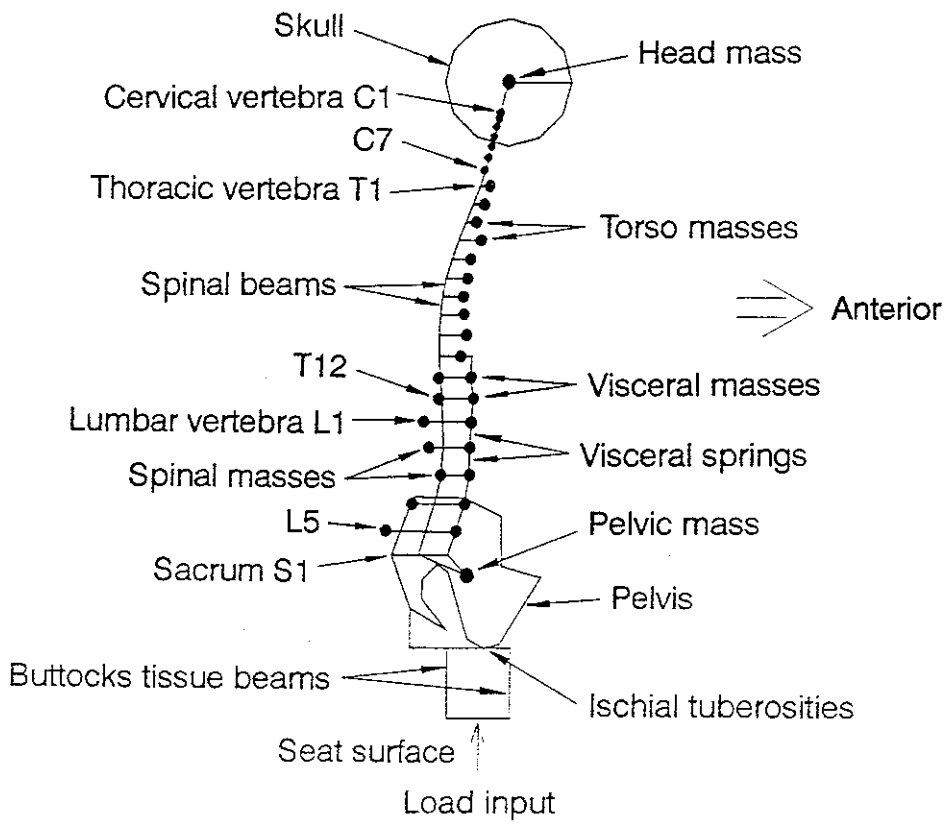

Figure 5.1 Modified expanded model in the normal posture.

5.2.2 Geometry and material properties

5.2.2.1 Geometry

Node locations for the spinal beams (geometrical centres of the vertebral bodies) were totally modified. The spinal curves in erect, normal and slouched postures were

determined based on the mean data of eight subjects measured using an anthropometric stand in the experiment in section 4.3. The postural data were measured on the posterior body surface of the subjects and transferred to the locations of the head mass centre, geometrical centres of the vertebral bodies and the pelvis with an initial angle (around the pivot at the ischial tuberosities) (Table 4.13). The locations of the vertebral body centres were obtained for the vertebrae T1, T6, T11, L3 and the sacrum S2, and the locations of the rest of the vertebrae were estimated for the modified expanded model. For the cervical spine, the locations of the head mass centre and the vertebrae C1 and T1 were almost on the straight line drawn from the head mass centre to the geometrical centre of the vertebral body of T1, although the cervical spine showed a convex forwards curve (Belytschko and Privitzer, 1978). The coordinates of the cervical vertebrae were approximated so that they divided the straight line from the head to the vertebra T1 in proportion to the lengths between the geometrical centres of the vertebral bodies and the head mass centre, which were calculated using equations (3.51) based on the data of Belytschko *et al.* (1976). For the thoraco-lumbar spine, unknown (unmeasured) vertical locations of the vertebrae were estimated, using a proportional relationship, from the vertical locations of the vertebrae for the expanded model (Table 3.13). Unknown horizontal locations of the vertebrae, corresponding to the estimated vertical locations, were then interpolated from the known (measured) locations of the vertebrae (Table 4.13), using the cubic spline interpolation (see Appendix 5).

The cubic spline interpolation for estimating spinal curves was validated, using the geometrical data for the expanded model (Table 3.13) which were originally determined based on radiographs of seated pilots by Belytschko *et al.* (1976). In the thoraco-lumbar spine, the vertical locations of all the vertebrae and the horizontal locations of the vertebrae T1, T6, T11, L3 and the sacrum S1 (S1 and S2 are fused) were assumed to be known. Horizontal locations of the rest of the vertebrae, corresponding to the known vertical locations, were interpolated from the known locations of the vertebrae T1, T6, T11, L3 and the sacrum S1. The interpolated horizontal locations were compared with the measured locations. The results are shown in Figure 5.2 and in Table 5.1 with the error defined by equation (5.1):

$$\text{Error}\ (\%) = \frac{|x_m(i) - x_i(i)|}{z_m(i) - z_m(i-1)} \times 100 \qquad \textbf{(5.1)}$$

where: $x_m(i)$ and $z_m(i)$ are measured horizontal and vertical locations of the vertebra i; $x_i(i)$ is interpolated horizontal location for the vertebra i. The cubic spline interpolation

estimated the curve of the thoraco-lumbar spine with negligible error from the five locations of the vertebrae, T1, T6, T11, L3 and the sacrum S1. The measured and the interpolated spinal curves for the three postures are shown in Figures 5.3, 5.4 and 5.5.

Table 5.1 Comparison between measured and interpolated locations of the vertebrae (x=horizontal location, z=vertical location with respect to the origin located at the ischial tuberosities).

	x ($m \times 10^{-2}$)			z ($m \times 10^{-2}$)(1)
Level	Measured	Interpolated	Error (%)	Measured
T1	-7.630(1)	—	—	63.321
T2	-8.138	-8.025	5.4	61.214
T3	-8.587	-8.428	7.6	59.136
T4	-8.962	-8.832	6.2	57.022
T5	-9.277	-9.210	3.0	54.900
T6	-9.557(1)	—	—	52.680
T7	-9.859	-9.837	0.9	50.382
T8	-10.036	-10.026	0.4	47.946
T9	-10.122	-10.082	1.5	45.401
T10	-10.122	-9.959	5.9	42.726
T11	-9.602(1)	—	—	39.942
T12	-8.776	-8.944	5.0	36.907
L1	-8.061	-8.050	0.3	33.551
L2	-7.052	-7.132	2.1	29.896
L3	-6.538(1)	—	—	26.003
L4	-6.488	-6.558	1.8	22.097
L5	-6.999	-6.912	2.7	18.227
S1	-7.188(1)	—	—	15.113

(1) Known values for the interpolation.

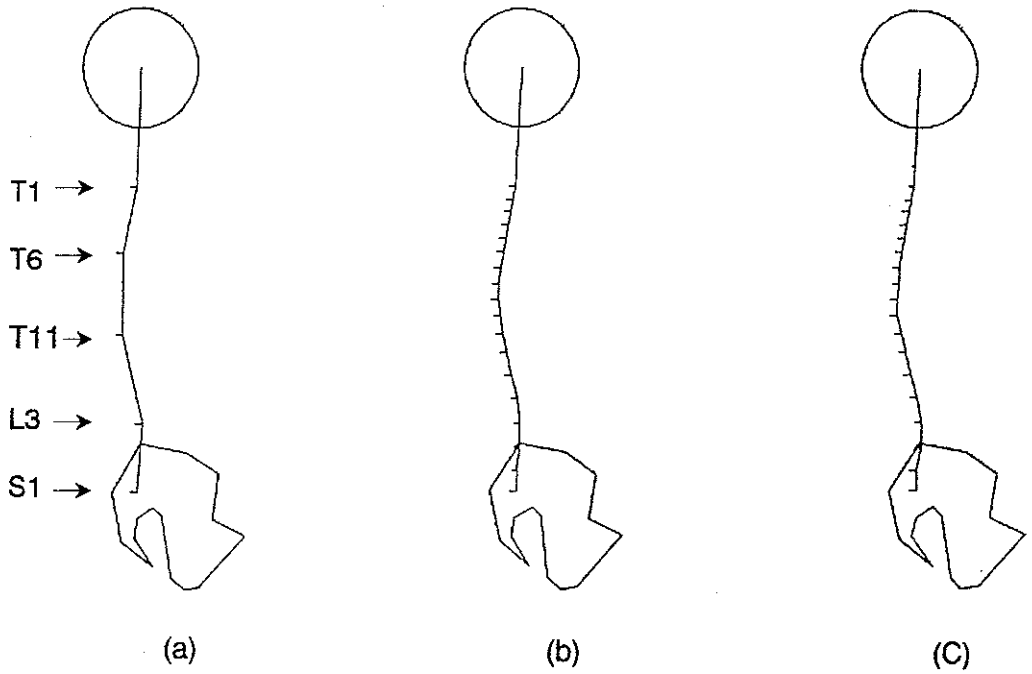

Figure 5.2 Validation of the cubic spline interpolation for estimating spinal curves: (a) known locations of the vertebrae and the sacrum; (b) interpolated locations of all the vertebrae in the thoraco-lumbar spine; (c) measured locations of all the vertebrae in the thoraco-lumbar spine.

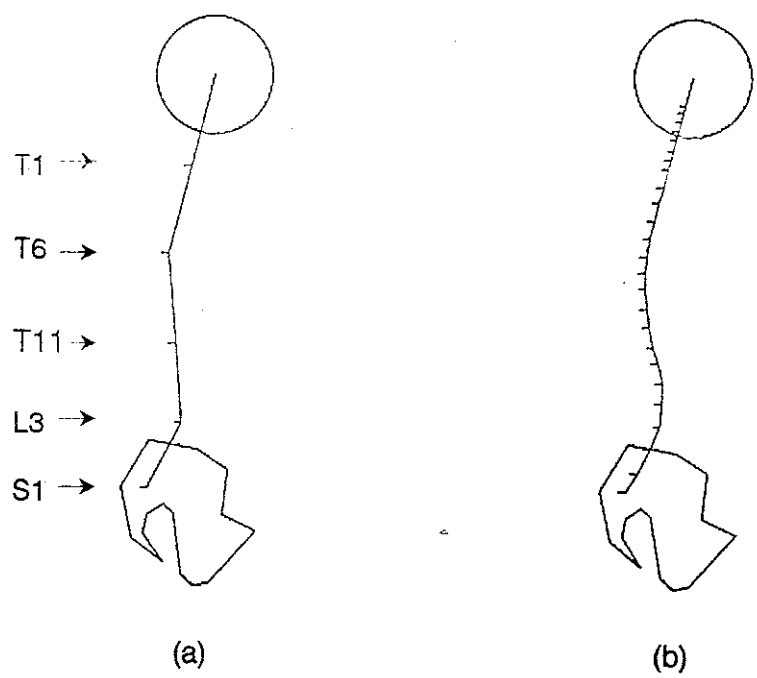

Figure 5.3 Estimation of the spinal curve: (a) measured erect posture (mean data of eight subjects); (b) interpolated spinal curve.

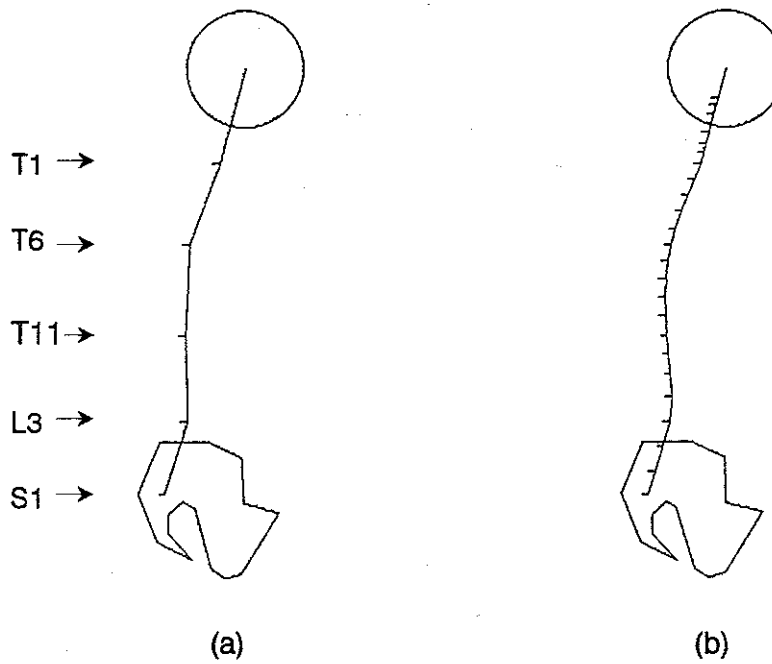

Figure 5.4 Estimation of the spinal curve: (a) measured normal posture (mean data of eight subjects); (b) interpolated spinal curve.

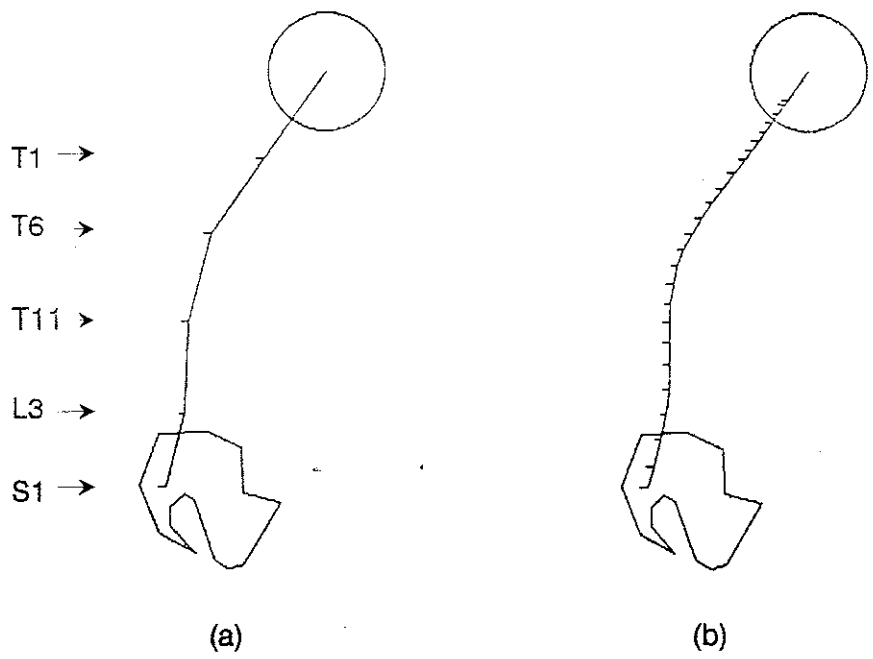

Figure 5.5 Estimation of the spinal curve: (a) measured slouched posture (mean data of seven subjects); (b) interpolated spinal curve.

The masses for the motion segments of the neck were assigned to the levels from C1 to C7 with no eccentricity from the spine because no data were available. The node locations for the torso masses above the T10 level were the same as those for the expanded model which corresponded to the mass centres of the torso motion segments measured by Liu and Wickstrom (1973). The node locations for the spinal masses and the visceral masses below the T10 level were assigned at each level so that the mass centre, the translational and the rotational masses coincided with those of each torso segment, and they were the same as those for the expanded model except at the L4 and L5 levels. At the L4 and L5 levels, the node locations for the spinal masses and the visceral masses were recalculated with L_v=2.0 x 10^{-2} m in equation (3.51) so that the visceral column became closer to vertical and avoided unwanted fore-and-aft motion of the visceral masses at these levels.

The location of the pelvic mass was defined by relative location with respect to the locations of the sacrum S1 and the ischial tuberosities, and it was rotated around the pivot at the ischial tuberosities when changing the pelvic angle with a postural change. The location of the pelvic mass affected rotational motion of the pelvis and it was determined, comparing the rotational modes of the pelvis between 8 and 9 Hz. Vertical harmonic load was applied, for the harmonic response analysis, at the middle of the span of the horizontal rigid link connecting the lower ends of the buttocks tissue beams. The node locations for the modified expanded model are shown in Tables 5.2, 5.3 and 5.4.

The acceleration responses were measured on the bite-bar (100 mm behind the mouth) and on the posterior body surface of the subjects in the experiment (section 4.3). Nodes were placed to the positions of the accelerometers (Table 5.5) via massless rigid links connecting them to the spinal beams so that the responses of the model could be calculated at these nodes and compared with the measurements directly.

Table 5.2 Node locations for the head mass, spinal beams and pelvic mass of the modified expanded model in the three postures.

Level	Erect posture ($m \times 10^{-2}$)		Normal posture ($m \times 10^{-2}$)		Slouched posture ($m \times 10^{-2}$)	
	x[1]	z	x	z	x	z
Head	2.983	80.863	2.570	80.250	14.856	78.157
C1	1.854	76.384	1.411	75.710	11.887	74.048
C2	1.629	75.493	1.180	74.807	11.296	73.230
C3	1.252	73.996	0.792	73.289	10.303	71.856
C4	0.877	72.507	0.407	71.780	9.316	70.490
C5	0.497	71.002	0.017	70.254	8.318	69.109
C6	0.088	69.379	-0.403	68.609	7.242	67.620
C7	-0.303	67.827	-0.805	67.036	6.214	66.196
T1	-0.694	66.275	-1.207	65.463	5.185	64.771
T2	-1.421	63.572	-2.176	62.861	3.521	62.435
T3	-2.192	60.908	-3.179	60.297	1.825	60.132
T4	-2.952	58.195	-4.179	57.686	0.124	57.786
T5	-3.608	55.474	-5.087	55.067	-1.472	55.434
T6	-4.094	52.625	-5.856	52.325	-2.930	52.971
T7	-4.296	50.032	-6.346	49.797	-4.135	50.415
T8	-4.276	47.283	-6.648	47.117	-5.085	47.705
T9	-4.036	44.411	-6.762	44.318	-5.769	44.873
T10	-3.591	41.392	-6.073	41.375	-6.202	41.897
T11	-2.969	38.250	-6.495	38.313	-6.407	38.800
T12	-2.364	35.528	-6.205	35.307	-6.436	35.622
L1	-1.792	32.519	-5.911	31.985	-6.391	32.108
L2	-1.529	29.239	-5.795	28.365	-6.437	28.280
L3	-1.961	25.748	-6.124	24.510	-6.829	24.203
L4	-3.472	21.933	-7.109	20.467	-7.742	20.077
L5	-5.522	18.202	-8.420	16.513	-8.915	16.042
S1	-7.188	15.113	-9.488	13.238	-9.871	12.700
I.T.[2]	0.0	0.0	0.0	0.0	0.0	0.0
Pelvis	-0.782	10.609	-2.436	10.355	-2.794	10.264
P.Angle[3]	-9.02 (degrees)		0.0 (degrees)		1.99 (degrees)	

(1) The coordinate system has x-axis for the fore-and-aft direction and z-axis for the vertical direction with the origin at the ischial tuberosities.
(2) Ischial tuberosities.
(3) Initial pelvic angle around the pivot at the ischial tuberosities, with respect to the angle in the normal posture.

Table 5.3 Node locations for the torso masses, spinal masses and visceral masses of the modified expanded model in common for the three postures.

Level	Torso or spinal mass[1] ($m \times 10^{-2}$)	Visceral mass[1] ($m \times 10^{-2}$)
C1	0.000	—
C2	0.000	—
C3	0.000	—
C4	0.000	—
C5	0.000	—
C6	0.000	—
C7	0.000	—
T1	1.351	—
T2	1.351	—
T3	1.351	—
T4	3.080	—
T5	2.500	—
T6	2.880	—
T7	2.800	—
T8	3.220	—
T9	3.810	—
T10	3.640	4.640[2]
T11	-0.636	4.390
T12	-0.558	4.470
L1	-2.917	3.980
L2	-2.233	3.650
L3	-1.007	3.970
L4	-3.542	4.240
L5	-6.335	4.280
S1	—	4.280[2]

(1) Relative horizontal coordinates with respect to the spinal column (vertebral body centres).
(2) Node without a mass.

Table 5.4 Node locations for the buttocks tissue beams and load application of the modified expanded model in common for the three postures.

Node	(m x 10^{-2}) x[(1)]	z
Upper end of the front beam	3.000	0.000
Upper end of the rear beam	-4.000	0.000
Lower end of the front beam	3.000	-10.000
Lower end of the rear beam	-4.000	-10.000
Load applying point	-0.500	-10.000

(1) The coordinate system has x-axis for the fore-and-aft direction and z-axis for the vertical direction with the origin at the ischial tuberosities.

Table 5.5 Node locations for calculating responses of the head[(1)] and the vertebrae[(2)], corresponding to the positions of accelerometers in the experiment (relative coordinates with respect to the head mass and the vertebral body centres).

Level	(m x 10^{-2}) x	z
Head	2.0	-6.5
T1	-6.456	-1.400
T6	-6.856	-1.400
T11	-7.293	-1.400
L3	-7.914	-0.460
S1	-4.000	0.000

(1) x and z are fore-and-aft and vertical directions. The listed relative coordinates are for the erect and the normal postures. For the slouched posture, the coordinates are rotated clockwise around the head mass by the angle determined by the forward inclination of the cervical spine from the normal or erect position.

(2) x and z are fore-and-aft and vertical directions and the listed relative coordinates are in common for the three postures.

5.2.2.2 Inertial properties

Inertial properties for the motion segments of the neck were based on the data of Williams and Belytschko (1981), which were obtained by distributing the total mass of the neck measured by Prasad and King (1974) to the segments according to the estimated volume of the segments with an assumption of uniform density. The translational and rotational torso masses above the T10 level were the same as those for the expanded model which were based on the data of Liu and Wickstrom (1973). The mass of the upper arms was divided equally and assigned to the translational torso masses for the levels from T1 to T6. Below the T10 level, the spinal masses and the visceral masses were distributed so that the translational and rotational masses at each level coincided with those for the corresponding torso segment at the mass centre measured by Liu and Wickstrom. The spinal and visceral masses below the T10 level were the same as those for the expanded model except the rotational masses at the L4 and L5 levels which were recalculated with L_v=2.0 x 10^{-2} m in equation (3.51). The rotational head mass was the same as that for the expanded model and the translational head mass was reduced from 5.0 kg for the expanded model to 4.5 kg for the modified expanded model, considering data of Mawn *et al.* (1992), Singley III and Haley (1978) and Hubbard and McLeod (1978). The translational pelvic mass was the same as that for the expanded model but 30 % of the translational masses of the thighs, forearms and hands were added to the translational mass of the pelvis for the modified expanded model instead of 50 % for the expanded model. The rotational pelvic mass was increased by 50% from that used for the expanded model, accounting for the additional rotational mass of the limbs. The total mass of the modified expanded model was 60.046 kg. The inertial properties for the modified expanded model are shown in Table 5.6.

Table 5.6 Inertial properties for the modified expanded model in common for the three postures.

Level	Torso or spinal mass		Visceral mass	
	Translational mass (kg)	Rotational mass[1] ($kgm^2 \times 10^{-2}$)	Translational mass (kg)	Rotational mass[1] ($kgm^2 \times 10^{-2}$)
Head	4.5	2.0	—	—
C1	0.815	0.0601	—	—
C2	0.815	0.0601	—	—
C3	0.815	0.0601	—	—
C4	0.815	0.0601	—	—
C5	0.815	0.0601	—	—
C6	0.900	0.0656	—	—
C7	1.200	0.0775	—	—
T1	2.114[2]	0.0745	—	—
T2	1.829[2]	0.2077	—	—
T3	1.915[2]	0.2878	—	—
T4	1.819[2]	0.3138	—	—
T5	1.930[2]	0.3838	—	—
T6	1.948[2]	0.4425	—	—
T7	1.308	0.5374	—	—
T8	1.326	0.5543	—	—
T9	1.417	0.6164	—	—
T10	1.352	0.6028	—	—
T11	0.3184	0.1283	1.282	0.5130
T12	0.3329	0.1270	1.341	0.5079
L1	0.2842	0.1036	1.676	0.5870
L2	0.3420	0.1253	1.670	0.6119
L3	0.4325	0.1482	1.720	0.5927
L4	0.5621	0.1427	1.625	0.4126
L5	0.4659	0.0993	1.774	0.3781
S1	—	—	1.708	0.1000
Pelvis	16.879[3]	14.13	—	—

(1) Rotational mass around the mass centre.
(2) Include the translational mass of the upper arms x 1/6 (0.755 kg).
(3) Sum of the masses for the pelvis (10.9 kg), thighs x 0.3 (4.86 kg) and hands x 0.3 (1.119 kg).

5.2.2.3 Stiffness data

The stiffness data for the spinal beams in the cervical region were initially based on the data of the intervertebral discs and the atlanto-occipital joint estimated by Williams and Belytschko (1981): for the axial stiffnesses, the mean values of tension and compression were used. The rest of the stiffness data were initially based on the data used for the expanded model. The initial values were adjusted, comparing the driving point apparent mass and the vibration mode shapes of the model with the measurements (section 4.3) below 10 Hz in the normal posture. The axial stiffnesses for the buttocks tissue beams and the visceral springs were determined, focusing on the entire body mode (buttocks mode) and the visceral mode included in the principal mode at about 5 Hz. The effects of the visceral constraint and the buttocks constraint were also calculated by increasing those stiffnesses so as to assess the contributions of the buttocks mode and the visceral mode to the principal mode, comparing them with the experimental results shown in section 4.4. The bending stiffnesses and the distribution of the axial stiffnesses for the front and rear buttocks tissue beams affected the rotational motion of the pelvis and they were determined so that the rotational mode of the pelvis occurred between 8 and 9 Hz. The bending stiffnesses for the spinal beams were determined, mainly focusing on the bending mode of the entire spine between 5 and 6 Hz. The bending stiffnesses for the lowest spinal beams were also adjusted so that the spine did not deform largely at the mode between 8 and 9 Hz where the pelvis rotated. The axial stiffnesses for the spinal beams were not altered because the axial deformation of the spine was not clear in the experiment.

The apparent masses in the three postures were compared. Only changing axial stiffnesses for the buttocks tissue beams achieved the resonance shift observed in the experiment. The axial stiffnesses for the buttocks tissue beams in the erect and the slouched postures were determined, comparing the principal resonance frequencies of the apparent mass and the natural frequencies for the entire body mode with the measurements. The stiffness data for the modified expanded model are shown in Tables from 5.7 to 5.13. The stiffness data for the spinal beams are listed for the three postures separately in Tables 5.7, 5.8 and 5.9 for the different Young's moduli due to slightly different lengths of the beams measured in the experiment. However, the axial and the bending stiffnesses for the spinal beams are exactly the same for the three postures.

Table 5.7 Stiffness data for the spinal beams of the expanded model in the erect posture.

Level	Axial stiffness ($N/mx10^6$)	Bending stiffness ($Nm \times 10^2$)	Length ($m \times 10^{-2}$)	Area ($m \times 10^{-3}$)	Young's modulus (N/m^2x10^7)	Second moment [1] ($m^4 \times 10^{-8}$)
Head-C1	0.550	10x0.40	4.618	1.0	2.540	10x7.272
C1-C2	0.300	10x0.90	0.919	1.0	0.276	10x29.96
C2-C3	0.700	10x0.08	1.544	1.0	1.081	10x1.143
C3-C4	0.760	10x0.10	1.536	1.0	1.167	10x1.316
C4-C5	0.794	10x0.12	1.552	1.0	1.232	10x1.511
C5-C6	0.967	10x0.16	1.673	1.0	1.618	10x1.655
C6-C7	1.014	10x0.22	1.601	1.0	1.623	10x2.169
C7-T1	1.334	10x0.37	1.601	1.0	2.136	10x2.774
T1-T2	0.70	7x0.20	2.799	1.0	1.959	7x2.857
T2-T3	1.20	7x0.40	2.773	1.0	3.328	7x3.333
T3-T4	1.50	7x0.60	2.818	1.0	4.227	7x4.000
T4-T5	2.10	7x1.00	2.799	1.0	5.878	7x4.762
T5-T6	1.90	7x1.00	2.890	1.0	5.491	7x5.263
T6-T7	1.80	7x1.00	2.601	1.0	4.682	7x5.556
T7-T8	1.50	7x1.00	2.749	1.0	4.124	7x6.666
T8-T9	1.50	7x1.10	2.882	1.0	4.323	7x7.333
T9-T10	1.50	7x1.10	3.051	1.0	4.577	7x7.333
T10-T11	1.50	7x1.20	3.203	1.0	4.805	7x8.000
T11-T12	1.50	7x1.00	2.789	1.0	4.184	7x6.666
T12-L1	1.80	7x0.90	3.063	1.0	5.513	7x5.000
L1-L2	2.13	7x0.90	3.290	1.0	7.008	7x4.225
L2-L3	2.00	7x0.90	3.518	1.0	7.036	7x4.500
L3-L4	2.00	7x0.90	4.103	1.0	8.206	7x4.500
L4-L5	1.87	7x0.80	4.256	1.0	7.959	7x4.278
L5-S1	1.47	1x0.70	3.510	1.0	5.160	1x4.762

(1) Second moment of area of the cross-section.

Table 5.8 Stiffness data for the spinal beams of the expanded model in the normal posture.

Level	Axial stiffness ($N/m \times 10^6$)	Bending stiffness ($Nm \times 10^2$)	Length ($m \times 10^{-2}$)	Area ($m \times 10^{-3}$)	Young's modulus ($N/m^2 \times 10^7$)	Second moment [1] ($m^4 \times 10^{-8}$)
Head-C1	0.550	10x0.40	4.685	1.0	2.577	10x7.272
C1-C2	0.300	10x0.90	0.932	1.0	0.280	10x29.96
C2-C3	0.700	10x0.08	1.566	1.0	1.096	10x1.143
C3-C4	0.760	10x0.10	1.558	1.0	1.184	10x1.316
C4-C5	0.794	10x0.12	1.575	1.0	1.251	10x1.511
C5-C6	0.967	10x0.16	1.698	1.0	1.642	10x1.655
C6-C7	1.014	10x0.22	1.624	1.0	1.647	10x2.169
C7-T1	1.334	10x0.37	1.624	1.0	2.166	10x2.774
T1-T2	0.70	7x0.20	2.776	1.0	1.943	7x2.857
T2-T3	1.20	7x0.40	2.754	1.0	3.305	7x3.333
T3-T4	1.50	7x0.60	2.796	1.0	4.194	7x4.000
T4-T5	2.10	7x1.00	2.772	1.0	5.821	7x4.762
T5-T6	1.90	7x1.00	2.848	1.0	5.411	7x5.263
T6-T7	1.80	7x1.00	2.575	1.0	4.635	7x5.556
T7-T8	1.50	7x1.00	2.697	1.0	4.046	7x6.666
T8-T9	1.50	7x1.10	2.802	1.0	4.203	7x7.333
T9-T10	1.50	7x1.10	2.943	1.0	4.415	7x7.333
T10-T11	1.50	7x1.20	3.070	1.0	4.605	7x8.000
T11-T12	1.50	7x1.00	3.019	1.0	4.529	7x6.666
T12-L1	1.80	7x0.90	3.335	1.0	6.003	7x5.000
L1-L2	2.13	7x0.90	3.622	1.0	7.715	7x4.225
L2-L3	2.00	7x0.90	3.869	1.0	7.738	7x4.500
L3-L4	2.00	7x0.90	4.162	1.0	8.324	7x4.500
L4-L5	1.87	7x0.80	4.166	1.0	7.790	7x4.278
L5-S1	1.47	1x0.70	3.445	1.0	5.064	1x4.762

(1) Second moment of area of the cross-section.

Table 5.9 Stiffness data for the spinal beams of the expanded model in the slouched posture.

Level	Axial stiffness ($N/mx10^6$)	Bending stiffness ($Nm \times 10^2$)	Length ($m \times 10^{-2}$)	Area ($m \times 10^{-3}$)	Young's modulus (N/m^2x10^7)	Second moment [1] ($m^4 \times 10^{-6}$)
Head-C1	0.550	10x0.40	5.070	1.0	2.789	10x7.272
C1-C2	0.300	10x0.90	1.009	1.0	0.303	10x29.96
C2-C3	0.700	10x0.08	1.695	1.0	1.187	10x1.143
C3-C4	0.760	10x0.10	1.686	1.0	1.281	10x1.316
C4-C5	0.794	10x0.12	1.704	1.0	1.353	10x1.511
C5-C6	0.967	10x0.16	1.837	1.0	1.776	10x1.655
C6-C7	1.014	10x0.22	1.757	1.0	1.782	10x2.169
C7-T1	1.334	10x0.37	1.757	1.0	2.344	10x2.774
T1-T2	0.70	7x0.20	2.868	1.0	2.008	7x2.857
T2-T3	1.20	7x0.40	2.860	1.0	3.432	7x3.333
T3-T4	1.50	7x0.60	2.897	1.0	4.346	7x4.000
T4-T5	2.10	7x1.00	2.842	1.0	5.968	7x4.762
T5-T6	1.90	7x1.00	2.862	1.0	5.438	7x5.263
T6-T7	1.80	7x1.00	2.826	1.0	5.087	7x5.556
T7-T8	1.50	7x1.00	2.872	1.0	4.308	7x6.666
T8-T9	1.50	7x1.10	2.913	1.0	4.370	7x7.333
T9-T10	1.50	7x1.10	3.007	1.0	4.511	7x7.333
T10-T11	1.50	7x1.20	3.104	1.0	4.656	7x8.000
T11-T12	1.50	7x1.00	3.178	1.0	4.767	7x6.666
T12-L1	1.80	7x0.90	3.514	1.0	6.325	7x5.000
L1-L2	2.13	7x0.90	3.829	1.0	8.156	7x4.225
L2-L3	2.00	7x0.90	4.096	1.0	8.192	7x4.500
L3-L4	2.00	7x0.90	4.226	1.0	8.452	7x4.500
L4-L5	1.87	7x0.80	4.202	1.0	7.858	7x4.278
L5-S1	1.47	1x0.70	3.476	1.0	5.110	1x4.762

(1) Second moment of area of the cross-section.

Table 5.10 Stiffness data for the visceral springs of the modified expanded model in common for the three postures.

Level	Axial stiffness ($N/m \times 10^4$)
T10-T11	2.86
T11-T12	2.62
T12-L1	2.42
L1-L2	2.24
L2-L3	1.91
L3-L4	1.64
L4-L5	1.68
L5-S1	1.29

For all the viscera-spine interconnecting springs: axial stiffness=3.0×10^4 N/m.

Table 5.11 Stiffness data for the buttocks tissue beams of the modified expanded model in the erect posture.

Buttocks tissue beam	Axial stiffness ($N/m \times 10^6$)	Bending stiffness ($Nm \times 10^2$)	Length ($m \times 10^{-2}$)	Area ($m \times 10^{-3}$)	Young's modulus ($N/m^2 \times 10^7$)	Second moment [1] ($m^4 \times 10^{-8}$)
Front	2x0.00983	0.04913	10.0	2.0	0.09825	50.0
Rear	16x0.00983	0.04913	10.0	16.0	0.09825	50.0

(1) Second moment of area of the cross-section.

Table 5.12 Stiffness data for the buttocks tissue beams of the modified expanded model in the normal posture.

Buttocks tissue beam	Axial stiffness ($N/m \times 10^6$)	Bending stiffness ($Nm \times 10^2$)	Length ($m \times 10^{-2}$)	Area ($m \times 10^{-3}$)	Young's modulus ($N/m^2 \times 10^7$)	Second moment [1] ($m^4 \times 10^{-8}$)
Front	1x0.00983	0.04913	10.0	1.0	0.09825	50.0
Rear	8x0.00983	0.04913	10.0	8.0	0.09825	50.0

(1) Second moment of area of the cross-section.

Table 5.13 Stiffness data for the buttocks tissue beams of the modified expanded model in the slouched posture.

Buttocks tissue beam	Axial stiffness ($N/m \times 10^6$)	Bending stiffness ($Nm \times 10^2$)	Length ($m \times 10^{-2}$)	Area ($m \times 10^{-3}$)	Young's modulus ($N/m^2 \times 10^7$)	Second moment [1] ($m^4 \times 10^{-8}$)
Front	0.6x0.0098	0.04913	10.0	0.6	0.09825	50.0
Rear	4.8x0.0098	0.04913	10.0	4.8	0.09825	50.0

(1) Second moment of area of the cross-section.

5.2.2.4 Effective damping ratios

The effective damping ratios (modal viscous damping) used for calculating the transfer functions of the modified expanded model are listed in Table 5.14. The damping loss factors extracted in the experiment (section 4.3) were used first with the approximation shown in equation (5.2). However, they tended to be too small and they were increased by means of trial and error.

$$\eta = 2\zeta \qquad \textbf{(5.2)}$$

where: η is the damping loss factor for the hysteretic damping; ζ is the damping ratio for the viscous damping.

Table 5.14 The effective damping ratios used for calculating the transfer functions of the modified expanded model.

Mode No.	Effective damping ratio
1	0.5
2	0.5
3	0.5
4	0.3
5	0.3
6	0.2
7	0.2
8 and higher	0.3

5.2.3 Calculation conditions

The master degrees of freedom were defined as the vertical, fore-and-aft and rotational (in the mid-sagittal plane) directions at the head mass, torso masses, spinal masses and the pelvic mass which were the same as for the previous models. They were defined as the direction along the visceral column at the visceral masses and as the vertical direction at the large mass placed at the force applied node. When calculating response displacements at some nodes in Ansys, their degrees of freedom must be defined as the master degrees of freedom. Additional master degrees of freedom newly defined for the modified expanded model were those at the nodes corresponding to the positions of the accelerometers at the head (on the bite-bar) and on the body surface in the experiment (Table 5.5). The master degrees of freedom were defined as the vertical, fore-and-aft and rotational directions at the head for the erect and the normal postures, whereas, for the slouched posture, their axes were rotated clockwise by the angle determined by the forward inclination of the cervical spine from the normal or erect position. They were defined as the longitudinal and transverse directions of the spine as well as the rotational direction at the nodes corresponding to the posterior body surface.

The vertical force was applied to the node at the middle of the span of the horizontal rigid link connecting the lower ends of the buttocks tissue beams, and some constraints and coupling motion were necessary to avoid unwanted motion of the buttocks beams. The vertical degrees of freedom of the nodes corresponding to the lower ends of the front and rear buttocks tissue beams were coupled, and the fore-and-aft and rotational degrees of freedom at those nodes were constrained to be zero. The rest of the conditions were the same as those for the previous models. The Ansys command list for the modal analysis of the modified expanded model is shown in Appendix 6.

5.2.4 Results and discussion

Calculated natural frequencies below 20 Hz of the modified expanded model in the normal posture are shown in Table 5.15 and the vibration mode shapes are shown in Figure 5.6. Figure 5.7 compares the calculated vibration mode shapes below 10 Hz in the normal posture with the measured mode shapes obtained in section 4.3. The modified expanded model produced seven modes below 10 Hz, whereas the experimental modal analysis (section 4.3) extracted eight modes in the same frequency range. The calculated mode shapes generally showed good agreement with the measurements below 10 Hz. The

material properties arbitrarily adjusted to achieve the calculated results were the location of the pelvic mass, axial and bending stiffnesses of the buttocks tissue beams, axial stiffnesses of the visceral springs, and the bending stiffnesses of the spinal beams as shown in Table 5.16.

Table 5.15 Natural frequencies below 20 Hz of the modified expanded model in the three postures.

Mode No.	Natural frequency (Hz)		
	Erect	Normal	Slouched
1	0.33	0.28	0.24
2	1.65	1.49	1.28
3	2.92	2.81	2.66
4	5.25	5.06	4.53
5	6.34	5.77	5.46
6	7.11	7.51	7.92
7	9.15	8.96	8.52
8	11.72	10.86	10.37
9	12.74	13.11	13.15
10	16.33	15.22	14.69
11	19.21	19.65	19.31
12	——	19.76	19.60

The normalised apparent mass calculated with no damping (Figure 5.8) indicated that the fourth mode at 5.06 Hz and the seventh mode at 8.96 Hz corresponded to the principal and the second principal resonances of the driving point apparent mass. The fourth mode in the calculation corresponded to the fourth mode in the measurement, and they consisted of an entire body mode with vertical and fore-and-aft pelvic motion due to buttocks tissue deformation in phase with a vertical visceral mode. A bending mode of the upper thoracic and the cervical spine was also found in the principal mode in the measurement, whereas it was included in the next higher mode in the calculation. The seventh mode in the calculation corresponded to either the seventh mode at 8.1 Hz or the eighth mode at 8.7 Hz (or possibly both of them) in the measurement, and they contained rotational modes of the pelvis. The calculated sixth mode was the second visceral mode with buttocks tissue deformation (rotation of the pelvis) which corresponded to the second visceral mode of the two degree-of-freedom model discussed in section 4.4. However, the second visceral mode was found to make a

small contribution to the second principal resonance of the apparent mass (Figure 5.8).

5.16 Adjusted parameters and their effects on the modes below 10 Hz in the normal posture (†; there was a large effect and the parameter was determined based on the comparison with the measurement, *; there was some effect).

Adjusted parameter	Mode number							Other factors considered to determine the parameter
	1	2	3	4	5	6	7	
Location of the pelvic mass						*	†	
Axial stiffness of the buttocks				† (1)		*	† (2)	Effect of buttocks constraint Effect of changing posture
Bending stiffness of the buttocks	*	*	*		*		†	
Axial stiffness of the viscera				†		*		Effect of visceral constraint
Bending stiffness of the spine	*	*	*		† (3)		† (4)	

(1) For the rear beam. (2) For the front beam.
(3) For the entire spine. (4) For the lowest spine.

Although the first mode was not clear in the measurement due to the low coherencies for the transfer functions caused by low levels of the bending responses of the spine at low frequencies (Figure 4.22), it was found by the calculation result that the first mode corresponded to the first mode of a beam with one (lower) end fixed. The second and the third modes both in the calculation and the measurement corresponded to the first and the second modes of a beam with both ends free. The natural frequencies for the first three modes of the modified expanded model were significantly lower than the measurements. Since the extracted modal properties in the experiment were less reliable below 5 Hz due to the low coherencies, the bending stiffnesses for the spinal beams of the modified expanded model were adjusted, comparing mainly the fifth mode at 5.77 Hz of the model with the fifth mode at 5.6 Hz in the measurement (Table 5.16). Therefore, the calculated natural frequencies for the first three modes were more reliable than the measurements.

The fourth mode was the principal mode mentioned above. The axial stiffnesses for the visceral springs and the buttocks tissue beams of the modified expanded model were

determined, comparing the principal modes of the calculation and the measurement. The effects of constraining the visceral motion and the buttocks deformation (see section 4.4) were also considered when determining the stiffnesses for the visceral springs and the buttocks tissue beams. The visceral constraint and the buttocks constraint were simulated by increasing the stiffnesses for the vertical visceral springs and the axial stiffnesses for the front and rear buttocks tissue beams. The amount of the resonance shifts tended to decrease as the stiffnesses for the viscera and the buttocks were increased. The values listed in Tables 5.10 and 5.12 for the normal posture and three-fold increases in the visceral stiffnesses and the buttocks stiffnesses for the constraints achieved almost the desired resonance shifts of the apparent mass as shown in Figure 5.9. The determined visceral stiffnesses were eventually the same as those used by Belytschko and Privitzer (1978), and the axial stiffness for the buttocks tissue (total axial stiffness of the front and rear beams) corresponded to a 35 % increase from that used by the same authors.

The fifth mode between 5 and 6 Hz was located close to the principal mode both in the calculation and the measurement. However, its contribution to the principal resonance was small (Figure 5.8). It was a bending mode of the entire spine, in the calculation, similar to the third mode of a beam with both ends free. A pitching mode of the head was also seen in the fifth mode. The calculated fifth mode corresponded to the measured fifth mode, although it was a bending mode of the lower thoracic and the lumbar spine in the measurement (i.e. the bending mode of the upper thoracic and the cervical spine was extracted in the principal mode). The bending stiffnesses for the spinal beams were increased so as to obtain the fifth mode between 5.5 and 6 Hz as observed in the experiment. The initial values for the bending stiffnesses of the spine were based on data from isolated intervertebral discs. Therefore, the increase in stiffnesses of the spinal beams for the model was reasonable, considering other elastic elements connecting the vertebrae such as the intervertebral ligaments or muscles, and the resistance of other parts of the torso against bending of the body.

The sixth mode in the measurement had a low correlation between the subjects and was less reliable. Rotational modes of the pelvis were found in the sixth mode at 7.51 Hz and the seventh mode at 8.96 Hz in the calculation, and in the measurement they were found in the seventh mode at 8.1 Hz and the eighth mode at 8.7 Hz. In the measured mode shape for the eighth mode, the lower lumbar spine below the vertebra L3 appeared to deform axially together with the pelvic rotation. However, the modified expanded model achieved the pelvic rotation with neither axial deformation of the lumbar spine nor bending

deformation of the upper spine, by assigning a lower bending stiffness for the lowest spine. This result supported the hypothesis discussed in section 4.3 that in the experiment the bending deformation of the lumbar spine and the pelvic rotation appeared as axial motion on the posterior body surface due to the depth of the lumbar spine below the posterior body surface.

The second visceral mode was found in the sixth mode at 7.51 Hz in opposite phase with the buttocks tissue deformation (rotation of the pelvis) in the calculation, which corresponded to the second visceral mode of the two degree-of-freedom model discussed in section 4.4. However, its contribution to the second principal resonance of the apparent mass was found to be small (Figure 5.8). In the measurement, the second visceral mode was found in the ninth mode at 9.3 Hz on its own. When increasing the visceral stiffnesses to obtain the second visceral mode at a frequency higher than 9 Hz as observed in the measurement, the effect of the visceral constraint on the principal resonance became too small. Although the mode shapes extracted from the mean transfer functions of the eight subjects (see section 4.3) showed the second visceral mode at 9.3 Hz, there were some subjects who showed the second visceral mode between 7.5 and 8 Hz (Table 4.15), and their mode shapes were similar to the sixth mode in the calculation. The difference of the second visceral mode between the calculation and the measurement might have been caused by the variability between the subjects in the measurement and also by the fact that the acceleration was measured at only one site on the abdominal wall in the experiment. Therefore, the calculation result was possibly more reliable.

The modes calculated above 10 Hz included higher visceral modes such as the ninth mode at 13.11 Hz and the eleventh mode at 19.65 Hz. However, they were not reliable because the visceral subsystem was originally constructed, assuming a one dimensional uniform rod having the fundamental natural frequency at about 5 Hz by Belytschko and Privitzer (1978), and the assumption was valid only for the fundamental mode of the visceral column which was seen in the fourth and the seventh modes. The eighth, tenth and the twelfth modes at 10.86, 15.22 and 19.76 Hz in the calculation were higher bending modes of the spine. The calculated eighth mode at 10.86 Hz appeared to correspond to the eleventh mode at 12.5 Hz in the measurement. The measured modes above 13 Hz had low correlations between the subjects and were less reliable. The calculated results also showed that the wavelengths of the bending modes of the spine in this frequency range were too short to measure the deformations correctly at the measuring sites used on the spine (i.e. T1, T6, T11, L3 and S2).

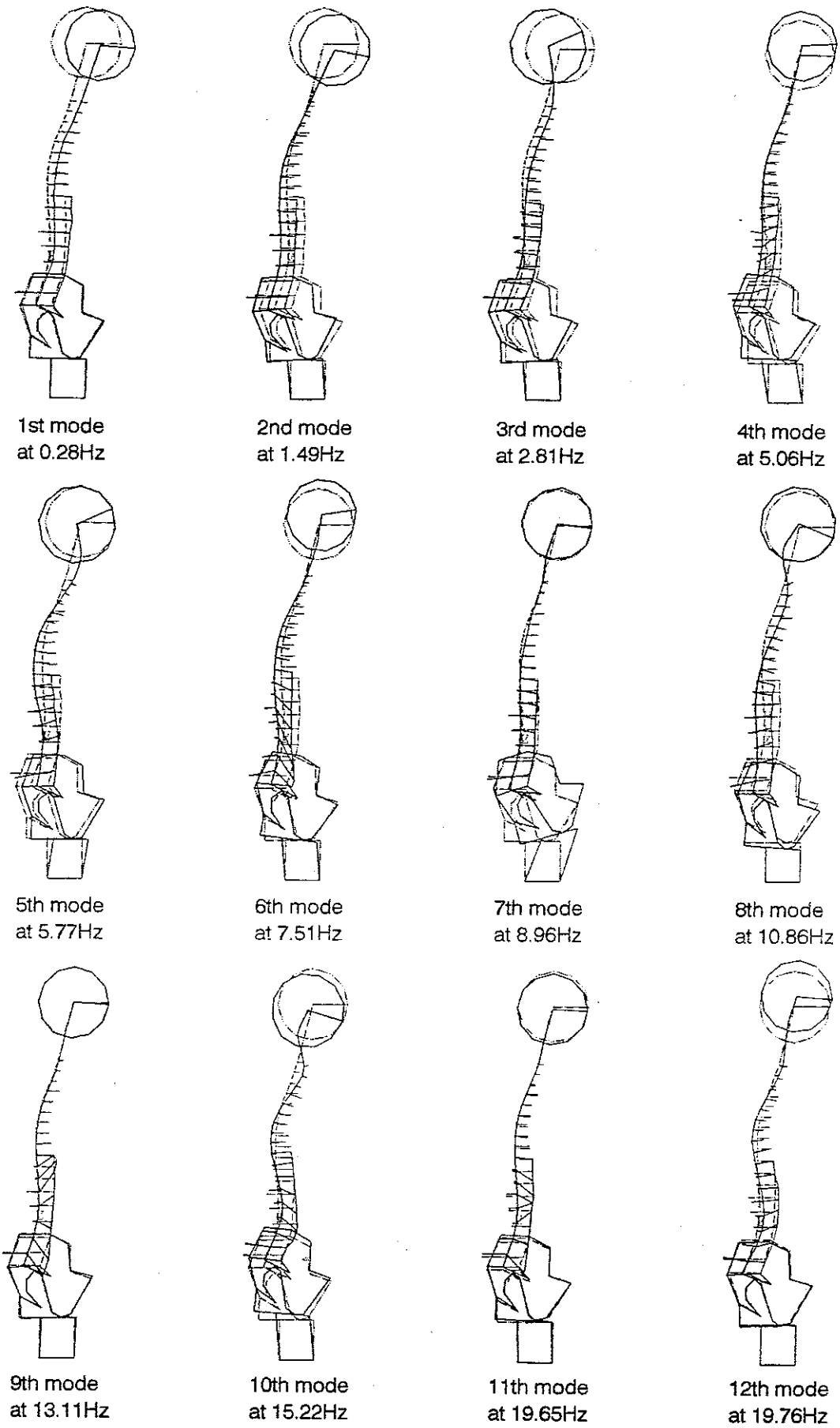

Figure 5.6 Calculated mode shapes of the modified expanded model in the normal posture (——) and the initial configuration (- - -).

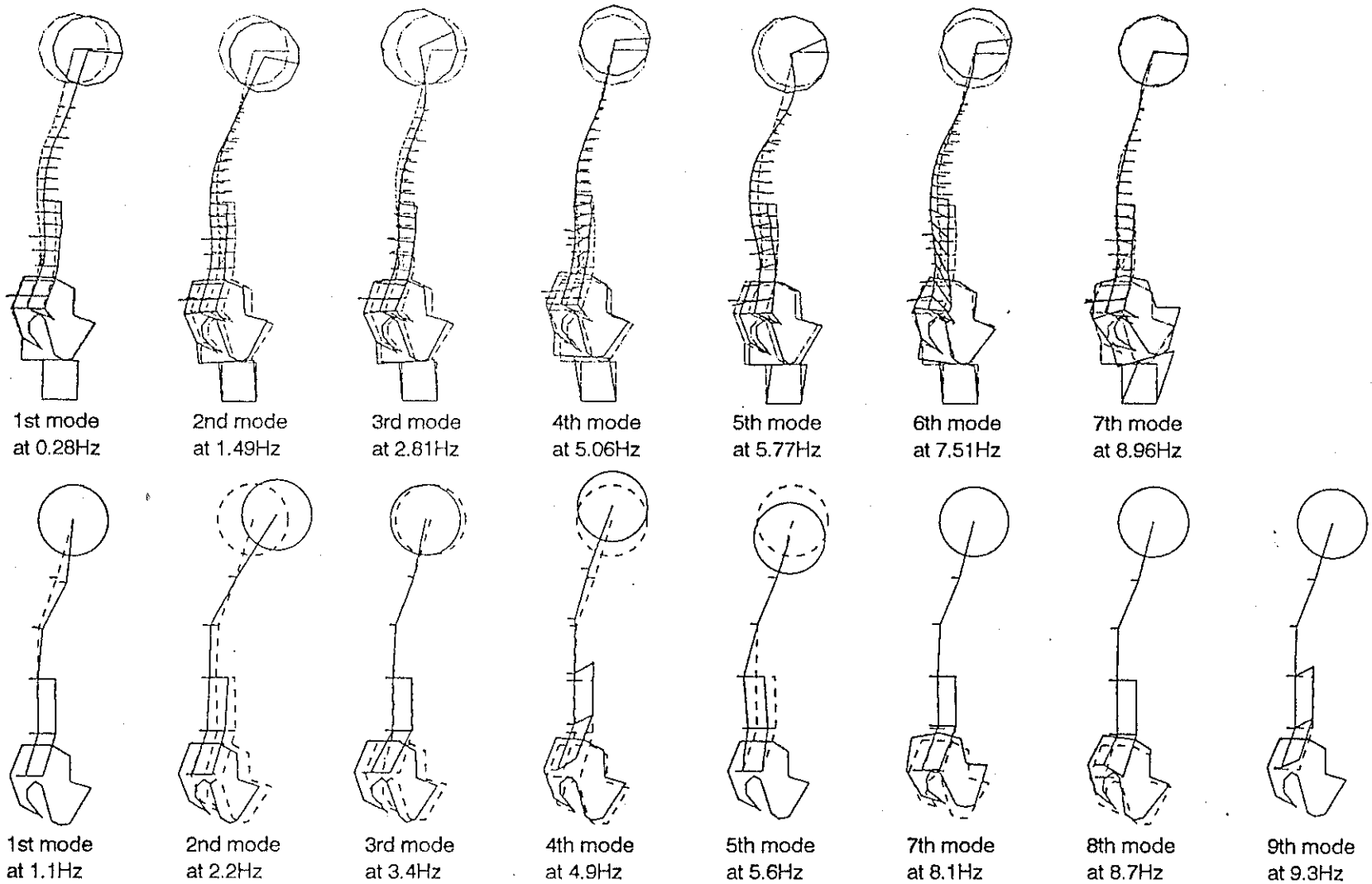

Figure 5.7 Calculated mode shapes (upper) and measured mode shapes (lower) below 10 Hz in the normal posture (6th mode of the measurements had a low correlation between the subjects and it was excluded).

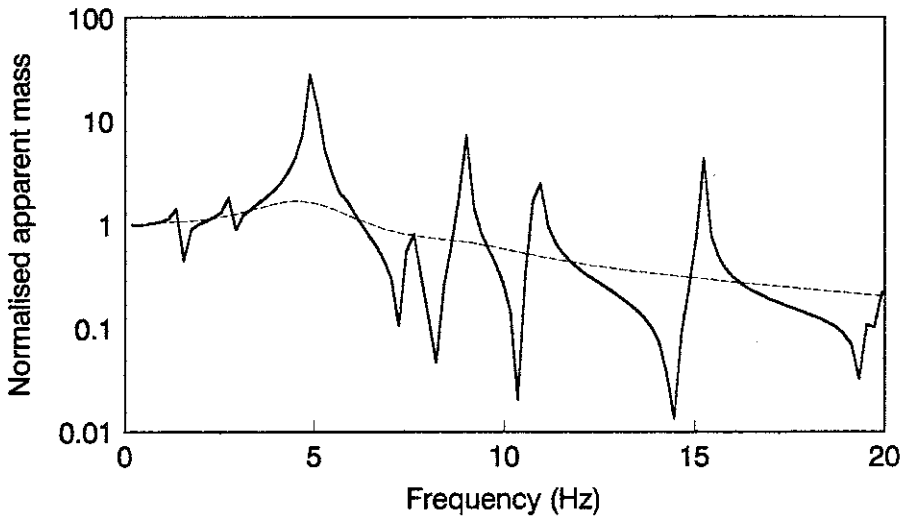

Figure 5.8 Normalised apparent masses of the modified expanded model in the normal posture calculated with no damping (——), and with the appropriate damping (- - -).

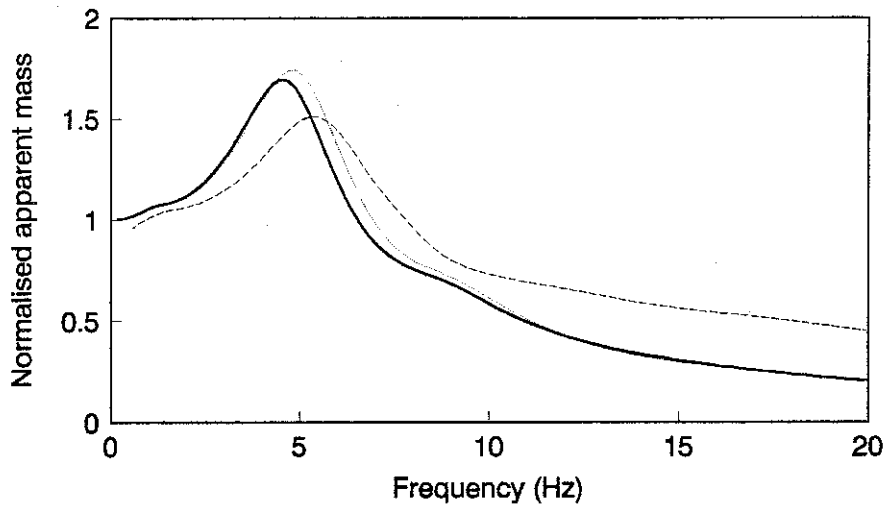

Figure 5.9 Normalised apparent masses of the modified expanded model in the normal posture (——), with increased visceral stiffnesses (three-fold) for the visceral constraint (.....), and with increased buttocks stiffness (three-fold) for the buttocks constraint (- - -).

Axial modes of the spine were not clear in Figure 5.6. They were calculated by increasing the bending stiffnesses for the spinal beams to constrain the bending deformation of the spine. The lowest axial mode of the spine of the modified expanded model was found at 16.21 Hz with the constraint (Figure 5.10) which was included in the tenth mode at 15.22 Hz without the constraint (Figure 5.6). The deformation of the spine in the lowest axial mode was calculated to occur in the cervical and the upper thoracic spine. The axial stiffnesses for the spinal beams of the modified expanded model were not altered from the initial values which were based on data from isolated intervertebral discs, and so a decrease in the axial stiffnesses was hardly justified. Therefore, pitching motion of the head, bending deformation of the spine and rotation of the pelvis were possibly misinterpreted as axial deformations of the spine in some of the measured mode shapes below 15 Hz (Figure 4.30).

The driving point responses and the acceleration (displacement) transmissibilities from vertical seat motion to motion of various parts of the body were compared with the experimental data reported in the literature as well as the results obtained in section 4.3 (Figures from 5.11 to 5.16). The driving point responses and the transmissibilities to vertical motion of the spine and the viscera of the modified expanded model showed good agreement with the experimental data. However, the transmissibilities to vertical head motion and to fore-and-aft motion of the spine showed some discrepancies between the model responses and the experimental data (Figures 5.13 and 5.15). In the transmissibility to vertical head motion, the discrepancy was large above the principal resonance: some experimental data, including the transmissibility obtained in section 4.3, showed a wide peak above 10 Hz, whereas the model response did not show any noticeable peaks above 10 Hz. The measured transmissibilities to vertical head motion in Figure 5.13 possibly include both the translational and rotational (pitching) motion of the head except the transmissibility measured by Messenger (1987). Although the cervical spine was modelled more precisely for the modified expanded model than the previous models and the atlanto-occipital joint was newly modelled, the transmissibility to vertical head motion of the modified expanded model did not improve dramatically. The head-neck region of the model needs to be modified further, based on more precise measurement of the response in this region. In the transmissibility to fore-and-aft motion of the spine, most of the experimental data, including the transmissibility obtained in section 4.3, were significantly smaller below 5 Hz and larger above 10 Hz than the model response. Although the modified expanded model produced similar vibration mode shapes and driving point responses to the experimental data, it needs further precise modification to

achieve closer transmissibilities.

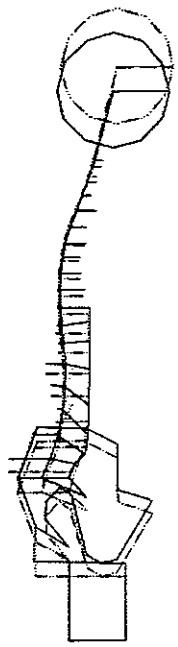

Figure 5.10 The lowest axial mode of the spine at 16.21 Hz of the modified expanded model in the normal posture (calculated by constraining the bending deformation of the spinal beams).

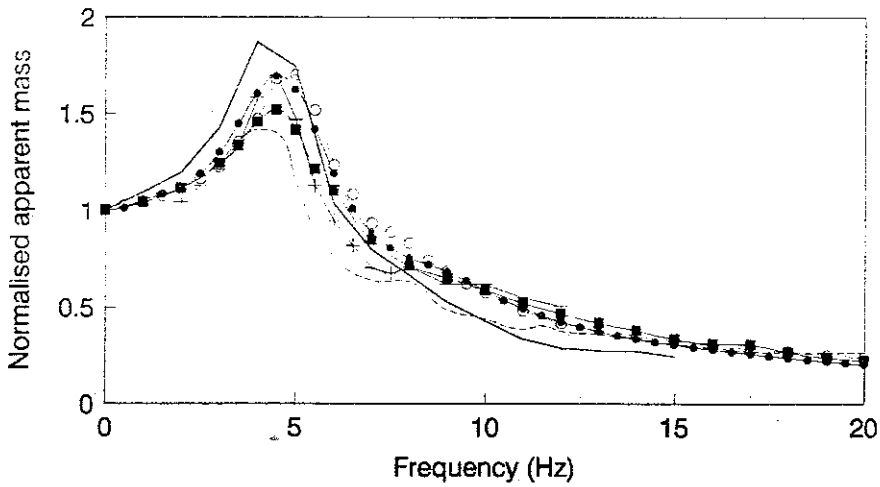

Figure 5.11 Normalised apparent masses: response of the modified expanded model in the normal posture (—•—); mean values of eight subjects in the normal posture obtained in section 4.3 (·····o·····); mean values of ten subjects by Vogt *et al.* (——); mean values of two subjects by Sandover (- - - -); mean values of four subjects by Hinz and Seidel (—+—); mean values of 60 subjects by Fairley and Griffin (—■—).

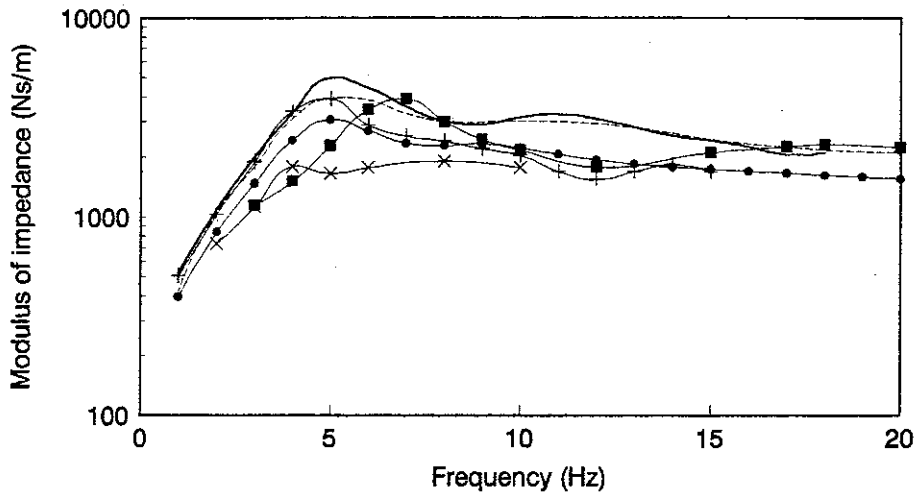

Figure 5.12 Moduli of the impedance: response of the modified expanded model in the normal posture (—•—); mean values of eight subjects by Coermann *et al.* (——); mean values of eight subjects by Miwa (—■—); mean values of ten subjects by Vogt *et al.* (—+—); mean values of 15 subjects by Donati and Bonthoux (—x—); International Standard 5982 (- - - -).

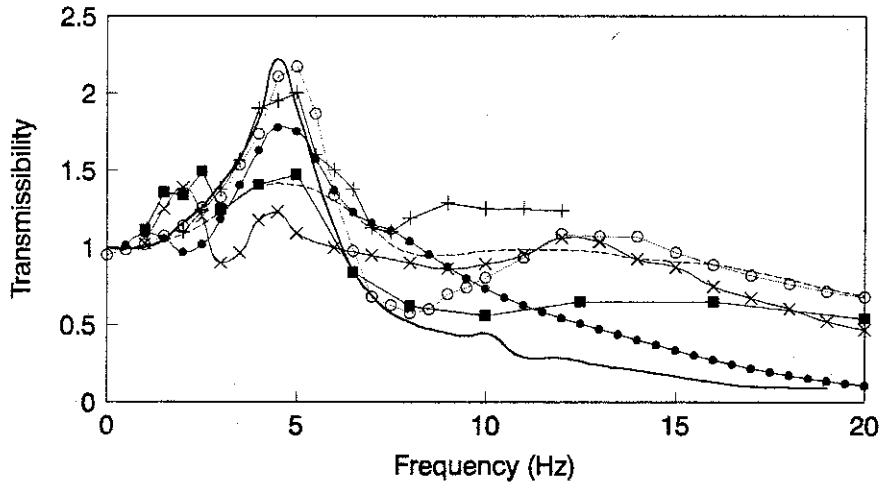

Figure 5.13 Acceleration transmissibilities from vertical seat motion to vertical head motion: response of the modified expanded model in the normal posture (—•—); mean values of eight subjects in the normal posture obtained in section 4.3 (·····o·····); values of a single subject by Coermann (——); mean values of 18 subjects by Griffin *et al.* (—■—); mean values of eight subjects by Messenger (—x—); mean values of four subjects by Hinz and Seidel (—+—); International Standard 7962 (- - - -).

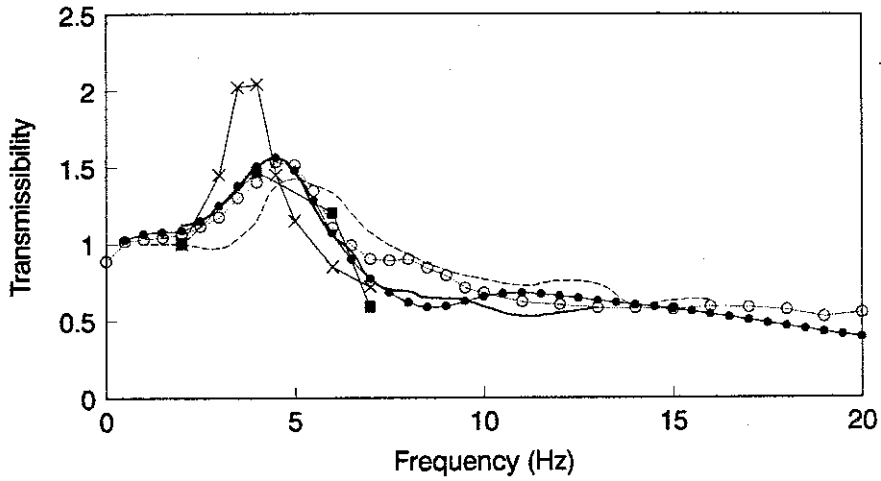

Figure 5.14 Transmissibilities from vertical seat motion to vertical spinal motion: acceleration (displacement) transmissibility to the vertebra L3 of the modified expanded model in the normal posture (—•—); mean acceleration transmissibility to the vertebra L3 of eight subjects in the normal posture obtained in section 4.3 (.....o.....); mean acceleration transmissibility to the vertebra L3 of five subjects by Panjabi *et al.* (——); displacement transmissibility to the vertebra L3 of a single subject by Pope *et al.* (—■—); displacement transmissibility to the vertebra L4 of a single subject by Sandover and Dupuis (—x—); mean acceleration transmissibility to the vertebra L3 of three subjects by Magnusson *et al.* (- - - -).

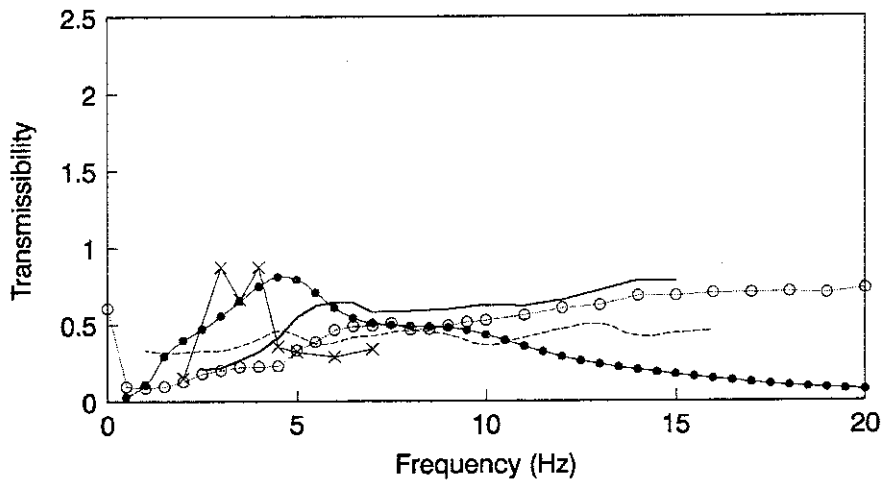

Figure 5.15 Transmissibilities from vertical seat motion to fore-and-aft (transverse) spinal motion: acceleration (displacement) transmissibility to the vertebra L3 of the modified expanded model in the normal posture (—•—); mean acceleration transmissibility to the vertebra L3 of eight subjects in the normal posture obtained in section 4.3 (.....o.....); mean acceleration transmissibility to the vertebra L3 of five subjects by Panjabi *et al.* (——); displacement transmissibility to the vertebra L4 of a single subject by Sandover and Dupuis (—x—); mean acceleration transmissibility to the vertebra L3 of three subjects by Magnusson *et al.* (- - - -).

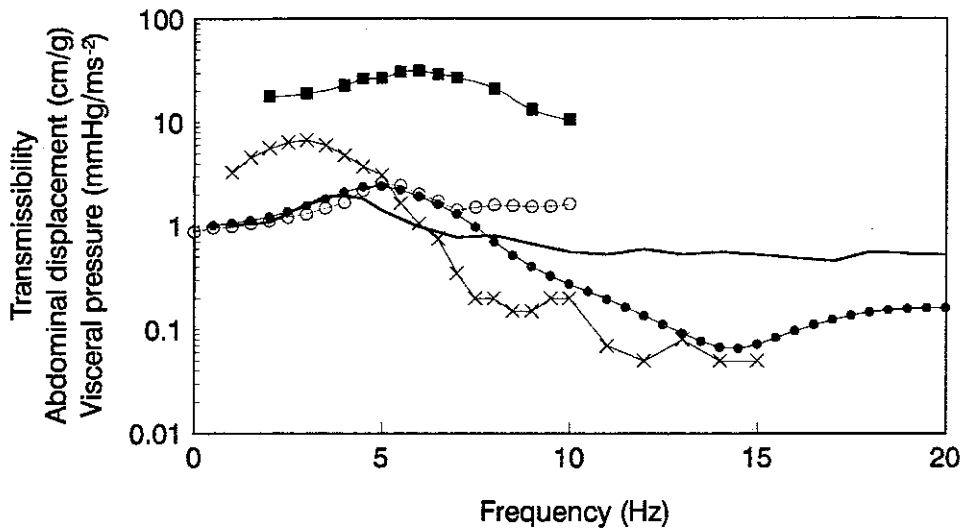

Figure 5.16 Acceleration (displacement) transmissibility from vertical seat motion to vertical visceral motion at the L3 level of the modified expanded model in the normal posture (—•—); mean acceleration transmissibility from vertical seat motion to vertical visceral motion at the L2 level of eight subjects in the normal posture obtained in section 4.3 (·····o·····); longitudinal abdominal wall displacement of a single subject by Coermann *et al.* (—x—); mean colon pressure of eight subjects by White *et al.* (——); intraabdominal pressure of a single subject by Sandover (—■—).

Changing posture from erect to slouched decreased the principal resonance frequency of the apparent mass in the experiment shown in section 4.3: the natural frequencies extracted from the principal resonance of the apparent masses were 5.2 Hz in the erect posture, 4.9 Hz in the normal posture and 4.4 Hz in the slouched posture. The natural frequency for the entire body mode also decreased due to the postural change, corresponding to the resonance shift: 5.2 Hz in the erect posture, 4.9 Hz in the normal posture and 4.0 Hz in the slouched posture. In the slouched posture, the visceral mode remained at 4.9 Hz and it was separated from the entire body mode. The apparent masses of the modified expanded model in the erect and the slouched postures were calculated, using the same material properties and the geometry as those for the normal posture except the node locations for the spinal curves (Figures 5.17 and 5.18). Although the change of posture from erect to slouched decreased the modulus of the apparent mass at the principal resonance, the frequency of the principal resonance was not decreased. Because the shift of the principal resonance of the apparent mass was caused by a shift of the entire body mode, only changing parameters affecting the entire body mode (buttocks mode) was expected to realise the resonance shift. The modified

expanded model achieved the shift of the principal resonance of the driving point responses by only decreasing the buttocks tissue stiffness with a change of posture from erect to slouched. Multiplying the axial stiffnesses of the front and rear buttocks tissue beams for the normal posture by factors of 2.0 and 0.6 achieved almost the desired shifts of the principal resonance (Figures 5.19 and 5.20) and the natural frequencies for the entire body mode: the natural frequencies for the entire body mode were 5.25 Hz in the erect posture, 5.06 Hz in the normal posture and 4.53 Hz in the slouched posture (Table 5.15). Calculated mode shapes below 20 Hz in the erect and the slouched postures are shown in Figures 5.21 and 5.22.

It was a reasonable hypothesis that changing posture from erect to slouched would increase the effective contact areas between the buttocks and thighs and the seat surface, resulting in a decrease in the total axial stiffness under the pelvis due to the non-linear force-deflection relationship of tissue as discussed in section 4.3. The resonance (natural frequency) shift was larger from the normal posture to the slouched posture than from the erect posture to the normal posture. This may be explained if the backward rotation of the pelvis from the erect posture to the normal posture increases contact of some part of the buttocks posterior to the ischial tuberosities, and if the forward inclination of the thoraco-cervical spine and the head from the normal posture to the slouched posture increases contact of the thighs. The increment in the axial stiffness to simulate the buttocks constraint, in which the subjects sat on the two wooden blocks (5 cm x 5 cm) beneath the ischial tuberosities (see section 4.4), was three times the stiffness for the normal posture. Therefore, the increment in the axial stiffnesses of the buttocks tissue beams from the normal posture to the erect posture (a factor of 2.0) and the decrement from the normal posture to the slouched posture (a factor of 0.6) seemed to be reasonable changes. Factors between the two extreme postures (erect and slouched) may lie between 0.6 and 2.0.

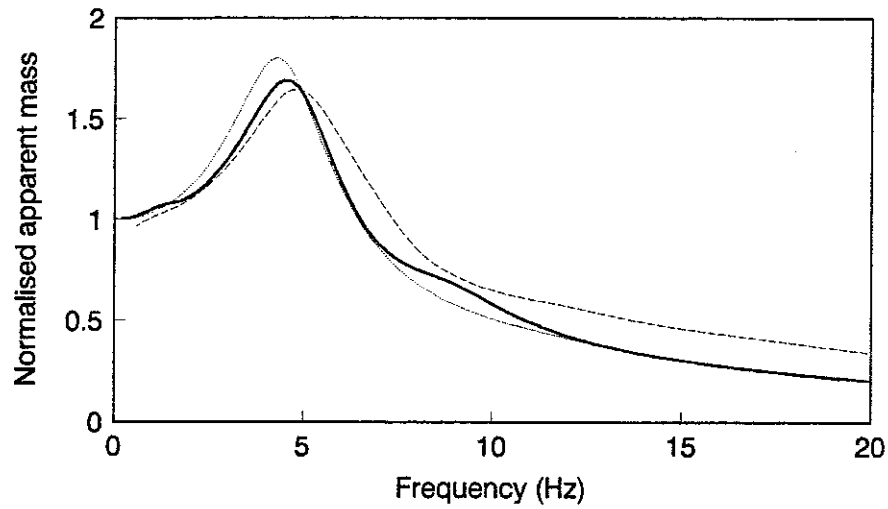

Figure 5.17 Normalised apparent masses of the modified expanded model in the normal posture (——), in the erect posture calculated with the same material properties as for the normal posture (·····), and in the erect posture calculated with increased buttocks tissue stiffness (- - -).

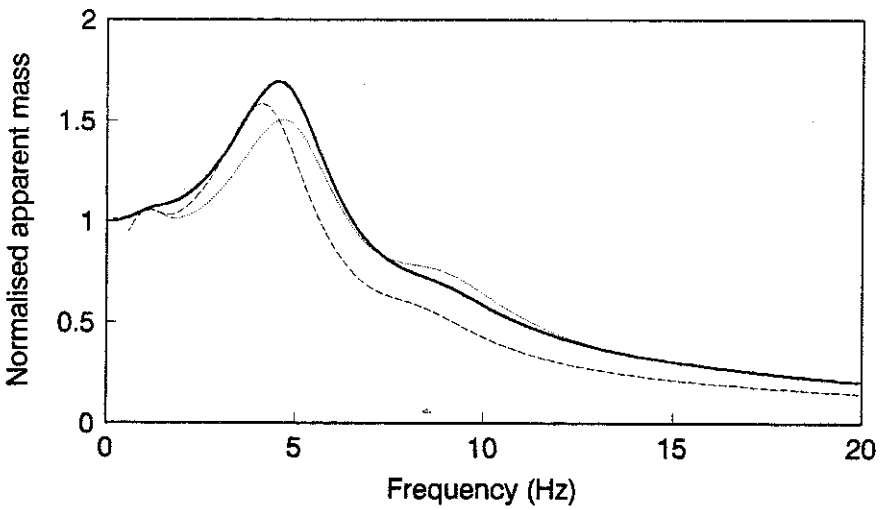

Figure 5.18 Normalised apparent masses of the modified expanded model in the normal posture (——), in the slouched posture calculated with the same material properties as for the normal posture (·····), and in the slouched posture calculated with decreased buttocks tissue stiffness (- - -).

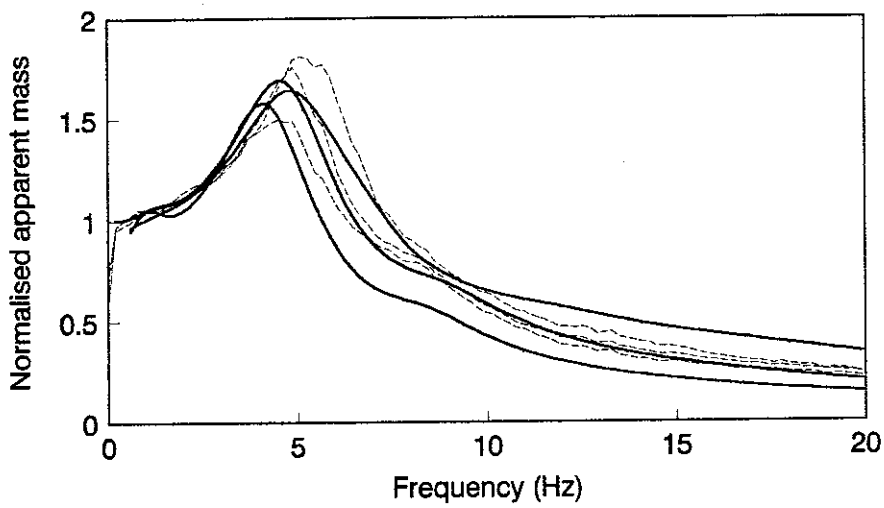

Figure 5.19 Normalised apparent masses of the modified expanded model in the three postures (——) and experimental data in the three postures obtained in section 4.3 (- - -). (The principal resonance frequency decreased both in the calculation and in the measurement when changing posture from erect to slouched).

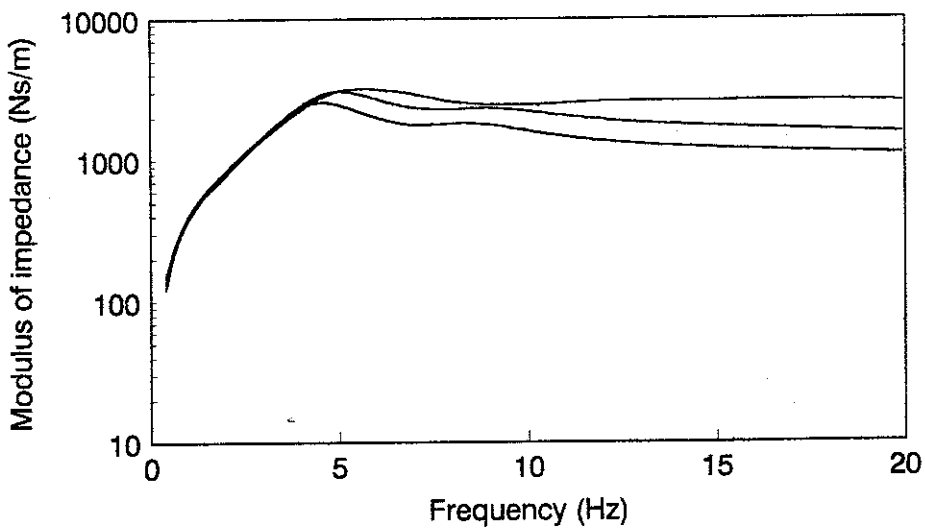

Figure 5.20 Moduli of the impedance of the modified expanded model in the three postures.

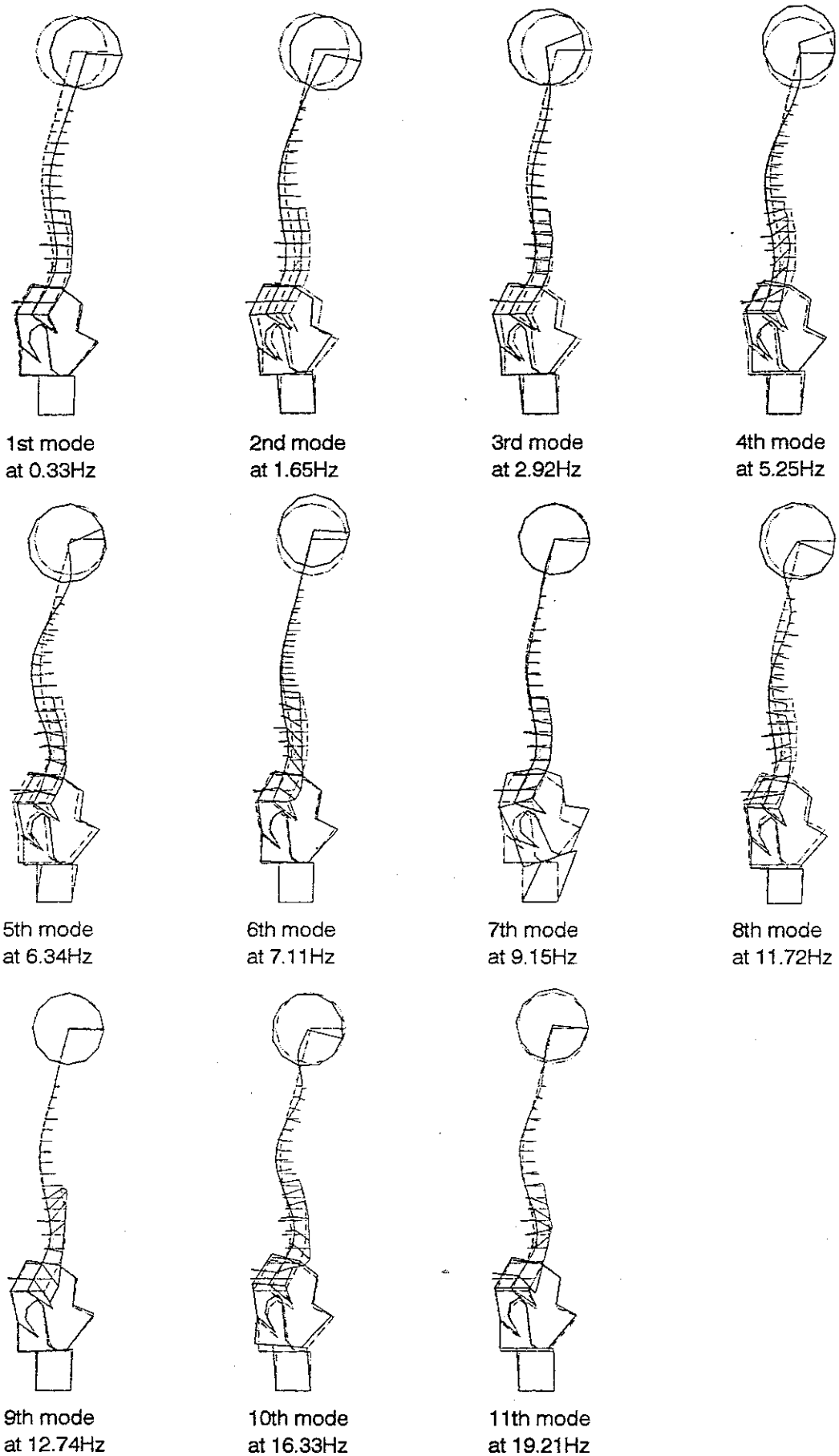

Figure 5.21 Calculated mode shapes of the modified expanded model in the erect posture (——) and the initial configuration (- - -).

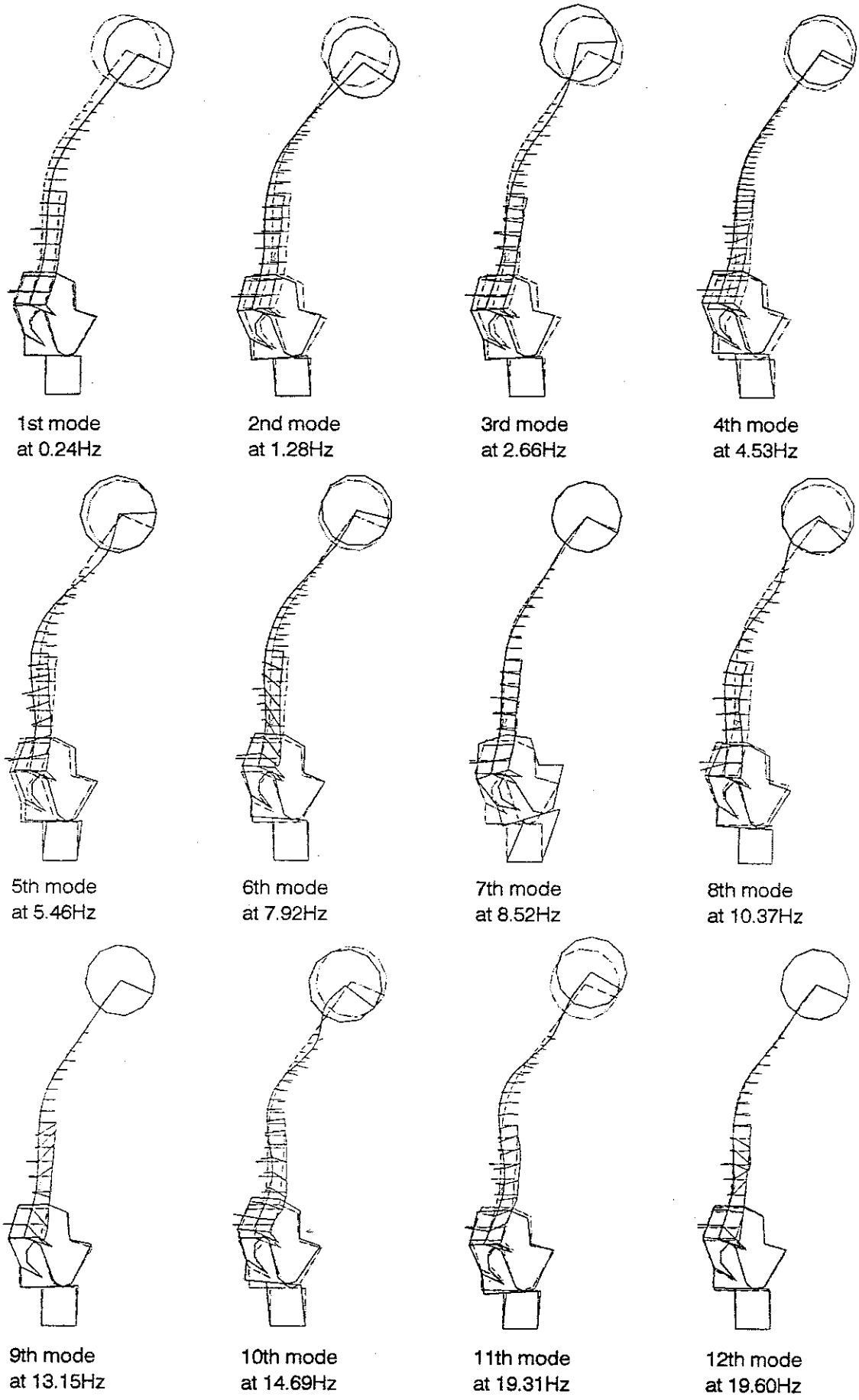

Figure 5.22 Calculated mode shapes of the modified expanded model in the slouched posture (——) and the initial configuration (- - -).

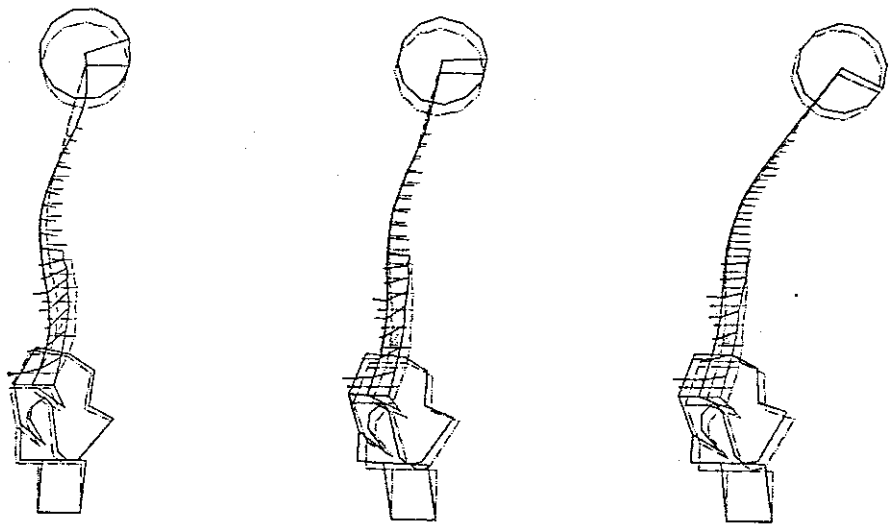

Figure 5.23 The mode shapes for the entire body mode of the modified expanded model in the three postures; (a) mode at 5.25 Hz in the erect posture; (b) mode at 5.06 Hz in the normal posture; (c) mode at 4.53 Hz in the slouched posture.

The calculated mode shapes for the entire body mode in the three postures are compared in Figure 5.23. It is seen that the fore-and-aft pelvic motion in the entire body mode, accompanying shear deformation of buttocks tissue, increased when changing posture from erect to slouched as observed in the experiment (Figure 4.34). The increase in the fore-and-aft pelvic motion may have been caused by the increased horizontal distance between the mass centre of the entire body and the excitation point which induced excitation moment. The increase in shear deformation of the buttocks tissue may also contribute to the decrease in the natural frequency for the entire body mode and the principal resonance frequency with the much lower shear stiffness of tissue than the axial stiffness (see section 4.2). This hypothesis was supported by a calculation: when the shear deformation of buttocks tissue was constrained by increasing the bending stiffnesses for the buttocks tissue beams by five-fold, the natural frequency for the entire body mode of the modified expanded model in the slouched posture increased from 4.53 Hz to 4.75 Hz.

The calculation did not separate the entire body mode and the visceral mode in the slouched posture. If the entire body mode and the visceral mode were coupled in the principal mode, the two degree-of-freedom model shown in Figure 4.37 is representative of the principal mode whose natural frequencies and mode shapes are determined by equations (4.56) and (4.57). Multiplying the buttocks tissue stiffness in the first parameter set in section 4.4.4 for the normal posture by the factors of 2.0 for the erect posture and

0.6 for the slouched posture, the first natural frequency shifted from 4.8 Hz to 5.15 and 4.29 Hz respectively, and the deformation ratio of the viscera to the buttocks tissue for the first mode changed from 4.7 to 10.86 and 2.69 respectively. Therefore, the principal mode in the slouched posture still would have included both the entire body mode and the visceral mode, although the contribution of the visceral mode would have decreased. The difference in the first visceral mode in the slouched posture between the calculation and the measurement might have been caused by the fact that the acceleration was measured at only one site on the abdominal wall in the experiment and also by the simplification of the visceral subsystem for the model.

Changing the posture of the modified expanded model from erect to slouched also decreased the natural frequency for the rotational mode of the pelvis which corresponded to the second principal resonance of the driving point responses: 9.15 Hz in the erect posture, 8.96 Hz in the normal posture and 8.52 Hz in the slouched posture. The shift of the natural frequency for the rotational mode of the pelvis coincided well with the measurements in section 4.3 where the natural frequencies were 9.2 and 8.4 Hz in the erect posture, 8.7 and 8.1 Hz in the normal posture, and 8.3 and 7.3 Hz in the slouched posture (two rotational modes of the pelvis were extracted in each posture in the experiment). The decreased axial stiffness and increased contribution of shear deformation of buttocks tissue due to the postural change towards the slouched posture also decreased the natural frequency for the rotational mode of the pelvis. Therefore, it was confirmed that changing posture also shifted the second principal resonance of the driving point responses, although the shift was not clear in Figures 5.19 and 4.31.

The acceleration (displacement) transmissibilities from vertical seat motion to motion of the body at the sites corresponding to the experiment in section 4.3 are shown in Figure 5.24 for the three postures. When changing posture from erect to slouched, the principal resonance frequency of the transmissibilities from vertical seat motion to vertical or longitudinal motion of the body decreased and the transmissibilities also decreased at most frequencies above the principal resonance. These trends coincided with the experimental results in section 4.3 (Figure 4.29), except the longitudinal transmissibility to the head whose principal resonance did not shift as much as the transmissibilities to the spine in the measurements. The transmissibilities from vertical seat motion to fore-and-aft or transverse motion of the body tended to increase below 5 Hz when changing posture from erect to slouched and this coincided with the trend in the measurement. However, the trend reversed in the calculation above 10 Hz, whereas it remained unchanged

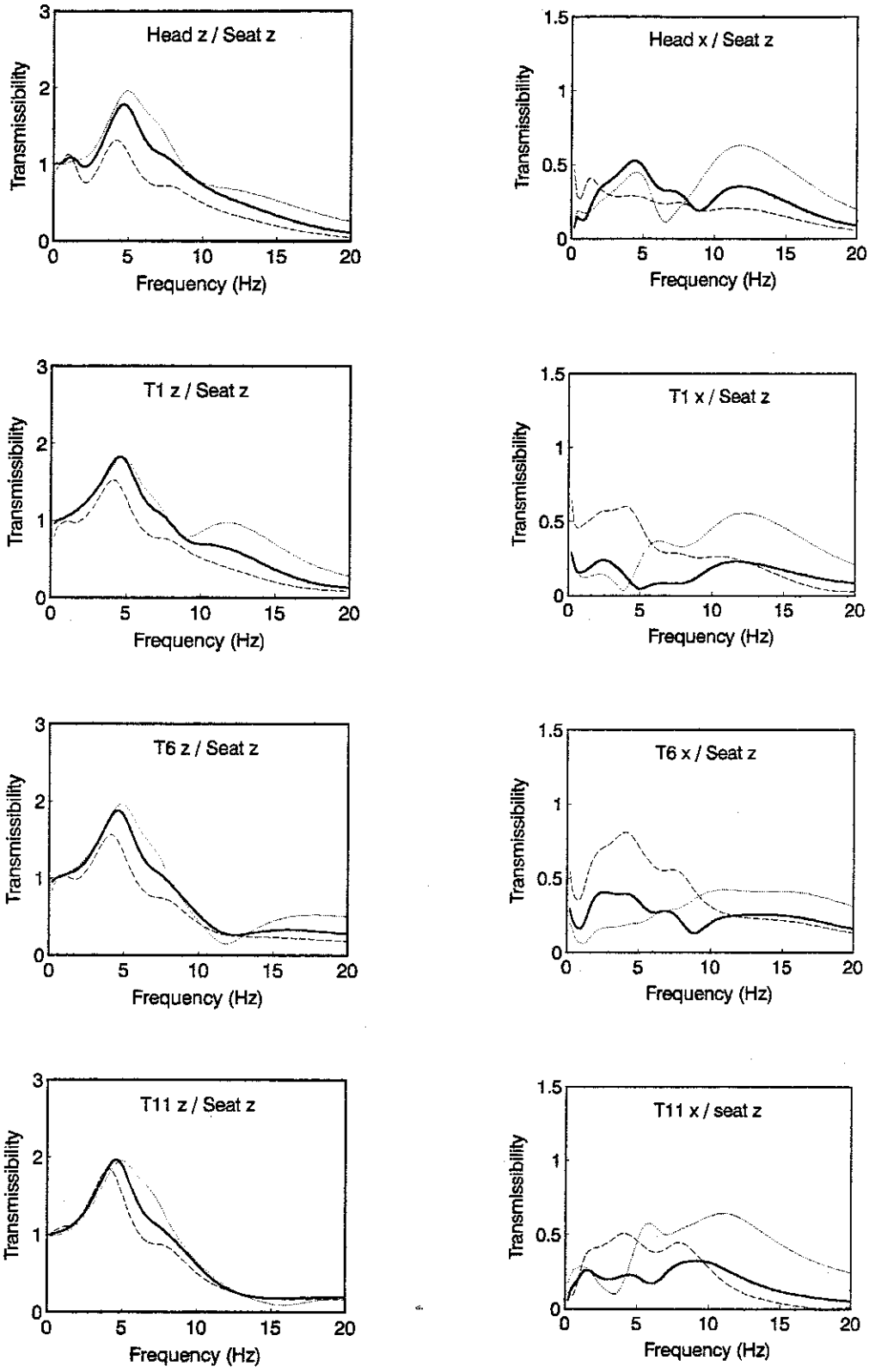

Figure 5.24 Transmissibilities from vertical seat motion to longitudinal and transverse motion of the body in the erect posture (·····), normal posture (——) and the slouched posture (- - -) (z=vertical or longitudinal direction of the spine; x=fore-and-aft or transverse direction of the spine).

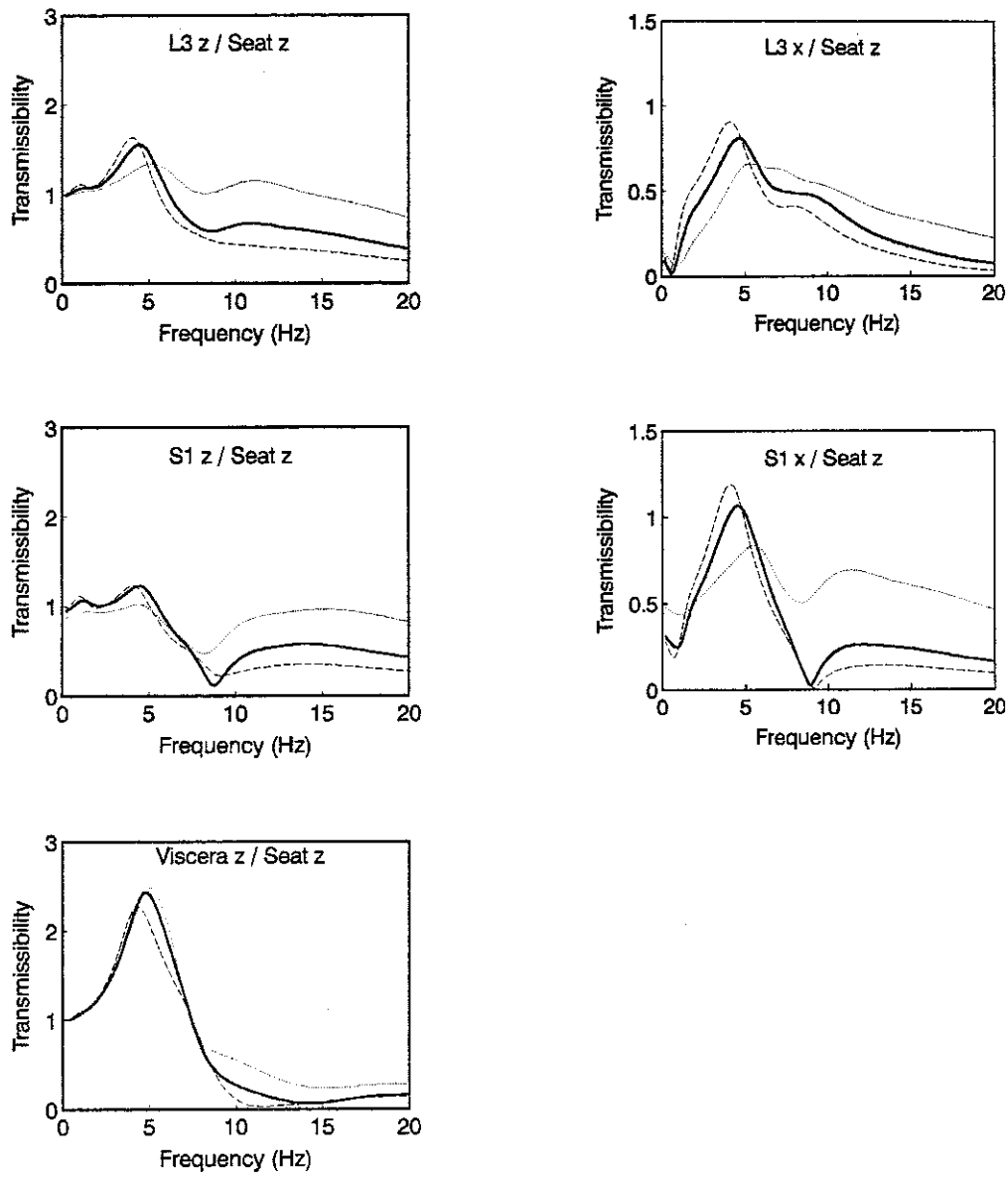

Figure 5.24 (Continued)

throughout the frequency range below 20 Hz in the measurement, except the transverse transmissibility to the head whose trend coincided with the calculation above 10 Hz. The model needs further precise modification to achieve closer transmissibilities in different postures to the experimental data

5.3 CONCLUSIONS FROM MODELLING: PART 2

The modified expanded model was developed. All the vertebrae (intervertebral discs) in the entire spine, including the cervical spine, were modelled by separate beam elements. The atlanto-occipital joint was also newly modelled by a beam element. The location of the pelvic mass, axial and bending stiffnesses of the buttocks tissue beams, axial stiffnesses of the visceral springs and the bending stiffnesses of the spinal beams were adjusted, comparing mainly the natural frequencies and the vibration mode shapes of the model with the experimental data. A total of ten reliable modes was calculated for the normal posture below 20 Hz (seven modes below 10 Hz), and the mode shapes of the model coincided well with the measurements below 10 Hz. The calculated driving point impedance and apparent mass were also similar to the experimental data reported in the literature as well as the measurements obtained in section 4.3.

The fourth mode at 5.06 Hz (in the normal posture) corresponded to the principal resonance of the human body, which consisted of an entire body mode with vertical and fore-and-aft pelvic motion due to deformation of tissue beneath the pelvis in phase with a vertical visceral mode. A bending mode of the lumbar spine was included in the next higher mode at 5.77 Hz with a pitching mode of the head. The seventh mode at 8.96 Hz corresponded to the second principal resonance of the body and contained a rotational mode of the pelvis. Any contribution of the second visceral mode found at 7.51 Hz to the second principal resonance was small.

The first mode at 0.28 Hz (in the normal posture) corresponded to the first mode of a beam with the lower end fixed. The second mode at 1.49 Hz and the third mode at 2.81 Hz corresponded to the first and the second modes of a beam with both ends free. The fourth mode at 5.06 Hz was the principal mode mentioned above. The fifth mode at 5.77 Hz was located close to the principal mode and it was a bending mode of the entire spine with a pitching mode of the head, similar to the third mode of a beam with both ends free. The six mode at 7.51 Hz was the second visceral mode in opposite phase with buttocks tissue deformation (rotation of the pelvis). The seventh mode at 8.96 Hz was the second principal mode mentioned above. Above 10 Hz, there were three higher bending modes of the spine calculated at 10.86, 15.22 and 19.76 Hz. The lowest axial mode of the spine was included in the mode at 15.22 Hz and the axial deformation occurred in the cervical and the upper thoracic spine.

Changing the posture of the modified expanded model from erect to slouched decreased the natural frequency for the entire body mode, which resulted in a decrease in the principal resonance frequency of the driving point responses and a decrease in the transmissibilities from vertical seat motion to vertical or longitudinal motion of various parts of the body. The resonance shifts were achieved only by means of changing the axial stiffness for buttocks tissue. It was hypothesised that changing posture would change the contact areas between the buttocks and the thighs and the seat surface, resulting in a change in the total axial stiffness under the pelvis due to the non-linear force-deflection relationship of tissue. When changing posture from erect to slouched, fore-and-aft motion of the pelvis, accompanying shear deformation of buttocks tissue, increased in the entire body mode due to the increased horizontal distance between the mass centre of the entire body and the excitation point which induced excitation moment. The increase in the shear deformation of buttocks tissue may also contribute to the decrease in the natural frequency for the entire body mode with the much lower shear stiffness of tissue than the axial stiffness. The natural frequency for the rotational mode of the pelvis also decreased, when changing posture from erect to slouched, due to the decreased axial stiffness under the pelvis and the increased contribution of the shear deformation of buttocks tissue, and it resulted in a decrease in the frequency of the second principal resonance of the driving point responses.

Although the modified expanded model produced similar vibration mode shapes and driving point responses to the experimental data, some discrepancies were found between the model responses and the measurements in the transmissibilities to some parts of the body. The model needs further precise modification, including modification of the head-neck region, to simulate the transmissibilities to various parts of the body more accurately.

CHAPTER 6

GENERAL CONCLUSIONS AND RECOMMENDATIONS

The literature review on measurement raised two questions to answer through this research. The first question was what the vibration mode shapes for the major resonance (between 4 and 6 Hz) and the second resonance (between 8 and 12 Hz) of the human body were. Because those two resonances produce large response magnitudes, their adverse effects on health, activities and comfort may be large. It was the primary interest to find how the body responded (deformed) at the resonances. The second question was how changes in posture affected the vibration mode shapes and how they shifted the major resonance of the body. It is also important to understand the effect of posture so that the adverse effects of whole-body vibration may be minimised by optimising the posture. The literature review on modelling concluded that a distributed parameter model was required to answer the questions and that the model should be based on anatomy and validated using dynamic responses measured at various parts of the body. Because of the difficulty of measuring the dynamic responses of the body accurately at the desired body parts and the complexity of the body structure with unknown material properties and geometry, it was also suggested that the two approaches of measurement and modelling would be complementary and achieve a fundamental understanding of the mechanical responses to whole-body vibration.

Three models were developed in modelling part 1. The simplified model was found to produce a lower frequency of the principal resonance than the experimental results. The modified simplified model, which was given increased stiffnesses for the visceral springs and the buttocks tissue spring, achieved similar driving point responses to the experimental data. However, changing the posture of the model from erect to slouched did not shift the principal resonance of the driving point responses. The vibration mode shapes of the expanded model demonstrated that the principal resonance of the body at about 5 Hz consisted of an entire body mode caused by buttocks tissue deformation in phase with a vertical visceral mode, and a small bending mode of the entire spine. Many bending modes of the spine were calculated throughout the frequency range below 20 Hz, and it was concluded that the models should be validated comparing the bending modes of the spine for further modification. The predicted transmissibilities from vertical seat motion to vertical and fore-and-aft motion of the vertebrae at several levels of the spine

were distinctive, indicating the feasibility of extracting the vibration modes from measured transmissibilities.

Experimental modal analysis was applied to whole-body vibration to extract the natural frequencies and the vibration mode shapes of the human body. The accelerations were measured on the body surface and corrected using the method developed to eliminate the effects of local tissue-accelerometer vibration from the measurements. For the subject group, a total of ten correlated modes was extracted for the normal posture below 13 Hz (eight modes below 10 Hz). The principal resonance of the driving point responses at about 5 Hz was found to correspond to a combination of an entire body mode with vertical and fore-and-aft pelvic motion due to buttocks tissue deformation in phase with a vertical visceral mode, and a bending mode of the upper thoracic and cervical spine. A bending mode of the lumbar and the lower thoracic spine was found in the next higher mode which was located close to the principal mode. It was found by an additional experiment that the entire body mode and the visceral mode made equal contributions to the principal resonance. The second principal resonance of the driving point responses at about 8 Hz seemed to correspond to rotational modes of the pelvis and might have some contribution of the second visceral mode. When a subject changed posture from erect to slouched, the natural frequencies for the entire body mode and the rotational modes of the pelvis decreased, which resulted in decreases in the frequencies for the principal and the second principal resonances of the driving point responses. It was also found that the fore-and-aft motion of the pelvis, including shear deformation of buttocks tissue, increased in the entire body mode due to the postural change towards the slouched posture.

The modified expanded model (final model) was developed in modelling part 2, comparing mainly the natural frequencies and the vibration mode shapes of the model with the experimental data. A total of ten reliable modes was calculated for the normal posture below 20 Hz (seven modes below 10 Hz), and the mode shapes of the model coincided well with the measurements below 10 Hz. The calculation results of the modified expanded model have answered the questions raised in the literature review. The principal resonance of the human body at about 5 Hz was found to correspond to an entire body mode with vertical and fore-and-aft pelvic motion due to deformation of tissue beneath the pelvis in phase with a vertical visceral mode. A bending mode of the lumbar spine was included in the next higher mode located close to the principal mode, which was a bending mode of the entire spine with a pitching mode of the head. The second principal resonance of the body at about 8 Hz corresponded to a rotational mode of the pelvis. The

contribution of the second visceral mode to the second principal resonance was found to be small. The lowest axial mode of the spine was found at about 15 Hz with a higher bending mode of the spine, and the axial deformation occurred in the cervical and the upper thoracic spine. The modified expanded model also showed that the shifts of the principal and the second principal resonances of the body due to changes in posture were caused by shifts of the natural frequencies for the entire body mode and the rotational mode of the pelvis. It was suggested that an increase in contact areas between the buttocks and the thighs and the seat surface, when changing posture from erect to slouched, decreased the axial stiffness beneath the pelvis with the non-linear force-deflection relationship of tissue, resulting in decreases in the natural frequencies. It was also found that a change in posture from erect to slouched increased the contribution of the shear deformation of tissue beneath the pelvis to the entire body mode, and the natural frequency was decreased with the much lower shear stiffness of tissue than the axial stiffness. Although the modified expanded model produced similar vibration mode shapes and driving point responses to the experimental data, it needs further precise modification, including modification of the head-neck region, to simulate the transmissibilities to various parts of the body more accurately.

The modified expanded model has provided much needed information for a fundamental understanding of the mechanical responses to whole-body vibration, and will be a powerful tool to analyse various vibration problems concerning health, activities and comfort. Although the principal mode produces a large response magnitude, it may not be hazardous for spinal injuries because the spine does not deform largely in the principal mode. The next higher mode to the principal mode and the second principal mode contain bending deformations of the spine, and may be more hazardous for spinal injuries. The response of the body contains many bending modes of the spine throughout the frequency range below 20 Hz but only one axial mode at about 15 Hz. Therefore, further intensive research should be concentrated on the bending modes of the spine so as to find the most hazardous modes and frequencies for spinal injuries. In the modified expanded model, each spinal beam is given stiffnesses for the intervertebral disc and the length of the beam represents the length between the geometrical centres of the adjacent vertebral bodies. With this simplification for the spine, the model is capable of predicting approximate (i.e. geometrically mean) internal forces within the spine at any level, although the model needs further modification to predict the transmissibilities quantitatively. If each spinal beam is separated into a rigid link representing the vertebral body and a deformable beam representing the intervertebral disc with a more accurate area of cross-

section, stress and strain distributions within the discs will be predicted so that the mechanism for spinal injuries may be understood more precisely.

When the head-neck region of the model is modified further, degradation of visual performance caused by translational and rotational head motion may be predicted at the frequencies where compensatory movements of eyes are not effective. When the arms are anatomically modelled and added to the model, it will become also possible to analyse degradation of manual control. However, it will require further intensive research to model voluntary and involuntary muscle activities which may be involved in manual control, because available material properties for tissue, such as muscles and ligaments, are extremely limited, and the layered structure of the muscles and the ligaments on the skeleton is anatomically complicated.

The vibration mode shapes obtained for the human body may assist understanding the effect of vibration on comfort. International standard 2631 (1985) shows the greatest and equal sensitivity to vertical acceleration between 4 and 8 Hz and British standard 6841 (1987) between 5 and 16 Hz in their frequency weighting curves for evaluating discomfort. Three modes and seven modes were found in the frequency ranges between 4 and 8 Hz and between 5 and 16 Hz respectively, and they create the greatest and equal sensitivity according to the standards. The modes include the buttocks modes, the first and the second visceral modes, the bending modes of the spine and the pitching modes of the head. Although the different modes within the frequency range cause the equal sensitivity, the feeling of whole-body vibration is different depending on the frequency within the range. This may be explained by the mode shapes, although the vibration feeling (discomfort) may be dominated by tissue vibration near the body surface at high frequencies that is not included in the model.

It is possible to investigate the effects of seat resilience on the body responses so as to improve the effects of vibration, by placing springs for the seat beneath the buttocks tissue beams in the model. The principal and the second principal resonances of the body will be largely affected by the presence of the seat which will reduce the total axial and shear stiffnesses beneath the pelvis. The model is also capable of calculating responses to excitations in other directions and at other points of contact in the mid-sagittal plane, that will be useful to analyse the effects of backrest vibration input. Some anthropometric parameters are included in the model and it may be possible to predict responses of subjects with different body constructions so as to investigate variability in responses

between subjects. Although the effect of posture on the vibration mode shapes and the mechanism for the resonance shift have been understood, the effect in the transmissibilities has not yet been explained by the model. It needs further modification of the model to predict the transmissibilities in different postures quantitatively and optimise the posture to minimise the adverse effects of whole-body vibration.

The modified expanded model can be extended to a three dimensional model by simply defining additional geometry and material properties so that it will be applied to problems in more practical situations. The model is entirely linear, although the effects of the non-linear force-deflection relationships of some intervertebral discs and the body weight preload are incorporated into the linearised (increased) stiffness data. The magnitude dependency of the responses is the most important non-linearity when applications of the model to practical situations are considered. Some part of the material properties for the model and the calculation results are valid for a magnitude range around 1.7 m/s^2 r.m.s. because the natural frequencies and the mode shapes were measured with an excitation magnitude of 1.7 m/s^2 r.m.s. in the experiment and the model was developed based on the measurements. The most efficient way to treat this non-linearity for the practical purposes may be to provide sets of stiffness data for different magnitudes of excitation. Systematic experimental work will be necessary to obtain such data sets.

It is recommended that the modified expanded model should be modified further to predict the transmissibilities quantitatively, the model should be applied to various practical vibration problems, and the model responses should be compared with physiological and psychological responses and epidemiological data for spinal injuries so as to solve problems as well as develop the model further.

APPENDIX 1

Responses of a single degree-of-freedom system

The driving point impedance, apparent mass and the acceleration (displacement) transfer function can be solved theoretically for a single degree-of-freedom system shown in Figure A1.1.

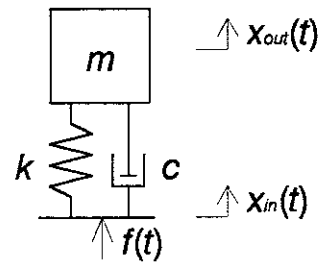

Figure A1.1 A single degree-of-freedom system.

The equation of motion of the mass, m, and the equilibrium of the reaction force from the base, $f(t)$, are:

$$m\ddot{x}_{out}(t) + c(\dot{x}_{out}(t) - \dot{x}_{in}(t)) + k(x_{out}(t) - x_{in}(t)) = 0 \qquad \textbf{(A1.1)}$$

$$f(t) = c(\dot{x}_{in}(t) - \dot{x}_{out}(t)) + k(x_{in}(t) - x_{out}(t)) \qquad \textbf{(A1.2)}$$

where: k is the stiffness; c is the damping coefficient; $x_{out}(t)$ is the vertical displacement response of the mass; $x_{in}(t)$ is the vertical excitation displacement given to the base; $f(t)$ is the vertical reaction force from the base.

Substituting $x_{in}(t)=X_{in}e^{i\omega t}$, $x_{out}(t)=X_{out}e^{i\omega t}$ and $f(t)=Fe^{i\omega t}$ into equations (A1.1) and (A1.2), and solving them, the driving point impedance, $Z(f)$, the driving point apparent mass, $M(f)$, and the transfer function, $T(f)$, are obtained:

$$Z(f) = \frac{F(f)}{i\omega X_{in}(f)} = m\omega_0 \frac{-2\zeta\beta(f)^2 + i\beta(f)}{1-\beta(f)^2 + 2i\zeta\beta(f)} \qquad \textbf{(A1.3)}$$

$$M(f) = \frac{F(f)}{-\omega^2 X_{in}(f)} = m \frac{1 + 2i\zeta\beta(f)}{1-\beta(f)^2 + 2i\zeta\beta(f)} \qquad \textbf{(A1.4)}$$

$$T(f) = \frac{X_{out}(f)}{X_{in}(f)} = \frac{1 + 2i\zeta\beta(f)}{1 - \beta(f)^2 + 2i\zeta\beta(f)} \quad \textbf{(A1.5)}$$

where: i^2=-1; $F(f)$ is equivalent to the Fourier transform of the reaction force, $f(t)$; $X_{out}(f)$ is equivalent to the Fourier transform of the displacement response of the mass, $x_{out}(t)$; $X_{in}(f)$ is equivalent to the Fourier transform of the excitation displacement given to the base, $x_{in}(t)$; $\beta(f)$ is the frequency ratio defined by equation (A1.6); ω is the excitation angular frequency; ω_o is the natural angular frequency obtained by equation (A1.7); f is the excitation frequency (ω=2πf); f_o is the natural frequency; ζ is the damping ratio obtained by equation (A1.8):

$$\beta(f) = \frac{\omega}{\omega_0} = \frac{f}{f_0} \quad \textbf{(A1.6)}$$

$$\omega_0 = \sqrt{\frac{k}{m}} = 2\pi f_0 \quad \textbf{(A1.7)}$$

$$\zeta = \frac{c}{2\sqrt{mk}} \quad \textbf{(A1.8)}$$

The modulus of the driving point impedance, $|Z(f)|$, the modulus of the driving point apparent mass, $|M(f)|$, and the transmissibility, $|T(f)|$, are:

$$|Z(f)| = m\,\omega_0 \frac{\sqrt{(-2\zeta\beta(f)^2)^2 + \beta(f)^2}}{\sqrt{(1-\beta(f)^2)^2 + (2\zeta\beta(f))^2}} \quad \textbf{(A1.9)}$$

$$|M(f)| = m \frac{\sqrt{1 + (2\zeta\beta(f))^2}}{\sqrt{(1-\beta(f)^2)^2 + (2\zeta\beta(f))^2}} \quad \textbf{(A1.10)}$$

$$|T(f)| = \frac{\sqrt{1 + (2\zeta\beta(f))^2}}{\sqrt{(1-\beta(f)^2)^2 + (2\zeta\beta(f))^2}} \quad \textbf{(A1.11)}$$

The exact resonance frequencies can be obtained by letting the derivatives of equations (A1.9), (A1.10) and (A1.11) equal 0. However the solutions are approximately β=1 with small ζ, hence the resonance frequency, f_r, is:

$$f_r \cong \frac{1}{2\pi}\sqrt{\frac{k}{m}} \quad \textbf{(A1.12)}$$

The resonance moduli of the driving point impedance, $|Z(f)|_r$, and the driving point apparent mass, $|M(f)|_r$, and the resonance transmissibility, $|T(f)|_r$, are obtained by substituting equation (A1.12) into equations (A1.9), (A1.10) and (A1.11):

$$|Z|_r \cong m\,\omega_0 \frac{1}{2\zeta} \qquad \textbf{(A1.13)}$$

$$|M|_r \cong m \frac{1}{2\zeta} \qquad \textbf{(A1.14)}$$

$$|T|_r \cong \frac{1}{2\zeta} \qquad \textbf{(A1.15)}$$

APPENDIX 2

Fundamentals of the finite element method (extracted from Petyt, 1990)

A2.1 Introduction

The response of simple structures, such as uniform axial, torque and beam elements, may be obtained by solving the differential equations of motion together with the appropriate boundary conditions. However, in practical situations where a structure has complicated geometry and consists of several materials, it is not possible to obtain analytical solutions to the equations of motion which satisfy the boundary conditions. The finite element displacement method is quite useful in such situations. The method treats a structure as an assemblage of components of simple elements such as rods, beams, plates and shells, and the matrices involved in the equations of motion for individual elements are derived based on the energy equations. The matrices for the equations of motion for the complete structure can be simply formed by assembling obtained matrices for individual elements, considering the geometrical boundary conditions. In this section, fundamentals of the finite element method are explained, using a beam as an example.

A2.2 Hamilton's principle and Lagrange's equation

Hamilton's principle and Lagrange's equation are useful to formulate the equations of motion for a complicated system. Application of Hamilton's principle described by equation (A2.1) directly leads to the equations of motion for any system.

$$\int_{t_1}^{t_2} (\delta(T - U) + \delta W)dt = 0 \qquad \textbf{(A2.1)}$$

where: T is the kinetic energy; U is the potential energy (strain energy); W is the virtual work done by a non-conservative force; t is time. When the principle is applied to discrete systems, it can be expressed by the Lagrange's equation (A2.2), using a dissipation function, D, defined by equation (A2.3):

$$\frac{d}{dt}\left(\frac{\partial T}{\partial \dot{u}}\right) + \frac{\partial D}{\partial \dot{u}} + \frac{\partial U}{\partial u} = f \qquad \textbf{(A2.2)}$$

$$D = \frac{1}{2} c \dot{u}^2 \qquad \textbf{(A2.3)}$$

where: u and $\dot{u}$ are the displacement and velocity; f is the externally applied force; c is a damping coefficient. Equation (A2.2) determines the equation of motion for a single degree-of-freedom system. In the case of a multi degree-of-freedom system, Lagrange's equation takes the form:

$$\frac{d}{dt}\left(\frac{\partial T}{\partial \dot{q}_j}\right)+\frac{\partial D}{\partial \dot{q}_j}+\frac{\partial U}{\partial q_j}=Q_j \qquad (j=1,2,\ldots,n) \tag{A2.4}$$

where: q_j and $\dot{q}_j$ are the generalised displacements and generalised velocities; Q_j are the generalised forces. The kinetic energy, dissipation function and strain energy can all be written in matrix forms:

$$T=\frac{1}{2}\{\dot{q}\}^T[M]\{\dot{q}\} \tag{A2.5a}$$

$$D=\frac{1}{2}\{\dot{q}\}^T[C]\{\dot{q}\} \tag{A2.5b}$$

$$U=\frac{1}{2}\{q\}^T[K]\{q\} \tag{A2.5c}$$

where: $\{q\}$ and $\{\dot{q}\}$ are the generalised displacement and velocity vectors; $[M]$, $[C]$ and $[K]$ are square symmetric matrices of inertia coefficients, damping coefficients and stiffness coefficients respectively. Substituting equation (A2.5) into (A2.4), the equations of motion are obtained in a matrix form:

$$[M]\{\ddot{q}\}+[C]\{\dot{q}\}+[K]\{q\}=\{Q\} \tag{A2.6}$$

where: $\{\ddot{q}\}$ is the generalised acceleration vector; $\{Q\}$ is the generalised applied force vector. Therefore, it is only necessary to obtain the energy expressions in matrix forms shown in equations (A2.5) in order to determine the matrix coefficients in the equations of motion.

A2.3 Rayleigh-Ritz method

The energy functions for a cantilever beam shown in Figure A2.1 are:

$$T=\frac{1}{2}\int_0^L \rho A\dot{v}^2\,dx \tag{A2.7}$$

$$U=\frac{1}{2}\int_0^L EI_z\left(\frac{\partial^2 v}{\partial x^2}\right)^2 dx \tag{A2.8}$$

The geometric boundary conditions are:

$$v(0,t)=0 \tag{A2.9a}$$

$$\frac{\partial v}{\partial x}(0,t)=0 \tag{A2.9b}$$

where: A is the constant cross-sectional area; E is Young's modulus for the material; I_z is

the second moment of area of the cross-section.

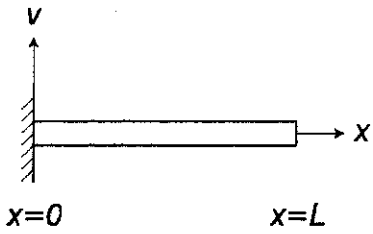

Figure A2.1 Cantilever beam.

The Rayleigh-Ritz method approximates the solution with a finite expansion of the form:

$$v(x,t) = \sum_{j=1}^{n} \phi_j(x) q_j(t) \qquad \textbf{(A2.10)}$$

where: $q_j(t)$ are unknown functions of time; $\phi_j(x)$ are prescribed functions of x, which must satisfy flowing criteria in order to ensure convergence of the solution.

(1) Be linearly independent, where a set of functions are linearly independent if:

$$\sum_{j=1}^{n} \alpha_j \phi_j(x) = 0 \qquad \text{for all } x \qquad \textbf{(A2.11)}$$

implies that:

$$\alpha_j = 0 \qquad \text{for } j = 1,2,\ldots,n \qquad \textbf{(A2.12)}$$

(2) Be continuous and have continuous derivatives up to order (p-1), where p is the highest order of derivative in energy equations. In the case of equations (A2.7) and (A2.8), p=2

(3) Satisfy the geometric boundary conditions.

(4) Form a complete series, where a series of functions is complete if the 'mean square error' vanishes in the limit:

$$\lim_{n\to\infty} \int_0^L \left(v - \sum_{j=1}^{n} \phi_j q_j \right)^2 dx = 0 \qquad \textbf{(A2.13)}$$

Polynomial functions defined by equation (A2.14) satisfy the above criteria and can be assumed for $\phi_j(x)$:

$$\phi_j(x) = x^{j+1} \qquad (j = 1,2,\ldots,n) \qquad \textbf{(A2.14)}$$

Each of the functions $\phi_j(x)$ surely satisfies the geometric boundary conditions (A2.9):

$$\phi_j(0) = 0 \qquad (j = 1,2,\ldots,n) \qquad \textbf{(A2.15a)}$$

$$\frac{d\phi_j}{dx}(0) = 0 \qquad (j = 1,2,\ldots,n) \qquad \textbf{(A2.15b)}$$

When the natural frequencies and the vibration mode shapes are to be obtained, damping and applied force are assumed to be zero and the Lagrange's equation (A2.4) yields:

$$\frac{d}{dt}\left(\frac{\partial T}{\partial \dot{q}_j}\right) + \frac{\partial U}{\partial q_j} = 0 \qquad (j = 1,2,\ldots,n) \tag{A2.16}$$

Substituting equation (A2.10) into equations (A2.7) and (A2.8), and then into (A2.16), equations of motion are obtained:

$$[M]\{\ddot{q}\} + [K]\{q\} = 0 \tag{A2.17}$$

where elements of the stiffness and inertial matrices are:

$$M_{jk} = \int_0^L \rho A x^{j+k+2} dx = \frac{1}{j+k+3}\rho A L^{j+k+3} \tag{A2.18a}$$

$$K_{jk} = \int_0^L EI_z (j+1)j(k+1)k x^{j+k-2} dx = \frac{(J+1)j(k+1)k}{j+k-1} EI_z L^{j+k-1} \tag{A2.18b}$$

Since the motion is harmonic, the displacements can be assumed:

$$q_j(t) = A_j \sin \omega t \qquad (j = 1,2,\ldots,n) \tag{A2.19}$$

Substituting equation (A2.19) into (A2.17), equation (A2.20) is obtained:

$$[K - \omega^2 M]\{A\} = 0 \tag{A2.20}$$

Equation (A2.20) describes a typical eigenvalue problem. Therefore, the eigenvalues ω_1^2, ω_2^2,..., ω_n^2 are obtained by letting the determinant of the matrix in equation (A2.20) equal zero:

$$|K - \omega^2 M| = 0 \tag{A2.21}$$

By substituting equations (A2.18) into (A2.21), the eigenvalues are obtained. The quantities, ω_1, ω_2,..., ω_n are approximate values of the first n natural frequencies. Substituting obtained ω_r^2 into equation (A2.20), an eigenvector $\{A\}_r$ is obtained. When the eigenvector $\{A\}_r$ are combined with the prescribed functions $\phi_j(x)$ by equation (A2.22), it corresponds to the vibration mode shape for the rth mode, $v_r(x)$, in an approximate sense:

$$v_r(x) = \sum_{j=1}^{n} \phi_j(x) A_{rj} \tag{A2.22}$$

The approximate natural frequencies obtained using the Rayleigh-Ritz method are always greater than the true values and they will converge to the true values as the number of terms in equation (A2.10) is increased.

A2.4 Finite element displacement method

The major drawback to the Rayleigh-Ritz method is the difficulty in constructing a set of prescribed functions. This difficulty can be overcome by using the finite element displacement method which provides an automatic procedure for constructing such functions. The prescribed functions are constructed in the following manner:

(1) Select a set of node points on the structure.

(2) Associate with each node point a given number of degrees of freedom (displacement, slope, etc.)

(3) Construct a set of functions such that each one gives a unit value for one degree of freedom and zero values for all the others.

This procedure is illustrated for the bending vibration of a beam in Figure A2.2.

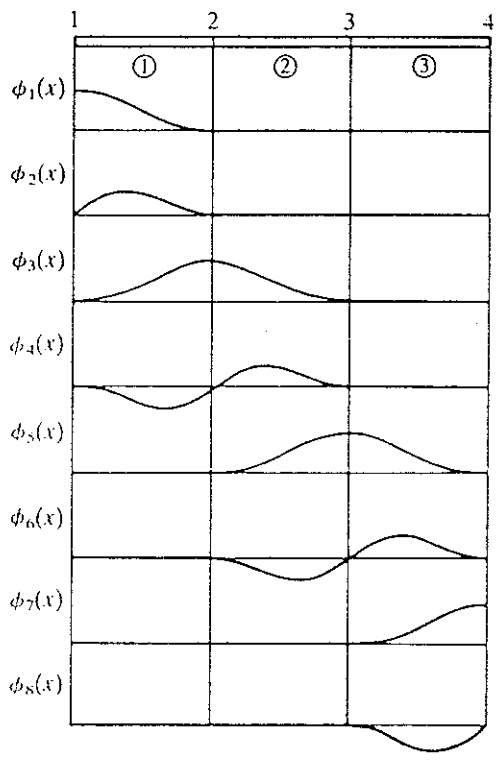

Figure A2.2 Prescribed functions for a beam (from Petyt,1990).

In Figure A2.2, four node points have been selected at equal intervals. The region between each pair of adjacent nodes is referred to as an 'element'. The highest derivative appearing in the energy expressions for a beam (equations (A2.7) and (A2.8)) is the second. Therefore, the Rayleigh-Ritz method requires the prescribed functions and their first

derivative to be continuous. Hence, it will be necessary to take v and $\partial v/\partial x$ as degrees of freedom at each node. In the figure, the odd numbered prescribed functions have been constructed by giving each node point in turn a unit lateral displacement, while maintaining zero displacements and zero rotations at all other nodes. The even numbered prescribed functions are constructed by giving each node in turn a unit rotation, while the rotations and the displacements at all other nodes are kept zero. The geometric boundary conditions are satisfied by omitting the appropriate functions. For example, the functions $\phi_1(x)$ and $\phi_2(x)$ are omitted when analysing a cantilever beam. Each element of the beam deforms in only four deformation patterns and the deformation patterns for each element are identical. Because of this feature, the emphasis is on determining deformation patterns for individual elements. It is also simpler to evaluate the energy expressions for each element and then add the contributions from the elements together. A function determining deformation patterns over a single element is referred to as an 'element displacement function'. Approached in this way, there is no reason why the elements should be identical and, for example, the elements could have different cross-sectional areas and densities as well as different length. In the Rayleigh-Ritz method, convergence is obtained as the number of prescribed functions is increased. In the finite element method, this corresponds to increasing the number of node points and, therefore, the number of elements.

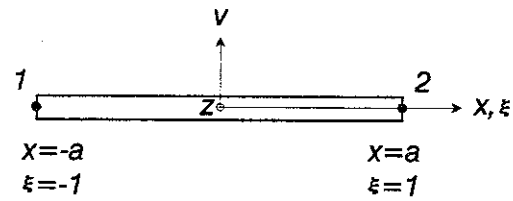

Figure A2.3 Geometry of a single beam element.

In the case of a bending beam element shown in Figure A2.3, the highest derivative appearing in the energy expressions is the second (equations (A2.7) and (A2.8)). Hence, it is necessary to take v and $\partial v/\partial x$ (θ_z) as degrees of freedom at each node. The element has a total of four degrees of freedom. The displacement function can be represented by a polynomial having four constants:

(A2.23)

$$v = \alpha_1 + \alpha_2\xi + \alpha_3\xi^2 + \alpha_4\xi^3$$

Equation (A2.23) can be written in a matrix form:

$$v = \lfloor 1 \ \xi \ \xi^2 \ \xi^3 \rfloor \begin{bmatrix} \alpha_1 \\ \alpha_2 \\ \alpha_3 \\ \alpha_4 \end{bmatrix} \tag{A2.24}$$

or:

$$v = \lfloor P(\xi) \rfloor \{\alpha\} \tag{A2.25}$$

Differentiating (A2.23) gives:

$$a\theta_z = a\frac{\partial v}{\partial x} = \frac{\partial v}{\partial \xi} = \alpha_2 + 2\alpha_3\xi + 3\alpha_4\xi^2 \tag{A2.26}$$

Evaluating equations (A2.23) and (A2.26) at $\xi = \mp 1$ gives:

$$\begin{bmatrix} v_1 \\ a\theta_{z1} \\ v_2 \\ a\theta_{z2} \end{bmatrix} = \begin{bmatrix} 1 & -1 & 1 & -1 \\ 0 & 1 & -2 & 3 \\ 1 & 1 & 1 & 1 \\ 0 & 1 & 2 & 3 \end{bmatrix} \begin{bmatrix} \alpha_1 \\ \alpha_2 \\ \alpha_3 \\ \alpha_4 \end{bmatrix} \tag{A2.27}$$

or:

$$\{v\}_e = [A]_e \{\alpha\} \tag{A2.28}$$

$\{\alpha\}$ is obtained by solving equation (A2.28):

$$\{\alpha\} = [A]_e^{-1} \{v\}_e \tag{A2.29}$$

where:

$$[A]_e^{-1} = \frac{1}{4} \begin{bmatrix} 2 & 1 & 2 & -1 \\ -3 & -1 & 3 & -1 \\ 0 & -1 & 0 & 1 \\ 1 & 1 & -1 & 1 \end{bmatrix} \tag{A2.30}$$

Substituting equation (A2.29) into (A2.25):

$$\begin{aligned} v &= \lfloor P(\xi) \rfloor [A]_e^{-1} \{v\}_e \\ &= \lfloor N(\xi) \rfloor \{v\}_e \end{aligned} \tag{A2.31}$$

where:

$$\lfloor N(\xi) \rfloor = \lfloor N_1(\xi) \ aN_2(\xi) \ N_3(\xi) \ aN_4(\xi) \rfloor \tag{A2.32}$$

and:

$$N_1(\xi) = \frac{1}{4}(2 - 3\xi + \xi^3)$$
$$N_2(\xi) = \frac{1}{4}(1 - \xi - \xi^2 + \xi^3) \qquad \textbf{(A2.33)}$$
$$N_3(\xi) = \frac{1}{4}(2 + 3\xi - \xi^3)$$
$$N_4(\xi) = \frac{1}{4}(-1 - \xi + \xi^2 + \xi^3)$$

Each function from $N_1(\xi)$ to $N_4(\xi)$ indicates the deformation pattern of the element as shown in Figure A2.4.

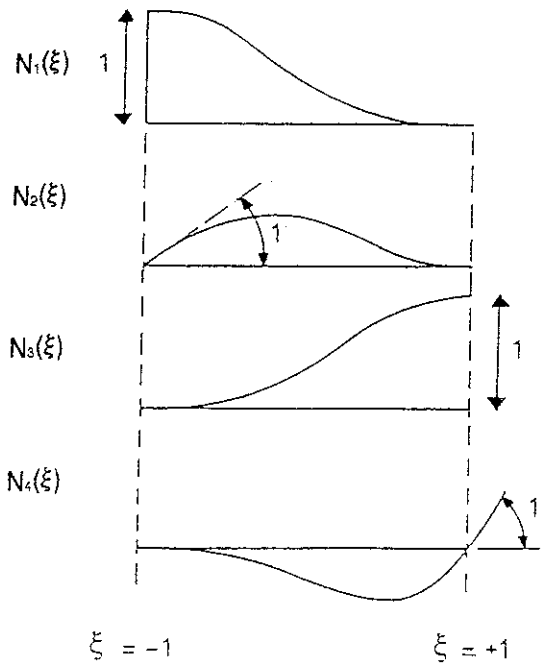

Figure A2.4 The functions from $N_1(\xi)$ to $N_4(\xi)$ (from Petyt, 1990).

The energy expressions for the single element are:

$$T_e = \frac{1}{2}\int_{-a}^{a} \rho A \dot{v}^2 dx = \frac{1}{2}\{\dot{v}\}_e^T [m]_e \{\dot{v}\}_e \qquad \textbf{(A2.34)}$$

$$U_e = \frac{1}{2}\int_{-a}^{a} EI_z \left(\frac{\partial^2 v}{\partial x^2}\right)^2 dx = \frac{1}{2}\{v\}_e^T [k]_e \{v\}_e \qquad \textbf{(A2.35)}$$

Substituting equation (A2.31) into (A2.34) and (A2.35) gives the element inertia matrix $[m]_e$ and the element stiffness matrix $[k]_e$:

$$[m]_e = \rho A a \int_{-1}^{1} \lfloor N(\xi) \rfloor^T \lfloor N(\xi) \rfloor d\xi \qquad \textbf{(A2.36)}$$

$$[k]_e = \frac{EI_z}{a^3}\int_{-1}^{1}\lfloor N''(\xi)\rfloor^T\lfloor N''(\xi)\rfloor d\xi \qquad \textbf{(A2.37)}$$

Substituting equations (A2.33) into (A2.36) and (A2.37) yields:

$$[m]_e = \frac{\rho Aa}{105}\begin{bmatrix} 78 & 22a & 27 & -13a \\ 22a & 8a^2 & 13a & -6a^2 \\ 27 & 13a & 78 & -22a \\ -13a & -6a^2 & -22a & 8a^2 \end{bmatrix} \qquad \textbf{(A2.38)}$$

$$[k]_e = \frac{EI_z}{2a^3}\begin{bmatrix} 3 & 3a & -3 & 3a \\ 3a & 4a^2 & -3a & 2a^2 \\ -3 & -3a & 3 & -3a \\ 3a & 2a^2 & -3a & 4a^2 \end{bmatrix} \qquad \textbf{(A2.39)}$$

The energy expressions for a complete beam are obtained by adding together the energies for all the individual elements. Before carrying this out it is necessary to relate the degrees of freedom of a single element, $\{v\}_e$, to the set of degrees of freedom for the complete beam, $\{v\}$. For the beam shown in Figure A2.2, the degrees of freedom are:

$$\{v\}^T = \lfloor v_1 \; a\theta_{z1} \; v_2 \; a\theta_{z2} \; v_3 \; a\theta_{z3} \; v_4 \; a\theta_{z4}\rfloor \qquad \textbf{(A2.40)}$$

For the element, e, the relationship is:

$$\{v\}_e = [a]\{v\} \qquad \textbf{(A2.41)}$$

where the transformation matrices $[a]_e$ for the three elements are:

$$[a]_1 = \begin{bmatrix} 1 & 0 & 0 & 0 & 0 & 0 & 0 & 0 \\ 0 & 1 & 0 & 0 & 0 & 0 & 0 & 0 \\ 0 & 0 & 1 & 0 & 0 & 0 & 0 & 0 \\ 0 & 0 & 0 & 1 & 0 & 0 & 0 & 0 \end{bmatrix}$$

$$[a]_2 = \begin{bmatrix} 0 & 0 & 1 & 0 & 0 & 0 & 0 & 0 \\ 0 & 0 & 0 & 1 & 0 & 0 & 0 & 0 \\ 0 & 0 & 0 & 0 & 1 & 0 & 0 & 0 \\ 0 & 0 & 0 & 0 & 0 & 1 & 0 & 0 \end{bmatrix} \qquad \textbf{(A2.42)}$$

$$[a]_3 = \begin{bmatrix} 0 & 0 & 0 & 0 & 1 & 0 & 0 & 0 \\ 0 & 0 & 0 & 0 & 0 & 1 & 0 & 0 \\ 0 & 0 & 0 & 0 & 0 & 0 & 1 & 0 \\ 0 & 0 & 0 & 0 & 0 & 0 & 0 & 1 \end{bmatrix}$$

Substituting the transformation (A2.41) into (A2.34) and (A2.35), and summing over all the elements gives:

$$T = \frac{1}{2}\{\dot{v}\}^T \sum_{e=1}^{3} [a]_e^T [m]_e [a]_e \{\dot{v}\} = \frac{1}{2}\{\dot{v}\}^T [M]\{\dot{v}\} \qquad \textbf{(A2.43)}$$

$$U = \frac{1}{2}\{v\}^T \sum_{e=1}^{3} [a]_e^T [k]_e [a]_e \{v\} = \frac{1}{2}\{v\}^T [K]\{v\} \qquad \textbf{(A2.44)}$$

where: $[M]$ and $[K]$ are the inertia and the stiffness matrices for the complete beam.

The matrix product $[a]_e^T[m]_e\ [a]_e$ and $[a]_e^T[k]_e\ [a]_e$ in equations (A2.43) and (A2.44) effectively locates the positions in $[M]$ and $[k]$ to which the elements of $[m]_e$ and $[k]_e$ have to be added. In practice it is not necessary to form $[a]_e$ and carry out the matrix multiplication. The information required can be obtained from the element node numbers. Element number e has nodes e and $(e+1)$ and each node has two degrees of freedom. Therefore, the four rows and columns in the element inertia matrix are added into the rows and columns from $2e$-1 to $2e$+2 of the inertia and the stiffness matrices for the complete beam. This procedure is known as the 'assembly process'. The geometric boundary conditions can be satisfied by omitting rows and columns corresponding to appropriate degrees of freedom from the inertia and the stiffness matrices for the complete beam.

Exactly the same procedure can be taken for other types of elements with corresponding energy equations and matrices for such elements are also incorporated into the matrices for the complete structure in the 'assembly process'. By the above means, the inertia and the stiffness matrices for the complete structure are constructed and, therefore, the equations of motion of the structure (A2.17) are determined for the modal analysis to calculate the natural frequencies and the vibration mode shapes (equation (A2.20)). For the case of forced vibration, the applied force vector can also be incorporated in the formulation. However, in this research, another type of technique (the mode superposition method) is used for the harmonic response analysis, which is based on the modal analysis (see section 3.2.3.1).

APPENDIX 3

A straight-line technique for extracting modal properties from frequency response data (extracted from Dobson, 1987)

The method used in this study to extract the modal properties are modified dynamic stiffness (1/receptance) method based on a single degree-of-freedom model developed by Dobson (1987). The method can calculate the complex modal constants and does not require calculation of the residual term in advance. The receptance around a resonance can be approximated to a single term corresponding to the dominant *r*th mode with a constant and complex residual term representing the contributions of the remaining modes (see equation 4.31):

$$\alpha \cong \frac{A + iB}{\omega_r^2 - \omega^2 + i\eta_r\omega_r^2} + residual \qquad \textbf{(A3.1)}$$

Considering the Argand diagram representation of the receptance between frequency limits ω_L and ω_U as shown in Figure A3.1, the receptance at a 'fixing' frequency, Ω, within the frequency band is:

$$\alpha_\Omega \cong \frac{A + iB}{\omega_r^2 - \Omega^2 + i\eta_r\omega_r^2} + residual \qquad \textbf{(A3.2)}$$

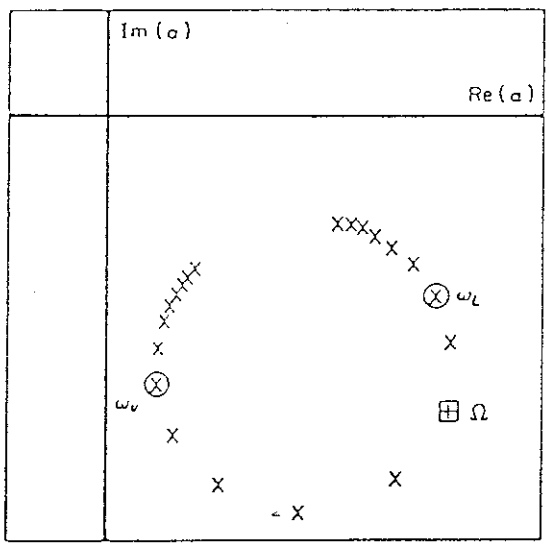

Figure A3.1 Argand diagram of receptance data showing the band width for analysis (from Dobson,1987).

The residual effects can be eliminated by subtracting equation (A3.2) from equation (A3.1):

$$\alpha - \alpha_{\Omega} = (A + iB)\left[\frac{1}{\omega_r^2 - \omega^2 + i\eta_r\omega_r^2} - \frac{1}{\omega_r^2 - \Omega^2 + i\eta_r\omega_r^2}\right] \qquad \textbf{(A3.3)}$$

Re-arranging and inverting equation (A3.3) yields:

$$\frac{\omega^2 - \Omega^2}{\alpha - \alpha_{\Omega}} = \Delta = \frac{A - iB}{A^2 + B^2}\left[(\omega_r^2 - \omega^2)(\omega_r^2 - \Omega^2) - \eta_r^2\omega_r^4 + i\eta_r\omega_r^2(2\omega_r^2 - \omega^2 - \Omega^2)\right] \qquad \textbf{(A3.4)}$$

The quantity, Δ, consists of real and imaginary components which are linear functions in ω^2. Thus:

$$\text{Re}\,(\Delta) = m_R\omega^2 + c_R \qquad \textbf{(A3.5a)}$$

$$\text{Im}\,(\Delta) = m_I\omega^2 + c_I \qquad \textbf{(A3.5b)}$$

where: the slopes are given by:

$$m_R = \frac{-1}{A^2 + B^2}\left[A(\omega_r^2 - \Omega^2) + B\eta_r\omega_r^2\right] \qquad \textbf{(A3.6a)}$$

$$m_I = \frac{-1}{A^2 + B^2}\left[A\eta_r\omega_r^2 - B(\omega_r^2 - \Omega^2)\right] \qquad \textbf{(A3.6b)}$$

By selecting different 'fixing' frequencies within the frequency band, $\omega_L \leq \Omega \leq \omega_U$, a family of linear curves will be obtained as shown in Figure A3.2. These curves will intersect at specific points defined by equations (A3.7a) and (A3.7b):

$$\text{Re}\,(\Delta): \omega^2_{\text{intersection}} = \frac{\omega_r^2(A + B\eta_r)}{A} \qquad \textbf{(A3.7a)}$$

$$\text{Im}\,(\Delta): \omega^2_{\text{intersection}} = \frac{\omega_r^2(B - A\eta_r)}{B} \qquad \textbf{(A3.7b)}$$

Therefore, if there is no complexity present (i.e. B=0), the real component curves will intersect at a point equivalent to the natural frequency and the imaginary curves will be parallel lines.

From equations (A3.6a) and (A3.6b) it can be seen that the slopes of the real and imaginary components of the quantity Δ are linear functions of Ω^2 such that:

$$m_R = n_R\Omega^2 + d_R \qquad \textbf{(A3.8a)}$$

$$m_I = n_I\Omega^2 + d_I \qquad \textbf{(A3.8b)}$$

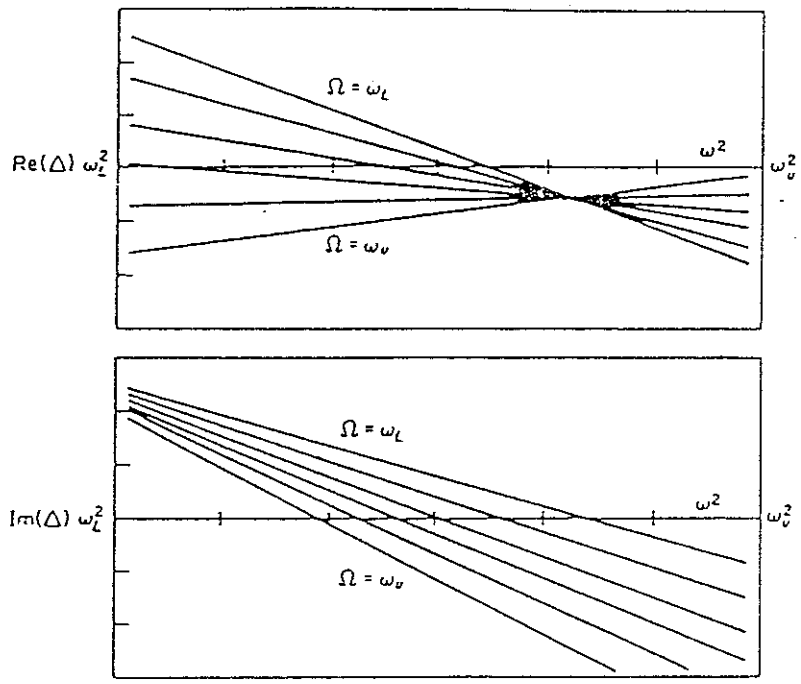

Figure A3.2 Re(Δ) and Im(Δ) versus ω^2 for different 'fixing' points (from Dobson,1987).

where: the slopes and intercepts are:

$$n_R = \frac{A}{A^2 + B^2} \qquad \textbf{(A3.9a)}$$

$$d_R = \frac{-\omega_r^{\,2}(A + B\eta_r)}{A^2 + B^2} \qquad \textbf{(A3.9b)}$$

$$n_I = \frac{-B}{A^2 + B^2} \qquad \textbf{(A3.9c)}$$

$$d_I = \frac{-\omega_r^{\,2}(A\eta_r - B)}{A^2 + B^2} \qquad \textbf{(A3.9d)}$$

This set of equations can be used to extract the modal properties. From equations (A3.9a) and (A3.9c):

$$B = -pA \qquad \textbf{(A3.10)}$$

where:

$$p = \frac{n_I}{n_R} \qquad \textbf{(A3.11)}$$

From equations (A3.9b) and (A3.9d), using equation (A.3.11):

where:

$$\eta_r = \frac{1 - pq}{p + q} \tag{A3.12}$$

$$q = \frac{d_R}{d_I} \tag{A3.13}$$

Therefore, from equation (A3.9b), using equation (A.3.11) :

$$\omega_r^2 = \frac{-1}{1 - p\eta_r} \frac{d_R}{n_R} \tag{A3.14}$$

and:

$$A = \frac{\omega_r^2}{d_R(1 + p^2)}(p\eta_r - 1) \tag{A.3.15}$$

Hence, B may be obtained by substituting equation (A3.15) into equation (A3.10).

The technique will extract exact values of the modal properties for a synthesised system with "well-separated" modes providing that the Argand diagram of receptance is reasonably well defined around each resonance. When the selected frequency band for the analysis with lower and upper frequency limits ω_L and ω_U are too wide and there are more than one mode exist within the band, the family of linear curves defined by equations (A3.7a) and (A3.7b) will reveal non-linearity as shown in Figure A3.3. Thus the non-linearity of the resulting curves indicates that further study of a particular mode may be necessary.

When there are closely located modes, the Argand diagram will show an ellipse instead of a circle and the Δ versus ω-curves will be highly non-linear: the Δ versus ω-curves are more sensitive to the presence of closely located modes. In such a situation, an iteration procedure is effective to separate the close modes. The frequency response functions are analysed from the lowest mode to the highest mode and after each analysis the effects of the analysed modes are removed from the data. Thus the magnitude of any residual effects from "out-of-range" modes can be diminished. The process is then repeated in the reverse direction (i.e. from the highest to the lowest). This "sweeping" to-and-fro through the frequency response functions yields results that converge rapidly to the exact solutions. If a series of transfer functions is analysed simultaneously, the rate of convergence is further improved.

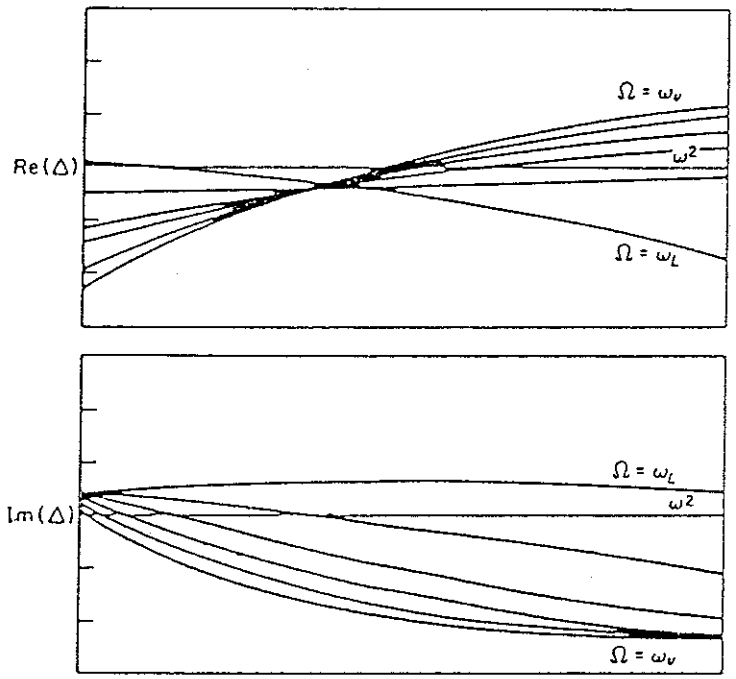

Figure A3.3 Effect of too wide bandwidth on Re(Δ) and Im(Δ) (from Dobson,1987).

APPENDIX 4

Modal matrices

Table A4.1a Modal matrix (real part) extracted from the mean transfer functions in the erect posture.

Site	Mode No.							
	1	2	3	4	5	6	7	8
Head z	0.0	0.0	0.0	0.0	-2.53E-1	-1.09E-1	0.0	0.0
Head x	-4.77E-3	1.51E-2	-1.07E-2	0.0	0.0	-3.04E-2	0.0	0.0
T1 z	0.0	0.0	0.0	0.0	-4.59E-2	0.0	0.0	0.0
T1 x	-2.11E-2	-4.56E-3	0.0	0.0	1.38E-1	5.15E-2	0.0	1.49E-2
T6 z	0.0	0.0	0.0	0.0	-1.09E-1	0.0	0.0	0.0
T6 x	-4.29E-3	-7.58E-3	0.0	0.0	4.48E-3	0.0	-3.79E-2	0.0
T11 z	0.0	0.0	0.0	0.0	-1.45E-1	0.0	0.0	0.0
T11 x	-5.81E-3	-5.31E-3	0.0	0.0	0.0	-1.50E-1	0.0	0.0
L3 z	0.0	0.0	0.0	0.0	-1.69E-1	0.0	0.0	-2.07E-2
L3 x	-9.75E-3	-1.46E-2	-6.49E-3	-5.06E-4	0.0	-6.93E-2	0.0	0.0
S2 z	0.0	0.0	0.0	0.0	-1.16E-1	0.0	0.0	0.0
S2 x	-2.72E-3	-1.03E-2	0.0	4.35E-2	1.90E-2	0.0	0.0	6.18E-2
FP z	0.0	0.0	0.0	0.0	-2.32E-1	0.0	0.0	-3.41E-1
AW z	0.0	0.0	0.0	0.0	-4.07E-1	0.0	0.0	0.0

Site	Mode No.					
	9	10	11	12	13	14
Head z	0.0	-5.98E-2	-3.26E-1	0.0	0.0	0.0
Head x	-5.03E-2	0.0	0.0	-3.16E-2	0.0	0.0
T1 z	0.0	-1.39E-1	0.0	-1.60E-2	0.0	0.0
T1 x	0.0	0.0	0.0	1.21E-2	0.0	9.31E-3
T6 z	0.0	-1.04E-1	0.0	-2.66E-2	0.0	-1.72E-2
T6 x	1.21E-2	0.0	0.0	1.05E-2	0.0	0.0
T11 z	0.0	-1.41E-1	0.0	-1.34E-1	-1.03E-1	0.0
T11 x	4.27E-3	-1.77E-2	0.0	2.06E-2	0.0	0.0
L3 z	0.0	0.0	-6.34E-2	0.0	-8.80E-4	0.0
L3 x	0.0	0.0	-6.63E-2	-4.48E-2	0.0	0.0
S2 z	-2.55E-1	0.0	-3.46E-2	-2.77E-2	-1.08E-2	0.0
S2 x	1.48E-2	0.0	0.0	0.0	-1.54E-2	0.0
FP z	-3.03E-2	0.0	-5.77E-3	0.0	0.0	1.44E-4
AW z	-2.39E-1	0.0	0.0	0.0	0.0	0.0

Table A4.1b Modal matrix (imaginary part) extracted from the mean transfer functions in the erect posture.

Site	Mode No.							
	1	2	3	4	5	6	7	8
Head z	0.0	0.0	0.0	0.0	-6.01E-2	3.74E-2	0.0	0.0
Head x	7.36E-3	-5.94E-3	-9.82E-3	0.0	0.0	-1.07E-1	0.0	0.0
T1 z	0.0	0.0	0.0	0.0	-1.13E-1	0.0	0.0	0.0
T1 x	-1.28E-3	2.10E-2	0.0	0.0	5.88E-3	-1.20E-2	0.0	2.37E-3
T6 z	0.0	0.0	0.0	0.0	-1.53E-1	0.0	0.0	0.0
T6 x	7.47E-3	6.52E-3	0.0	0.0	-1.90E-3	0.0	1.01E-2	0.0
T11 z	0.0	0.0	0.0	0.0	-2.06E-1	0.0	0.0	0.0
T11 x	-1.21E-2	-4.80E-3	0.0	0.0	0.0	-4.07E-2	0.0	0.0
L3 z	0.0	0.0	0.0	0.0	-1.76E-1	0.0	0.0	1.11E-2
L3 x	-1.50E-3	-8.40E-3	2.32E-4	2.07E-3	0.0	-3.55E-2	0.0	0.0
S2 z	0.0	0.0	0.0	0.0	-2.12E-1	0.0	0.0	0.0
S2 x	-8.63E-3	-3.42E-3	0.0	5.40E-2	3.88E-2	0.0	0.0	-4.36E-2
FP z	0.0	0.0	0.0	0.0	-3.08E-1	0.0	0.0	2.04E-1
AW z	0.0	0.0	0.0	0.0	-1.73E-1	0.0	0.0	0.0

Site	Mode No.					
	9	10	11	12	13	14
Head z	0.0	-1.85E-1	1.03E-1	0.0	0.0	0.0
Head x	-7.80E-2	0.0	0.0	6.26E-2	0.0	0.0
T1 z	0.0	-8.45E-2	0.0	8.50E-3	0.0	0.0
T1 x	0.0	0.0	0.0	5.39E-4	0.0	-1.59-3
T6 z	0.0	-4.36E-2	0.0	-5.59E-3	0.0	-1.13E-2
T6 x	3.36E-2	0.0	0.0	1.67E-3	0.0	0.0
T11 z	0.0	-2.18E-2	0.0	7.61E-2	-2.79E-2	0.0
T11 x	8.42E-3	7.68E-3	0.0	8.39E-2	0.0	0.0
L3 z	0.0	0.0	2.60E-2	0.0	4.00E-3	0.0
L3 x	0.0	0.0	2.18E-1	-1.09E-2	0.0	0.0
S2 z	1.02E-1	0.0	-5.42E-2	-1.68E-2	-1.52E-3	0.0
S2 x	9.10E-3	0.0	0.0	0.0	-1.61E-2	0.0
FP z	-1.81E-2	0.0	-3.34E-2	0.0	0.0	5.91E-3
AW z	1.58E-1	0.0	0.0	0.0	0.0	0.0

Table A4.2a Modal matrix (real part) extracted from the mean transfer functions in the normal posture.

Site	Mode No.							
	1	2	3	4	5	6	7	8
Head z	0.0	1.69E-2	0.0	-3.39E-1	-2.05E-1	0.0	0.0	0.0
Head x	-7.13E-3	4.91E-2	-4.25E-2	0.0	-1.19E-2	0.0	0.0	0.0
T1 z	0.0	0.0	2.34E-3	-1.27E-1	0.0	0.0	0.0	0.0
T1 x	-6.01E-2	0.0	0.0	2.05E-1	0.0	0.0	-1.27E-3	0.0
T6 z	0.0	0.0	-4.95E-4	-1.64E-1	0.0	0.0	0.0	0.0
T6 x	-1.93E-2	-1.95E-2	0.0	4.83E-2	0.0	-5.73E-2	0.0	0.0
T11 z	0.0	0.0	0.0	-1.58E-1	0.0	0.0	0.0	0.0
T11 x	0.0	-1.44E-2	-5.58E-4	0.0	-1.26E-1	0.0	0.0	0.0
L3 z	0.0	0.0	-7.79E-4	-2.15E-1	0.0	0.0	-4.95E-2	0.0
L3 x	0.0	-2.34E-2	-8.06E-3	0.0	-8.64E-2	0.0	0.0	0.0
S2 z	0.0	0.0	0.0	-1.37E-1	0.0	0.0	0.0	-3.19E-1
S2 x	-5.86E-4	-2.55E-2	-6.61E-2	7.08E-2	0.0	-6.49E-4	5.45E-2	0.0
FP z	0.0	0.0	0.0	-1.29E-1	0.0	0.0	-4.68E-1	-2.85E-2
AW z	0.0	0.0	0.0	-4.23E-1	0.0	0.0	-5.06E-2	0.0

Site	Mode No.					
	9	10	11	12	13	14
Head z	0.0	-1.05E-1	-2.70E-1	0.0	0.0	0.0
Head x	0.0	-1.40E-1	0.0	0.0	0.0	0.0
T1 z	0.0	-1.68E-1	0.0	0.0	0.0	0.0
T1 x	0.0	0.0	0.0	2.17E-2	0.0	0.0
T6 z	0.0	-4.77E-2	0.0	0.0	0.0	0.0
T6 x	0.0	1.37E-2	0.0	0.0	0.0	0.0
T11 z	0.0	-7.76E-2	0.0	0.0	0.0	-1.08E-1
T11 x	0.0	0.0	-5.92E-2	0.0	0.0	0.0
L3 z	0.0	0.0	0.0	0.0	-1.42E-2	0.0
L3 x	0.0	0.0	-8.96E-2	0.0	0.0	0.0
S2 z	0.0	0.0	0.0	-4.78E-2	0.0	0.0
S2 x	-1.43E-2	0.0	0.0	1.02E-3	0.0	-2.74E-2
FP z	0.0	0.0	-2.74E-3	0.0	0.0	1.37E-2
AW z	-3.32E-1	0.0	0.0	0.0	0.0	0.0

Table A4.2b Modal matrix (imaginary part) extracted from the mean transfer functions in the normal posture.

Site	Mode No.							
	1	2	3	4	5	6	7	8
Head z	0.0	-3.48E-2	0.0	-2.02E-3	1.65E-1	0.0	0.0	0.0
Head x	-9.10E-4	1.63E-3	5.28E-3	0.0	-2.05E-1	0.0	0.0	0.0
T1 z	0.0	0.0	-7.33E-3	-8.46E-2	0.0	0.0	0.0	0.0
T1 x	8.59E-2	0.0	0.0	-1.27E-2	0.0	0.0	5.22E-3	0.0
T6 z	0.0	0.0	1.62E-2	-1.21E-1	0.0	0.0	0.0	0.0
T6 x	5.06E-3	1.01E-2	0.0	1.60E-2	0.0	2.16E-2	0.0	0.0
T11 z	0.0	0.0	0.0	-1.31E-1	0.0	0.0	0.0	0.0
T11 x	0.0	-9.32E-3	1.66E-4	0.0	1.97E-2	0.0	0.0	0.0
L3 z	0.0	0.0	-1.27E-2	-1.27E-1	0.0	0.0	-3.64E-3	0.0
L3 x	0.0	-1.56E-2	-1.02E-3	0.0	-6.05E-3	0.0	0.0	0.0
S2 z	0.0	0.0	0.0	-1.48E-1	0.0	0.0	0.0	5.03E-2
S2 x	2.31E-3	1.23E-2	2.06E-2	-3.82E-3	0.0	4.48E-3	2.32E-3	0.0
FP z	0.0	0.0	0.0	-1.54E-1	0.0	0.0	2.49E-1	-8.66E-2
AW z	0.0	0.0	0.0	-1.81E-1	0.0	0.0	8.22E-4	0.0

Site	Mode No.					
	9	10	11	12	13	14
Head z	0.0	-1.73E-1	9.73E-2	0.0	0.0	0.0
Head x	0.0	-3.24E-2	0.0	0.0	0.0	0.0
T1 z	0.0	-5.73E-2	0.0	0.0	0.0	0.0
T1 x	0.0	0.0	0.0	-1.71E-2	0.0	0.0
T6 z	0.0	-3.43E-2	0.0	0.0	0.0	0.0
T6 x	0.0	7.00E-3	0.0	0.0	0.0	0.0
T11 z	0.0	-5.15E-2	0.0	0.0	0.0	-2.49E-2
T11 x	0.0	0.0	1.52E-1	0.0	0.0	0.0
L3 z	0.0	0.0	0.0	0.0	5.41E-3	0.0
L3 x	0.0	0.0	1.50E-1	0.0	0.0	0.0
S2 z	0.0	0.0	0.0	-1.59E-2	0.0	0.0
S2 x	-5.23E-2	0.0	0.0	-2.00E-2	0.0	7.39E-3
FP z	0.0	0.0	1.11E-2	0.0	0.0	2.62E-2
AW z	2.00E-1	0.0	0.0	0.0	0.0	0.0

Table A4.3a Modal matrix (real part) extracted from the mean transfer functions in the slouched posture.

Site	Mode No.							
	1	2	3	4	5	6	7	8
Head z	8.00E-2	5.99E-2	0.0	-1.47E-1	-3.95E-1	0.0	-2.53E-2	3.98E-2
Head x	-2.06E-2	1.22E-1	0.0	0.0	9.65E-2	0.0	0.0	0.0
T1 z	-4.50E-2	1.84E-2	0.0	-1.05E-1	0.0	0.0	0.0	0.0
T1 x	-4.35E-2	3.99E-2	0.0	0.0	2.11E-1	0.0	0.0	1.36E-2
T6 z	5.58E-3	0.0	0.0	-1.45E-1	0.0	0.0	0.0	0.0
T6 x	-4.95E-2	0.0	0.0	6.51E-2	0.0	1.44E-2	-1.02E-2	0.0
T11 z	0.0	0.0	0.0	-1.65E-1	0.0	0.0	0.0	-8.83E-3
T11 x	-4.91E-2	-9.82E-2	0.0	-1.09E-2	0.0	-2.74E-2	0.0	0.0
L3 z	0.0	0.0	0.0	-1.74E-1	0.0	0.0	0.0	-7.61E-2
L3 x	-1.68E-2	-9.82E-2	-2.33E-2	0.0	-2.99E-2	-1.62E-2	0.0	0.0
S2 z	0.0	0.0	0.0	-1.47E-1	0.0	0.0	0.0	-2.81E-1
S2 x	-3.89E-4	-1.22E-1	9.22E-3	4.18E-2	0.0	-4.11E-2	0.0	2.92E-2
FP z	0.0	0.0	0.0	-6.61E-2	0.0	0.0	-3.17E-2	-5.17E-1
AW z	0.0	-8.00E-3	0.0	0.0	-1.65E-1	0.0	0.0	0.0

Site	Mode No.					
	9	10	11	12	13	14
Head z	7.08E-3	0.0	0.0	-1.04E-1	0.0	-6.59E-2
Head x	-5.25E-3	-7.71E-2	0.0	-1.72E-2	0.0	-1.81E-2
T1 z	0.0	-4.34E-2	0.0	0.0	1.08E-2	0.0
T1 x	0.0	0.0	0.0	0.0	1.39E-1	0.0
T6 z	0.0	-2.14E-2	0.0	0.0	0.0	-1.87E-2
T6 x	0.0	3.96E-2	0.0	0.0	0.0	0.0
T11 z	0.0	0.0	0.0	0.0	0.0	-5.33E-3
T11 x	0.0	-1.36E-1	0.0	0.0	0.0	0.0
L3 z	0.0	0.0	6.45E-3	0.0	-1.70E-2	0.0
L3 x	0.0	-3.27E-2	0.0	0.0	0.0	1.35E-2
S2 z	0.0	0.0	0.0	-1.18E-2	0.0	0.0
S2 x	1.22E-2	0.0	1.72E-2	0.0	-2.83E-2	0.0
FP z	0.0	0.0	0.0	2.74E-2	0.0	0.0
AW z	0.0	-3.09E-3	0.0	0.0	0.0	0.0

Table A4.3B Modal matrix (imaginary part) extracted from the mean transfer functions in the slouched posture.

Site	Mode No.							
	1	2	3	4	5	6	7	8
Head z	-8.71E-2	-9.39E-3	0.0	-1.33E-1	-7.24E-2	0.0	8.03E-2	7.48E-2
Head x	4.09E-2	-4.15E-2	0.0	0.0	-1.03E-1	0.0	0.0	0.0
T1 z	-4.74E-2	-7.59E-3	0.0	-1.59E-1	0.0	0.0	0.0	0.0
T1 x	3.88E-3	1.56E-2	0.0	0.0	7.10E-2	0.0	0.0	3.86E-3
T6 z	-1.84E-2	0.0	0.0	-1.64E-1	0.0	0.0	0.0	0.0
T6 x	-8.46E-2	0.0	0.0	1.85E-1	0.0	-1.49E-2	2.45E-2	0.0
T11 z	0.0	0.0	0.0	-1.58E-1	0.0	0.0	0.0	-1.44E-3
T11 x	-3.06E-2	-7.10E-2	0.0	1.25E-3	0.0	3.34E-2	0.0	0.0
L3 z	0.0	0.0	0.0	-2.05E-1	0.0	0.0	0.0	1.60E-2
L3 x	-4.53E-2	-5.22E-2	5.57E-2	0.0	-6.94E-2	-1.15E-2	0.0	0.0
S2 z	0.0	0.0	0.0	-1.26E-1	0.0	0.0	0.0	-1.84E-2
S2 x	-9.71E-3	9.45E-3	9.15E-2	-6.117E-3	0.0	-6.55E-3	0.0	-3.59E-2
FP z	0.0	0.0	0.0	-1.52E-1	0.0	0.0	6.62E-2	1.47E-1
AW z	0.0	-3.14E-2	0.0	0.0	-4.01E-1	0.0	0.0	0.0

Site	Mode No.					
	9	10	11	12	13	14
Head z	1.26E-1	0.0	0.0	5.89E-3	0.0	-3.98E-3
Head x	-1.34E-2	-1.71E-1	0.0	3.23E-2	0.0	9.77E-3
T1 z	0.0	-7.88E-4	0.0	0.0	3.26E-2	0.0
T1 x	0.0	0.0	0.0	0.0	-1.51E-1	0.0
T6 z	0.0	1.90E-2	0.0	0.0	0.0	-2.37E-2
T6 x	0.0	6.78E-2	0.0	0.0	0.0	0.0
T11 z	0.0	0.0	0.0	0.0	0.0	-9.47E-3
T11 x	0.0	2.02E-1	0.0	0.0	0.0	0.0
L3 z	0.0	0.0	2.79E-2	0.0	5.80E-3	0.0
L3 x	0.0	4.21E-2	0.0	0.0	0.0	3.83E-2
S2 z	0.0	0.0	0.0	9.45E-3	0.0	0.0
S2 x	-1.16E-2	0.0	-1.45E-2	0.0	-2.12E-2	0.0
FP z	0.0	0.0	0.0	4.95E-3	0.0	0.0
AW z	0.0	-5.18E-2	0.0	0.0	0.0	0.0

APPENDIX 5

Cubic spline interpolation

The cubic spline interpolation estimates a value of a function, $y=f(x)$, for an arbitrary variable, x, from known values of the function, $y_i=f(x_i)$, for a set of points, x_i ($i=1,2,\cdots,N$), so as to draw a smooth curve. The value $f(x)$ for x in the interval $[x_i, x_{i+1}]$ is calculated from the known y_i and y_{i+1} and the second derivatives y''_i and y''_{i+1} at the end points of the interval, x_i and x_{i+1}, by equation (A5.1):

$$f(x) = A\,y_i + B\,y_{i+1} + C\,y''_i + D\,y''_{i+1} \qquad \textbf{(A5.1)}$$

where:

$$A = \frac{x_{i+1} - x}{x_{i+1} - x_i} \qquad \textbf{(A5.2a)}$$

$$B = 1 - A = \frac{x - x_i}{x_{i+1} - x_i} \qquad \textbf{(A5.2b)}$$

$$C = \frac{1}{6}(A^3 - A)(x_{i+1} - x_i)^2 \qquad \textbf{(A5.2c)}$$

$$D = \frac{1}{6}(B^3 - B)(x_{i+1} - x_i)^2 \qquad \textbf{(A5.2d)}$$

From equation (A5.1) the first and the second derivatives of the function are:

$$f'(x) = \frac{y_{i+1} - y_i}{x_{i+1} - x_i} + \frac{3A^2 - 1}{6}(x_{i+1} - x_i)y''_i + \frac{3B^2 - 1}{6}(x_{i+1} - x_i)y''_{i+1} \qquad \textbf{(A5.3)}$$

$$f''(x) = A\,y''_i + B\,y''_{i+1} \qquad \textbf{(A5.4)}$$

From equation (A5.2a) and (A5.2b), $A=1$ and $B=0$ at $x=x_i$, and $A=0$ and $B=1$ at $x=x_{i+1}$. Therefore, from equations (A5.1) and (A5.4):

$$f(x) = y_i \quad \text{and} \quad f''(x) = y''_i \quad \text{at} \quad x = x_i \qquad \textbf{(A5.5a)}$$

$$f(x) = y_{i+1} \quad \text{and} \quad f''(x) = y''_{i+1} \quad \text{at} \quad x = x_{i+1} \qquad \textbf{(A5.5b)}$$

The function, $f(x)$, and the second derivative of the function, $f''(x)$, are continuous across the boundary between the adjacent two intervals, $[x_{i-1}, x_i]$ and $[x_i, x_{i+1}]$. Now the requirement is continuity of the first derivative, $f'(x)$, at the boundary. This is obtained by letting $f'(x_i)$ evaluated by equation (A5.3) in the interval $[x_{i-1}, x_i]$ equal to $f'(x_i)$ evaluated

by equation (A5.3) in the interval $[x_i, x_{i+1}]$, and the equation (A5.6) is obtained:

$$\frac{x_i - x_{i-1}}{6} y''_{i-1} + \frac{x_{i+1} - x_{i-1}}{3} y''_i + \frac{x_{i+1} - x_i}{6} y''_{i+1} = \frac{y_{i+1} - y_i}{x_{i+1} - x_i} - \frac{y_i - y_{i-1}}{x_i - x_{i-1}} \qquad \textbf{(A5.6)}$$

Equations (A5.6) are N-2 linear equations and y''_i (i=1,2,···,N) can be solved with two more conditions which are the first derivatives at the both ends of the entire interval, y'_1 and y'_N. By the above means, value of the function $y=f(x)$ for an arbitrary x is determined when $y_i=f(x_i)$ (i=1,2,···,N), $y'_1=f'(x_1)$ and $y'_N=f'(x_N)$ are given, and the function and the first and the second derivatives of the function are continuous at x_i.

APPENDIX 6

Ansys command list for the modal analysis of the modified expanded model

The command file shown below can be loaded into Ansys Prep7 by /INPUT, filename, ext.

```
c*****************************************************************
c*****************************************************************
c***                                                           ***
c***    Modified expanded model in normal posture              ***
c***                                                           ***
c***    Command list for ANSYS PREP7 (Preprocessional phase)   ***
c***    for modal analysis                                     ***
c***                                                           ***
c*****************************************************************
c*****************************************************************
/COM
     /TITLE,  MODIFIED EXPANDED MODEL
/COM=============================================================
/COM============        Chose analysis type       ================
/COM=============================================================
/COM
     KAN,2                 * Chose modal analysis
     KAY,2,-1              * Expand modes below 50 Hz to draw mode
     EXMODE,0.,50          * shapes
/COM
/COM=============================================================
/COM============          Type of elements        ================
/COM=============================================================
/COM
     ET,1,3                  * STIFF3 (2-D beam)
/COM
     ET,2,21,,,3             * STIFF21 (mass with rotary inertia)
/COM
     ET,3,14,,,2             * STIFF14 (longitudinal spring)
/COM
/COM=============================================================
/COM====    Material properties and geometrical constants    ====
/COM=============================================================
/COM
/COM-------------------- For spinal beams ----------------------
/COM
     MP,EX,1,5.064E7         * Young's modulus for the disc S1-L5
     MP,DENS,1,0.1           * Density (very light)
     R,1,1.E-3,1.*4.762E-8,0.035 * Area,Iyy,Height
/COM
     MP,EX,2,7.790E7         * Young's modulus for the disc L5-L4
     MP,DENS,2,0.1           * Density (very light)
     R,2,1.E-3,7.*4.278E-8,0.035 * Area,Iyy,Height
/COM
     MP,EX,3,8.234E7         * Young's modulus for the disc L4-L3
     MP,DENS,3,0.1           * Density (very light)
     R,3,1.E-3,7.*4.500E-8,0.035 * Area,Iyy,Height
/COM
     MP,EX,4,7.738E7         * Young's modulus for the disc L3-L2
     MP,DENS,4,0.1           * Density (very light)
     R,4,1.E-3,7.*4.500E-8,0.035 * Area,Iyy,Height
/COM
     MP,EX,5,7.715E7         * Young's modulus for the disc L2-L1
     MP,DENS,5,0.1           * Density (very light)
```

```
      R,5,1.E-3,7.*4.225E-8,0.035 * Area,Iyy,Height
/COM
      MP,EX,6,6.003E7          * Young's modulus for the disc L1-T12
      MP,DENS,6,0.1            * Density (very light)
      R,6,1.E-3,7.*5.000E-8,0.035 * Area,Iyy,Height
/COM-------------------------------------------------------------
      MP,EX,7,4.529E7          * Young's modulus for the disc T12-T11
      MP,DENS,7,0.1            * Density (very light)
      R,7,1.E-3,7.*6.666E-8,0.035  * Area,Iyy,Height
/COM
      MP,EX,8,4.605E7          * Young's modulus for the disc T11-T10
      MP,DENS,8,0.1            * Density (very light)
      R,8,1.E-3,7.*8.000E-8,0.035  * Area,Iyy,Height
/COM
      MP,EX,9,4.415E7          * Young's modulus for the disc T10-T9
      MP,DENS,9,0.1            * Density (very light)
      R,9,1.E-3,7.*7.333E-8,0.035  * Area,Iyy,Height
/COM
      MP,EX,10,4.203E7         * Young's modulus for the disc T9-T8
      MP,DENS,10,0.1           * Density (very light)
      R,10,1.E-3,7.*7.333E-8,0.035 * Area,Iyy,Height
/COM
      MP,EX,11,4.046E7         * Young's modulus for the disc T8-T7
      MP,DENS,11,0.1           * Density (very light)
      R,11,1.E-3,7.*6.666E-8,0.035 * Area,Iyy,Height
/COM
      MP,EX,12,4.635E7         * Young's modulus for the disc T7-T6
      MP,DENS,12,0.1           * Density (very light)
      R,12,1.E-3,7.*5.556E-8,0.035 * Area,Iyy,Height
/COM
      MP,EX,13,5.411E7         * Young's modulus for the disc T6-T5
      MP,DENS,13,0.1           * Density (very light)
      R,13,1.E-3,7.*5.263E-8,0.035 * Area,Iyy,Height
/COM
      MP,EX,14,5.821E7         * Young's modulus for the disc T5-T4
      MP,DENS,14,0.1           * Density (very light)
      R,14,1.E-3,7.*4.762E-8,0.035 * Area,Iyy,Height
/COM
      MP,EX,15,4.194E7         * Young's modulus for the disc T4-T3
      MP,DENS,15,0.1           * Density (very light)
      R,15,1.E-3,7.*4.000E-8,0.035 * Area,Iyy,Height
/COM
      MP,EX,16,3.305E7         * Young's modulus for the disc T3-T2
      MP,DENS,16,0.1           * Density (very light)
      R,16,1.E-3,7.*3.333E-8,0.035 * Area,Iyy,Height
/COM
      MP,EX,17,1.943E7         * Young's modulus for the disc T2-T1
      MP,DENS,17,0.1           * Density (very light)
      R,17,1.E-3,7.*2.857E-8,0.035 * Area,Iyy,Height
/COM
      MP,EX,18,2.166E7         * Young's modulus for the disc T1-C7
      MP,DENS,18,0.1           * Density (very light)
      R,18,1.E-3,10.*2.774E-8,0.035 * Area,Iyy,Height
/COM-------------------------------------------------------------
      MP,EX,19,1.647E7         * Young's modulus for the disc C7-C6
      MP,DENS,19,0.1           * Density (very light)
      R,19,1.E-3,10.*2.169E-8,0.035 * Area,Iyy,Height
/COM
      MP,EX,20,1.642E7         * Young's modulus for the disc C6-C5
      MP,DENS,20,0.1           * Density (very light)
      R,20,1.E-3,10.*1.655E-8,0.035 * Area,Iyy,Height
/COM
      MP,EX,21,1.251E7         * Young's modulus for the disc C5-C4
      MP,DENS,21,0.1           * Density (very light)
```

```
      R,21,1.E-3,10.*1.511E-8,0.035 * Area,I_yy,Height
/COM
      MP,EX,22,1.184E7        * Young's modulus for the disc C4-C3
      MP,DENS,22,0.1          * Density (very light)
      R,22,1.E-3,10.*1.316E-8,0.035 * Area,I_yy,Height
/COM
      MP,EX,23,1.096E7        * Young's modulus for the disc C3-C2
      MP,DENS,23,0.1          * Density (very light)
      R,23,1.E-3,10.*1.143E-8,0.035 * Area,I_yy,Height
/COM
      MP,EX,24,0.280E7        * Young's modulus for the disc C2-C1
      MP,DENS,24,0.1          * Density (very light)
      R,24,1.E-3,10.*29.96E-8,0.035 * Area,I_yy,Height
/COM
      MP,EX,25,2.577E7        * Young's modulus for the disc C1-HEAD
      MP,DENS,25,0.1          * Density (very light)
      R,25,1.E-3,10.*7.272E-8,0.035 * Area,I_yy,Height
/COM
/COM
/COM---------------- For spinal or torso masses -----------------
/COM
      R,121,0.4659,0.09929E-2          * M,I at L5 level
      R,122,0.5621,0.1427E-2           * M,I at L4 level
      R,123,0.4325,0.1482E-2           * M,I at L3 level
      R,124,0.3420,0.1253E-2           * M,I at L2 level
      R,125,0.2842,0.1036E-2           * M,I at L1 level
/COM-------------------------------------------------------------
      R,126,0.3329,0.1270E-2           * M,I at T12 level
      R,127,0.3184,0.1283E-2           * M,I at T11 level
      R,128,1.352,0.6028E-2            * M,I at T10 level
      R,129,1.417,0.6164E-2            * M,I at T9 level
      R,130,1.326,0.5543E-2            * M,I at T8 level
      R,131,1.308,0.5374E-2            * M,I at T7 level
      R,132,1.948,0.4425E-2            * M,I at T6 level
      R,133,1.930,0.3838E-2            * M,I at T5 level
      R,134,1.819,0.3138E-2            * M,I at T4 level
      R,135,1.915,0.2878E-2            * M,I at T3 level
      R,136,1.829,0.2077E-2            * M,I at T2 level
      R,137,2.114,0.0745E-2            * M,I at T1 level
/COM-------------------------------------------------------------
      R,138,1.200,0.0775E-2            * M,I at C7 level
      R,139,0.900,0.0656E-2            * M,I at C6 level
      R,140,0.815,0.0601E-2            * M,I at C5 level
      R,141,0.815,0.0601E-2            * M,I at C4 level
      R,142,0.815,0.0601E-2            * M,I at C3 level
      R,143,0.815,0.0601E-2            * M,I at C2 level
      R,144,0.815,0.0601E-2            * M,I at C1 level
/COM
/COM
/COM------------------ For visceral springs --------------------
/COM
      R,42,1.29E4              * Spring rate for S1-L5 level
      R,43,1.68E4              * Spring rate for L5-L4 level
      R,44,1.64E4              * Spring rate for L4-L3 level
      R,45,1.91E4              * Spring rate for L3-L2 level
      R,46,2.24E4              * Spring rate for L2-L1 level
      R,47,2.42E4              * Spring rate for L1-T12 level
      R,48,2.62E4              * Spring rate for T12-T11 level
      R,49,2.86E4              * Spring rate for T11-T10 level
/COM
      R,50,3.E4                * Spring rate for the viscera-spine
                                 interconnecting springs
/COM
/COM
/COM
```

```
/COM------------------- For visceral masses --------------------
/COM
      R,51,1.708,0.1000E-2                * M,I at S1 level
      R,52,1.774,0.3781E-2                * M,I at L5 level
      R,53,1.625,0.4126E-2                * M,I at L4 level
      R,54,1.720,0.5927E-2                * M,I at L3 level
      R,55,1.670,0.6119E-2                * M,I at L2 level
      R,56,1.676,0.5870E-2                * M,I at L1 level
      R,57,1.341,0.5079E-2                * M,I at T12 level
      R,58,1.282,0.5130E-2                * M,I at T11 level
/COM
/COM
/COM---------------------- For pelvic mass ----------------------
/COM
      R,70,16.879,1.5*0.0942          * M,I
/COM
/COM
/COM----------------------- For head mass -----------------------
/COM
      R,80,4.5,2.0E-2                 * M,I
/COM
/COM
/COM---------------- For buttocks tissue springs -----------------
/COM
/COM  For the front beam
      MP,EX,71,9.825E5                * Young's modulus
      MP,DENS,71,0.1                  * Density (very light)
      R,71,0.1E-2,5.E-7,0.01          * Area,Iyy,Height
/COM  For the rear beam
      MP,EX,73,9.825E5                * Young's modulus
      MP,DENS,73,0.1                  * Density (very light)
      R,73,0.8E-2,5.E-7,0.01          * Area,Iyy,Height
/COM
/COM
/COM------- For large mass at the seat-buttocks interface -------
/COM
      R,72,1000,0                     * M(very heavy),I
/COM
/COM
/COM---------------------- For rigid links ----------------------
/COM
      MP,EX,60,1.E10                 * Young's modulus (very stiff)
      MP,DENS,60,0.1                 * Density (very light)
      R,60,0.1E-3,1.E-2,0.01         * Area,Iyy,Height
/COM
/COM
/COM================================================================
/COM===  Definition of nodes                                     ===
/COM===  Model is built in X-Y plane (X+;foreword,Y+;upward).    ===
/COM===  The origin of the global coordinate system is           ===
/COM===  located at the centre of the L3 body.                   ===
/COM================================================================
/COM
/COM------ Locate the origin at the L3 vertebral body centre ----
/COM
      X0=-6.124E-2
      Y0=24.510E-2
/COM
/COM
/COM---------- Location of the ischial tuberosities ------------
/COM
      XTUB=0.E-2-X0       * Location of the ischial tuberosities
      YTUB=0.E-2-Y0
/COM
```

```
/COM
/COM--------- Location of the vertebral body centres ------------
/COM
      XS1=-9.488E-2-X0
      YS1=13.238E-2-Y0
      N,41,XS1,YS1                    * Location of S1
/COM
      XL5=-8.420E-2-X0
      YL5=16.513E-2-Y0
      N,35,XL5,YL5                    * Location of L5
/COM
      XL4=-7.109E-2-X0
      YL4=20.467E-2-Y0
      N,34,XL4,YL4                    * location of L4
/COM
      XL3=-6.124E-2-X0
      YL3=24.510E-2-Y0
      N,33,XL3,YL3                    * Location of L3
/COM
      XL2=-5.795E-2-X0
      YL2=28.365E-2-Y0
      N,32,XL2,YL2                    * Location of L2
/COM
      XL1=-5.911E-2-X0
      YL1=31.985E-2-Y0
      N,31,XL1,YL1                    * Location of L1
/COM
/COM-------------------------------------------------------------
/COM
      XT12=-6.205E-2-X0
      YT12=35.307E-2-Y0
      N,22,XT12,YT12                  * Location of T12
/COM
      XT11=-6.495E-2-X0
      YT11=38.313E-2-Y0
      N,21,XT11,YT11                  * Location of T11
/COM
      XT10=-6.703E-2-X0
      YT10=41.375E-2-Y0
      N,20,XT10,YT10                  * Location of T10
/COM
      XT9=-6.762E-2-X0
      YT9=44.318E-2-Y0
      N,19,XT9,YT9                    * Location of T9
/COM
      XT8=-6.648E-2-X0
      YT8=47.117E-2-Y0
      N,18,XT8,YT8                    * Location of T8
/COM
      XT7=-6.346E-2-X0
      YT7=49.797E-2-Y0
      N,17,XT7,YT7                    * Location of T7
/COM
      XT6=-5.856E-2-X0
      YT6=52.325E-2-Y0
      N,16,XT6,YT6                    * Location of T6
/COM
      XT5=-5.087E-2-X0
      YT5=55.067E-2-Y0
      N,15,XT5,YT5                    * Location of T5
/COM
      XT4=-4.179E-2-X0
      YT4=57.686E-2-Y0
      N,14,XT4,YT4                    * Location of T4
```

```
/COM
      XT3=-3.179E-2-X0
      YT3=60.297E-2-Y0
      N,13,XT3,YT3                  * Location of T3
/COM
      XT2=-2.176E-2-X0
      YT2=62.861E-2-Y0
      N,12,XT2,YT2                  * Location of T2
/COM
      XT1=-1.207E-2-X0
      YT1=65.463E-2-Y0
      N,11,XT1,YT1                  * Location of T1
/COM
/COM-------------------------------------------------------------
/COM
      XC7=-0.805E-2-X0
      YC7=67.036E-2-Y0
      N,7,XC7,YC7                   * Location of C7
/COM
      XC6=-0.403E-2-X0
      YC6=68.609E-2-Y0
      N,6,XC6,YC6                   * Location of C6
/COM
      XC5=0.017E-2-X0
      YC5=70.254E-2-Y0
      N,5,XC5,YC5                   * Location of C5
/COM
      XC4=0.407E-2-X0
      YC4=71.780E-2-Y0
      N,4,XC4,YC4                   * Location of C4
/COM
      XC3=0.792E-2-X0
      YC3=73.289E-2-Y0
      N,3,XC3,YC3                   * Location of C3
/COM
      XC2=1.180E-2-X0
      YC2=74.807E-2-Y0
      N,2,XC2,YC2                   * Location of C2
/COM
      XC1=1.411E-2-X0
      YC1=75.710E-2-Y0
      N,1,XC1,YC1                   * Location of C1
/COM
/COM
/COM------------ Location of the head mass centre ---------------
/COM
      XHM=2.5700E-2-X0
      YHM=80.250E-2-Y0
      N,300,XHM,YHM             * Location of the head mass centre
/COM
/COM
/COM------------ Locations of spinal or torso masses ------------
/COM
      LOCAL,35,0,XL5,YL5        * Local coordinate system as No.35
      N,135,-6.335E-2,0.        * Spinal mass for the L5 level
/COM
      LOCAL,34,0,XL4,YL4        * Local coordinate system as No.34
      N,134,-3.542E-2,0.        * Spinal mass for the L4 level
/COM
      LOCAL,33,0,XL3,YL3        * Local coordinate system as No.33
      N,133,-1.007E-2,0.        * Spinal mass for the L3 level
/COM
      LOCAL,32,0,XL2,YL2        * Local coordinate system as No.32
      N,132,-2.233E-2,0.        * Spinal mass for the L2 level
```

```
/COM
      LOCAL,31,0,XL1,YL1        * Local coordinate system as No.31
      N,131,-2.917E-2,0.        * Spinal mass for the L1 level
/COM
/COM-----------------------------------------------------------------
/COM
      LOCAL,22,0,XT12,YT12      * Local coordinate system as No.22
      N,122,-0.558E-2,0.        * Spinal mass for the T12 level
/COM
      LOCAL,21,0,XT11,YT11      * Local coordinate system as No.21
      N,121,-0.636E-2,0.        * Spinal mass for the T11 level
/COM
      LOCAL,20,0,XT10,YT10      * Local coordinate system as No.20
      N,120,3.64E-2,0.          * Torso mass for the T10 level
/COM
      LOCAL,19,0,XT9,YT9        * Local coordinate system as No.19
      N,119,3.81E-2,0.          * Torso mass for the T9 level
/COM
      LOCAL,18,0,XT8,YT8        * Local coordinate system as No.18
      N,118,3.22E-2,0.          * Torso mass for the T8 level
/COM
      LOCAL,17,0,XT7,YT7        * Local coordinate system as No.17
      N,117,2.80E-2,0.          * Torso mass for the T7 level
/COM
      LOCAL,16,0,XT6,YT6        * Local coordinate system as No.16
      N,116,2.88E-2,0.          * Torso mass for the T6 level
/COM
      LOCAL,15,0,XT5,YT5        * Local coordinate system as No.15
      N,115,2.50E-2,0.          * Torso mass for the T5 level
/COM
      LOCAL,14,0,XT4,YT4        * Local coordinate system as No.14
      N,114,3.08E-2,0.          * Torso mass for the T4 level
/COM
      LOCAL,13,0,XT3,YT3        * Local coordinate system as No.13
      N,113,1.351E-2,0.         * Torso mass for the T3 level
/COM
      LOCAL,12,0,XT2,YT2        * Local coordinate system as No.12
      N,112,1.351E-2,0.         * Torso mass for the T2 level
/COM
      LOCAL,11,0,XT1,YT1        * Local coordinate system as No.11
      N,111,1.351E-2,0.         * Torso mass for the T1 level
/COM
/COM
/COM------------- Locations of the visceral masses --------------
/COM
      LOCAL,39,0,XS1,YS1  * Local coordinate system as No.39
      N,241,4.28E-2,0.    * Visceral mass at the S1 level
/COM
      CSYS,35             * Activate local coordinate system No.35
      N,235,4.28E-2,0.    * Visceral mass at the L5 level
/COM
      CSYS,34             * Activate local coordinate system No.34
      N,234,4.24E-2,0.    * Visceral mass at the L4 level
/COM
      CSYS,33             * Activate local coordinate system No.33
      N,233,3.97E-2,0.    * Visceral mass at the L3 level
/COM
      CSYS,32             * Activate local coordinate system No.32
      N,232,3.65E-2,0.    * Visceral mass at the L2 level
/COM
      CSYS,31             * Activate local coordinate system No.31
      N,231,3.98E-2,0.    * Visceral mass at the L1 level
/COM
      CSYS,22             * Activate local coordinate system No.22
```

```
      N,222,4.47E-2,0.     * Visceral mass at the T12 level
/COM
      CSYS,21              * Activate local coordinate system No.21
      N,221,4.39E-2,0.     * Visceral mass at the T11 level
/COM
      CSYS,20              * Activate local coordinate system No.20
      N,220,4.64E-2,0.     * Viscera fixing point at the level T10
/COM
/COM
/COM--- Rotate the degrees of freedom of the visceral masses ----
/COM
      CS,38,0,241,235,41
      NROTATE,241,241,1
      CS,38,0,235,234,135
      NROTATE,235,235,1
      CS,38,0,234,233,134
      NROTATE,234,234,1
      CS,38,0,233,232,133
      NROTATE,233,233,1
      CS,38,0,232,231,132
      NROTATE,232,232,1
      CS,38,0,231,222,131
      NROTATE,231,231,1
      CS,38,0,222,221,122
      NROTATE,222,222,1
      CS,38,0,221,220,121
      NROTATE,221,221,1
/COM
/COM
/COM---------- Reference points on the body surface -------------
/COM
      CSYS,39              * Activate local coordinate system No.39
      N,641,-4.000E-2,0.   * Body surface on S1
      CS,19,0,41,35,641
      NROTATE,641,641,1    * Rotate the degrees of freedom
/COM
      CSYS,33              * Activate local coordinate system No.33
      N,633,-7.914E-2,-0.460E-2    * Body surface on L3
      CS,19,0,33,32,633
      NROTATE,633,633,1    * Rotate the degrees of freedom
/COM
      CSYS,21              * Activate local coordinate system No.21
      N,621,-7.293E-2,-1.400E-2    * Body surface on T11
      CS,19,0,21,20,621
      NROTATE,621,621,1    * Rotate the degrees of freedom
/COM
      CSYS,16              * Activate local coordinate system No.16
      N,616,-6.856E-2,-1.400E-2    * Body surface on T6
      CS,19,0,16,15,616
      NROTATE,616,616,1    * Rotate the degrees of freedom
/COM
      CSYS,11              * Activate local coordinate system No.11
      N,611,-6.456E-2,-1.400E-2    * Body surface on T1
      CS,19,0,11,7,611
      NROTATE,611,611,1    * Rotate the degrees of freedom
/COM
      HANG=-14.33+14.15    * Head angle
      LOCAL,38,0,XHM,YHM,,HANG  * Local coordinate system as No.38
      N,610,2.E-2,-6.5E-2  * Point on the bite-bar
      NROTATE,610,610,1    * Rotate the degrees of freedom
/COM
/COM
/COM------------------- Define head shape ----------------------
/COM
```

```
      LOCAL,38,1,XHM,YHM,,HANG     * Local cylindrical coord.Sys.
      N,311,9.013E-2,-180.         * No.38
      N,322,9.013E-2,150.
      FILL,311,322,10,312,1        * Circle chape
/COM
/COM
/COM------------------ Define pelvis shape ----------------------
/COM
      SCPV=1.29                    * Scale factor for the pelvis
/COM
      LOCAL,11,0,XTUB,YTUB,,-0.8   * Initial pelvic angle
/COM
      N,411,-8.231E-2*SCPV,16.457E-2*SCPV
      N,412,-10.558E-2*SCPV,10.078E-2*SCPV
      N,413,-8.317E-2*SCPV,4.259E-2*SCPV
      N,414,-4.098E-2*SCPV,1.889E-2*SCPV
      N,415,-6.981E-2*SCPV,5.251E-2*SCPV
      N,416,-6.981E-2*SCPV,7.406E-2*SCPV
      N,417,-5.300E-2*SCPV,9.130E-2*SCPV
      N,418,-4.007E-2*SCPV,8.268E-2*SCPV
      N,419,-1.723E-2*SCPV,0.940E-2*SCPV
      N,420,0.000E-2*SCPV,0.000E-2*SCPV  *<-- Ischial tuberosities
      N,421,1.816E-2*SCPV,0.423E-2*SCPV
      N,422,6.209E-2*SCPV,7.837E-2*SCPV
      N,423,1.812E-2*SCPV,9.031E-2*SCPV
      N,424,1.683E-2*SCPV,14.518E-2*SCPV
      N,425,-2.412E-2*SCPV,16.457E-2*SCPV
/COM
/COM
/COM--------------- Location of the pelvic mass -----------------
/COM
      XPM=-2.E-2*SCPV
      YPM=8.E-2*SCPV
      N,400,XPM,YPM                      * Pelvic mass
/COM
/COM
/COM---------- Locations of the buttocks tissue beams -----------
/COM
      LOCAL,11,0,XTUB,YTUB,,0    * Local coordinate system as No.11
      N,450,-8.257E-2*SCPV,0.    * Node for a rigid link
      N,460,-4.E-2*SCPV,0.       * Rear upper end
      N,430,-4.E-2*SCPV,-0.1     * Rear lower end
      N,470,3.E-2*SCPV,0.        * Front upper end
      N,440,3.E-2*SCPV,-0.1      * Front lower end
/COM
/COM
/COM------------ Location of the force applied node ------------
/COM
      N,500,-0.5E-2*SCPV,-0.1    * Load applied node
/COM
/COM
/COM================================================================
/COM===                                                          ===
/COM===              Definition of elements                      ===
/COM===                                                          ===
/COM================================================================
/COM
/COM------------------ Place spinal beams ----------------------
/COM
      TYPE,1
      REAL,1
      MAT,1
      E,41,35                          * Beam for the spine S1-L5
/COM
```

```
      REAL,2
      MAT,2
      E,35,34                          * Beam for the spine L5-L4
/COM
      REAL,3
      MAT,3
      E,34,33                          * Beam for the spine L4-L3
/COM
      REAL,4
      MAT,4
      E,33,32                          * Beam for the spine L3-L2
/COM
      REAL,5
      MAT,5
      E,32,31                          * Beam for the spine L2-L1
/COM
      REAL,6
      MAT,6
      E,31,22                          * Beam for the spine L1-T12
/COM-------------------------------------------------------------
      REAL,7
      MAT,7
      E,22,21                          * Beam for the spine T12-T11
/COM
      REAL,8
      MAT,8
      E,21,20                          * Beam for the spine T11-T10
/COM
      REAL,9
      MAT,9
      E,20,19                          * Beam for the spine T10-T9
/COM
      REAL,10
      MAT,10
      E,19,18                          * Beam for the spine T9-T8
/COM
      REAL,11
      MAT,11
      E,18,17                          * Beam for the spine T8-T7
/COM
      REAL,12
      MAT,12
      E,17,16                          * Beam for the spine T7-T6
/COM
      REAL,13
      MAT,13
      E,16,15                          * Beam for the spine T6-T5
/COM
      REAL,14
      MAT,14
      E,15,14                          * Beam for the spine T5-T4
/COM
      REAL,15
      MAT,15
      E,14,13                          * Beam for the spine T4-T3
/COM
      REAL,16
      MAT,16
      E,13,12                          * Beam for the spine T3-T2
/COM
      REAL,17
      MAT,17
      E,12,11                          * Beam for the spine T2-T1
/COM
```

```
      REAL,18
      MAT,18
      E,11,7                          * Beam for the spine T1-C7
/COM-------------------------------------------------------------
      REAL,19
      MAT,19
      E,7,6                           * Beam for the spine C7-C6
/COM
      REAL,20
      MAT,20
      E,6,5                           * Beam for the spine C6-C5
/COM
      REAL,21
      MAT,21
      E,5,4                           * Beam for the spine C5-C4
/COM
      REAL,22
      MAT,22
      E,4,3                           * Beam for the spine C4-C3
/COM
      REAL,23
      MAT,23
      E,3,2                           * Beam for the spine C3-C2
/COM
      REAL,24
      MAT,24
      E,2,1                           * Beam for the spine C2-C1
/COM
      REAL,25
      MAT,25
      E,1,300                         * Beam for the joint C1-HEAD
/COM
/COM
/COM-------------- Place spinal or torso masses -----------------
/COM
      TYPE,2
      REAL,121
      E,135                           * Spinal mass at L5 level
/COM
      REAL,122
      E,134                           * Spinal mass at L4 level
/COM
      REAL,123
      E,133                           * Spinal mass at L3 level
/COM
      REAL,124
      E,132                           * Spinal mass at L2 level
/COM
      REAL,125
      E,131                           * Spinal mass at L1 level
/COM-------------------------------------------------------------
      REAL,126
      E,122                           * Spinal mass at T12 level
/COM
      REAL,127
      E,121                           * Spinal mass at T11 level
/COM
      REAL,128
      E,120                           * Torso mass at T10 level
/COM
      REAL,129
      E,119                           * Torso mass at T9 level
/COM
```

```
      REAL,130
      E,118                          * Torso mass at T8 level
/COM
      REAL,131
      E,117                          * Torso mass at T7 level
/COM
      REAL,132
      E,116                          * Torso mass at T6 level
/COM
      REAL,133
      E,115                          * Torso mass at T5 level
/COM
      REAL,134
      E,114                          * Torso mass at T4 level
/COM
      REAL,135
      E,113                          * Torso mass at T3 level
/COM
      REAL,136
      E,112                          * Torso mass at T2 level
/COM
      REAL,137
      E,111                          * Torso mass at T1 level
/COM-----------------------------------------------------------------
      REAL,138
      E,7                            * Neck mass at C7 level
/COM
      REAL,139
      E,6                            * Neck mass at C6 level
/COM
      REAL,140
      E,5                            * Neck mass at C5 level
/COM
      REAL,141
      E,4                            * Neck mass at C4 level
/COM
      REAL,142
      E,3                            * Neck mass at C3 level
/COM
      REAL,143
      E,2                            * Neck mass at C2 level
/COM
      REAL,144
      E,1                            * Neck mass at C1 level
/COM
/COM
/COM--------------- Connect spinal beams and spinal -------------
/COM--------------- or torso masses by rigid links  -------------
/COM
      TYPE,1
      REAL,60
      MAT,60
      E,35,135                 * Connect spine L5 and spinal mass
      E,34,134                 * Connect spine L4 and spinal mass
      E,33,133                 * Connect spine L3 and spinal mass
      E,32,132                 * Connect spine L2 and spinal mass
      E,31,131                 * Connect spine L1 and spinal mass
      E,22,122                 * Connect spine T12 and spinal mass
      E,21,121                 * Connect spine T11 and spinal mass
      E,20,120                 * Connect spine T10 and torso mass
      E,19,119                 * Connect spine T9 and torso mass
      E,18,118                 * Connect spine T8 and torso mass
      E,17,117                 * Connect spine T7 and torso mass
      E,16,116                 * Connect spine T6 and torso mass
```

```
      E,15,115                  * Connect spine T5 and torso mass
      E,14,114                  * Connect spine T4 and torso mass
      E,13,113                  * Connect spine T3 and torso mass
      E,12,112                  * Connect spine T2 and torso mass
      E,11,111                  * Connect spine T1 and torso mass
/COM
/COM
/COM------------------- Place pelvic mass ----------------------
/COM
      TYPE,2
      REAL,70
      E,400
/COM
/COM
/COM----------- Place rigid links for pelvis shape -------------
/COM
      TYPE,1
      REAL,60
      MAT,60
      E,411,412
      EGEN,14,1,-1
      E,425,411
/COM
/COM
/COM-------- Connect the bottom of the viscera to the pelvis ----
/COM
      E,400,241
      E,41,241
      E,41,400
      E,41,412
/COM
/COM
/COM------- Connect the top of the viscera to the spine ---------
/COM
      E,20,220
/COM
/COM
/COM------------------ Place visceral springs -------------------
/COM
      TYPE,3
      REAL,42
      E,241,235           * Between visceral masses at S1 and L5
/COM
      REAL,43
      E,235,234           * Between visceral masses at L5 and L4
/COM
      REAL,44
      E,234,233           * Between visceral masses at L4 and L3
/COM
      REAL,45
      E,233,232           * Between visceral masses at L3 and L2
/COM
      REAL,46
      E,232,231           * Between visceral masses at L2 and L1
/COM
      REAL,47
      E,231,222           * Between visceral masses at L1 and T12
/COM
      REAL,48
      E,222,221           * Between visceral masses at T12 and T11
/COM
      REAL,49
      E,221,220           * Between visceral mass at T11 and T10
/COM
```

```
/COM
/COM-------- Place viscera-spine interconnecting springs --------
/COM
      REAL,50
      E,35,235                          * At L5 level
      E,34,234                          * At L4 level
      E,33,233                          * At L3 level
      E,32,232                          * At L2 level
      E,31,231                          * At L1 level
      E,22,222                          * At T12 level
      E,21,221                          * At T11 level
      E,20,220                          * At T10 level
/COM
/COM
/COM------------------ Place visceral masses ---------------------
/COM
      TYPE,2
      REAL,51
      E,241                             * Mass at S1 level
      REAL,52
      E,235                             * Mass at L5 level
      REAL,53
      E,234                             * Mass at L4 level
      REAL,54
      E,233                             * Mass at L3 level
      REAL,55
      E,232                             * Mass at L2 level
      REAL,56
      E,231                             * Mass at L1 level
      REAL,57
      E,222                             * Mass at T12 level
      REAL,58
      E,221                             * Mass at T11 level
/COM
/COM
/COM---------------------- Place head mass -----------------------
/COM
      TYPE,2
      REAL,80
      E,300
/COM
/COM
/COM------------- Place rigid links for head shape --------------
/COM
      TYPE,1
      REAL,60
      MAT,60
      E,311,312
      EGEN,11,1,-1
      E,322,311
      E,300,317
/COM
/COM
/COM--------- Connect the reference points on the body ----------
/COM--------- surface to the spine                    ----------
/COM
      TYPE,1
      REAL,60
      MAT,60
      E,641,41                           * At S1 level
      E,633,33                           * At L3 level
      E,621,21                           * At T11 level
      E,616,16                           * At T6 level
      E,611,11                           * At T1 level
```

```
      E,610,315                          * At the head
/COM
/COM
/COM-------------- Place buttocks tissue springs ---------------
/COM
      TYPE,1
      REAL,71                            * Front beam
      MAT,71
      E,470,440
/COM
      REAL,73                            * Rear beam
      MAT,73
      E,460,430
/COM
/COM
/COM-------- Place a large mass at the force applied node -------
/COM
      TYPE,2
      REAL,72
      E,500
/COM
/COM
/COM--------- Connect buttocks tissue beams to the pelvis -------
      TYPE,1
      REAL,60
      MAT,60
      E,413,450
      E,450,460
      E,460,470
      E,470,420
/COM
      E,430,500
      E,440,500
/COM
/COM
/COM-------- Coupling and constraining motion for load input ----
/COM
      CP,1,UY,430,440                    * Coupling motion
/COM
      D,430,UX,0,0,440,10,ROTZ           * Constraining displacement
/COM
/COM
/COM================================================================
/COM============                                    ===============
/COM============          Control calculation       ===============
/COM============                                    ===============
/COM================================================================
/COM
/COM-------- Sort wave front for efficient calculation ----------
/COM
      WSORT,Y
/COM
/COM
/COM------------ Define master degrees of freedom ---------------
/COM
      M,1,UY,1,1,UX,ROTZ                 * All degrees of freedom at the
      M,2,UY,2,1,UX,ROTZ                 * neck masses
      M,3,UY,3,1,UX,ROTZ
      M,4,UY,4,1,UX,ROTZ
      M,5,UY,5,1,UX,ROTZ
      M,6,UY,6,1,UX,ROTZ
      M,7,UY,7,1,UX,ROTZ
/COM-----------------------------------------------------------
      M,111,UY,111,1,UX,ROTZ             * All degrees of freedom at the
```

```
      M,112,UY,112,1,UX,ROTZ        * torso masses
      M,113,UY,113,1,UX,ROTZ
      M,114,UY,114,1,UX,ROTZ
      M,115,UY,115,1,UX,ROTZ
      M,116,UY,116,1,UX,ROTZ
      M,117,UY,117,1,UX,ROTZ
      M,118,UY,118,1,UX,ROTZ
      M,119,UY,119,1,UX,ROTZ
      M,120,UY,120,1,UX,ROTZ
      M,121,UY,121,1,UX,ROTZ
      M,122,UY,122,1,UX,ROTZ
      M,131,UY,131,1,UX,ROTZ
      M,132,UY,132,1,UX,ROTZ
      M,133,UY,133,1,UX,ROTZ
      M,134,UY,134,1,UX,ROTZ
      M,135,UY,135,1,UX,ROTZ
/COM-----------------------------------------------------------------
      M,241,UX,241,1                * Only longitudinal direction
      M,235,UX,235,1                * at the visceral masses
      M,234,UX,234,1                * (axes have been rotated)
      M,233,UX,233,1
      M,232,UX,232,1
      M,231,UX,231,1
      M,222,UX,222,1
      M,221,UX,221,1
/COM
      M,641,UY,641,1,UX,ROTZ        * All degrees of freedom at the
      M,633,UY,633,1,UX,ROTZ        * reference points on the body
      M,621,UY,621,1,UX,ROTZ        * surface
      M,616,UY,616,1,UX,ROTZ        * (axes have been rotated)
      M,611,UY,611,1,UX,ROTZ
      M,610,UY,610,1,UX,ROTZ
/COM
      M,400,UY,400,1,UX,ROTZ        * At the pelvic mass
      M,300,UY,300,1,UX,ROTZ        * At the head mass
      M,500,UY,500,1                * For load input
/COM
/COM
/COM------------------ Control output listing --------------------
/COM
      ITER,1,1,1
/COM
/COM
/COM-------- Define frequency range for mode extraction ---------
/COM
      EXTMODE,0.,50                 * Extract modes below 50 Hz
/COM
/COM
/COM----------------------- Plot model ----------------------------
/COM
      /PBC,ALL,1
      EPLOT
/COM
/COM
/COM--------------- Write data into FILE27.DAT -------------------
/COM
      AFWRITE
      SAVE
```

REFERENCES

Amirouche,F.M.L. and Ider,S.K. (1988). Simulation and analysis of a biodynamic human model subjected to low accelerations-A correlation study. *Journal of Sound and Vibration 123(2): 281-292.*

Bartz,J.A. (1972). Validation of a three dimensional methematical model of the crash victim. *Proceedings of a Symposium on Human Impact and Response, Warren, Michigan 1973.*

Belytschko,T., Schwer,L. and Schultz,A. (1976). A model for analytic investigation of three dimensional head-spine dynamics. *Aerospace Medical Research Laboratory, Wright-Patterson Air Force Base, Ohio, Report No. AMRL-TR-76-10.*

Belytschko,T., Schwer,L. and Privitzer,E. (1978). Theory and application of a three-dimensional model of the human spine. *Aviation, Space, and Environmental Medicine: 158-165.*

Belytschko,T. and Privitzer,E. (1978a). A three dimensional discrete element dynamic model of the spine, head and torso. *AGARD Conference Proceedings 253(A9): 1-15.*

Belytschko,T. and Privitzer,E. (1978b). Refinement and validation of a three-dimensional head-spine model. *Aerospace Medical Research Laboratory, Wright-Patterson Air Force Base, Ohio, Report No. AMRL-TR-78-7.*

Belytschko,T., Rencis,M. and Williams,J. (1985). Head-spine structure modelling: enhancements to secondary loading path model and validation of head-cervical spine model. *Armstrong Airospace Medical Research Laboratory, Wright-Patterson Air Force Base, Ohio, Report No. AAMRL-TR-85-019.*

British Standards Institution (1987). Measurement and evaluation of human exposure to whole-body mechanical vibration and repeated shock. *BS6841. London: British Standards Institution.*

Broman,H., Pope,M.H., Benda,M., Svensson,M., Ottosson,C. and Hansson,T. (1991). The impact response of the seated subject. *Journal of Orthopaedic Research 9: 150-154.*

Christ,W. and Dupuis,H. (1963). The influence of vertical vibrations on the spine and stomach. *Zentralblatt fur Arbeitsmedizin und Arbeitsschutz 13:3-9. (Translated from the German by Brown,B.M., National Institute of Agricultural Engineering Translation 153).*

Christ,W. and Dupuis,H. (1966). Uber die Beanspruchung der Wirbelsaule unter dem Einfluss sinusformiger und stochastischer Schwingungen. *International Zeitschrift angewandte Physiologie einschliesslich Arbeitsphysiologie 22: 258-278.*

Coermann,R.R. (1962). The mechanical impedance of the human body in sitting and standing position at low frequencies. *Human Factors 4(10): 227-253.*

Coermann,R.R., Ziegenruecker,G.H., Wittwer,A.L. and Von Gierke,H.E. (1960). The passive dynamic mechanical properties of the human thorax-abdomen system and of the whole body system. *Aerospace Medicine 31: 443-455.*

Collier,R.J. and Donarski,R.J. (1987). Non-invasive method of measuring resonant frequency of a human tibia *in vivo* part 1. *Journal of Biomechanical Engineering, Vol.9, 321-328.*

Cramer,H.J., Liu,Y.K. and von Rosenberg,D.U. (1976). A distributed parameter model of the inertially loaded human spine. *Journal of Biomechanics 9: 115-130.*

Dobson,B.J. (1987). A straight-line technique for extracting modal properties from frequency response data. *Mechanical systems and signal processing 1(1): 29-40.*

Donati.P.M. and Bonthoux,C. (1983). Biodynamic response of the human body in the sitting position when subjected to vertical vibration. *Journal of Sound and Vibration 90(3): 423-442.*

Eycleshymer,A.C. and Shoemaker,D.M. (1970). A cross-section anatomy. *Meredith corporation.*

Fairley,T.E. and Griffin,M.J. (1989). The apparent mass of the seated human body: vertical vibration. *Journal of Biomechanics 22(2): 81-94.*

Griffin,M.J. (1975). Vertical vibration of seated subjects: effects of posture, vibration level, and frequency. *Aviation, Space and Environmental Medicine 46(3): 269-276.*

Griffin,M.J. (1990). Handbook of human vibration. *Academic press, London, ISBN 0-12-303040-4.*

Griffin,M.J., Lewis,C.H., Parsons,K.C. and Whitham,E.M. (1978). The biodynamic response of the human body and its application to standards. *AGARD Conference Proceedings 253 (A28): 1-18.*

Hagena,F.W., Wirth,C.J., Piehler,C.J., Plitz,W., Hofmann,G.O. and Zwingers,Th. (1985). In-vivo experiments on the response of the human spine to sinusoidal Gz-vibration. *AGARD Conference Proceeings 378(16): 1-12.*

Hagena,F.W., Piehler,C.J., Hofmann,G.O. and Zwingers,Th. (1986). The dynamic response of the human spine to sinusoidal Gz-vibration. In-vivo-Experiments. *Neuro-Orthopedics 2: 29-33.*

Hess,J.L. and Lombard,C.F. (1958). Theoretical investigations of dynamic response of man to high vertical accelerations. *Aviation Medicine 29: 66-75.*

Hinz,B. and Seidel,H. (1987). The nonlinearity of the human body's dynamic response during sinusoidal whole body vibration. *Industrial Health 25: 169-181.*

Hinz,B., Seidel,H., Brauer,D., Menzel,G., Bluthner,R. and Erdmann,U. (1988a). Bidimensional accelerations of lumbar vertebrae and estimation of internal spinal load during sinusoidal vertical whole-body vibration: a pilot study. *Clinical Biomechanics 3: 241-248.*

Hinz,B., Seidel,H., Brauer,D., Menzel,G., Bluthner,R. and Erdmann,H. (1988b). Examination of spinal column vibrations: a non-invasive approach. *European Journal of Applied Physiology, Vol.57, 707-713.*

Hopkins,G.R. (1971). Nonlinear lumped parameter mathematical model of dynamic

response of the human body. *Aerospace Medical Research Laboratory, Wright-Patterson Air Force Base, Ohio, Report No. AMRL-TR-71-29: 649-699.*

Hubbard,R.P. and McLeod D.G. (1978). Geometric, inertial and joint characteristics of two part 572 dummies for occupant modelling. *Society of automotive engineers SAE 770937: 3252-3267.*

International Organization for Standardization (1981). Vibration and shock – Mechanical driving point impedance of the human body. *ISO5982. International Organization for Standardization, Geneva.*

International Organization for Standardization (1985). Evaluation of human exposure to whole-body vibration – Part1: General requirements. *ISO2631/1-1985. International Organization for Standardization, Geneva.*

International Organization for Standardization (1987). Mechanical vibration and shock – Mechanical transmissibility of the human body in the z direction. *ISO7962. International Organization for Standardization, Geneva.*

Kim,W., Voloshin,A.S. and Johnson,S.H. (1993). Measurement of the impulsive bone motion by skin-mounted accelerometers. *Journal of Biomechanical Engineering, Vol.115, 47-52.*

Krause,H.E. and Shirazi,M. (1971). The transverse response of the lumbar spine under longitudinal loads. *Aerospace Medical Research Laboratory, Wright-Patterson Air Force Base, Ohio, Report No. AMRL-TR-71-29: 621-648.*

Latham,F. (1957). A study in body ballistics: seat ejection. *Proceedings of the Royal Society B-147: 121-139.*

Li,T.F.,Advani,S.H. and Lee,Y-C. (1971). The effect of initial curvature on the dynamic response of the spine to axial acceleration. *Aerospace Medical Research Laboratory, Wright-Patterson Air Force Base, Ohio, Report No. AMRL-TR-71-29: 553-569.*

Liu,Y.K. and Murray,J.D. (1966). A theoretical study of the effect of impulse on the human torso. *Proceedings of American Society of Mechanical Engineers Symposium on Biomechanics: 167-186.*

Liu,Y.K. and Wickstrom,J.K. (1973). Estimation of the inertial property distribution of the human torso from segmented cadaveric data. *Perspectives in Biomedical Engineering, Proceedings of a symposium organised in association with the Biological Engineering Society at Glasgow, 1972.*

Magnusson,M., Pope,M., Rostedt,M. and Hansson,T. (1993). Effect of backrest inclination on the transmission of vertical vibrations through the lumbar spine. *Clinical Biomechanics 8:5-12.*

Mawn,S.V., Lambert,J.J. and Catyb,Jr,J.L. (1992). The relationship between head and neck anthropometry and kinematic response during impact acceleration. *Aviation, Space and Environmental Medicine: 32-36*

McConville,J.T., Churchill,T.D., Kaleps,I., Clauser,C.E. and Cuzzi,J. (1980). Anthropometric relationships of body and body segment inertia. *Air Force Aerospace Medical Research Laboratory, Wright-Patterson Air Force Bace, Ohio, Report No. AFAMRL-TR-80-119.*

Mertens,H. and Vogt,L. (1978). The response of a realistic computer model for sitting humans to different types of shocks. *AGARD Coference Proceedings 253(A26): 1-17.*

Messenger,A.J. (1987). Effects of pelvic angle on the transmission of vertical vibration to the heads of seated subjects. *Proceedings of the United Kingdom Informal Group Meeting on Human Response to Vibration.*

Messenger,A.J. (1989). Correlation of spinal posture and the transmission of vertical vibration to the heads of seated subjects. *Proceedings of the United Kingdom Informal Group Meeting on Human Response to Vibration.*

Miwa,T. (1975). Mechanical impedance of human body in various postures. *Industrial Health 13(1):1-22.*

Moffatt,C.A., Advani,S.H. and Lin,C-J. (1971). Analytical and experimental investigations of human spine flexure. *American Society of Mechanical Engineers, 71-WA/BHF-7: 1-12.*

Muksian,R. and Nash,Jr,C.D. (1974). A model for the response of seated humans to sinusoidal displacements of the seat. *Journal of Biomechanics 7: 209-215.*

Muksian,R. and Nash,Jr,C.D. (1976). On frequency-dependent damping coefficients in lumped-parameter models of human beings. *Journal of Biomechanics 9: 339-342.*

NASA (1978). Anthropometric source book Volume 1: Anthropometry for designers. *NASA Reference publication 1024.*

Nigam,S.P. and Malik,M. (1987). A study on a vibratory model of a human body. *Journal of Biomechanical Engineering 109(2): 149-153.*

Nokes,L., Fairclough,J.A., Mintowt-Czyz,W.J., Mackie,I. and Williams,J. (1984). Vibration analysis of human tibia: the effect of soft tissue on the output from skin-mounted accelerometers. *Journal of Biomechanical Engineering, Vol.6, 223-226.*

Oliver,J. and Middleditch,A. (1991). Functional anatomy of the spine. *Butterworth-Heinemann Ltd., Oxford, ISBN 0-7506-0052-7.*

Orne,D. and Liu,Y.K. (1971). A mathematical model of spinal response to impact. *Journal of Biomechanics 4: 49-71*

Paddan,G.S. and Griffin,M.J. (1988). The transmission of translational seat vibration to the head-I. vertical seat vibration. *Journal of Biomechanics 21(3): 191-197.*

Paddan,G.S. and Griffin,M.J. (1993). Transmission of vibration through the human body to the head: a summary of experimental data. *University of Southampton ISVR Technical Report 218.*

Panjabi,M.M. (1973). Three-dimensional mathematical model of the human spine structure. *Journal of Biomechanics 6: 671-680.*

Panjabi,M.M., Andersson,G.B.J., Jorneus,L., Hult,E. and Mattsson,L. (1986). *In vivo* measurement of spinal column vibrations. *Journal of Bone and Joint Surgery 68-A(5): 695-702.*

Payne,P.R. (1965). Personnel restraint and support system dynamics. *Aerospace Medical*

Research Laboratory, Wright-Patterson Air Force Base, Ohio, Report No. AMRL-TR-65-127.

Payne,P.R. and Band,E.G.U. (1971). A four-degree-of-freedom lumped parameter model of the seated human body. *Aerospace Medical Research Laboratory, Wright-Patterson Air Force Base, Ohio, Report No. AMRL-TR-70-35.*

Petyt,M. (1990). Introduction to finite element vibration analysis. *Cambridge University Press, ISBN 0-521-26607-6.*

Pope,M.H., Svensson,M., Broman,H. and Andersson,G.B.J. (1986). Mounting of the transducers in measurement of segmental motion of the spine. *Journal of Biomechanics 19(8): 675-677.*

Pope,M.H., Wilder,D.G., Jorneus,L., Broman,H., Svensson,M. and Andersson,G. (1987). The response of the seated human to sinusoidal vibration and impact. *Journal of Biomechanical Engineering 109:279-284.*

Pope,M.H., Kaigle,A.M., Magnusson,M., Broman,H. and Hansson,T. (1991). Intervertebral motion during vibration. *Journal of Engineering in Medicine 205(1): 39-44.*

Prasad,P. and King,A.I. (1974). An experimentally validated dynamic model of the spine. *Transactions of the American Society of Mechanical Engineers: 546-550.*

Privitzer,E. and Belytschko,T. (1980). Impedance of a three-dimensional head-spine model. *Mathematical modelling 1: 189-209.*

Saha,S. and Lakes,R.S. (1977). The effect of soft tissue on wave-propagation and vibration tests for determining *in vivo* properties of bone. *Journal of Biomechanics, Vol.10, 393-401.*

Sandover,J. (1978). Modelling human response to vibration. *Aviation, Space and Environmental Medicine 49(1): 335-339.*

Sandover,J. and Dupuis,H. (1987). A reanalysis of spinal motion during vibration. *Ergonomics 30(6): 975-985.*

Schultz,A.B. and Galante,J.O. (1970). A mathematical model for the study of the mechanics of the human vertebral column. *Journal of Biomechanics 3: 405-416.*

Schultz,A.B., Belytschko,T.B. and Andriacchi,T.P. (1973). Analog studies of forces in the human spine: mechanical properties and motion segment behavior. *Journal of Biomechanics 6: 373-383.*

Singley III,G.T. and Haley,J.L. (1978). The use of mathematical modeling in crashworthy helicopter seating systems. *AGARD Coference Proceedings 253(A22): 1-17.*

Smeathers,J.E. (1989). Measurement of transmissibility for the human spine during walking and running. *Clinical Biomechanics 4, 34-40.*

Suggs,C.W., Abrams,C.F. and Stikeleather,L.F. (1969). Application of a damped spring-mass human vibration simulator in vibration testing of vehicle seats. *Ergonomics 12(1): 79-90.*

Tortora,G.J. and Anagnostakos,N.P. (1990). Principles of anatomy and physiology (sixth edition). *Harper & Row Publishers, New York, ISBN 0-06-046694-4.*

Toth,R. (1966). Multiple degree-of-freedom, nonlinear spinal model. *Engineering in Medicine and Biology, proceeding of the 19th annual conference: 102.*

Valiant,G.A., McMahon,T.A. and Frederick,E.C. (1987). A new test to evaluate the cushioning properties of athletic shoes. *International Series on Biomechanics, Biomechanics X-B, Vol.6B, 937-941.*

Vogt,H.L., Coermann,R.R. and Fust,H.D. (1968). Mechanical impedance of the sitting human under sustained acceleration. *Aerospace Medicine 39: 675-679.*

White,G.H.Jr., Lange,K.O., and Coermann,R.R. (1962). The effects of simulated buffeting on the internal pressure of man, *Human Factors 4:275-290.*

Williams,J.L. and Belytschko,T. (1981). A dynamic model of the cervical spine and head. *Air Force Airospace Medical Research Laboratory, Wright-Patterson Air Force Base, Ohio, Report No. AFAMRL-TR-81-5.*

Williams,J.L. and Belytschko,T. (1983). A three-dimensional model of the human cervical spine for impact simulation. *Transactions of American Society of Mechanical Engineers, Journal of Biomechanical Engineering 105: 321-331.*

Wittmann,T.J. and Phillips,N.S. (1969). Human body nonlinearity and mechanical impedance analyses. *Journal of Biomechanics 2:281-288.*

Woods,A.G. (1967). Human response to low frequency sinusoidal and random vibration. *Aircraft Engineering 39(7): 6-14.*

Ziegert,J.C. and Lewis,J.L. (1979). The effect of soft tissue on measurements of vibrational bone motion by skin-mounted accelerometers. *Journal of Biomechanical Engineering, Vol.101,218-220.*